Chemistry Dissertations   Department of Chemistry

6-23-2009

On the Preorganization of the Active Site of Choline Oxidase for Hydride Transfer and Tunneling Mechanism

Osbourne Quaye
Georgia State University

ON THE PREORGANIZATION OF THE ACTIVE SITE OF CHOLINE OXIDASE FOR HYDRIDE TRANSFER AND TUNNELING MECHANISM

by

OSBOURNE QUAYE

Under the Direction of Giovanni Gadda

ABSTRACT

Choline oxidase catalyzes the two-step oxidation of choline to glycine betaine, one of limited osmoprotectants, with the formation of betaine aldehyde as an enzyme bound intermediate. Glycine betaine accumulates in the cytoplasm of plants and bacteria as a defensive mechanism to withstand hyperosmolarity and elevated temperatures. This makes the genetic engineering of relevant plants which lack the property of salt accumulation of economic interest, and the biosynthetic pathway of the osmolyte a potential drug target in microbial infections. The reaction of alcohol oxidation occurs via a hydride ion tunneling transfer from the substrate donor to a flavin acceptor within a highly preorganized active site environment in which choline and FAD are in a rigidly close proximity.

In this dissertation, factors contributing to the enzyme-substrate preorganization which is required for the hydride ion tunneling reaction mechanism in choline oxidase have been investigated. Crystallographic studies of wild-type choline oxidase revealed a covalent linkage

between C8M atom of the FAD isoalloxazine ring and the N(3) atom of the side chain of a histidine at position 99, and a solvent excluded cavity in the substrate binding domain containing glutamic acid at position 312 as the only negatively charged amino acid residue in the active site of the enzyme. The role of the histidine residue and the contribution of the 8α-N(3)-histidyl covalent linkage of the flavin cofactor to the reaction of alcohol oxidation was investigated in a variant form of choline oxidase in which the histidine residue was replaced with an asparagine. The role of the glutamate residue and the importance of the spatial location of the negative charge at position 312 was investigated in variant forms of choline oxidase in which the negatively charged residue was replaced with glutamine and aspartate. Mechanistic data obtained for the variant enzymes and their comparison to previous data obtained for wild-type choline oxidase are consistent with the residues at positions 99 and 312 being important for relative positioning of the hydride ion donor and acceptor. The residues are important for the enzyme-substrate preorganization that is required for the hydride tunneling reaction in choline oxidase.

INDEX WORDS: Flavoproteins, Flavinylation, Quantum Mechanical Tunneling, Hydride Ion
                Transfer, Preorganization, Choline Oxidase, Alcohol Oxidizing Enzymes

ON THE PREORGANIZATION OF THE ACTIVE SITE OF CHOLINE OXIDASE FOR HYDRIDE TRANSFER AND TUNNELING MECHANISM

by

OSBOURNE QUAYE

A Dissertation Submitted in Partial Fulfillment of the Requirements for the Degree of

Doctor of Philosophy

in the College of Arts and Sciences

Georgia State University

2009

ON THE PREORGANIZATION OF THE ACTIVE SITE OF CHOLINE OXIDASE FOR

HYDRIDE TRANSFER AND TUNNELING MECHANISM

by

OSBOURNE QUAYE

Committee Chair: Dr. Giovanni Gadda

Committee: Dr. Dabney W. Dixon

Dr. Yujun G. Zheng

Electronic Version Approved:

Office of Graduate Studies

College of Arts and Sciences

Georgia State University

August 2009

To God Be The Glory

&

Dedicated To All Who Draw Inspiration From Me To

Achieve Their Personal Academic Goals

ACKNOWLEDGEMENTS

In as much as completion of my Ph.D. is obviously a great feat, it is not an accomplishment that I can solely take credit for. Just like a newborn child growing up, my study started with baby steps and needed the watch and support of many in order to develop the necessary skill and discipline to achieve the goal of becoming a seasoned scientist.

It is with immeasurable appreciation that I acknowledge my program advisor, Dr. Giovanni Gadda. Even though I have sometimes honestly felt the "knocks" were unjustifiably too hard, your unwavering support and "push" is what has really taken me to the "Olympics". If I made it all the way through, it is because you made it all happen. Over the years as your student, my attitude to science and research, as well as working life in general, has tremendously changed for the better; not to mention the confidence you have inadvertently imbibed in me as a result of your knowledgeable prowess and pedigree in your field of research. The disciplined training I have acquired under your tutelage and direction will forever remain a tall-standing fortress in my life in the future. Thank you very much for the crafty touch you gave my career.

My second appreciation goes to my advisory committee members, Drs. Dabney W. Dixon and Yujun G. Zheng, for your prompting questions and suggestions, and the fine tunings of some of the rough edges of my study. Dr. Dixon, I would like you to exceptionally know that your motherly and career goals talk/advice are not only going to be used right after my program but for a lifetime. My appreciation also goes to all the professors who in one way or the other taught or offered me advice in my Ph.D. studies, both in Georgia and Ghana. To my academic god-parents, Professor and Professor Mrs. Ernest and Ellen Aryeetey, Professor Marian E. Addy, and Professor Alex Nyarko, I say thank you and I am particularly highly appreciative of you for believing in me. I also want to take this opportunity to thank Professor Nigel Scrutton, Dr. Sam

Hay, Dr. Chris Pudney and all the members of Nigel Scrutton's laboratory at the University of Manchester, UK for hosting me when I came to do part of my study in Manchester.

There is always something to learn from people however brief the interaction with them may be. It is and would forever be a wonderful experience getting to meet and working with all the past and present members of Dr. Giovanni Gadda's laboratory that I met. Fan, Mahmoud, Kevin, Trang, Tran Bao, Kunchala, Merid, Steffan, Slavica, Andrea, Anthony, Hongling, Sharonda, Lydia, Philip, Nicole, Stephen and Danila you all provided the serene laboratory environment in your own individual ways for this successful Ph.D. story to be told. Tore (Kunchala), for all the enjoyment and fun I had in your black Toyota Camry, I have considered owning a Toyota Camry in the future; you are such a sweet-hearted angel. I would also like to mention the cheerfully receiving faces of the staff at the Chemistry Department of Georgia State University. Edna, Sina, Stephanie, Diane, Marina, Lita, Robert, Will, Dan, Chris Long (My Hero), Don Hardon etc. your smiles and willingness to always provide the needed help were so soothing they will never be forgotten. To Julianne, Cathy, Rong, Jia and all of my student friends, thank you for being special to me.

I am indebted to my wife Naa and daughter Gift for being the backbone that kept me going whenever the going got tough. I denied you your rightfully deserving time and attention during my Ph.D. study. Naa, I left you in the mornings almost everyday (at least every weekday) to take care of Gift and the home, and came back late in the evening too tired to even help you with anything. You took care of me and even picked up after me as if I were a baby too, just so I could find the time to do my school work. For all the sacrifice you had to make, no amount of "Thank you" I say and in whatever language I say it will suffice. I equally share the honors with

you and more than ready to make it up to you in every way possible. I pledge my love to you and I pray God richly bless you.

I would like to say "Thank you" to my parents Poppyyy and Mommyyy, my grandma Yoomo, Mama Belinda, all my siblings, and my entire extended family for your unending love to me. I feel so blessed for all the emotional support from the rank and file of the whole family. Without all of you, there would have been no me.

To my friends David and Rosemond, Ben and Amma, Serwaa and Kufour, Heather, Selina, Josephine, Andy Andoh, and Abena Ajobi all of Atlanta, GA, Adriana of West Orange, NJ, Norine, Ernest, Joseline and Jonathan, I appreciate you being there when it mattered most during my Ph.D. program.

My final thanks go to all those who could not be mentioned; your contributions and support are very much appreciated and are by no means less of importance.

Thank you once again to all and sundry and God richly bless each and every one of you.

TABLE OF CONTENTS

LIST OF TABLES

LIST OF FIGURES

LIST OF SCHEMES

CHAPTER 1

Introduction

1.1.   Flavoproteins

Flavoproteins are proteins that employ a flavin cofactor, either flavin mononucleotide (FMN) or flavin adenine dinucleotide (FAD), for their biological processes. Flavins are derived from riboflavin, which has an isoalloxazine ring as the basic structure (Figure 1.1), with substituted groups. The FMN contains a monophosphate and FAD contains an adenine diphosphate attached to the riboflavin (Figure 1.2). Flavoproteins are involved in a variety of functions which are crucially determined by the mode of interaction of the isoalloxazine ring of the flavin with the protein moiety. The versatility of flavoproteins is due to the ability of the flavin cofactor to readily and reversibly undergo both one- and two-electron transfers, thus allowing for the transfer of electrons, hydrogen atoms, hydride ions and protons (*1-3*). The flavin cofactor can also accept and emit photons as in the case of the oxygenation reaction catalyzed by bacterial luciferase, and the reaction that results in illumination of marine bacteria at night as examples (*4-8*). Other electronic states involving a partial charge transfers to or from the redox states and called charge-transfer species have also been shown in flavins. Depending on the redox, ionic or electronic state, the flavin cofactor assumes a unique color such as yellow for the oxidized, and red and blue for the semiquinone species. The oxidized flavin cofactor is susceptible to nucleophilic attack at different positions of the isoalloxazine ring allowing the formation of a variety of covalent intermediates (*9, 10*). The majority of the known flavoproteins are flavoenzymes which include, but are not limited to, monooxygenases, oxidases and transferases. The grouping of flavoenzymes into classes is based on common properties shared

within the same class which include the number of electrons involved in a catalytic cycle (*11*), the type of reaction catalyzed, the ability to use molecular oxygen as electron acceptor, the substrate subjected to catalysis, and the nature of the auxiliary redox centers among others (*2*). The reactions catalyzed by flavin-dependent enzymes consist of a reductive half in which an electron donor or a substrate is oxidized with a concomitant reduction of the flavin cofactor, and an oxidative half in which the reduced flavin is re-oxidized by an electron acceptor or another substrate.
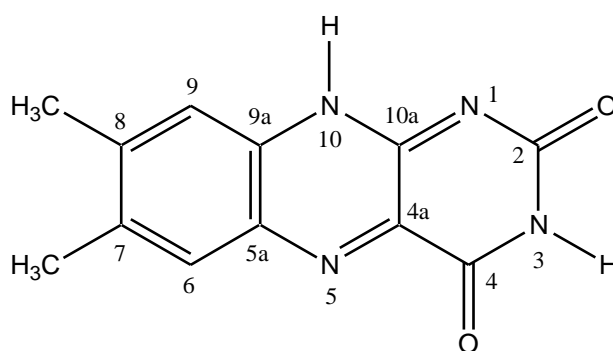
Figure 1.1. The flavin isoalloxazine ring.
Modified from ref. (12).
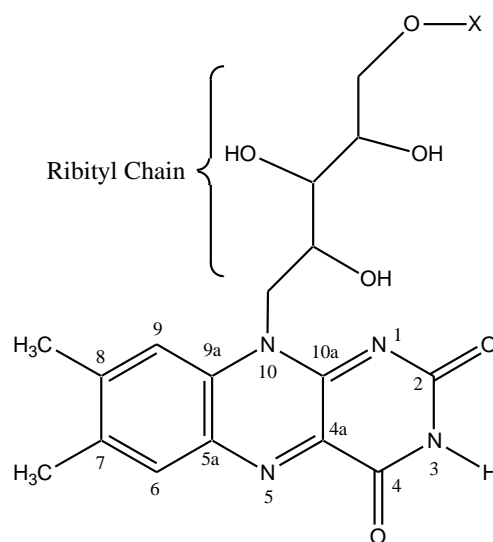
Figure 1.2. FMN and FAD riboflavin structures.
Riboflavin, $X = H$; FMN, $X = PO_3^{2-}$; FAD, $X = ADP$.

Flavin monooxygenases. This group of flavoproteins catalyzes the detoxification of a wide range of chemicals in animals including therapeutic drugs and dietry compounds (*13*). In plants, they are involved in the metabolism of glucosinolates, biosynthesis of auxin, and defense (*14*). The reduced enzyme reacts with molecular oxygen to form an observable C(4a)-hydroperoxide intermediate in the reaction catalyzed by flavin monooxygenases, with either NADH or NADPH as a reducing agent (*2*). In the presence of an organic substrate, an oxygen atom is transferred to the substrate from the hydroperoxide intermediate to form a C(4a)-hydroxy flavin which is subsequently converted to oxidized flavin upon dehydration. In the absence of the substrate, the flavin hydroperoxide is slowly converted to the oxidized flavin with the formation of hydrogen peroxide (*2*). The preferred substrates for flavin monooxygenases contain a nucleophilic heteroatom, such as nitrogen and sulfur, as the site for oxygenation, and are converted to more polar and excretable products which are less toxic or pharmacologically less active. Flavin monooxygenases have been further grouped into subclasses A-F based on sequence similarity, fold or structural features, and function (*1, 15*). Subclass A are flavoprotein hydroxylases which typically react with aromatic substrates with high regioselectivity and exhibit shuttling conformations between "in" and "out" positions of the flavin cofactor during catalysis (*16, 17*). Subclass B contains two dinucleotide binding domains (*18*). Subclass C monooxygenases are FMN dependent and display a TIM barrel fold (*19*). Subclass D has the unusual ability of using both FAD and FMN with similar degree of efficiency and has the fold of acyl-CoA dehydrogenase (*20-23*). The rare subclass E monooxygenases oxidize styrene and styrene derivatives to their corresponding epoxides (*24*) and have structural properties similar to *p*-hydroxybenzoate hydroxylase (*25-27*). Subclass F monooxygenases catalyze the chlorination and

bromination of activated organic molecules and play an important role in the biosynthetic pathways of antibiotics and other natural products (*28-31*).

Flavin oxidases. In the flavin oxidases, the reduced enzyme reacts with molecular oxygen by transferring hydride equivalents to form the oxidized flavin with the production of hydrogen peroxide (*10*). Even though the formation of stable flavin intermediates is rare among the flavin oxidases, the presence of a C(4a)-adduct has recently been demonstrated in pyranose 2-oxidase (*32*) and choline oxidase (*33*). Flavoprotein oxidases catalyze the oxidation of a wide range of organic substrates which include amines and amino acids, alcohols, carbohydrates, nitroalkanes and sulfhydryl groups [for recent reviews see (*1, 34, 35*)]. In the reactions catalyzed by the flavin oxidases, the negative charge of the anionic reduced flavin is localized at the N(1)-C(2)=O region of the isoalloxazine ring and stabilized by a positive charged locus of the protein (*36-38*). The stabilization is thought to be necessary to facilitate flavinylation in the enzymes with covalently linked flavin cofactors (*39*), to elevate the mid-point reduction-oxidation potential for a thermodynamically favorable flavin reduction (*40, 41*), and for the reactivity of the reduced flavin with molecular oxygen (*40, 41*).

Flavin electron transferases. In the flavin electron transferases, the flavoenzymes catalyze one-electron transfer reactions with the formation of the neutral form of flavin semiquinone and $O_2^{\cdot-}$ (*2*). The benzene ring of the isoalloxazine has been shown to be the only part of the flavin cofactor that is solvent accessible in the flavin electron transferases. Unlike oxidases, this group of flavoenzymes cannot stabilize benzoquinoid forms of 6- and 8- substituted flavins and flavin-N(5)-sulfite adducts (*12*).

1.1.1. Flavin Attachments

Flavins may be bound to flavoproteins via electrostatic interactions and hydrogen bonding so that the cofactor becomes dissociable under mild denaturing conditions, or permanently attached through a covalent linkage. Differences in reduction-oxidation potential for the two types of bound flavins (higher for the covalently attached flavin) suggest that the covalent linkage may increase the efficiency of a particular reaction and selectively enhance a metabolic pathway [for a recent review see (*42*)]. It is thus interesting to note in this regard that both covalently and non-covalently bound FAD in cholesterol oxidase has been identified in one organism, *Brevibacterium sterolicum* (*43, 44*). As to whether the covalently linked flavin has evolved from the non-covalently linked flavin to enhance catalysis is yet unknown. However, the importance of covalent attachments of flavins in catalysis is acknowledged in various contexts.

Proteins with covalently linked flavins constitute about one-tenth of all flavoproteins with the flavin either attached to the 8α-methyl position via histidine, tyrosine or cysteine residues, or to the 6α-methyl position via a cysteine residue (*42, 45*). There are five different types of covalent linkages (Figure 1.3); flavoproteins and their different types of linkages are shown in (Table 1.1). Identification of covalently linked flavoproteins has generally been made using acid precipitation followed by proteolytic fragmentation of the polypeptide, or polyacrylamide gel electrophoresis under denaturing conditions followed by fluorescence at acid pH before or after spraying the gel with performic acid. The identity of the covalent attachment with respect to the amino acid residue and position of the linkage have required more rigorous approaches ranging from chemical analysis and/or synthesis, UV-visible and/or fluorescence spectroscopy, to nuclear magnetic resonance spectroscopy (*45*). The aminoacyl flavin identification involves generation of flavinylated peptide by proteolytic digestion. The flavinylated peptide is dephosphorylated by

treating with nucleotide and alkaline phosphatases, and purified. The purified peptide is treated with aminopeptidase M to yield a flavinylated amino acid which is further purified by a chromatographic technique such as ion-exchange, reverse-phase high pressure liquid, or thin-layer using synthetic standards as controls (*45*). 6-S-cysteinyl flavin has unusual UV-visible absorption spectra that allow for readily identification. The cysteinyl flavin is more light-sensitive compared to the other aminoacyl flavins, giving rise to a blue fluorescent photoproduct at low pH but a non-fluorescent product at high pH. Comparison of the quantum yield of fluorescence at low (<3.5) and neutral pH, and the enhancement of fluorescence after performic acid oxidation affords a preliminary identification of the 8α-substituted flavins. The reduction of the performic acid oxidation product of 8α-S-cysteinyl flavin produces free cysteine and free flavin, and the reduction of 8α-O-tyrosyl flavin with dithionite produces free tyrosine and free flavin (*46*). 8α-N1- and 8α-N3-hystidyl flavins can be distinguished by paper electrophoresis at pH 5, isoelectric focusing (*47*), or by high voltage electrophoresis after sequential treatment with sodium borohydride, methyliodide and prolonged exposure to acid (*48*).

Proteolytic fragmentation of flavoproteins in which the protein cofactor is covalently linked to the protein has allowed the determination of peptide sequences around the site of flavinylation, which have shown little sequence homology (*45*). Similarities in sequences around the point of flavin attachment have only been shown in cases where the entire primary sequences of the proteins are related (*49, 50*). Often, regions of multiple glycine residues are found near the sites of covalent attachment. These are thought to be present to allow for flexibility and accommodation of the bulky flavin and the amino acid residues required for flavin attachment and/or catalysis in the active site since the glycyl residues are small (*51*). The lack of a specific recognition sequence around the site of flavin attachment, which would be required by a

common modifying enzyme to prevent covalent addition of the flavin to similar residues in the polypeptide chain, suggested that the process of flavinylation is self-catalytic, and the specificity of the linkage to a particular residue acquired after protein folding (*45*). The covalently linked flavoproteins are thought to form an active site that initiates and/or mediates the formation of covalent linkage between the flavin and the protein.

8α-(N3)-Histidyl

8α-S-Cysteinyl

8α-(N1)-Histidyl

8α-O-Tyrosyl

6-S-Cysteinyl
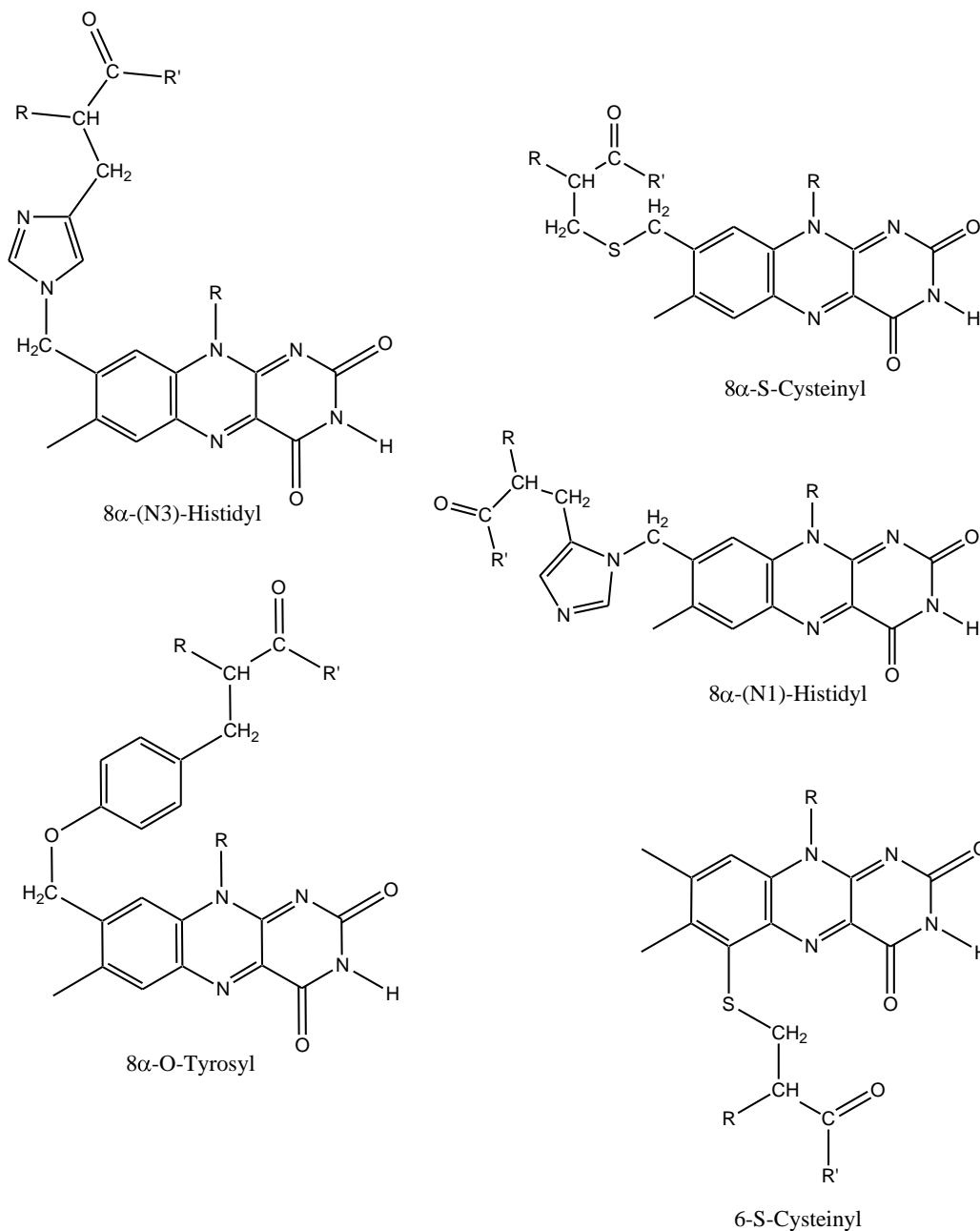
Figure 1.3. Mode of covalent attachment of flavin to the protein in flavoproteins.

Table 1.1. Examples of Flavoenzymes with Covalently Linked Flavin Cofactors[a]

Mode of Flavin Attachment	Enzyme	References
8-α-*N1*-Histidyl FAD	Alditol oxidase	(*52*)
	Cytokinin dehydrogenase	(*53*)
	6-Hydroxy-D-nicotine oxidase	(*54*)
	Cholesterol oxidase	(*55*)
	Thiamin dehydrogenase	(*56*)
	L-Galactonolactone oxidase	(*57*)
	L-Gulono-γ-lactone oxidase	(*58*)
	Cyclopiazonate oxidocyclase	(*56*)
8-α-*N3*-Histidyl FAD	Choline oxidase	(*59*)
	Pyranose 2-oxidase	(*60*)
	Fumarate reductase	(*56*)
	Sarcosine dehydrogenase	(*56*)
	Succinate dehydrogenase	(*61*)
	Vanillyl-alcohol oxidase	(*62*)
	Eugenol oxidase	(*63*)
	L-Gluconolactone oxidase	(*64*)
	Dimethylglycine dehydrogenase	(*56*)
	Dimethylglycine oxidase	(*65*)
8-α-*O*-Tyrosyl-FAD	*p*-Cresol methylhydroxylase	(*66*)
8-α-S-Cysteinyl FAD	Monoamine oxidase A	(*67*)
	Monoamine oxidase B	(*68*)
	Monomeric sarcosine oxidase	(*69*)
	Amadoriase I	(*70*)
	Pipecolate oxidase	(*69*)
	N-methyltryptophan oxidase	(*69, 71*)
	Sarcosine oxidase	(*72*)
	NikD	(*73*)
	Flavocytochrome c	(*74, 75*)

8α-Histidyl-6-S-cysteinyl FAD	Glucooligosaccharide oxidase	(*76*)
	Chito-oligosaccharide oxidase	70
	Berberine bridge enzyme	(*77*)
	Hexose oxidase	(*78*)
	Aclacinomycin oxidoreductase	(*79*)
	Δ-Tetrahydrocannabinolic acid synthase	(*80*)
	Cannabidiolic acid synthase	(*80*)
6-S-Cysteinyl FMN	Dimethylamine dehydrogenase	(*50*)
	Trimethylamine dehydrogenase	(*81*)
	Histamine dehydrogenase	(*82*)
8α-histidyl FMN	Heterotetrameric sarcosine oxidase	(*83*)
	NADH dehydrogenase type II	(*84*)
8α-histidyl-6-S-cysteinyl FMN	Dbv29	(*85*)
Phosphoester-threonyl	NqrB	(*86*)
	NqrC	(*86*)

[a]Modified from ref. (*42*)

Different mechanisms have been proposed for the flavinylation process in different enzymes. The mechanisms of covalent flavinylation in *p*-cresol methylhydroxylase (*87*), 6-hydroxy-D-nicotine oxidase (*88*), monomeric sarcosine oxidase (*69*), trimethylamine dehydrogenase (*39*) and N-methyltryptophan (*89*) require a positively charged amino acid residue in close proximity to the N(1)-C(2)=O region of the bound flavin cofactor. The positively charged residue is important for the stabilization of a negative charge that develops at the N1/C2 locus during the flavinylation reaction. Arginine residues, specifically Arg447, Arg67 and Arg222, have been shown to be the positively charged residues that stabilizes the negative charged at the N(1)-C(2)=O loci in *p*-cresol methylhydroxylase (*87*), 6-hydroxy-D-nicotine

oxidase (*90*) and trimethylamine dehydrogenase (*39*), respectively. Removal or reversal of the positive charge in trimethylamine dehydrogenase, using site-directed mutagenesis, resulted in mutant proteins that were devoid of the flavin cofactor. Studies on succinate dehydrogenase from *S. cerevisiae* in which the flavin is covalently attached to histidine 90 showed that flavinylation takes place in the mitochondrial matrix after the flavoprotein subunit is transported into the matrix and a lead peptide sequence cleaved (*91*). The flavinylation process is stimulated by the presence of citric acid intermediates but the intermediates are not absolutely required. C-terminal deletion mutants of succinate dehydrogenase with the deletions far from the postulated site of the covalent linkage do not recognize FAD. The overall data in this study suggested that binding of citric acid intermediates may stabilize a protein conformation that allows flavinylation to occur and that a precise structural configuration of the flavoprotein subunit may be required for the process. In 6-hydroxy-D-nicotine oxidase (6HDNO), the incorporation and covalent linkage of ^{14}C-labelled riboflavin into the apoprotein to form a functional enzyme was consistent with a self-catalytic flavinylation process (*88, 92*). Holoenzyme reconstitution from the apoprotein of 6HDNO with FAD required the presence of 3-carbon mediating compounds thought to stabilize a protein conformation that favors flavinylation (*88*), as for the case of succinate dehydrogenase. Using site-directed mutagenesis, an arginine residue at position 67 has been shown to be important for flavinylation in 6HDNO, and also demonstrated the requirement of a positive charge at that position (*90*). The general proposed mechanism for flavinylation is shown in Figure 1.4. Crystallographic studies coupled with site-directed mutagenesis in berberine bridge enzyme, chitooligosaccharide oxidase, hexose oxidase, Dbv29 and glucooligosaccharide oxidase, all containing double covalent linkage in each molecule of FAD, suggest that flavinylation of the individual covalent attachments is independent of each other (*78, 85, 93-95*).
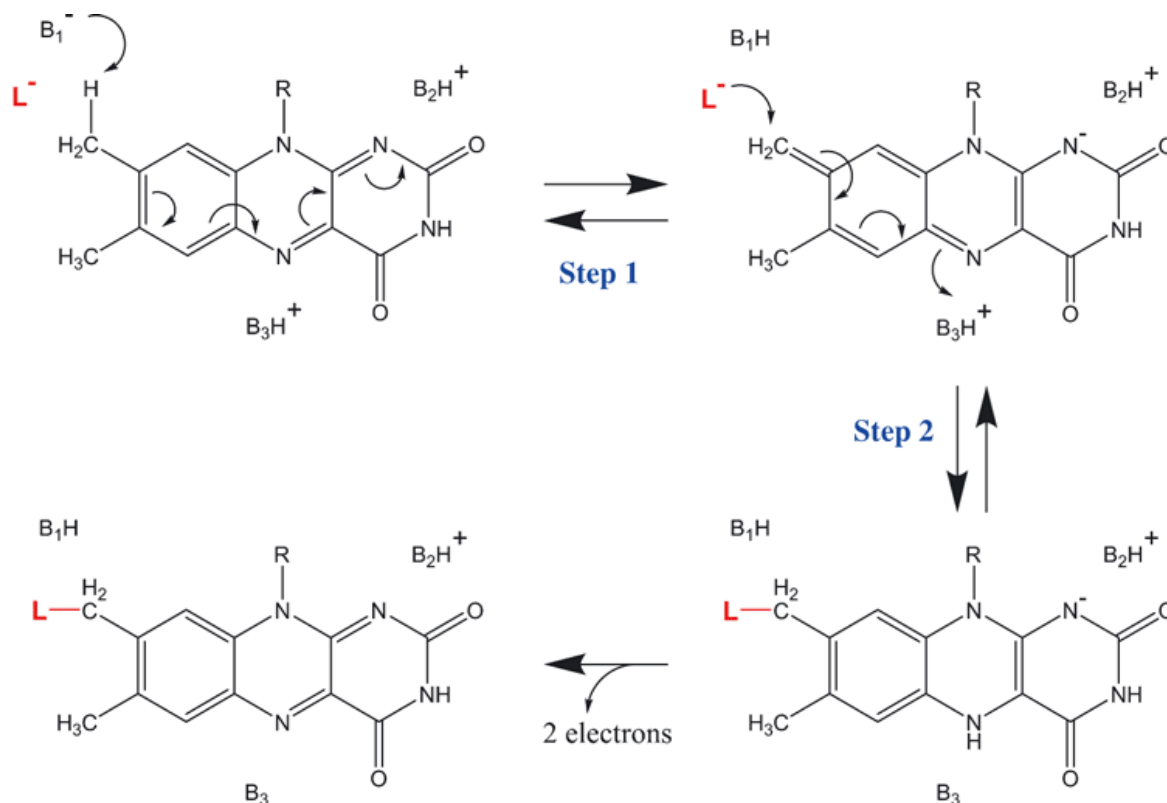
Figure 1.4. General proposed mechanism for flavinylation.
 Modified from ref. (42).

Studies on the effects of pH on the redox potentials of 8α-N-imidazolylflavins showed that increases in pH result in a decrease in the oxidation-reduction potential, suggesting that the redox potential of the flavin can be influenced by the histidyl group modulation of the flavin microenvironment (*96*). A correlation between the flavin covalent attachment and redox properties was proposed in a study that demonstrated that oxidation-reduction potentials of aminoacyl flavins were ~50-60 mV more positive compared to the unmodified flavins (*97*). This proposal has recently been supported by studies in which removal of the covalent linkage in flavin-dependent enzymes containing the covalently linked flavin resulted in a decrease in the redox potential of ~100 mV (*62, 98, 99*).

1.1.2. Roles of the Flavin Covalent Linkage

The flavin covalent linkage has been shown to play a number of roles in covalently linked flavoproteins.

Glucooligosaccharide oxidase, which catalyzes the oxidation of glucose, lactose, maltose, cello- and malto-oligosaccharides (*100*), contains a double-covalent linkage in each FAD molecule linking the 6 and 8α positions of the isoalloxazine ring to Cys130 and His70, respectively (*76*). Double site-directed mutation of the residues involved in the covalent attachments to alanine resulted in a protein with no detectable FAD bound (*94*). Even though the protein folded into an overall similar structure to the wild-type enzyme, the double mutant did not contain an appropriate cavity for binding the oxidized flavin suggesting that the covalent attachment is important for the organization of the FAD binding domain (*94*). Due to the relatively bulky substrates for the enzyme, glucooligosaccharide oxidase has an open substrate bindng cavity. It appears that the double covalent linkage serves as an anchor that properly orients the flavin cofactor for binding and oxidation of the substrate (*94*). Heat and guanidine HCl treatments of the wild-type and the double mutant form of glucooligosaccharide oxidase resulted in a higher melting temperature and greater guanidine HCl resistance for the wild-type enzyme compared to the mutant consistent, with the double covalent attachment contributing to the structural stability of the protein.

Histidine at position 69 is the residue involved in covalent linkage with the flavin cofactor (FAD) in cholesterol oxidase (*55, 101, 102*). Replacement of the histidine residue with an alanine resulted in an enzyme with a non-covalently bound FAD (*99*) with similar topology to the wild-type enzyme (*103*). The cholesterol oxidase variant however unfolded at a lower urea concentration and has melting temperature that ~15 $^{\circ}$C as compared to wild-type cholesterol

oxidase suggesting that the covalent linkage is important for the overall stability of the structure of the cholesterol oxidizing enzyme (*104*).

In monomeric sarcosine oxidase, mutation of the amino acid residue (Cys315) involved in covalent attachment with FAD to alanine produced an apoprotein with no catalytic activity (*105*). Reconstitution of the apoprotein with exogenous FAD or 8-nor-8-chloro-FAD, an FAD analogue, resulted in the formation of an unstable complex suggesting differences in the reconstituted C315A holoenzyme compared to the wild-type enzyme with the covalently bound flavin cofactor (*105*). Oxidation of a reconstituted C315A with reduced 5-deazaFAD using sarcosime amine was accompanied by release of the oxidized 5-deazaFAD suggesting a weak interaction of the oxidized FAD analogue with the protein, and consistent with the flavin covalent linkage preventing loss of the loosely bound flavin cofactor analogue (*105*).

Berberine bridge enzyme (BBE) is a bicovalently flavinylated enzyme that catalyzes the oxidative cyclization of (S)-reticuline to (S)-scoulerine in the alkaloid biosynthetic pathway in plants (*77*). The flavin cofactor is linked via C(8)M and C(6)M atoms of the flavin isoalloxazine ring to histidine 104 (8α-histidyl) and cysteine 166 (6-S-cysteinyl), respectively (*77*). The wild-type has a redox potential of +132 mV but removal of one of the covalent linkages in His104Ala and Cys166Ala mutant enzymes resulted in a decrease in the redox potential of about 80 to 100 mV (*95, 106*). Even though the decrease of ~100 mV is expected for the removal of a flavin covalent linkage, as has been observed in other covalently linked flavoenzymes. There were differences in the stabilization of the mutant enzymes; whereas the C166A enzyme could be expressed and purified using the same protocol as for the case of the wild-type enzyme (*95*), the H104A mutant enzyme could only be obtained by co-overexpressing the protein with disulfide isomerase (*106*). Removal of each one of the covalent linkages resulted in ~20-fold decrease in

enzymatic activity (*106*). The research group of Vrielink in has cautioned that a direct quantitative correlation of redox potential with decreases in enzymatic activity may not be appropriate because other factors such as the geometry of the transition state or mode of orbital reorganization could also affect the kinetics of the reaction (*103*). X-ray crystal structures of the two singly flavinylated variants of BBE compared to the wild-type enzyme suggest no significant changes in the overall structure and the positioning of the flavin cofactor. However, the side chains of amino acid residues that interact with the substrate have been significantly affected suggesting an important role of the covalent linkages in substrate binding and product release (*106*), similar to the observation made in glucooligosaccharide oxidase (*94*). Computational studies of 6-S-cysteinylation in trimethyamine dehydrogenase suggest that substrate binding could also be affected by the change in electrostatic potential of the isoalloxazine ring due to removal of the covalent linkage (*107*). It is interesting to note that most of the observed properties of the flavin cofactor in the wild-type and mutant enzymes of BBE have also been observed in other bicovalently linked flavoprotein systems (*93, 94*). In chito-oligosaccharide oxidase the FAD cofactor is covalently linked to His94 and Cys154 and replacement of the respective amino acid residues is also consistent with the requirement of the covalent linkages for protein stability (*93*). The results obtained from the spectroelectrochemical and kinetic studies with the wild-type and singly flavinylated variant forms of chito-oligosaccharide oxidase suggest that high redox potential is not the only prerequisite for efficient catalysis, and the bi-covalent linkage of the flavin cofactor is essential for a catalytically relevant conformational change in the active site of the enzyme (*93*).

1.2.   Quantum Mechanical Tunneling

A chemical reaction may occur through the classical transition state (over-the-barrier) or through quantum mechanical tunneling (through the barrier) processes. Transition state theory describes the ground state or minimum potential energy and the transition state or maximum potential energy for the reactant and transition state species, respectively, of a reaction. Enzymatic catalysis from the perspective of the transition state theory is based on the stabilization of the transition state at a reduced energy, thus reduction of the activation barrier and resulting in enhancement of the rate of the reaction (*108*). Figure 1.5 describes the transition state model. Mathematically, the transition state theory has been explained using the Arrhenius (eq 1) and Eyring (eq 2) equations where k is the rate of reaction, k_B is Boltzmann constant, h is Planck's constant, $\Delta H^{\ddagger}$ is the enthalpy of activation and describes the thermodynamics of bond breaking or formation at the transition state, $\Delta S^{\ddagger}$ is the entropy of activation and describes the transition state, R is gas constant, T is temperature, A is the Arrhenius pre-exponential factor, and E_a is the energy of activation. The transition state theory was formulated with the assumption that there is no re-crossing of the transition state species, and subsequently led to the requirement of a correction factor in order to fit other reaction models (*109, 110*). One of such models is the quantum mechanical tunneling.

$$k = A\exp(-E_a/RT) \qquad\qquad 1$$

$$k = \frac{k_B T}{h}\exp\left(\frac{\Delta S^{\ddagger}}{R} - \frac{\Delta H^{\ddagger}}{RT}\right) \qquad\qquad 2$$
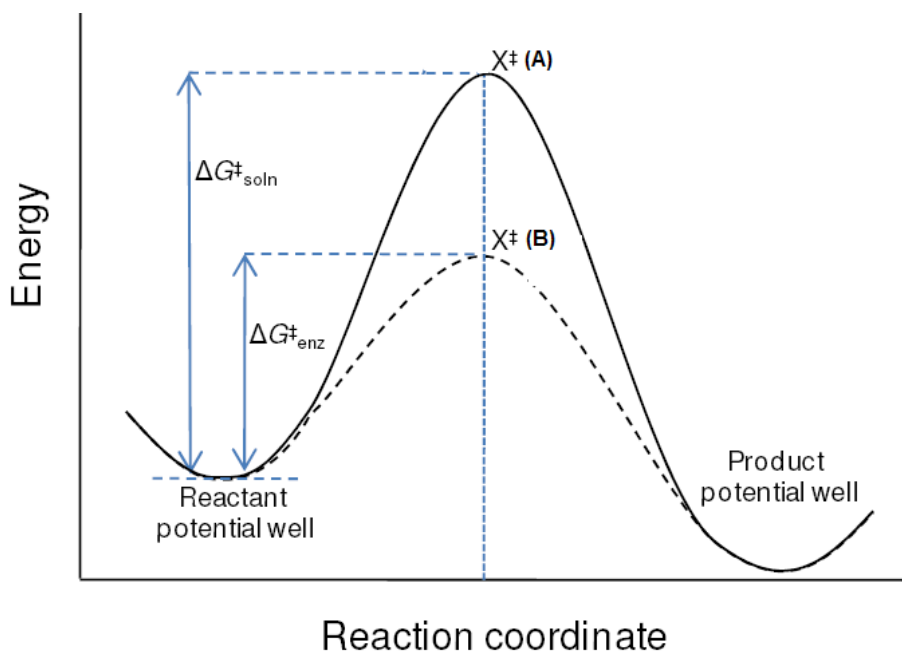
Figure 1.5. Transition state theory model of catalysis.
X‡(A) is the transition state for a reaction in solution. X‡(B) is the transition state for the enzyme-mediated reaction. Modified from ref. (*111*).

Quantum tunneling effects have been shown to be responsible for deviations from classical theories in chemical reactions (*112*). The phenomenon of quantum tunneling was developed on the basis that matter has both wave-like and particle properties, otherwise referred to as the concept of wave-particle duality, that manifests itself in various reactions including chemical catalysis and enzymology. Expression of the concept of wave-particle duality by the de Broglie relation establishes that rather than having a fixed position, a particle has a certain probability of existence at any particular point in space which is described by the wave function of the particle (*113*). Small particles have large wave functions (~0.6Å for a hydrogen) that approach the width of an energy barrier and causing the particle to avoid obtaining the energy required to reach transition state. The particle may only need to surmount a barrier at a point where its function for both reactants and products overlaps, hence crossing the barrier at a lower energy or "tunneling".

The tunneling model therefore become relevant for small particles or species with very small mass and suggests a minimum energy term which is referred to as the zero point energy (ZPE). The ZPE is given by the equation E=1/2hv, where h is Planck's constant and v is the frequency of the particle in ground state.

Electron transfers are the simplest chemical reactions and can proceed at very high rates from an electron donor to an acceptor. Marcus contribution to the tunneling model as it applies to the transfer of electrons was the recognition of a reorganizational energy required for the reaction to proceed (*114-118*). This contribution was thought of as the energy required to move the nuclei of the reactant species from a configuration where the electron is on the donor, to another configuration where the electron is favored to be on the acceptor (*119*). The electronic energy levels of the reactants must be equal for electrons to tunnel as stated by the Franck-Condon principle. The Franck-Condon principle states that since masses of nuclei are greater than those of an electron, their position and momenta change much slower, thus the nuclei do not have much time to change position and momenta during electron transfer. The electrons must therefore be transferred at or near the intersection of the donor and acceptor potential surfaces in order to satisfy the Franck-Condon principle and conserve total energy. Marcus predicted that in electron transfer reactions, all of the reaction may occur by nuclear tunneling at sufficiently low temperatures since the reaction is occurring at an energy that is close to the ZPE suggesting a temperature independent rate constant at low temperatures and a temperature dependent rate constant at high temperature for electron transfer due to nuclear tunneling effects (*118*). Temperature dependence of rate is a key feature that differentiates the classical and tunneling pathways. Based on the inverse relation of the wavelike properties of a particle to its mass, a large de Broglie wavelength (*120*) is manifested in chemical systems due to the small mass of an

electron. The electron tunneling in chemistry and biology have been demonstrated and discussed in literature but not presented in this dissertation. The mass of a proton, a hydrogen atom, or a hydride ion, even though much larger than an electron, is also small and therefore has a de Broglie wavelength that is on the order of the distances over which it is expected to be transferred.

The Bell tunneling correction model, which provides an explanation for experimental observations in small molecules and enzyme systems, has been used to interpret aberrant kinetic isotope effects data that did not conform to the Marcus theory (*121-123*). The inclusion of the correction factor to the Arrhenius equation for the classical transition state theory accounted for tunneling below the energy barrier. However, as the kinetic isotope effects of more enzymatic systems were determined, the Bell tunneling correction model became inadequate, resulting in the consideration of absolute tunneling contributions particularly for the rate enhancement for the transfer of hydrogen atoms. Also considered to promote the hydrogen transfer reactions is enzyme dynamics, which could be passive (conformational fluctuations that lead to optimal tunneling) or active (environmentally coupled enzyme motions).

1.2.1. Use of Kinetic Isotope Effects as Mechanistic Probes of Quantum Mechanical Tunneling Reactions

Kinetic isotope effects, particularly with hydrogen isotopes, but also with carbon (*124*), oxygen (*125*) and nitrogen (*126*) have been used to study the kinetics of enzymatic reactions. Kinetic isotope effects are derived from the different energies of nuclear motions which are implicitly due to the mass of the isotopic nuclei (*127*). This is based on the assumption that the

electronic, vibrational, rotational and translational energies of a molecule can be treated separately. Since the potential energy surfaces of isotopic molecules are essentially the same, the effect of the mass difference is to alter vibrational modes of the bonds which are being broken and formed in a reaction. This can explain the observed rates for isotopes of the same element. In other words, it is the difference in the ZPE due to the difference in the isotopic mass that accounts for a large number of the observed kinetic isotope effects. The primary kinetic isotope effect is the ratio of the rate of transfer of an atom to the rate of transfer of an isotope of the same atom. The secondary kinetic isotope effect is the ratio of the rate of transfer where the secondary or proximal atom is non-isotopically and isotopically labeled (*128*). In this dissertation, only the use of hydrogen isotopes is discussed. The masses of the three isotopes of hydrogen are 1.007 for protium, 2.014 for deuterium and 3.106 for tritium, giving rise to relative frequencies of 1.00, 0.71 and 0.57 for C-H, C-D and C-T bonds, respectively. The stretching frequency for a C-H bond is ~2,900 cm^{-1} and that for a C-D bond is ~2,100 cm^{-1}, corresponding to ZPEs of ~17.4 kJmol^{-1} and 12.6 kJmol^{-1}, respectively, giving a difference of ~4.8 kJmol^{-1}. Since the C-H bond stretching (one of the vibrational degrees of freedom) becomes translational in transition state theory, the primary kinetic isotope effect is entirely determined by the ratio of the ZPEs for the C-H and C-D bonds (*129, 130*). Due to restricted motions of D compared to H in C-D and C-H, respectively, caused by the potential energy surfaces in the two isotopes, a change in charge distribution by replacing an H with a D at the secondary position will result in a change in force constant which will affect the H more than the D by virtue of the larger ZPE in the H (*127*). This difference in effect caused by the change in charge distribution or dipole moments as a result of a change in vibrational frequencies upon re-hybridizing a sp^3 hybridized carbon to a sp^2 is the basis for secondary kinetic isotope effect (*131, 132*). In the classical transfer reaction, the

secondary kinetic isotope effect value has been estimated to be between unity and the equilibrium isotope effect (EIE) (*133*). The value of the secondary kinetic isotope is close to unity where the transition state species resemble the reactants which suggests minimal re-hybridization, and close to the EIE value where the transition state resembles the product.

Kinetic isotope effects can be measured using steady state and pre-steady state approaches. The steady state approach only reports on the observed isotope effect. This is the weighted average of all the individual kinetic steps involved in the enzyme turnover reaction and therefore cannot determine the presence of kinetic complexities. Pre-steady state kinetics are purported at directly examining single chemical steps and therefore give the intrinsic or true kinetic isotope effect even in the presence of kinetic complexities. The observation of anomalously large kinetic isotope effects in enzymatic reactions results in the suggestion of the H-tunneling model of hydrogen atom transfer. The modes of hydrogen atom transfer by quantum mechanical tunneling in enzymatic systems have been demonstrated to be either tunneling in a highly preorganized active site with minimal independent movements other than vibrations of the C-H bond along the reaction coordinates or environmentally assisted. Temperature dependence of the kinetic isotope effect has been used as a tool for determining whether an enzymatic hydrogen transfer reaction is by tunneling or not. Tunneling within a highly pre-organized active site with minimal independent movements has been shown to be associated with kinetic isotope effects that are independent of temperature whereas environmentally coupled tunneling is associated with temperature dependence of the kinetic isotope effect in combination/consideration with other thermodynamic parameters. It is worth mentioning that the temperature dependence of the kinetic isotope effect alone will not be adequate to choose between the mechanism between environmentally assisted tunneling and transition state mechanisms.

1.2.2. Proton, Hydrogen and Hydride Ion Transfer

The mechanism of proton transfer, which is ubiquitous in chemical and biological reactions, was initially explained with a model in which the activation energy was thought to be caused by the necessity to stretch the hydrogen covalent bond in a proton donor to a distance at which the formation of a bond with a the proton acceptor becomes possible. The quantum mechanical corrections, taking into account the energies of zero-point vibrations and proton tunneling at the top of the barrier, were later introduced to further develop the bond-stretching model. As a results of rigorous theoretical analysis based on the concept of quantum and classical degrees of freedom, the model suggested that activation energy and preexponential factors are determined by physically different barriers. There is the possibility of the existence of two different types of transition, overbarrier and underbarrier types. The possibility of an underbarrier transition (tunneling) depends on the energy of the particle that tunnel. For the theoretical analysis of the model for proton transfer see the following references (*134-136*).

Tunneling of hydrogen species could occur within static or dynamic barrier systems. Hydrogen tunneling in a static system is associated with inflated kinetic isotope effects which are temperature independent, large differences in the activation energies for protium and deuterium transfer ($\Delta H^{\ddagger}$), and non-classical values for the ratio of Arrhenius preexponential factors (A_H'/A_D') (classical values are close to unity). Such behavior has been shown in alcohol dehydrogenase (*137*), lipoxygenase (*138, 139*), glucose oxidase (*140*), bovine serum amine oxidase (*141*), and monoamine oxidase (*142*), among other enzymes. For hydrogen tunneling in enzymes, a role for protein dynamics has been described as environmentally assisted or vibrationally enhanced ground state tunneling (VEGST) theory, in which thermal fluctuations of the protein scaffold are responsible for shortening the hydrogen tunneling distance (*143*).

Dynamic motions for environmentally assisted tunneling have also been addressed from the perspectives of vibrations in the substrate (*134*).

A tunneling mechanism which is environmentally assisted may occur with gating or active dynamics on the picosecond timescale and affects the donor and acceptor distance, or with passive enzyme motions on the millisecond timescale. The passive motions are similar to the reorganizational energy requirement for a tunneling reaction in the Marcus theory (*116, 118*). The concept of dynamic motions has been extensively discussed in literature using a variety of terminologies such as gating, sampling and reorganization. It has been argued that for the model to be reasonable, the magnitude of the contribution due to dynamic motion should be different in the enzyme catalyzed reaction compared to the same reaction in solution or water, and the transition state for the enzyme catalyzed reaction should have a higher tendency of forming the reaction product. Transmission coefficients determined in enzyme catalyzed systems using computational simulations were shown to be similar to the same reaction in solution (*144, 145*). The extent of tunneling was measured in an enzyme system (methyl malonyl CoA mutase) and an identically enzyme-free system. There was no significant difference in the extent of tunneling in the two systems, suggesting no enzyme enhancement or assistance in the tunneling reaction in methyl malonyl CoA mutase due to protein dynamic motion (*146, 147*).

The tunneling mechanisms for the hydride transfer reactions in the mutant enzymes of choline oxidase presented in Chapters II and III in this dissertation are interpreted as being environmentally assisted.

1.2.3. Enzyme Preorganization

Preferential stabilization of the transition state has been accepted as a contributing factor to rate acceleration observed in enzyme catalysis compared to non-enzymatic reactions or reactions that occur in solution (*148, 149*). Over the years however, considerable evidence has implicated the contribution of active site preorganization in promoting the formation of reactive near attack conformers as the origin of rate enhancement in enzymatic reactions (*150-152*). The active site of an enzyme is preorganized to a geometry that electrostatically stabilizes the transition state (*153, 154*). Warshel's group suggested the contribution of electrostatic effects towards enzyme catalysis stating that although the electrostatic interaction between reacting systems and the surrounding environment is similar in enzymes and solution, the reorganization energy for stabilizing the transition state is removed by the preorganized dipolar environment in the enzyme (*155, 156*). Even though solvent organization around a reacting molecule can be slow compared to the reaction itself in solution thereby limiting the rate of the reaction (*109*), a preorganized enzyme is not subject to such limitations since it can employ relatively fixed dipoles to stabilize the transition state (*153, 154, 157-159*). In accordance with a relatively rigid model system implied by preorganization, various techniques have been used to demonstrate a higher mobility of non-catalytic residues compared to catalytic ones which include comparison of crystal structures in the absence and presence of a ligand (*160*), vibrational modes from Gaussian Network Modeling (GNM) (*161*), calculated motions in dynamic simulations (*162*), and temperature effects (*163*). The observation of multiple steps and intermediates in enzymatic reactions consistent with the requirement for stabilization of each transition state intermediate suggest that enzyme active site preorganization does not imply a geometry that is completely rigid (*164*). Due to slightly different geometric and electrostatic profiles in the transition state

intermediate, some degree of transition state reorganization would be expected (*165, 166*). Based on this premise, it is not surprising that the dogma about enzyme catalysis have changed over the years from the static "lock-and-key" to the more fluid "induced fit" and to the current idea that enzyme catalysis is promoted by dynamic motions. The observations of fixed dipoles and dynamic motions argue in favor of both preorganization and reorganization contributing to enzyme catalysis.

In a comparison study of experimental and theoretically ideal active site geometries in serine esterase, crystal structures of the enzyme in the presence and absence of a ligand and quantum mechanical modeling was used to calculate the optimum arrangement of catalytic side chains (*167*). In the quantum mechanical modeling, the active site was modeled using just the functional groups involved in catalysis, neglecting the surrounding environment, i.e., their attachment to the protein and in the absence of solvent. The theoretical quantum mechanical modeling results suggest that serine esterases can deploy a catalytic triad and oxyanion hole in a three-dimensional consensus geometry that optimally stabilizes each step in the catalytic cycle. Comparison of the consensus geometry from the theoretical modeling to the geometry in the natural enzymes, as observed in the crystal structures, led to the conclusion that the active site of serine esterases have evolved to achieve the catalytic geometry, performing multiple steps with minimum conformational rearrangements (*167*). The conclusion agrees with the principle of minimal frustration which states that "proteins proceed from the unfolded to the folded state along an energy landscape that has minimized conformational barriers by avoiding thermodynamic traps" (*168, 169*). Examples of enzymes in which preorganization has been demonstrated is subsequently reviewed.

Dihydrofolate reductase (DHFR) has been shown to have several secondary

structural elements, including eight stranded β-sheet and four α-helices which are interspersed with loop regions that guide the substrate and cofactor through the catalytic pathway (*170-172*). The protein structure of DHFR can be divided into an adenosine binding subdomain, and a loop subdomain which contains three loops (*173*). Essential hydrophobic contacts exist between the substrate 7,8-dihydrofolate and the active site residues Leu28, Phe31, Ile50, and Leu54 which are disrupted after reduction of the substrate to 5,6,7,8-tetrahydrofolate (*174, 175*). Data on single mutants of Leu28 and Leu54, and their double mutation on one hand, and single mutants of Phe31 and Ile50, and their double mutation on the other hand, suggest that DHFR adopts different conformations during its catalytic cycle (*176*). Compilation of structures that represent complexes and the transition state by cocrystallization of the enzyme with substrate and cofactor analogues and then tracing vibrations in the subdomains and loop positions coupled with kinetic data revealed various differences in conformations within the enzyme structure which implicated a series of conformational states that are characteristic of extensive loop movements that guide the reaction cycle. Further evidence to complement the involvement of dynamic motions in the reaction catalyzed by DHFR was conducted using NMR and molecular dynamics simulation studies. The additional studies suggested connections between distant positions which promote substrate binding and give rise to vibrations that act along the reaction coordinate to facilitate hydride transfer (*176*). In a study by Liu and Warshel on "the catalytic effect of DHFR and its mutants is determined by reorganization energies" quantum mechanical and molecular modeling techniques suggest that preorganization of the polar groups of enzymes is the key catalytic factor and anticatalytic mutations destroy the preorganization (*177*). The authors pointed out that all reactions in a condensed phase, both in enzymes and in solutions, involve correlated motions that are affected by a change in the shape of a multidimensional reaction path which is associated

with a change in the solvent reorganizational energy upon mutation of active site residues. The study therefore supports an active site preorganization in DHFR where the reorganization energy is reduced to the minimum as has been demonstrated in other enzyme systems (*178*).

Preorganization and reorganization factors as related in the enzymatic rearrangement of chorismate to prephenate catalyzed by chorismate mutase from *Bacillus subtilis* was studied to understand the factors that contribute to rate enhancement using a combination of statistical quantum mechanics/molecular modeling simulation methods and potential energy surface exploration techniques (*151*). Different conformational equilibria for chorismate in aqueous solution and in the active site of the enzyme suggest that chorismate mutase preferentially binds the reactive conformer of the substrate, which means that the enzyme acts on the reactants that are geometrically similar to the transition state, favoring the reactive structures of the substrate more than does the solvent. Energy decomposition analysis of the potential energy barrier for the rearrangement of chorismate in solution and in the enzymatic environment were carried out to determine whether the enzyme is suited to better interact with a particular reactant conformation or with the transition state structure of the reaction. The results suggest that in solution, the solvent interacts better with the transition state structure than with the reactant, but to obtain this interaction, an energy cost due to solvent polarization must be paid by the system. Decomposition of the contribution of the interaction energy to the potential energy barrier into electrostatic and non-electrostatic components suggested that the preference of the enzyme for the transition state structure is electrostatic in nature (*151*). The data is consistent with chorismate mutase structure being able to decrease the reaction energy barrier by optimizing electrostatic interactions with the transition state structure while minimizing the reorganization energy. Thus the enzyme does not pay an energy cost to optimize interaction with the transition

state since it is preorganized, whereas the energy price is paid in solution due to a more broken solvent structure. A structural analysis of the spatial arrangements of the substrate inside of the enzyme for the transition state is very similar to the reactive reactant but very different from the non-reactive reactant, and a quantitative analysis of the averaged distances between the substrate and the amino acids showed more similarities in the enzyme active site when the substrate is in the reactive reactant conformation and transition state form than with the non-reactive conformer.

1.3.   Quantum Mechanical Tunneling Enzymes

1.3.1. Alcohol Dehydrogenase

Alcohol dehydrogenase (ADH) is a zinc containing enzyme that catalyzes the oxidation of alcohol substrates to aldehydes by the transfer of a hydride from the substrate to the nicotinamide ring of NAD^+ (*179*). ADH has been extensively studied and data thus far obtained come from horse liver, thermophilic and yeast ADHs.

Horse liver ADH is a homodimer with a molecular mass of 80 kDa. Each monomer subunit contains a catalytic domain and an NAD^+-binding domain, with the catalytic domain containing two zinc atoms (*180, 181*). In the reaction catalyzed by horse liver ADH, the NAD^+ binds to the enzyme followed by the substrate in an ordered bi-bi steady state mechanism (*179*), with the chemical step being masked by the release of the coenzyme (*182-184*). The rate of the coenzyme dissociation from the enzyme was increased in mechanistic studies using hydroxybutyrimidyled enzyme and resulting in kinetic isotope effect values between 3 and 4 on

the overall enzyme turnover (*185*). The crystal structure of horse liver ADH was used to design mutant enzymes with increased rate of substrate binding and product release by using site-directed mutagenesis to replace an active site phenylalanine at position 93, which forms a van der Waals contact with the alcohol substrate with tryptophan. Temperature dependence of the KIE determined for the mutant enzyme showed A_H/A_T and A_D/A_T values lower than the predicted values using semi-classical models, and suggested that the wild-type enzyme is characterized by significant tunneling (*184*). In active site mutants, the size of a valine side chain at the back of the nicotinamide ring of the NAD^+ was changed by mutating it to leucine, alanine and glycine with and without the mutation at position 93, suggesting that hydrogen tunneling may directly be related to an increase in catalytic efficiency for the enzyme (*186*). The temperature dependence of steady state kinetic parameters at subzero temperatures was used to probe hydrogen tunneling in horse liver ADH. The Phe93Trp variant enzyme showed much less kinetic complexity compared to the wild-type enzyme between 3 and -35 ^{o}C, with the analysis of the data suggesting the involvement of substantial hydrogen tunneling down to -35 ^{o}C (*187*). The effect of methanol on the kinetic properties of the mutant enzyme indicated a more random bi-bi kinetic mechanism compared to the ordered bi-bi mechanism for the same enzyme in water.

In thermophilic ADH, the hydrogen transfer was shown to occur by tunneling as exhibited by the Swain-Schaad exponent on the secondary KIEs which exceeded 3.3 at all temperatures (*138*). The exponent increased with increasing temperature, suggesting an increase in tunneling as a function of temperature. The observation is consistent with promotion of the hydrogen transfer via environmental oscillations which has previously been demonstrated in thermophilic ADH (*188*). A distinct transition was seen in the form of a break point at around 30 ^{o}C for the dependence of the rate of hydride transfer and KIE on temperature. This added to the

accumulated evidence suggesting that the tunneling reaction in thermophilic ADH is dynamically coupled to protein vibrational modes that are thermally activated (*188*). The breaking point in the temperature dependent studies was supported by hydrogen-deuterium exchange mass spectroscopy which provided evidence for thermal activation of some collective protein motions. The mass spectrometry data suggested that a large region in the substrate-binding domain of the enzyme undergoes a transition from a relatively rigid structure to a more dynamic structure at ~30 ^{o}C (*189*). A linear correlation was also observed between the overall enzyme turnover and the average hydrogen-deuterium exchange rate constant for the peptides with the substrate-binding region.

In yeast ADH, the hydride transfer step is mostly rate-limiting, resulting in primary and secondary KIEs of 3.6 and 10.2, respectively (*137*). The anomalously large secondary KIE could not be explained by semi-classical mechanics but was consistent with the incorporation of a quantum mechanical correction. This led to the proposal that both tunneling and coupled motion contribute to the hydride transfer reaction in the enzyme, where coupled motion refers to the contribution of both primary and secondary motions to the reaction coordinate (*137*). Secondary KIEs are generally small (close to one) so the value observed in yeast ADH could only be satisfied by invoking tunneling (*190*). The anomalous secondary KIE was also seen in later experiments using *para*-substituted benzyl alcohols for the yeast enzyme (*191*).

1.3.2. Soybean Lipoxygenase-1

Soybean lipoxygenase (SLO-1) is a metalloenzyme with a molecular mass of 94 kDa (*192-195*). The enzyme contains a non-heme iron which cycles between the ferric and ferrous

states during the catalytic cycle (*196*) and catalyzes the oxidation of linoleic acid to produce fatty acid hydroperoxides. In the reaction catalyzed by SLO-1, a hydrogen is transferred from the substrate to molecular oxygen to form a peroxyl radical intermediate, which is subsequently reduced by the ferrous center and protonated by a water ligand. Steady state kinetic studies suggest that interaction of the enzyme with oxygen follows the hydride transfer step and reduction of the metal center (*197*). Deuterium KIE values in the range from 20 to 80 have been observed under a wide range of conditions and isotopic substitution patterns suggesting that the reaction of linoleic acid oxidation by SLO-1 is limited by the abstraction of a hydrogen atom from the substrate. The involvement of α-secondary KIE on the hydrogen transfer step was investigated using singly deuterated substrates. A primary KIE of ~40 was measured for the wild-type enzyme with the stereospecifically deuterated linoleic acid substrates (*198*) which is ~2-fold less compared to the primary KIE for the enzyme with the doubly deuterated substrate. The effect of the hydrogen atom that is not transferred during the oxidation on the hydrogen atom transfer (α-secondary KIE) was probed by comparing the KIE of the 11-(S)-[^{2}H$_1$]-linoleic acid and the doubly deuterated substrate. An α-secondary KIE of ~2.1 was observed which is significantly larger than that for a semi-classical effect (between 1.0 to 1.2). It was therefore expected that if coupled motion is responsible for the large α-secondary KIE measured with a deuterium at the primary position then the α-secondary KIE with a protium at the primary position would even be larger. However, a value of ~1.1 was obtained which is in stark contrast to what was expected (*198*). The replacement of a leucine residue at position 546, which is in close proximity to C11 atom of linoleic acid, with alanine by site-directed mutagenesis gave a 4-fold decrease in primary KIE compared to the wild-type enzyme, but an increase in the observed α-secondary KIE of 5.6. The anomalous α-secondary KIE was shown to arise as a result of

imperfect stereoselectivity of the hydrogen abstraction step. A large primary KIE value in the range from 76-84 and a small α-secondary KIE in the range from 1.1 to 1.2 were calculated after kinetic corrections for both the wild-type and mutant enzymes, suggesting the involvement of tunneling in the hydrogen transfer reaction catalyzed by SLO-1 (*198*). Wild-type SLO-1 exhibits a nearly temperature independent KIE resulting in a small activation energy and large isotope effect on the Arrhenius preexponential factors. This is consistent with a hydrogen tunneling in which the reaction coordinate is dominantly controlled by environmental reorganizational energy. Other bulky hydrophobic residues in the substrate-binding pocket of SLO-1 and close to the Fe^{3+} center in addition to Leu546, i.e., Leu754 and Ile553, were replaced with alanine to create a larger space within the binding pocket. The effect of the reduced bulkiness in the substrate-binding pocket on the hydrogen transfer reaction catalyzed by the enzyme was investigated using temperature dependence of the KIE and compared with the data for the wild-type enzyme. The leucine to alanine mutant enzymes yielded moderate temperature dependent KIEs and increased activation energies, suggesting increased environmental reorganizational energies with moderate contributions of gating (modulations of the hydrogen transfer distance) to the reaction coordinate (*199*). The data for the Ile553Ala mutant enzyme are, however, consistent with a tunneling mechanism for the hydrogen transfer reaction with extensive gating suggesting a relatively relaxed active site. The analysis of the results for the wild-type and mutant enzymes allowed the separation of "passive" and "active" dynamics, where the former refers to the environmental reorganization of the active site and the latter refers to modulation of the hydrogen tunneling barrier (*199*). The overall data suggest that the active site structure of SLO-1 is organized for the hydrogen tunneling which is significantly affected by structural perturbations of the elements that support the mechanism. Based on the results obtained for the Ile553Ala

variant of SLO-1, the isoleucine residue at position 553 in the wild-type enzyme was mutated to leucine, valine and glycine, thus obtaining variable lengths of the side chain (progressive reduction of bulkiness). All the mutant enzymes showed increases in KIE with increasing temperature, which is significantly different from that of the wild-type enzyme (*200*). The X-ray crystal structures of the 553 position mutant enzymes were found to be superimposable with the wild-type enzyme with minimal differences at the site of the mutations suggesting no significant overall structural differences in the variant enzymes compared to the wild-type. Consequently, comparison of the mechanistic data for the kinetic parameters that affect hydrogen tunneling was used to determine the contribution of the side chain at position 553 to the reaction catalyzed by SLO-1. The change in activation energy increases with decreasing size of the side chain (or increasing cavity at position 553) whereas the isotope effect on the preexponential factors decreases with decreasing side chain size (*200*). The results indicate difficulty of the deuterium in transferring from the donor to the acceptor due to its small wavelength as the transfer distance is altered (probably increased with decreasing side chain size) and therefore require significant distance sampling. The data were interpreted as interplay of preorganization and reorganization motion terms controlling the hydrogen transfer reaction in SLO-1 (*200*). Tunneling with minimal distance sampling or gating has generally been associated with Arrhenius preexponential factors that are significantly larger than unity and tunneling with extensive sampling or gating associated with preexponential factors significantly lower than unity. However, a compelling argument using the preexponential factors for the wild-type and mutant SLO-1 enzymes has implicated tunneling modes for preexponential factors that are close to unity (*201*).

Using molecular dynamics calculations for wild-type SLO-1, the theoretical results obtained for the dependence of temperature on the rate of hydrogen abstraction and KIE overlaid

the experimental data (*202, 203*). The theoretical studies indicated that hydrogen tunneling and environmental contribution play significant roles in the reaction catalyzed by SLO-1 and hydrogen donor and acceptor distance decreases relative to its equilibrium value for efficient tunneling reaction. Conformational changes that facilitate the transfer of the hydrogen result from equilibrium thermal motions of the protein with nonequilibrium dynamical motions having negligible effect on the transfer reaction (*203*).

1.3.3. Glucose Oxidase

Glucose oxidase (GO) catalyzes the oxidation of β-D-glucose to δ-gluconolactone according to a ping-pong steady state kinetic mechanism (*204, 205*). The δ-gluconolactone is subsequently hydrolyzed spontaneously to gluconic acid and hydrogen peroxide (*206*). The enzyme requires FAD which is tightly but non-covalently bound to the protein moiety for catalysis, and uses molecular oxygen as its natural electron acceptor. GO is a homodimer with each monomer subunit having a molecular mass of 65-180 kDa depending on the extent of glycosylation (*207*). The native enzyme is glycosylated, having a carbohydrate mass of percentage of ~20% (*204, 208, 209*). In the reaction catalyzed by GO, a proton is abstracted from the C1 position of glucose by an active site base followed by a hydride ion transfer from the α-carbon to the N5 position of the flavin cofactor. The catalytic base in GO has been identified as histidine at position 516 (*210*) and the residue is fully conserved in the glucose-methanol-choline enzyme superfamily (*211*). The kinetic properties of three glycoforms of GO with different molecular weights due to their varying degrees in glycosylation were investigated to determine the contribution of glycosylation to the mechanism of hydrogen transfer in the reaction catalyzed

by GO. There was no significant difference in the kinetic parameters for the different glycoforms of GO (*140*). The dependence of competitive KIEs for the three glycoforms of GO in the range from 0 to 45 ^{o}C were determined using 2-deoxyglucose as substrate. The isotope effect on the Arrhenius preexponential factors were significantly larger than unity in all the glycoforms, consistent with the hydrogen being transferred by a tunneling mechanism, but varying as a function of glycosylation. The similarities in the active site conformation in the different glycoforms of GO suggested that the tunneling mechanism in the glucose oxidizing enzyme is affected by the carbohydrate mass; with the hydrogen tunneling decreasing with increasing extent of glycosylation (*140*). The data are also an indication of a dynamic transmission of protein surface effect, since the polysaccharides are on the surface of the enzyme, to the active site. Additional surface variants of GO containing more extensive glycosylation and polyethylene glycol (PEG) were prepared and used in a study to distinguish simple mass effects from other sources of altered catalytic functions. Similar Arrhenius preexponential factors in the range from 0.55 to 0.62 were obtained for the surface variants of GO compared to ~1 for the non-glycosylated enzyme suggesting a role of the protein structure and dynamics in the hydrogen tunneling reaction (*212*). A study with GO containing cofactor analogs unveiled a correlation of the rate of reaction to driving force (*213*). Electrochemical and equilibrium data analyses for two enzymes studied suggested that the reaction thermodynamics is not significantly altered by the surrounding protein due to a large reorganizational energy barrier revealed by applying Marcus theory.

1.3.4. Dihydrofolate Reductase

Dihydrofolate reductase (DHFR) catalyzes the reduction of 7,8-dihydrofolate to 5,6,7,8-tetrahydrofolate using NADPH as cofactor. A pro-R hydrogen is stereospecifically transferred from the cofactor to C6 of the pterin center of the substrate (*214*). X-ray crystallographic studies of DHFR from *E. coli* suggest that, depending on the ligand bound to the active site, the enzyme adopts different conformations along the reaction pathway (*172*). Relaxation measurements of the frequency and amplitude of amide backbone motions for DHFR with bound folate using nuclear magnetic resonance spectroscopy indicated enhanced flexibility at regions that are not close to the binding site suggesting that binding of substrate and cofactor alters the dynamic properties of protein segments that are far from the active site (*215, 216*). The flexible regions include the methionine 20 loop, the FG loop, the adenosine binding loop, and the hinge regions. The first two loops have also been shown to undergo conformational changes during the reaction (*215*). Site-directed mutagenesis of a series of amino acid residues in the flexible loop regions suggest that these residues are important determinants of the rate of reaction in DHFR despite being far away from the active site (*217, 218*). A hybrid quantum-classical molecular dynamics simulation of the hydride transfer reaction coupled with genomic sequence analysis and kinetic measurement revealed kinetic complexities that were thought to be consistent with the involvement of a network of coupled promoting motions in the tunneling mechanism (*219*).

The kinetic mechanism for the reduction of dihydrofolate catalyzed by DHFR was determined by measuring the association and dissociation rate constants under steady state and pre-steady state conditions. During steady state turnover, product dissociation follows a specific and preferred pathway occurring after $NADP^+$ is replaced by NADPH in a ternary complex as suggested by binding kinetic studies (*220, 221*), and transient pre-steady state measurements.

These suggest that the transfer of the hydride from NADPH to the pterin ring of dihydrofolate is patially rate-limiting with a deuterium KIE of 3 at pH 6 (*220*). The hydride transfer step was shown to be more rate-limiting at high pH (*222*). The mechanism for the hydride transfer reaction was investigated by probing the effect of temperature on the KIE for DHFR form *Thermogota maritima*. The reaction rates were measured by fluorescence energy transfer from the protein to the reduced nicotinamide moiety of the cofactor in the temperature range from 6 to 65 ^{o}C. The KIE values increase with decreasing temperature below 25 ^{o}C, but no significant effect was observed for temperatures above 25 ^{o}C resulting in a breakpoint at 25 ^{o}C (*223*). The effect of temperature on the KIE values in DHFR is similar to the trend observed in thermophilic ADH (see Section 1.3.1.) (*188*). The isotope effect on the preexponential factors for the temperature dependence KIEs below 25 ^{o}C was close to zero whereas the isotope effect on the preexponential factors above 25 ^{o}C was 1.6 ± 0.5. These data are consistent with the hydride transfer reaction in DHFR occurring via quantum mechanical tunneling (*223*). Associated with the temperature independent KIE values above 25 ^{o}C are large but similar activation energies for the C-H and C-D bond cleavages (E_A^H = 53.5 ± 0.4 kJ/mol and E_A^D = 56.0 ± 0.8 kJ/mol) suggesting a vibrationally enhanced tunneling mechanism. The enzyme from *E. coli* was used in a mixed labeling experiment to obtain the intrinsic KIEs and probe coupling between primary and secondary hydrogens (*222*). The intrinsic KIEs were calculated according to the description for peptidylglycine-hydroxylating monooxygenase (*224*) and fitted to Arrhenius formalism. The fit resulted in temperature independence of the KIE, an isotope effect on the preexponential factor significantly larger than unity, and activation energies that are significantly larger than zero (~4 kcal/mol) (*222*). The temperature dependent data for DHFR from both E. coli and *Thermogota maritima* agree with the molecular dynamics simulation analysis previously carried

out on the enzyme from *E. coli* and support the hypothesis that the hydride transfer reaction which occurs via environmentally assisted quantum mechanical tunneling is coupled to protein motions.

Mixed simulations for mutations residues including Gly121 and Met42 suggest alterations to the sampled configurations conducive for the hydride ion transfer (*225*). The study also indicated a possible functional grouping for Gly121 and Met42 in the turnover cycle for DHFR. The role of the two distal residues were investigated in single mutants and double mutant enzymes in the dynamic network previously shown to be coupled to the reaction coordinate (*218, 225, 226*). Competitve KIE and their temperature dependent for the mutant enzymes indicated that even though there was a large effect on the rate of hydride ion transfer, the effect of the single mutations on the mode of transfer was small compared to the double mutant as suggested by poor reorganization and extensive gating in the double mutant enzyme (*227, 228*). The data are consistent with participation of Gly121 and Met42 in the dynamic network of coupled motions.

1.3.5. Morphinone Reductase

Morphinone reductase (MR) catalyzes the reduction of morphinone and codeinone to hydromorphone and hydrocodone, respectively, with NADH as cofactor (*229*). The enzyme is a flavoprotein homodimer with a molecular mass of 82 kDa and contains a non-covalently bound FMN in each monomer subunit (*230, 231*). In the reductive half-reaction of MR, a hydride from C4 of the nicotinamide ring is transferred to the N5 position of the flavin, and the oxidative half-reaction involves a hydride transfer from the N5 position of the reduced FMN to the substrate.

The hydride transfer step in the reductive half-reaction is preceded by accumulation of a charge transfer (CT) complex (*229*). The KIE on the rate of flavin reduction increases with increasing temperature from 15 to 35 $^{\circ}$C and yielded large and significantly different enthalpies of activation ($\Delta H^{\ddagger}_{D}$ = ~44 kJ/mol and $\Delta H^{\ddagger}_{H}$ = ~35 kJ/mol) and an isotope effect on the preexpenential factor that is significantly lower than unity (A_{H}/A_{D} = 0.13 ± 0.01). These observations are consistent with a tunneling mechanism for the hydride ion transfer from the NADH to the flavin cofactor that is gated by vibrations coupled to the reaction coordinate (*232*). The hydride transfer reaction for the reoxidation of the reduced FMN was investigated in an experimental design where MR was reduced with stoichiometric amount of NADH and the reduced enzyme mixed with the substrate analog 2-cyclohexenone. The oxidative half-reaction have previously been shown to be rate-limiting in steady state studies based on comparable rates for the oxidative half-reaction and the overall enzyme turnover (*230*) and confirmed in the study with 2-cyclohexenone as substrate (*232*). A large solvent isotope effect was observed on k_{cat} suggesting that the oxidative half-reaction is accompanied by a protonation step. Double primary and solvent isotope effect data on the oxidative half-reaction are consistent with a concerted reaction which involves a simultaneous transfer of a hydride and a proton (*232*). The KIE for the oxidative half-reaction carried out in a protiated solvent is independent of temperature and resulted in similar enthalpies of activation values for the C-H and C-D bond cleavages. Coupled with an isotope effect on the preexpnential factor of ~3.7 are consistent with the hydride transfer reaction occurring via quantum mechanical tunneling. Similar mechanistic data were obtained when the experiments were carried out in deuterated solvent, suggesting that the proton transfer reaction also occurs via quantum mechanical tunneling (*232*). There was no viscosity effect on the enzyme turnoever using glycerol up to 35% as viscosigen, suggesting that the measured

solvent isotope effect is not due to the increased viscosity of the deuterated solvent. It is intriguing to note that the three hydrogen transfer reactions in MR occur by quantum mechanical tunneling.

High-pressure stopped-flow experiments showed large increases in observed rates of FMN reduction with increasing hydrostatic pressure in the range from 1 to 2000 bar (*233*). The primary KIE was shown to be directly proportional to pressure, resulting in no significant difference in $\Delta\Delta H^{\ddagger}$ and an isotope effect on the preexponential factor that is close to zero consistent with an environmentally coupled model of hydride tunneling. Similar dependences of the primary KIE on pressure at different viscosities for the hydride ion transfer from NADH to FMN suggest that the promoting motions in MR are likely localized to the active site of the enzyme and not sensitive to bulk solvent properties (*234*).

1.3.6. Other Enzymes with Quantum Mechanical Hydrogen Tunneling Reactions

A number of enzymes other than those reviewed in this section in which hydrogen atoms are transferred have been studied and shown to employ quantum mechanical tunneling. The list includes, but is not limited to, trimethylamine dehydrogenase (*235*), methylamine dehydrogenase (*236*), thymidylate synthase (*237*), sarcosine oxidase (*238*), aromatic amine dehydrogenase (*239*), copper amine oxidase (*240*), peptidylglycine α-hydroxylating monooxygenase (*224*), monoamine oxidase B (*142*), bovine serum amine oxidase (*141*) and pentaerythritol tetranitrate reductase (*232*).

1.4.   Choline Oxidase

1.4.1   Choline Oxidase from *Arthrobacter globiformis*

Choline oxidase from *Arthrobacter globiformis* was first purified and characterized by Ikuta *et al*. in 1977 (*241*). The enzyme was shown to be a flavoprotein. It catalyzes the four-electron oxidation of choline to glycine betaine (N,N,N-trimethylglycine, betaine) with betaine aldehyde as intermediate and molecular oxygen as the final electron acceptor, with the capability of also using betaine aldehyde as substrate (*241*). The prosthetic group of the enzyme was determined by subjecting the enzyme to trypsin-chymotrypsin digestion and the digest purified for fluorescence intensity analysis. The fluorescence intensity of the purified flavin peptide tested after enzymatic hydrolysis with nucleotide pyrophosphatase was consistent with the presence of FAD rather than FMN as the cofactor (*242*). The inability of the purified flavin peptide to be reduced with sodium borohydride suggests that the covalent attachment is 8α-N(3)-histidyl linkage. A more recent analysis of an acid hydrolyzed choline oxidase from *A. globiformis* aimed at identifying the type of flavin linkage was conducted using mass spectroscopy and nucleotide sequence mapping of the *codA* gene. Even though the results suggest that choline oxidase contains 8α-N(1)-histidyl linkage attached to histidine at position 87 (*243*), the *codA* gene sequence used, which was previously deposited in the Genbank (accession no. X84895) (*244*), had seven flaws thus resulting in a translated protein containing altered amino acid sequence (*245*).

The steady state kinetic mechanism for the oxidation of choline and betaine aldehyde for the commercially available choline oxidase form *A. globiformis* (Sigma-Aldrich, St. Louis, MO) was determined by measuring the initial rates of reaction at varying concentrations of both

choline (or betaine aldehyde) and oxygen (*246*). The data indicated a sequential mechanism with the formation of a ternary complex with both choline and betaine aldehyde as substrate, but the maximum velocity at saturating oxygen concentrations is independent of betaine aldehyde concentration where the aldehyde is used as substrate. The kinetic data are consistent with the catalytic mechanism shown in Scheme 1.1. Choline is oxidized to betaine aldehyde after the formation of the oxidized enzyme-substrate complex upon binding of choline and the enzyme is reduced, resulting in the reduced enzyme in complex with betaine aldehyde. The reduced enzyme-betaine aldehyde complex reacts with oxygen to form the oxidized enzyme-betaine aldehyde complex which is subsequently converted to the reduced enzyme-glycine betaine complex. The reduced enzyme-product complex finally reacts with oxygen before the release of glycine betaine (*246*). The transient aldehyde intermediate was shown to be predominantly bound to the active site of choline oxidase, and activation of the reduced flavin species by the enzyme is to similar degrees when in complex with either betaine aldehyde or glycine betaine (*246*).
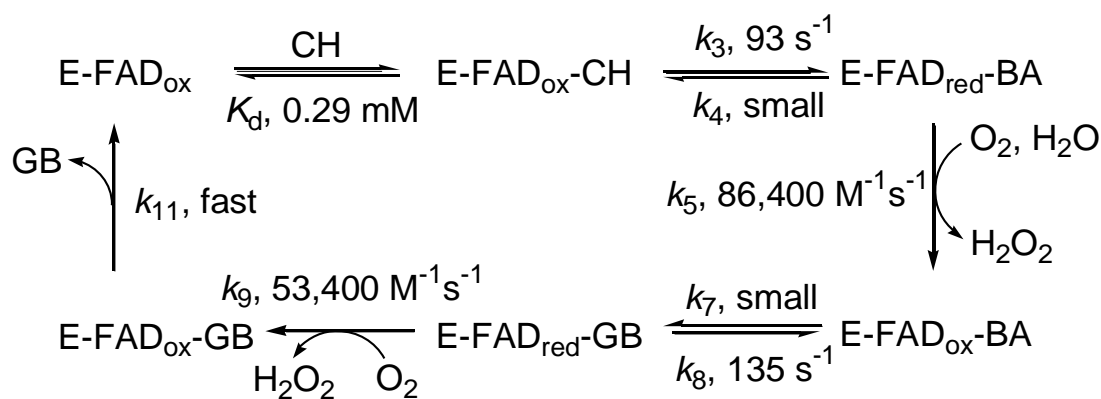
Scheme 1.1. Steady State Kinetic Mechanism for Choline Oxidase at pH 10[a].
E, enzyme; FAD_{ox}, oxidized flavin; FAD_{red}, reduced flavin; CH, choline; BA, betaine aldehyde; GB, glycine betaine. [a]Modified from (*247*)

The gene that encodes for choline oxidase (*codA* gene) from *Arthrobacter globiformis*, previously cloned in the binary vector plasmid *p*GAH was amplified and sub-cloned into pET20b(+) and the recombinant gene expressed and purified using ammonium sulfate precipitation followed by anion exchange chromatography (*245*). The molecular weight of the recombinant enzyme was determined by MALDI-TOF mass spectrometry using the positive ion mode and a value of 60,614 calculated from the mass spectroscopic data. Size exclusion chromatography and PAGE both under non-denaturing conditions suggested that choline oxidase exist as a dimer (*245*). UV-visible absorbance spectrum of choline oxidase with oxidized flavin bound to the enzyme shows absorbance maxima at 359 and 452 nm at pH 8, and a visible florescence emission peak at 530 nm upon excitation at 452 nm. The enzyme forms a sulfite adduct with a binding constant of ~50 μM at pH 7 and 15 $^{\circ}$C, and anaerobic reduction of the enzyme with dithionite goes through an anionic flavosemiquinone species to form anionic hydroquinone (*245*). This is consistent with stabilization of a negative charge (both one and two electrons) at the N(1)-C(2) region of the isoalloxazine. Indeed, a mixture of oxidized and anionic semiquinone flavin species was observed upon purification of the recombinant enzyme.

Using choline and glycine betaine analogues as substrates and inhibitors for choline oxidase, competitive inhibition patterns were observed with K_{is} values that increase with decreasing number of methyl groups at the ammonium portion of the substrate suggesting that the trimethylammonium headgroup is important for binding (*248*). The alcohol or carboxylic acid portions of the substrate or product, respectively, do not however contribute to the binding. Consistent with the inhibition patterns is the contribution of ~29 kJ/mol estimated for the specificity of the enzyme to the trimethylammonium headgroup of the substrate. In agreement to the observed specificity of the trimethylammonium portion of the substrate to the active site of

choline oxidase, a contribution of ~13 kJ/mol was estimated for the positively charged headgroup towards substrate binding whereas only ~2 kJ/mol was the contribution towards catalysis, in a study in which the isosteric analogue 3,3-dimethylbutan-1-ol was used as substrate (*249*).

The enzyme was devoid of enzymatic activity at pH 6 and 25 $^{\circ}$C when stored at pH 6 and -20 $^{\circ}$C but regains activity at pH 7 and 25 $^{\circ}$C with a slow onset of steady state which is observed as significant hysteretic behavior (*250*). The enzyme also shows a significant lag in achieving steady state upon flash-freezing in a mixture of dry-ice and acetone bath when assayed at pH 6. No lag, however, was observed when the enzyme was stored at pH 6 and 0 $^{\circ}$C or -20. The enzymatic activity was also without hysteresis when stored at pH 6 and -20 or -80 $^{\circ}$C in the presence of 30 or 50% glycerol as an anti-freezing agent, or stored at pH 6 on ice for 26 h. Measurement of the enzymatic activity in the presence of glycine betaine (~90% of the ligand bound to the enzyme) for the enzyme frozen at pH 6 also showed a hysteretic behavior suggesting that the formation of enzyme with the altered catalytic properties occurs whether or not a ligand is bound to the enzyme (*250*). The data suggest that storage at low pH and -20 $^{\circ}$C results in a reversible conformational change which is associated with loss of activity at pH 6. A fit of the progress curves for oxygen consumption to a modified version of Frieden equation for hysteretic enzymes is consistent with the rate constant for the transition from the altered to the original enzyme before storage at pH 6 and -20 $^{\circ}$C being independent of ionic strength, as well as substrate and enzyme concentrations. The rate of conversion increases with increasing pH to a limiting value at high pH between pH 6.5 and 9.5, resulting in a pK_a value of 7.3 ± 0.1 (*250*). UV-visible absorbance, fluorescence and circular dichroism spectroscopies of the altered and unaltered enzyme forms suggest that choline oxidase undergoes a conformational change which

significantly affects the flavin microenvironment. Activation of the altered enzyme was shown to be enthalpy-driven. Prolonged incubation of the active enzyme at pH 6 and temperature higher than 20 $^{\circ}$C resulted in full recovery of activity (*250*).

Kinetic isotope effects were determined at varying concentrations of the organic substrate and oxygen using both steady state and rapid kinetic approaches to elucidate the chemical mechanism for choline oxidation catalyzed by choline oxidase. An enzyme turnover of 60 ± 1 s^{-1} and a k_{cat}/K_m value of 240,000 M^{-1}s^{-1} were determined for the enzyme with choline as substrate at pH 10 and 25 $^{\circ}$C (*247*). pH-independent values for the substrate kinetic isotope effects of 10.6 ± 0.6 and 7.5 ± 0.3 on k_{cat}/K_m and k_{cat}, respectively, were measured at saturating concentrations of choline and oxygen, consistent with the hydride transfer step being rate limiting in both the reductive half-reaction and the overall turnover of the enzyme and lack of external forward or reverse commitments to catalysis. Solvent kinetic isotope effects were measured to probe the timing of kinetic steps that involve solvent exchangeable protons, and multiple kinetic isotope effects were determined to probe the relative timing of the C-H and O-H bond cleavages. The data are consistent with the O-H bond cleavage occurring before the C-H bond cleavage in two different kinetic steps, resulting in the formation of an alkoxide species due to the removal of the hydroxyl proton before the transfer of the hydride from the α-carbon of the substrate to the flavin (*247*). The overall enzyme turnover with choline as substrate was shown to be limited by both transfers of hydride equivalents from choline and the betaine aldehyde intermediate. To further characterize the chemical mechanism, the effect of oxygen concentration on substrate kinetic isotope effect was used to probe the reversibility of the hydride transfer reaction, and the effect of temperature was used to probe the involvement of quantum mechanical tunneling in the reaction catalyzed by choline oxidase (*251*). At non-saturating oxygen concentrations, $^{D}(k_{cat}/K_m)$

and $^D k_{cat}$ values decrease between limiting values from low to high pH with defined pK_a values of ~7.5 and 6.0, respectively. The limiting values at high pH decreases with decreasing concentration of oxygen whereas the limiting values at low pH were not significantly different from the limiting values obtained at saturating oxygen concentrations. The results at non-saturating oxygen concentration suggest the presence of reverse commitment to catalysis, and consistent with the forward partitioning of the reduced enzyme-betaine aldehyde complex rather than reverting to the oxidized enzyme-choline alkoxide complex being dependent on the availability of oxygen (*251*). The effect of temperature on the kinetic isotope effect was determined in the range from 10 to 45 ^{o}C at saturating oxygen concentration and the data analyzed according to the Eyring's and Arrhenius' formalisms. The analysis of the temperature dependence showed a monotonic increase in the $In(k_{cat}/K_m T)$ and $In(k_{cat}/T)$ values with increasing temperature yielding similar slopes for choline and 1,2-[^{4}H$_2$]-choline, thus resulting in temperature independent kinetic isotope effects, and similar enthalpies and entropies of activation for the C-H and C-D bond cleavages (*251*). Associated with the temperature-independent kinetic isotope effects is a large isotope effect on the preexponential factors (A_H/A_D) with a value of ~14. The data are consistent with the hydride transfer reaction in wild-type choline oxidase occurring via quantum mechanical tunneling within a highly preorganized active site (*251*). The effect of temperature on the kinetic isotope effects was also determined at sub-saturating concentrations of oxygen with $^D(k_{cat}/K_m)$ increasing with decreasing temperature which either suggests a change in the hydride transfer mechanism or a temperature effect on the kinetic complexity (reverse commitment to catalysis) of the reaction catalyzed by choline oxidase under the reversible catalytic regime. The kinetic complexity increases with increasing

temperature suggesting that the hydride transfer reaction becomes more reversible with increasing temperature (*251*).

The crystal structure of choline oxidase was solved by collecting X-ray diffraction data sets consisting of 381,317 observations of 97,546 unique reflections in a resolution range of from 50 to 1.86 Å (*59*). The structure was determined by molecular replacement with a search model based on glucose oxidase from *Aspergillus niger*. Choline oxidase crystallized as a homo-dimer with the dimer interface having two sets of six identical inter-subunit contacts between charged complementary residues clustered on the outer edges of the interface, with few close contacts at the central portion of the dimer interface (*59*). The enzyme has a typical *p*-hydroxybenzoate hydroxylase (PHBH) fold (*40*), and the fold of each subunit resembles that of other members of the glucose-methanol-choline (GMC) oxidoreductase superfamily (*44, 102, 207, 211, 252-257*). The FAD-binding domain consist of a six stranded parallel β-sheets that is surrounded by eight α-helices and flanked on one side by a three-stranded anti-parallel β-sheets, and the topology of the substrate binding domain is made up of a distorted six-stranded anti-parallel β-sheets which forms the bottom of the active site and flanked on the top by three α-helices that extend into the bulk solution (*59*). The isoalloxazine ring portion of the flavin cofactor, which is buried within the protein, is physically constrained through a covalent linkage via the FAD C(8) methyl atom and the N(3) atom of the histidine side chain at position 99. A solvent excluded cavity with a volume of ~125 Å in the substrate binding domain, and adjacent to the re face of the FAD is sufficient enough to accommodate a 93 Å choline molecule (*59*). The substrate binding cavity is partially surrounded by hydrophobic residues with a glutamate residue at position 312 and two histidine residues at positions 351 and 466 being the only polar residues. The active site of choline oxidase is secluded from the solvent by a loop that has been shown to be a common

feature of other members of the GMC enzyme superfamily (*44, 102, 207, 211, 252, 254, 256, 258, 259*), and may serve as a lid that allow entry and exit of the substrate and product, respectively, to and from the active site. The manual docking of choline into the substrate binding cavity of the resolved crystal structure of choline oxidase suggests an electrostatic interaction between the positively charged trimethylammonium headgroup of choline and the negatively charged side chain of Glu312 (*59*). The involvement of the negative charge at position 312 in substrate binding was investigated by replacing the glutamate residue with a glutamine in a Glu312Gln variant enzyme. Determination of the thermodynamic equilibrium constant (K_d) for binding of choline to the glutamine variant enzyme under anaerobic conditions using the stopped-flow spectrophotometer yielded a value that was at least 500-times larger than the K_d value for the wild-type enzyme, and consistent with Glu312 participating in substrate binding (*59*).

Even though circular dichroism and florescence spectroscopy as well as other biophysical studies suggest similar protein fold and overall enzyme structure, the mutant enzyme upon replacing histidine 466 with alanine resulted in a 60- and 1000-fold decreases in k_{cat} and k_{cat}/K_m with no effect on reactivity with oxygen, and a midpoint redox potential that is ~25 mV more negative as compared to the wild-type enzyme (*260*). Partial rescue of the enzymatic activity of the His466Ala mutant enzyme with exogenous imidazolium but not imidazole suggested that the protonated form of the histidine plays a role in the catalytic mechanism of choline oxidase. Substrate and solvent kinetic isotope effects of the histidine to alanine variant enzyme are consistent with the OH bond cleavage being concerted with the hydride transfer step. The overall data for the variant enzyme of choline oxidase in which the histidine residue at position 466 was replaced with alanine suggest that apart from modulating the electrophilicity of the enzyme-

bound flavin and the polarity of the active site, His466 stabilizes the transition state for the oxidation of choline to betaine aldehyde (*260*). Reversal of the charge at position 466 by replacing the histidine residue with aspartate resulted in a protein that forms a stable complex with choline but could not catalyze the oxidation of the substrate (*261*). Anaerobic incubation of the aspartate 466 mutant enzyme with xanthine and xanthine oxidase at pH 6 resulted in the formation of neutral hydroquinone, with no stabilization of flavin semiquinone intermediate suggesting that a negatively charged N(1)-C(2) locus cannot be stabilized in CHO-H466D leading to defective flavinylation and a decreased in midpoint redox potential of ~160 mV (*261*).

There is no effect upon replacing His466 with alanine on the reactivity of the reduced flavin species with oxygen in CHO-H466A compared to the wild-type enzyme. This observation led to the speculation that the positively charged side chain that might be needed for oxygen reactivity, as has been shown in glucose oxidase, could be His351 since the two histidine residues (His466 and His351) are the only ionizable groups in the active site of choline oxidase as suggested by the crystal structure (*59*). A variant enzyme of choline oxidase in which the histidine residue at position 351 was replaced with alanine was prepared and kinetically characterized (*262*). In keeping with the wild-type enzyme, there was no significant difference in k_{cat}/K_{O2} value, suggesting that the histidine residue is not involved in the activation of the reduced flavin species with oxygen. Other observations made in the studies of the His351 variant enzyme suggest that the histidine residue at position 351 in wild-type choline oxidase plays a role in substrate binding and positioning, as well as stabilizing the transition state for the hydride transfer reaction, likely by hydrogen bonding to the hydroxyl oxygen and the oxygen atom of the alkoxide species, respectively (*262*). In the His351Ala mutant enzyme, His351 was shown to contribute to the overall polarity of the active site in choline oxidase, based on a shift in the pK_a

value for the group that needs to be unprotonated, even though the group is still required for catalysis. The authors proposed that one of the two histidine residues may be the active site base in the wild-type enzyme, with the other residue picking up the role in the absence of the "true" base. An alternative explanation could be the possibility of a synergistic role of multiple active site residues, and not the responsibility of a single amino acid acting as the base (*262*). The former proposal is currently under investigation in a double mutant enzyme of choline oxidase where the two histidine residues have been replaced with glutamine. It was interestingly observed that all of the choline oxidase variant enzymes in which the ionizable histidine residues were singly replaced [His351Ala (*262*), His466Ala (*260*) and His466Asp (*261*)] could stabilize the neutral hydroquinone species of the flavin cofactor at high pH. In contrast, the wild-type enzyme stabilizes the anionic hydroquinone between pH 6 and 10, suggesting that one positively charged side chain in the active site of the enzyme is not enough to stabilize the anionic flavin hydroquinone. The fact that the oxidative half-reaction is not significantly affected in the choline oxidase histidine variants compared to the wild-type also suggests that the neutral and anionic flavin hydroquinone species have similar reactivity with molecular oxygen.

The role of the histidine residue at position 99, which is involved in a covalent linkage with the isoalloxazine ring of the FAD, to the reaction catalyzed by choline oxidase was investigated in a variant enzyme in which the residue was replaced with asparagine (see Chapter II).

In order to understand the mechanism of betaine aldehyde oxidation, betaine aldehyde and its isosteric analogue, 3,3-dimethylbutyraldehyde, were used in a spectroscopic and kinetic analyses to further characterize the reaction catalyzed by choline oxidase. The enzyme-bound flavin was completely reduced upon mixing with betaine aldehyde and choline to similar rates

under anaerobic conditions in the stopped-flow spectrophotometer, with only 10 to 26% of the enzyme getting reduced upon mixing with 3,3-dimethylbutyraldehyde between pH 6 and 10 (*263*). To determine whether 3,3-dimethylbutyraldehyde may be an inhibitor of choline oxidase, initial rates of reaction were measured at varying concentrations of choline and different fixed concentrations of 3,3-dimethylbutyraldehyde in air-saturated buffer at pH 8. A double reciprocal plot of 1/rate against 1/[choline] yielded line patterns that intersect on the y-axis, consistent with the substrate analogue being a competitive inhibitor against choline with a K_{is} value of ~7 mM (*263*). Since aldehydes are known to exist in equilibrium with their hydrated species when in solution, the hydration ratios of betaine aldehyde and 3,3-dimethylbutyraldehyde were determined to investigate whether the different reactivity of choline oxidase with the two aldehydes may be due to their different diol/aldehyde ratio. Using nuclear magnetic resonance spectroscopy, ~99% of betaine aldehyde was shown to be hydrated whereas only ~30% of 3,3-dimethylbutyraldehyde was hydrated when both aldehydes are in aqueous solution, consistent with betaine aldehyde predominantly existing in the diol form (*263*).

Even though one may think of charged residues as the catalytically relevant for an enzymatic reaction, a recent study in which an active site valine was replaced with alanine or threonine suggested that the hydrophobic residue at position 464 in choline oxidase is important for positioning the catalytic residues in the enzyme (*264*). The close proximity of the valine at position 464 to the N(5) atom and its side chain in van der Waals contact with the C(2) atom of the isoalloxazine of the flavin cofactor as demonstrated in the three-dimensional crystal structure of choline oxidase (*59*) suggested that the V464 may play an important role in the reaction catalyzed by choline oxidase. Anaerobic reduction of the variant 464 forms of choline oxidase with substrate at pH 10 using a stopped-flow spectrophotometer showed a double exponential

process with a fast phase of ~70% of the change in absorbance (*264*). The percentage absorbance change for the fast phase decreased to ~50% at pH 6. The interpretation of the data was given as two forms of the enzyme that interconvert between a fast and slow species (Scheme 1.2). Even though the rate of hydride ion transfer from the α-carbon of the substrate alkoxide to N(5) position of the flavin was not significantly affected, the preceding abstraction of the hydroxyl proton is significantly slowed in the valine choline oxidase variants as shown by solvent kinetic isotope effects (*264*). The hydroxyl proton abstraction step in the valine variants is associated with a solvent sensitive internal equilibrium, and suggests disruption of the highly preorganized enzyme-substrate complex in the wild-type enzyme.

$$\begin{array}{c} \text{fast phase} \\ \overbrace{\phantom{E_{ox}+S\xrightleftharpoons{K_d}E_{ox}S\xrightarrow{k_{red}}E_{red}+P}} \end{array}$$

$$\text{slow phase} \left\{ \begin{array}{ccc} E_{ox} + S \xrightleftharpoons{K_d} E_{ox}S \xrightarrow{k_{red}} E_{red} + P \\ k_1 \Big\Updownarrow k_2 \qquad k_3 \Big\Updownarrow k_4 \\ E^{*}_{ox} + S \xrightleftharpoons{K_d^{*}} E^{*}_{ox}S \end{array} \right.$$
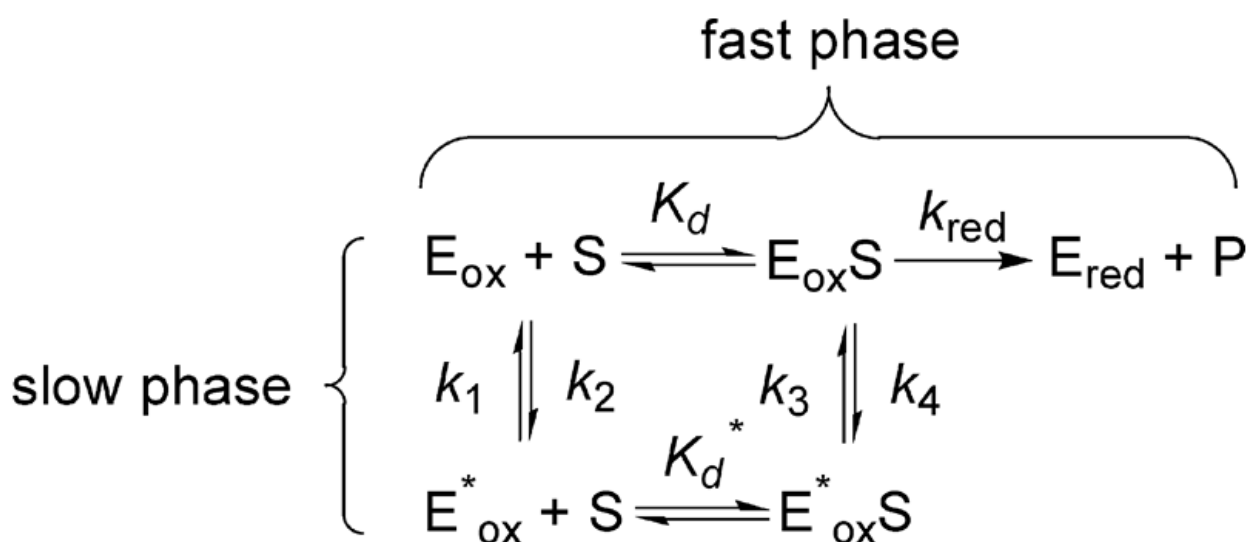
Scheme 1.2.   Proposed Kinetic Mechanism for the Oxidation of Choline Catalyzed by the V464T and V464A enzymes.
 Scheme from ref. (*264*)

Several studies over the past three decades have demonstrated the biotechnological relevance of glycine betaine, the final product of the reaction catalyzed by choline oxidase. A

number of these studies have genetically engineered plants of economical interest with the *codA* gene and the survival or susceptibility of the transgenic plants under stress conditions such as extreme temperatures, hyperosmolarity and drought were investigated. Introduction of a cloned *codA* gene into cyanobacterium *Synechococcus sp.* resulted in the accumulation of 60-80 mM levels of intracellular glycine betaine when expressed under the control of a strong constitutive promoter (*244*). Photosynthesis of the transgenic cyanobacterium was more tolerant to light at low temperatures due to enhanced ability of the photosynthetic machinery to recover from low temperature photo-inhibition than control cells, and suggesting that glycine betaine enhances the tolerance of photosynthesis to low temperature (*265*). Similarly, transformation of *Arabidopsis thaliana* with the *codA* gene from *A. globiformis* resulted in enhanced salt (*266*), high temperature (*267*), light stress (*268*) and freezing tolerance (*269*). Other plants or chloroplast containing organisms in which glycine betaine accumulation and stress tolerance have been demonstrated as a result of biotechnological transformation of the *codA* gene from *A. globiformis* include rice (*270, 271*), tomato (*272, 273*) and *Chlamydomonas reinhardtii* (*274*). The concern of genetically modified food causing food allergy led to a study in which the allergenicity of *Brassica juncea* (mustard) was investigated. In assessing the allergenicity of expressing the *codA* gene from *A. globiformis*, comparison of choline oxidase sequence with allergenic protein databases show no sequence homology, and no immunoreactive polypeptide was observed (*275*). Allergenic and toxicity studies in respiratory allergic patients and pre-sensitized mice with extracts from the genetically modified mustard and compared with data for native mustard suggest similar reactions for the two mustard types.

1.4.2. Choline Oxidase from Other Sources

The gene encoding for choline oxidase in the gram-positive soil bacterium *A. pascens* was isolated and characterized to determine the involvement of the enzyme in osmo-tolerance (*276*). The metabolic role of recombinant Ap-CHO was investigated by examining the activity of the enzyme when *A. pascens* is cultured in the presence of different carbon sources, and its osmoprotective functions evaluated in the presence of inhibitory amount of sodium chloride. The results suggest that Ap-CHO is related to carbon metabolism but not involved in osmo-tolerance (*276*). Transfer of the Ap-CHO gene to an *E. coli* mutant that is defective in betaine biosynthesis however resulted in an osmo-tolerant phenotype with the ability of the host to synthesize and assemble an active enzyme that could catalyze the biosynthesis of betaine from an exogenous supply of choline (*276*). Glycine betaine was not found to be an osmolyte in *A. pascens* but utilized as a carbon source.

Plasmids containing the choline oxidase gene were introduced into rice genome by *Agrobacterium*-mediated transformation and the transgenes verified by Southern blot hybridization analysis (*277*). The gene was fused to a chloroplast targeting gene sequence and expressed under the control of ABA-inducible promoter (stress-induced promoter) or a constitutive ubiquitin gene promoter. Choline oxidase activity was detected to various levels in extracts of the different transgenes with no detectable activity in the non-transgenic plant extract, confirming the expression of the genes in the transgenic plants (*277*). The results suggest that expression with the well-studied stress-inducible promoter did not give rise to enhanced glycine betaine accumulation compared to the constitutive promote under high salt stress conditions.

In an attempt to study the properties of Ap-CHO from *A. pascens*, a recombinant enzyme from a synthetic gene was created based on a published sequence (*278*). The gene was

successfully expressed in *E. coli* strain BL21(DE3) using pET52b(+) as vector but no enzymatic activity could be detected (*276*). Assembly polymerase chain reaction was used for the synthesis of chimeric genes from the homologous choline oxidase gene from *A. globiformis* in order to see if activity of the enzyme from *A. pascens* could be restored by homologous recombination. Homologous recombination in this case is being used as a systematic chimeric replacement and DNA repair in addition to promoting genetic diversity (*279*). Individual segments between Ag-CHO and Ap-CHO-syn were exchanged stepwise with increasing fragments from Ag-CHO until an active recombinant protein was expressed (*280*). Exchange of the first 144 amino acid recidues from Ag-CHO did not restore activity but exchange of the following 74 amino acids did restore enzymatic activity in Ap-CHO. A sequence alignment of the region amino acids from 144 to 218 for Ap-CHO with the sequence of the same region for choline oxidase from *A. globiformis*, *A. aurescens* and *A. nicotianae* showed the residue at position 200 to be a conserved asparagine with the exception of the enzyme from *A. pascens* where the residue is a threonine (*280*). Even though the amino acid sequence for Ap-CHO-syn differs in more than one position to one or two of the other choline oxidases, it is only at position 200 that it differs with all the other three sequences. The threonine residue in Ap-CHO-syn was back mutated to asparagine and the T200N variant enzyme yielded an active enzyme with similar properties to the chimeric recombinant choline oxidase and the enzyme from *A. globiformis* (*280*). Consequently, the published gene sequence for Ap-CHO (*278*) turned out to be incorrect. The application enabled the identification of active chimeric proteins by systematic replacement of individual gene segments.

The interest of the detergent industry to make use of biological bleaching, such as an enzyme that produces hydrogen peroxide from suitable substrates *in situ* during the wash, led to

the screening of oxidases as potential candidates. The advantages of the use of enzymes in detergents include their turnover number and the properties of the substrate and/or product. In this regard betaine the final product of the reaction catalyzed by choline oxidase has an additional advantage in cleaning procedures since quaternary ammonium ions functions as fabric softeners. The production and release of hydrogen peroxide from the reaction of choline oxidation catalyzed by choline oxidase passed the enzyme for screening. A soil sample screen with choline chloride as the sole carbon source resulted in the isolation of various bacteria strains showing choline oxidase activity (*281*). Consequently, the gene for choline oxidase from *A. nicotianae* was cloned, sequenced analyzed, and heterologously overexpress in E. coli for biochemical and catalytic characterization. *A. nicotianae* was identified as the organism with the highest activity. An-CHO was purified by a single-step anion exchange chromatography on Q sepharose Fast Flow and eluted with ammonium sulfate. Cofactor determination studies are consistent with the presence of FAD which is covalently linked to the enzyme (*281*). pH and temperature optima for the enzymatic activity of An-CHO are 7.4 and 55 ^{o}C, respectively. NMR spectroscopy identification of the reaction products formed by An-CHO during oxidation of choline chloride after incubation of the reaction mixture at 30 ^{o}C for 8 h showed the presence of choline chloride, glycine betaine and the intermediate betaine aldehyde (found in the hydrated form in solution) (*281*).

1.5.   Goals

Choline oxidase catalyzes the two-step, four electron oxidation of choline to glycine betaine with betaine aldehyde as intermediate and molecular oxygen as the final electron

acceptor. The aldehyde intermediate is predominantly bound to the enzyme and almost entirely forms a gem-diol when in solution (*246, 263*). The accumulation of glycine betaine in the cytoplasm of plants and bacteria as a defensive mechanism against stress conditions makes the genetic engineering of relevant plants of economic interest (*282-288*), and the biosynthetic pathway for the osmolyte a potential drug target to curb human microbial infections (*289-291*). The first oxidation step in the reaction catalyzed by choline oxidase involves the transfer of a hydride ion from the α-carbon of choline to the N(5) position of the enzyme-bound flavin to form betaine aldehyde and anionic flavin hydroquinone, followed by reactivity of the flavin hydroquinone with oxygen and a concomitant release of hydrogen peroxide (*245, 246, 292*).

Enzymatic catalysis in choline oxidase is initiated by the hydroxyl proton abstraction from choline after the formation of the enzyme-substrate complex (*246, 247, 293*). The use of substrate analogues and inhibition studies with glycine betaine suggested the requirement of an unprotonated species for catalysis with a thermodynamic pK_a of 7.5 (*248, 293*). Substrate, solvent and multiple kinetic isotope effects are consistent with the transfers of the hydride ions from the choline alkoxide and the gem-diol betaine aldehyde intermediate to the enzyme-bound flavin being rate-limiting in the overall enzyme turnover, with the proton abstraction step being kinetically fast and mechanistically decoupled from the relatively slow hydride transfer step (*247, 293*). Mechanistic data on the effect of temperature on steady state kinetic parameters demonstrated that the reaction of hydride ion transfer in which choline is oxidized to betaine aldehyde occurs via a quantum tunneling mechanism within a highly pre-organized enzyme-substrate complex (*247, 251, 294*). This pre-supposes a close proximity of the hydride donor and acceptor in an active site environment where minimal independent movements of the alkoxide α-carbon (donor) relative to the N(5) atom of the flavin isoalloxazine ring (acceptor) are permitted.

The pre-organization which is required to assemble the hydride ion donor and acceptor is triggered by the hydroxyl proton abstraction from the substrate, and attained through a thermodynamically relevant conformational change of the enzyme-alkoxide complex. The goal of this dissertation is to understand some of the key contributors (especially the amino acid residues) to the mechanistic properties of the reaction of alcohol oxidation catalyzed by choline oxidase with respect to pre-organization of the active site for the quantum tunneling mechanism.

A better understanding of the mechanistic properties of choline oxidase required the determination of the three-dimensional structure of the enzyme. X-ray crystallography provides structural information about the identity of the amino acid residues that interact with the substrate or involved in substrate binding, and the amino acid residues that stabilize the enzyme-substrate complex or intermediates and/or modulate the polarity and electrophilicity of the active site environment. The crystal structure of choline oxidase was needed to complement the mechanistic data that have been obtained for the wild-type as well as choline oxidase variant enzymes. Some of the insights expected to be gained from the three-dimensional structure were the identity of the unprotonated species that is required for catalysis and the probable orientation of the substrate in the active site of the enzyme. The crystal structure of choline oxidase is described in Chapter III.

Based on the crystal structure of choline oxidase, a glutamate residue at position 312, which is the only negatively charged residue in the active site, and a histidine residue at position 99, which is involved in a covalent linkage with the flavin cofactor, were investigated for their mechanistic roles in the reaction catalyzed by the enzyme. To investigate the contribution of the spatial location of the negative charge at position 312, and the physical constraint of the flavin cofactor requires the replacement of the respective amino acid residues with other residues to

make variant forms of the enzyme. This was achieved using site-directed mutagenesis and optimization of the protein expression and purification based on previous protocol for the wild-type enzyme to obtain large quantities and high purity of the variant enzymes for the mechanistic studies.

Mechanistic data on glutamate 312 and histidine 99 variant enzymes provide important information about the roles of the active site residues, thus allowing analysis of some of the key contributors to the pre-organization of the active site of choline oxidase for the hydride tunneling mechanism.

1.5.1. References

1.   Joosten, V., and van Berkel, W. J. (2007) Flavoenzymes, *Curr. Opin. Chem. Biol. 11*, 195-202.

2.   Massey, V. (1995) Introduction: flavoprotein structure and mechanism, *F.A.S.E.B. J. 9*, 473-475.

3.   Massey, V. (2000) The chemical and biological versatility of riboflavin, *Biochem. Soc. Trans. 28*, 283-296.

4.   Shimomura, O., Johnson, F. H., and Kohama, Y. (1972) Reactions involved in bioluminescence systems of limpet (Latia neritoides) and luminous bacteria, *Proc. Natl. Acad. Sci. U S A 69*, 2086-2089.

5.   Lei, B., Liu, M., Huang, S., and Tu, S. C. (1994) *Vibrio harveyi* NADPH-flavin oxidoreductase: cloning, sequencing and overexpression of the gene and purification and characterization of the cloned enzyme, *J. Bacteriol. 176*, 3552-3558.

6. Hastings, J. W., and Nealson, K. H. (1977) Bacterial bioluminescence, *Annu. Rev. Microbiol. 31*, 549-595.

7. Tu, S. C. (2008) Activity coupling and complex formation between bacterial luciferase and flavin reductases, *Photochem. Photobiol. Sci. 7*, 183-188.

8. Tu, S. C., Lei, B., Liu, M., Tang, C. K., and Jeffers, C. (2000) Probing the mechanisms of the biological intermolecular transfer of reduced flavin, *J. Nutr. 130*, 331S-332S.

9. Ghisla, S., and Massey, V. (1989) Mechanisms of flavoprotein-catalyzed reactions, *Eur. J. Biochem. 181*, 1-17.

10. Massey, V. (1994) Activation of molecular oxygen by flavins and flavoproteins, *J. Biol. Chem. 269*, 22459-22462.

11. Miura, R. (2001) Versatility and specificity in flavoenzymes: control mechanisms of flavin reactivity, *Chem. Rec. 1*, 183-194.

12. Ghisla, S., and Massey, V. (1986) New flavins for old: artificial flavins as active site probes of flavoproteins, *Biochem. J. 239*, 1-12.

13. Krueger, S. K., and Williams, D. E. (2005) Mammalian flavin-containing monooxygenases: structure/function, genetic polymorphisms and role in drug metabolism, *Pharmacol. Ther. 106*, 357-387.

14. Schlaich, N. L. (2007) Flavin-containing monooxygenases in plants: looking beyond detox, *Trends Plant Sci. 12*, 412-418.

15. van Berkel, W. J., Kamerbeek, N. M., and Fraaije, M. W. (2006) Flavoprotein monooxygenases, a diverse class of oxidative biocatalysts, *J. Biotechnol. 124*, 670-689.

16. Entsch, B., Cole, L. J., and Ballou, D. P. (2005) Protein dynamics and electrostatics in the function of *p*-hydroxybenzoate hydroxylase, *Arch. Biochem. Biophys. 433*, 297-311.

17.   Westphal, A. H., Matorin, A., Hink, M. A., Borst, J. W., van Berkel, W. J., and Visser, A. J. (2006) Real-time enzyme dynamics illustrated with fluorescence spectroscopy of p-hydroxybenzoate hydroxylase, *J. Biol. Chem. 281*, 11074-11081.

18.   van den Heuvel, R. H., Tahallah, N., Kamerbeek, N. M., Fraaije, M. W., van Berkel, W. J., Janssen, D. B., and Heck, A. J. (2005) Coenzyme binding during catalysis is beneficial for the stability of 4-hydroxyacetophenone monooxygenase, *J. Biol. Chem. 280*, 32115-32121.

19.   Eichhorn, E., Davey, C. A., Sargent, D. F., Leisinger, T., and Richmond, T. J. (2002) Crystal structure of *Escherichia coli* alkanesulfonate monooxygenase SsuD, *J. Mol. Biol. 324*, 457-468.

20.   Galan, B., Diaz, E., Prieto, M. A., and Garcia, J. L. (2000) Functional analysis of the small component of the 4-hydroxyphenylacetate 3-monooxygenase of *Escherichia coli* W: a prototype of a new Flavin:NAD(P)H reductase subfamily, *J. Bacteriol. 182*, 627-636.

21.   Chaiyen, P., Suadee, C., and Wilairat, P. (2001) A novel two-protein component flavoprotein hydroxylase, *Eur. J. Biochem. 268*, 5550-5561.

22.   Thotsaporn, K., Sucharitakul, J., Wongratana, J., Suadee, C., and Chaiyen, P. (2004) Cloning and expression of p-hydroxyphenylacetate 3-hydroxylase from *Acinetobacter baumannii*: evidence of the divergence of enzymes in the class of two-protein component aromatic hydroxylases, *Biochim. Biophys. Acta. 1680*, 60-66.

23.   Sucharitakul, J., Chaiyen, P., Entsch, B., and Ballou, D. P. (2005) The reductase of p-hydroxyphenylacetate 3-hydroxylase from *Acinetobacter baumannii* requires p-hydroxyphenylacetate for effective catalysis, *Biochemistry 44*, 10434-10442.

24.   Park, J. B., Buhler, B., Habicher, T., Hauer, B., Panke, S., Witholt, B., and Schmid, A. (2006) The efficiency of recombinant *Escherichia coli* as biocatalyst for stereospecific epoxidation, *Biotechnol. Bioeng. 95*, 501-512.

25.   O'Leary, N. D., Duetz, W. A., Dobson, A. D., and O'Connor, K. E. (2002) Induction and repression of the sty operon in *Pseudomonas putida* CA-3 during growth on phenylacetic acid under organic and inorganic nutrient-limiting continuous culture conditions, *F.E.M.S. Microbiol. Lett. 208*, 263-268.

26.   Kantz, A., Chin, F., Nallamothu, N., Nguyen, T., and Gassner, G. T. (2005) Mechanism of flavin transfer and oxygen activation by the two-component flavoenzyme styrene monooxygenase, *Arch. Biochem. Biophys. 442*, 102-116.

27.   Santos, P. M., Blatny, J. M., Di Bartolo, I., Valla, S., and Zennaro, E. (2000) Physiological analysis of the expression of the styrene degradation gene cluster in *Pseudomonas fluorescens* ST, *Appl. Environ. Microbiol. 66*, 1305-1310.

28.   van Pee, K. H., Dong, C., Flecks, S., Naismith, J., Patallo, E. P., and Wage, T. (2006) Biological halogenation has moved far beyond haloperoxidases, *Adv. Appl. Microbiol. 59*, 127-157.

29.   Yeh, E., Garneau, S., and Walsh, C. T. (2005) Robust in vitro activity of RebF and RebH, a two-component reductase/halogenase, generating 7-chlorotryptophan during rebeccamycin biosynthesis, *Proc. Natl. Acad. Sci. U S A 102*, 3960-3965.

30.   Dong, C., Flecks, S., Unversucht, S., Haupt, C., van Pee, K. H., and Naismith, J. H. (2005) Tryptophan 7-halogenase (PrnA) structure suggests a mechanism for regioselective chlorination, *Science 309*, 2216-2219.

31. Keller, S., Wage, T., Hohaus, K., Holzer, M., Eichhorn, E., and van Pee, K. H. (2000) Purification and partial characterization of tryptophan 7-Halogenase (PrnA) from *Pseudomonas fluorescens* This work was supported by the Deutsche Forschungsgemeinschaft (DFG) through the Graduiertenkolleg "Struktur-Eigenschafts-Beziehungen bei Heterocyclen", the Environment and Climate Research and Technology Development Programme of the European Union, the Sachsische Staatsministerium fur Umwelt und Landesentwicklung, the Max-Buchner-Stiftung, and the Fonds der Chemischen Industrie. Samples of *P. fluorescens* BL915DeltaORF1-4 with pPEH14(prnA) and pPEH14(prnC) were obtained from Dr. J. M. Ligon, Novartis Agribusiness Biotechnology Research, Inc., Research Triangle, NC (USA) and NADH oxidase (from *Thermus thermiphilus*) from Prof. Helmut Erdmann, Fachhochschule Flensburg (Germany), *Angew Chem Int Ed Engl 39*, 2300-2302.

32. Sucharitakul, J., Prongjit, M., Haltrich, D., and Chaiyen, P. (2008) Detection of a C4a-hydroperoxyflavin intermediate in the reaction of a flavoprotein oxidase, *Biochemistry 47*, 8485-8490.

33. Orville, A. M., Lountos, G. T., Finnegan, S., Gadda, G., and Prabhakar, R. (2009) Crystallographic, spectroscopic, and computational analysis of a flavin C4a-oxygen adduct in choline oxidase, *Biochemistry 48*, 720-728.

34. van Hellemond, E. W., Leferink, N. G., Heuts, D. P., Fraaije, M. W., and van Berkel, W. J. (2006) Occurrence and biocatalytic potential of carbohydrate oxidases, *Adv. Appl. Microbiol. 60*, 17-54.

35. De Colibus, L., and Mattevi, A. (2006) New frontiers in structural flavoenzymology, *Curr. Opin. Struct. Biol. 16*, 722-728.

36.   Massey, V., and Hemmerich, P. (1980) Active-site probes of flavoproteins, *Biochem. Soc. Trans. 8*, 246-257.

37.   Fitzpatrick, P. F., and Massey, V. (1983) The reaction of 8-mercaptoflavins and flavoproteins with sulfite. Evidence for the role of an active site arginine in D-amino acid oxidase, *J. Biol. Chem. 258*, 9700-9705.

38.   Massey, V., Ghisla, S., and Moore, E. G. (1979) 8-Mercaptoflavins as active site probes of flavoenzymes, *J. Biol. Chem. 254*, 9640-9650.

39.   Mewies, M., Packman, L. C., Mathews, F. S., and Scrutton, N. S. (1996) Flavinylation in wild-type trimethylamine dehydrogenase and differentially charged mutant enzymes: a study of the protein environment around the N1 of the flavin isoalloxazine, *Biochem. J. 317 (Pt 1)*, 267-272.

40.   Fraaije, M. W., and Mattevi, A. (2000) Flavoenzymes: diverse catalysts with recurrent features, *Trends Biochem. Sci. 25*, 126-132.

41.   Trimmer, E. E., Ballou, D. P., Galloway, L. J., Scannell, S. A., Brinker, D. R., and Casas, K. R. (2005) Aspartate 120 of *Escherichia coli* methylenetetrahydrofolate reductase: evidence for major roles in folate binding and catalysis and a minor role in flavin reactivity, *Biochemistry 44*, 6809-6822.

42.   Heuts, D. P., Scrutton, N. S., McIntire, W. S., and Fraaije, M. W. (2009) What's in a covalent bond?, *FEBS J.*

43.   Croteau, N., and Vrielink, A. (1996) Crystallization and preliminary X-ray analysis of cholesterol oxidase from *Brevibacterium sterolicum* containing covalently bound FAD, *J. Struct. Biol. 116*, 317-319.

44. Li, J., Vrielink, A., Brick, P., and Blow, D. M. (1993) Crystal structure of cholesterol oxidase complexed with a steroid substrate: implications for flavin adenine dinucleotide dependent alcohol oxidases, *Biochemistry 32*, 11507-11515.

45. Mewies, M., McIntire, W. S., and Scrutton, N. S. (1998) Covalent attachment of flavin adenine dinucleotide (FAD) and flavin mononucleotide (FMN) to enzymes: the current state of affairs, *Protein Sci. 7*, 7-20.

46. McIntire, W., Edmondson, D. E., Hopper, D. J., and Singer, T. P. (1981) 8 alpha-(O-Tyrosyl)flavin adenine dinucleotide, the prosthetic group of bacterial *p*-cresol methylhydroxylase, *Biochemistry 20*, 3068-3075.

47. McIntire, W., Singer, T. P., Ameyama, M., Adachi, O., Matsushita, K., and Shinagawa, E. (1985) Identification of the covalently bound flavins of D-gluconate dehydrogenases from Pseudomonas aeruginosa and Pseudomonas fluorescens and of 2-keto-D-gluconate dehydrogenase from *Gluconobacter melanogenus*, *Biochem. J. 231*, 651-654.

48. Singer, T. P., and McIntire, W. S. (1984) Covalent attachment of flavin to flavoproteins: occurrence, assay, and synthesis, *Methods Enzymol. 106*, 369-378.

49. Boyd, G., Mathews, F. S., Packman, L. C., and Scrutton, N. S. (1992) Trimethylamine dehydrogenase of bacterium W3A1. Molecular cloning, sequence determination and over-expression of the gene, *FEBS Lett. 308*, 271-276.

50. Yang, C. C., Packman, L. C., and Scrutton, N. S. (1995) The primary structure of *Hyphomicrobium X* dimethylamine dehydrogenase. Relationship to trimethylamine dehydrogenase and implications for substrate recognition, *Eur. J. Biochem. 232*, 264-271.

51. Yan, B. X., and Sun, Y. Q. (1996) Glycine residues provide flexibility for enzyme active site, *J. Biol. Chem. 272*, 3190-3194.

52. Forneris, F., Heuts, D. P., Delvecchio, M., Rovida, S., Fraaije, M. W., and Mattevi, A. (2008) Structural analysis of the catalytic mechanism and stereoselectivity in *Streptomyces coelicolor* alditol oxidase, *Biochemistry 47*, 978-985.

53. Malito, E., Coda, A., Bilyeu, K. D., Fraaije, M. W., and Mattevi, A. (2004) Structures of Michaelis and product complexes of plant cytokinin dehydrogenase: implications for flavoenzyme catalysis, *J. Mol. Biol. 341*, 1237-1249.

54. Koetter, J. W., and Schulz, G. E. (2005) Crystal structure of 6-hydroxy-D-nicotine oxidase from *Arthrobacter nicotinovorans*, *J. Mol. Biol. 352*, 418-428.

55. Coulombe, R., Yue, K. Q., Ghisla, S., and Vrielink, A. (2001) Oxygen access to the active site of cholesterol oxidase through a narrow channel is gated by an Arg-Glu pair, *J. Biol. Chem. 276*, 30435-30441.

56. Decker, K. F., (Ed.) (1991) *Covalent flavoproteins*, Vol. 2, CRC Press, Boca Raton, FL.

57. Kenney, W. C., Edmondson, D. E., Singer, T. P., Nishikimi, M., Noguchi, E., and Yagi, K. (1979) Identification of the covalently-bound flavin of L-galactonolactone oxidase from yeast, *FEBS Lett. 97*, 40-42.

58. Kenney, W. C., Edmondson, D. E., and Singer, T. P. (1976) Identification of the covalently bound flavin of L-gulono-gamma-lactone oxidase, *Biochem. Biophys. Res. Commun 71*, 1194-1200.

59. Quaye, O., Lountos, G. T., Fan, F., Orville, A. M., and Gadda, G. (2008) Role of Glu312 in binding and positioning of the substrate for the hydride transfer reaction in choline oxidase, *Biochemistry 47*, 243-256.

60.   Halada, P., Leitner, C., Sedmera, P., Haltrich, D., and Volc, J. (2003) Identification of the covalent flavin adenine dinucleotide-binding region in pyranose 2-oxidase from *Trametes multicolor*, *Anal. Biochem. 314*, 235-242.

61.   Walker, W. H., Singer, T. P., Ghisla, S., and Hemmerich, P. (1972) Studies on succinate dehydrogenase. 8 -Histidyl-FAD as the active center of succinate dehydrogenase, *Eur. J. Biochem. 26*, 279-289.

62.   Fraaije, M. W., van den Heuvel, R. H., van Berkel, W. J., and Mattevi, A. (1999) Covalent flavinylation is essential for efficient redox catalysis in vanillyl-alcohol oxidase, *J. Biol. Chem. 274*, 35514-35520.

63.   Jin, J., Mazon, H., van den Heuvel, R. H., Janssen, D. B., and Fraaije, M. W. (2007) Discovery of a eugenol oxidase from *Rhodococcus sp*. strain RHA1, *F.E.B.S. J. 274*, 2311-2321.

64.   Shimizu, M., Murakawa, S., and Takahashi, T. (1977) The covalently bound flavin prosthetic group of D-gluconolactone dehydrogenase of *Penicillium cyaneo-fulvum*, *Agric. Biol. Chem. 41*, 2107-2108.

65.   Leys, D., Basran, J., and Scrutton, N. S. (2003) Channelling and formation of 'active' formaldehyde in dimethylglycine oxidase, *E.M.B.O. J. 22*, 4038-4048.

66.   Mathews, F. S., Chen, Z. W., Bellamy, H. D., and McIntire, W. S. (1991) Three-dimensional structure of p-cresol methylhydroxylase (flavocytochrome c) from *Pseudomonas putida* at 3.0-A resolution, *Biochemistry 30*, 238-247.

67.   Edmondson, D. E., Binda, C., and Mattevi, A. (2004) The FAD binding sites of human monoamine oxidases A and B, *Neurotoxicology 25*, 63-72.

68.   Zhou, B. P., Lewis, D. A., Kwan, S. W., and Abell, C. W. (1995) Flavinylation of monoamine oxidase B, *J. Biol. Chem. 270*, 23653-23660.

69.   Wagner, M. A., Khanna, P., and Jorns, M. S. (1999) Structure of the flavocoenzyme of two homologous amine oxidases: monomeric sarcosine oxidase and N-methyltryptophan oxidase, *Biochemistry 38*, 5588-5595.

70.   Ferri, S., Miura, S., Sakaguchi, A., Ishimura, F., Tsugawa, W., and Sode, K. (2004) Cloning and expression of fructosyl-amine oxidase from marine yeast *Pichia species* N1-1, *Mar. Biotechnol. (NY) 6*, 625-632.

71.   Ilari, A., Bonamore, A., Franceschini, S., Fiorillo, A., Boffi, A., and Colotti, G. (2008) The X-ray structure of N-methyltryptophan oxidase reveals the structural determinants of substrate specificity, *Proteins 71*, 2065-2075.

72.   Goyer, A., Johnson, T. L., Olsen, L. J., Collakova, E., Shachar-Hill, Y., Rhodes, D., and Hanson, A. D. (2004) Characterization and metabolic function of a peroxisomal sarcosine and pipecolate oxidase from *Arabidopsis*, *J. Biol. Chem. 279*, 16947-16953.

73.   Carrell, C. J., Bruckner, R. C., Venci, D., Zhao, G., Jorns, M. S., and Mathews, F. S. (2007) NikD, an unusual amino acid oxidase essential for nikkomycin biosynthesis: structures of closed and open forms at 1.15 and 1.90 A resolution, *Structure 15*, 928-941.

74.   Chen, Z. W., Koh, M., Van Driessche, G., Van Beeumen, J. J., Bartsch, R. G., Meyer, T. E., Cusanovich, M. A., and Mathews, F. S. (1994) The structure of flavocytochrome c sulfide dehydrogenase from a purple phototrophic bacterium, *Science 266*, 430-432.

75.   Van Driessche, G., Koh, M., Chen, Z. W., Mathews, F. S., Meyer, T. E., Bartsch, R. G., Cusanovich, M. A., and Van Beeumen, J. J. (1996) Covalent structure of the flavoprotein

subunit of the flavocytochrome c: sulfide dehydrogenase from the purple phototrophic bacterium *Chromatium vinosum*, *Protein Sci. 5*, 1753-1764.

76.   Huang, C. H., Lai, W. L., Lee, M. H., Chen, C. J., Vasella, A., Tsai, Y. C., and Liaw, S. H. (2005) Crystal structure of glucooligosaccharide oxidase from *Acremonium strictum*: a novel flavinylation of 6-S-cysteinyl, 8alpha-N1-histidyl FAD, *J. Biol. Chem. 280*, 38831-38838.

77.   Winkler, A., Hartner, F., Kutchan, T. M., Glieder, A., and Macheroux, P. (2006) Biochemical evidence that berberine bridge enzyme belongs to a novel family of flavoproteins containing a bi-covalently attached FAD cofactor, *J. Biol. Chem. 281*, 21276-21285.

78.   Rand, T., Qvist, K. B., Walter, C. P., and Poulsen, C. H. (2006) Characterization of the flavin association in hexose oxidase from *Chondrus crispus*, *F.E.B.S. J. 273*, 2693-2703.

79.   Alexeev, I., Sultana, A., Mantsala, P., Niemi, J., and Schneider, G. (2007) Aclacinomycin oxidoreductase (AknOx) from the biosynthetic pathway of the antibiotic aclacinomycin is an unusual flavoenzyme with a dual active site, *Proc. Natl. Acad. Sci. U S A 104*, 6170-6175.

80.   Taura, F., Sirikantaramas, S., Shoyama, Y., and Morimoto, S. (2007) Phytocannabinoids in *Cannabis sativa*: recent studies on biosynthetic enzymes, *Chem. Biodivers. 4*, 1649-1663.

81.   Steenkamp, D. J., McIntire, W., and Kenney, W. C. (1978) Structure of the covalently bound coenzyme of trimethylamine dehydrogenase. Evidence for a 6-substituted flavin, *J. Biol. Chem. 253*, 2818-2824.

82. Fujieda, N., Tsuse, N., Satoh, A., Ikeda, T., and Kano, K. (2005) Production of completely flavinylated histamine dehydrogenase, unique covalently bound flavin, and iron-sulfur cluster-containing enzyme of nocardioides simplex in *Escherichia coli*, and its properties, *Biosci. Biotechnol. Biochem. 69*, 2459-2462.

83. Willie, A., Edmondson, D. E., and Jorns, M. S. (1996) Sarcosine oxidase contains a novel covalently bound FMN, *Biochemistry 35*, 5292-5299.

84. Bandeiras, T. M., Salgueiro, C., Kletzin, A., Gomes, C. M., and Teixeira, M. (2002) *Acidianus ambivalens* type-II NADH dehydrogenase: genetic characterisation and identification of the flavin moiety as FMN, *F.E.B.S. Lett. 531*, 273-277.

85. Li, Y. S., Ho, J. Y., Huang, C. C., Lyu, S. Y., Lee, C. Y., Huang, Y. T., Wu, C. J., Chan, H. C., Huang, C. J., Hsu, N. S., Tsai, M. D., and Li, T. L. (2007) A unique flavin mononucleotide-linked primary alcohol oxidase for glycopeptide A40926 maturation, *J. Am. Chem. Soc. 129*, 13384-13385.

86. Hayashi, M., Nakayama, Y., Yasui, M., Maeda, M., Furuishi, K., and Unemoto, T. (2001) FMN is covalently attached to a threonine residue in the NqrB and NqrC subunits of Na(+)-translocating NADH-quinone reductase from *Vibrio alginolyticus, F.E.B.S. Lett. 488*, 5-8.

87. Kim, J., Fuller, J. H., Kuusk, V., Cunane, L., Chen, Z. W., Mathews, F. S., and McIntire, W. S. (1995) The cytochrome subunit is necessary for covalent FAD attachment to the flavoprotein subunit of *p*-cresol methylhydroxylase, *J. Biol. Chem. 270*, 31202-31209.

88. Brandsch, R., and Bichler, V. (1991) Autoflavinylation of apo6-hydroxy-D-nicotine oxidase, *J. Biol. Chem. 266*, 19056-19062.

89. Khanna, P., and Jorns, M. S. (2003) Tautomeric rearrangement of a dihydroflavin bound to monomeric sarcosine oxidase or N-methyltryptophan oxidase, *Biochemistry 42*, 864-869.

90. Mauch, L., Bichler, V., and Brandsch, R. (1990) Lysine can replace arginine 67 in the mediation of covalent attachment of FAD to histidine 71 of 6-hydroxy-D-nicotine oxidase, *J. Biol. Chem. 265*, 12761-12762.

91. Robinson, K. M., and Lemire, B. D. (1996) Covalent attachment of FAD to the yeast succinate dehydrogenase flavoprotein requires import into mitochondria, presequence removal, and folding, *J. Biol. Chem. 271*, 4055-4060.

92. Brandsch, R., and Bichler, V. (1985) In vivo and in vitro expression of the 6-hydroxy-D-nicotine oxidase gene of *Arthrobacter oxidans*, cloned into *Escherichia coli*, as an enzymatically active, covalently flavinylated polypeptide, *F.E.B.S. Lett. 192*, 204-208.

93. Heuts, D. P., Winter, R. T., Damsma, G. E., Janssen, D. B., and Fraaije, M. W. (2008) The role of double covalent flavin binding in chito-oligosaccharide oxidase from *Fusarium graminearum*, *Biochem. J. 413*, 175-183.

94. Huang, C. H., Winkler, A., Chen, C. L., Lai, W. L., Tsai, Y. C., Macheroux, P., and Liaw, S. H. (2008) Functional roles of the 6-S-cysteinyl, 8alpha-N1-histidyl FAD in glucooligosaccharide oxidase from *Acremonium strictum*, *J. Biol. Chem. 283*, 30990-30996.

95. Winkler, A., Kutchan, T. M., and Macheroux, P. (2007) 6-S-cysteinylation of bi-covalently attached FAD in berberine bridge enzyme tunes the redox potential for optimal activity, *J. Biol. Chem. 282*, 24437-24443.

96. Williamson, G., and Edmondson, D. E. (1985) Effect of pH on oxidation-reduction potentials of 8 alpha-N-imidazole-substituted flavins, *Biochemistry 24*, 7790-7797.

97. Edmondson, D. E., and De Francisco, R., (Eds.) (1992) *Structure, Synthesis and Physical Properties of Covalently Bound Flavins and 6- 8-hydroxyflavins*, CRC Press, Boca Raton, FL.

98. Efimov, I., Cronin, C. N., and McIntire, W. S. (2001) Effects of noncovalent and covalent FAD binding on the redox and catalytic properties of *p*-cresol methylhydroxylase, *Biochemistry 40*, 2155-2166.

99. Motteran, L., Pilone, M. S., Molla, G., Ghisla, S., and Pollegioni, L. (2001) Cholesterol oxidase from *Brevibacterium sterolicum*. The relationship between covalent flavinylation and redox properties, *J. Biol. Chem. 276*, 18024-18030.

100. Lee, M. H., Lai, W. L., Lin, S. F., Hsu, C. S., Liaw, S. H., and Tsai, Y. C. (2005) Structural characterization of glucooligosaccharide oxidase from *Acremonium strictum*, *Appl. Environ. Microbiol. 71*, 8881-8887.

101. Vrielink, A., Lloyd, L. F., and Blow, D. M. (1991) Crystal structure of cholesterol oxidase from *Brevibacterium sterolicum* refined at 1.8 Å resolution, *J. Mol. Biol. 219*, 533-554.

102. Yue, Q. K., Kass, I. J., Sampson, N. S., and Vrielink, A. (1999) Crystal structure determination of cholesterol oxidase from Streptomyces and structural characterization of key active site mutants, *Biochemistry 38*, 4277-4286.

103. Lim, L., Molla, G., Guinn, N., Ghisla, S., Pollegioni, L., and Vrielink, A. (2006) Structural and kinetic analyses of the H121A mutant of cholesterol oxidase, *Biochem. J. 400*, 13-22.

104. Caldinelli, L., Iametti, S., Barbiroli, A., Bonomi, F., Fessas, D., Molla, G., Pilone, M. S., and Pollegioni, L. (2005) Dissecting the structural determinants of the stability of cholesterol oxidase containing covalently bound flavin, *J. Biol. Chem. 280*, 22572-22581.

105. Hassan-Abdallah, A., Zhao, G., and Jorns, M. S. (2006) Role of the covalent flavin linkage in monomeric sarcosine oxidase, *Biochemistry 45*, 9454-9462.

106. Winkler, A., Motz, K., Riedl, S., Puhl, M., Macheroux, P., and Gruber, K. (2009) Structural and mechanistic studies reveal the functional role of bicovalent flavinylation in berberine bridge enzyme, *J. Biol. Chem.*

107. Trickey, P., Basran, J., Lian, L. Y., Chen, Z., Barton, J. D., Sutcliffe, M. J., Scrutton, N. S., and Mathews, F. S. (2000) Structural and biochemical characterization of recombinant wild type and a C30A mutant of trimethylamine dehydrogenase from *Methylophilus methylotrophus* (sp. W(3)A(1)), *Biochemistry 39*, 7678-7688.

108. Pineda, J. R., and Schwartz, S. D. (2006) Protein dynamics and catalysis: the problems of transition state theory and the subtlety of dynamic control, *Philos. Trans. R. Soc. Lond. B Biol Sci 361*, 1433-1438.

109. Gertner, B. J., Wilson, K. R., and Hynes, J. T. (1989) Nonequilibrium solvation effects of reaction-rates for model Sn2 reactions in water, *J. Chem. Phys. 90*, 3537-3558.

110. Wang, M. L., Lu, Z. Y., and Yang, W. T. (2004) Transmission coeffient calculation for proton transfer in triosephosphate isomerase based on the reaction path potential method, *J. Chem. Phys. 121*, 101-105.

111. Pudney, C. (2008) Kinetic isotope effects as probes of the mechanism of enzymatic hydride transfer, *Thesis Submitted to the Faculty of Life Sciences*, p 192, University of Manchester, Manchester, UK.

112. Bell, R. P. (1980) *The Tunnel Effect in Chemistry*, Chapman and Hall, New York City, NY.

113. Caldin, E. (1969) Tunneling in proton-transfer reactions in solution, *Chem. Rev. 69*, 135.

114. Marcus, R. A. (1959) On the theory of electrochemical and chemical electron transfer processes, *Can. J. Chem. 37*, 155-163.

115. Marcus, R. A. (1964) Chemical and electrochemical electron transfer theory, *Annu. Rev. Phys. Chem. 15*, 155-196.

116. Marcus, R. A. (1965) Theory of electron transfer reaction rates of solvated electrons, *J. Chem. Phys. 43*, 3477.

117. Marcus, R. A. (1997) Electron transfer reactions in chemistry; theory and experiment, *J. Electroanaly. Chem. 438*, 251-259.

118. Marcus, R. A. (1985) Electron transfers in chemistry and biology, *Biochim. Biophys. Acta 118*, 256-322.

119. Moser, C. C., Farid, T. A., Chobot, S. E., and Dutton, P. L. (2006) Electron tunneling chains of mitochondria, *Biochim. Biophys. Acta 1757*, 1096-1109.

120. de Broglie, L. (1925) Researches on the quantum theory, *Ann. Phys. 3*, 22.

121. Bell, R. P. (1959) The tunnel effect correction for parabolic potential barriers, *T. Faraday. Soc. 55*, 1.

122. Bell, R. P. (1980) *The Tunnel Effect in Chemistry*, Chapman and Hall, New York City, NY.

123. Bell, R. P. (1973) *The Proton in Chemistry*, Cornell University Press, New York City, NY.

124. Park, H., Girdaukas, G. G., and Northrop, D. B. (2006) Effect of pressure on a heavy-atom isotope effect of yeast alcohol dehydrogenase, *J. Am. Chem. Soc. 128*, 1868-1872.

125. Roth, J. P. (2007) Advances in studying bioinorganic reaction mechanisms: isotopic probes of activated oxygen intermediates in metalloenzymes, *Curr. Opin. Chem. Biol. 11*, 142-150.

126. Ralph, E. C., Hirschi, J. S., Anderson, M. A., Cleland, W. W., Singleton, D. A., and Fitzpatrick, P. F. (2007) Insights into the mechanism of flavoprotein-catalyzed amine oxidation from nitrogen isotope effects on the reaction of N-methyltryptophan oxidase, *Biochemistry 46*, 7655-7664.

127. Thornton, E. R. (1966) Secondary deuterium isotope effects, *Ann. Rev. Phys. Chem. 17*, 349-372.

128. Romesberg, F. E., and Schowen, R. L. (2004) Isotope effects and quantum tunneling in enzyme-catalyzed hydrogen transfer: Part I. The experimental basis, *Adv. Phys. Org. Chem. 39*, 27.

129. Westheimer, F. H. (1961) The magnitude of the primary kinetic isotope effect for compounds of hydrogen and deuterium, *Chem. Rev. 61*, 265.

130. Masgrau, L., Basran, J., Hothi, P., Sutcliffe, M. J., and Scrutton, N. S. (2004) Hydrogen tunneling in quinoproteins, *Arch. Biochem. Biophys.428*, 41-51.

131. Streitwieser, A. (1958) Kinetic isotope effects in the acetolyses of deuterated cyclopentyl tosylates, *J. Am. Chem. Soc. 80*, 2326.

132. Wolfsber, M. (1969) Isotope effects, *Ann. Rev. Phys. Chem. 20*, 449.

133. Kurz, L. C., and Frieden, C. (1980) Anomalous equilibrium and kinetic alpha-deuterium secondary isotope effects accompanying hydride transfer from reduced nicotinamide adenine dinucleotide, *J. Am. Chem. Soc. 102*, 4198.

134. Antoniou, D., and Schwartz, S. D. (1997) Large kinetic isotope effects in enzymatic proton transfer and the role of substrate oscillations, *Proc. Natl. Acad. Sci. U S A 94*, 12360-12365.

135. Bruno, W. J., and Bialek, W. (1992) Vibrationally enhanced tunneling as a mechanism for enzymatic hydrogen transfer, *Biophys. J. 63*, 689-699.

136. Hammes-Schiffer, S. (2001) Theoretical perspectives on proton-coupled electron transfer reactions, *Acc. Chem. Res. 34*, 273-281.

137. Cha, Y., Murray, C. J., and Klinman, J. P. (1989) Hydrogen tunneling in enzyme reactions, *Science 243*, 1325-1330.

138. Knapp, M. J., and Klinman, J. P. (2002) Environmentally coupled hydrogen tunneling. Linking catalysis to dynamics, *Eur. J. Biochem. 269*, 3113-3121.

139. Knapp, M. J., Rickert, K., and Klinman, J. P. (2002) Temperature-dependent isotope effects in soybean lipoxygenase-1: correlating hydrogen tunneling with protein dynamics, *J. Am. Chem. Soc. 124*, 3865-3874.

140. Kohen, A., Jonsson, T., and Klinman, J. P. (1997) Effects of protein glycosylation on catalysis: changes in hydrogen tunneling and enthalpy of activation in the glucose oxidase reaction, *Biochemistry 36*, 2603-2611.

141. Grant, K. L., and Klinman, J. P. (1989) Evidence that both protium and deuterium undergo significant tunneling in the reaction catalyzed by bovine serum amine oxidase, *Biochemistry 28*, 6597-6605.

142. Jonsson, T., Edmondson, D. E., and Klinman, J. P. (1994) Hydrogen tunneling in the flavoenzyme monoamine oxidase B, *Biochemistry 33*, 14871-14878.

143. Scrutton, N. S., Basran, J., and Sutcliffe, M. J. (1999) New insights into enzyme catalysis. Ground state tunnelling driven by protein dynamics, *Eur. J. Biochem. 264*, 666-671.

144. Neria, E., and Karplus, M. (1997) Molecular dynamics of an enzyme reaction: proton transfer in TIM, *Chem. Phys. Lett. 267*, 23.

145. Villa, J., and Warshel, A. (2001) Energetics and dynamics of enzymatic reactions, *J. Phys. Chem. B. 105*, 7887.

146. Doll, K. M., Bender, B. R., and Finke, R. G. (2003) The first experimental test of the hypothesis that enzymes have evolved to enhance hydrogen tunneling, *J. Am. Chem. Soc. 125*, 10877-10884.

147. Doll, K. M., and Finke, R. G. (2003) A compelling experimental test of the hypothesis that enzymes have evolved to enhance quantum mechanical tunneling in hydrogen transfer reactions: the beta-neopentylcobalamin system combined with prior adocobalamin data, *Inorg. Chem. 42*, 4849-4856.

148. Kraut, J. (1988) How do enzymes work?, *Science 242*, 533-540.

149. Schramm, V. L. (1998) Enzymatic transition states and transition state analog design, *Annu. Rev. Biochem. 67*, 693-720.

150. Kim, K. S., Kim, D., Lee, J. Y., Tarakeshwar, P., and Oh, K. S. (2002) Catalytic mechanism of enzymes: preorganization, short strong hydrogen bond, and charge buffering, *Biochemistry 41*, 5300-5306.

151. Marti, S., Andres, J., Moliner, V., Silla, E., Tunon, I., and Bertran, J. (2003) Preorganization and reorganization as related factors in enzyme catalysis: the chorismate mutase case, *Chemistry 9*, 984-991.

152. Marti, S., Roca, M., Andres, J., Moliner, V., Silla, E., Tunon, I., and Bertran, J. (2004) Theoretical insights in enzyme catalysis, *Chem. Soc. Rev. 33*, 98-107.

153. Warshel, A. (1978) Energetics of enzyme catalysis, *Proc. Natl. Acad. Sci. U S A 75*, 5250-5254.

154. Warshel, A., Sharma, P. K., Kato, M., Xiang, Y., Liu, H., and Olsson, M. H. (2006) Electrostatic basis for enzyme catalysis, *Chem. Rev. 106*, 3210-3235.

155. Warshel, A. (1998) Electrostatic origin of the catalytic power of enzymes and the role of preorganized active sites, *J. Biol. Chem. 273*, 27035-27038.

156. Warshel, A., and Florian, J. (1998) Computer simulations of enzyme catalysis: finding out what has been optimized by evolution, *Proc. Natl. Acad. Sci. U S A 95*, 5950-5955.

157. Cannon, W. R., Singleton, S. F., and Benkovic, S. J. (1996) A perspective on biological catalysis, *Nat. Struct. Biol. 3*, 821-833.

158. Olsson, M. H., Parson, W. W., and Warshel, A. (2006) Dynamical contributions to enzyme catalysis: critical tests of a popular hypothesis, *Chem. Rev. 106*, 1737-1756.

159. Roca, M., Moliner, V., Tunon, I., and Hynes, J. T. (2006) Coupling between protein and reaction dynamics in enzymatic processes: application of Grote-Hynes Theory to catechol O-methyltransferase, *J. Am. Chem. Soc. 128*, 6186-6193.

160. Gutteridge, A., and Thornton, J. (2005) Conformational changes observed in enzyme crystal structures upon substrate binding, *J. Mol. Biol. 346*, 21-28.

161. Yang, L. W., Liu, X., Jursa, C. J., Holliman, M., Rader, A. J., Karimi, H. A., and Bahar, I. (2005) iGNM: a database of protein functional motions based on Gaussian Network Model, *Bioinformatics 21*, 2978-2987.

162. Sacquin-Mora, S., and Lavery, R. (2006) Investigating the local flexibility of functional residues in hemoproteins, *Biophys. J. 90*, 2706-2717.

163. Yuan, Z., Zhao, J., and Wang, Z. X. (2003) Flexibility analysis of enzyme active sites by crystallographic temperature factors, *Protein Eng. 16*, 109-114.

164. Holliday, G. L., Almonacid, D. E., Mitchell, J. B., and Thornton, J. M. (2007) The chemistry of protein catalysis, *J. Mol. Biol. 372*, 1261-1277.

165. Hedstrom, L. (2002) Serine protease mechanism and specificity, *Chem. Rev. 102*, 4501-4524.

166. Knowles, J. R. (1991) Enzyme catalysis: not different, just better, *Nature 350*, 121-124.

167. Smith, A. J., Muller, R., Toscano, M. D., Kast, P., Hellinga, H. W., Hilvert, D., and Houk, K. N. (2008) Structural reorganization and preorganization in enzyme active sites: comparisons of experimental and theoretically ideal active site geometries in the multistep serine esterase reaction cycle, *J. Am. Chem. Soc. 130*, 15361-15373.

168. Bryngelson, J. D., and Wolynes, P. G. (1987) Spin glasses and the statistical mechanics of protein folding, *Proc. Natl. Acad. Sci. U S A 84*, 7524-7528.

169. Onuchic, J. N., and Wolynes, P. G. (2004) Theory of protein folding, *Curr. Opin. Struct. Biol. 14*, 70-75.

170. Bystroff, C., Oatley, S. J., and Kraut, J. (1990) Crystal structures of *Escherichia coli* dihydrofolate reductase: the NADP+ holoenzyme and the folate.NADP+ ternary

complex. Substrate binding and a model for the transition state, *Biochemistry 29*, 3263-3277.

171. Lee, H., Reyes, V. M., and Kraut, J. (1996) Crystal structures of *Escherichia coli* dihydrofolate reductase complexed with 5-formyltetrahydrofolate (folinic acid) in two space groups: evidence for enolization of pteridine O4, *Biochemistry 35*, 7012-7020.

172. Sawaya, M. R., and Kraut, J. (1997) Loop and subdomain movements in the mechanism of *Escherichia coli* dihydrofolate reductase: crystallographic evidence, *Biochemistry 36*, 586-603.

173. Miller, G. P., and Benkovic, S. J. (1998) Stretching exercises--flexibility in dihydrofolate reductase catalysis, *Chem. Biol. 5*, R105-113.

174. Huang, Z., Wagner, C. R., and Benkovic, S. J. (1994) Nonadditivity of mutational effects at the folate binding site of *Escherichia coli* dihydrofolate reductase, *Biochemistry 33*, 11576-11585.

175. Wagner, C. R., Huang, Z., Singleton, S. F., and Benkovic, S. J. (1995) Molecular basis for nonadditive mutational effects in *Escherichia coli* dihydrofolate reductase, *Biochemistry 34*, 15671-15680.

176. Rajagopalan, P. T., and Benkovic, S. J. (2002) Preorganization and protein dynamics in enzyme catalysis, *Chem. Rec. 2*, 24-36.

177. Liu, H., and Warshel, A. (2007) The catalytic effect of dihydrofolate reductase and its mutants is determined by reorganization energies, *Biochemistry 46*, 6011-6025.

178. Bjelic, S., and Aqvist, J. (2006) Catalysis and linear free energy relationships in aspartic proteases, *Biochemistry 45*, 7709-7723.

179. Wratten, C. C., and Cleland, W. W. (1963) Product inhibition studies on yeast and liver alcohol dehydrogenases, *Biochemistry 2*, 935-941.

180. Eklund, H., Nordstrom, B., Zeppezauer, E., Soderlund, G., Ohlsson, I., Boiwe, T., Soderberg, B. O., Tapia, O., Branden, C. I., and Akeson, A. (1976) Three-dimensional structure of horse liver alcohol dehydrogenase at 2-4 A resolution, *J. Mol. Biol. 102*, 27-59.

181. Eklund, H., and Branden, C. I. (1979) Structural differences between apo- and holoenzyme of horse liver alcohol dehydrogenase, *J. Biol. Chem. 254*, 3458-3461.

182. Dalziel, K. (1963) Kinetic studies of liver alcohol dehydrogenase and pH effects with coenzyme preparations of high purity, *J. Biol. Chem. 238*, 2850-2858.

183. Dalziel, K. (1963) Interpretation of inhibition kinetics of coenzyme-substrate reactions, and the role of zinc in alcohol dehydrogenases, *Nature 197*, 462-464.

184. Bahnson, B. J., Park, D. H., Kim, K., Plapp, B. V., and Klinman, J. P. (1993) Unmasking of hydrogen tunneling in the horse liver alcohol dehydrogenase reaction by site-directed mutagenesis, *Biochemistry 32*, 5503-5507.

185. Dworschack, R. T., and Plapp, B. V. (1977) pH, isotope, and substituent effects on the interconversion of aromatic substrates catalyzed by hydroxybutyrimidylated liver alcohol dehydrogenase, *Biochemistry 16*, 2716-2725.

186. Bahnson, B. J., Colby, T. D., Chin, J. K., Goldstein, B. M., and Klinman, J. P. (1997) A link between protein structure and enzyme catalyzed hydrogen tunneling, *Proc. Natl. Acad. Sci. U S A 94*, 12797-12802.

187. Tsai, S., and Klinman, J. P. (2001) Probes of hydrogen tunneling with horse liver alcohol dehydrogenase at subzero temperatures, *Biochemistry 40*, 2303-2311.

188. Kohen, A., Cannio, R., Bartolucci, S., and Klinman, J. P. (1999) Enzyme dynamics and hydrogen tunnelling in a thermophilic alcohol dehydrogenase, *Nature 399*, 496-499.

189. Liang, Z. X., Lee, T., Resing, K. A., Ahn, N. G., and Klinman, J. P. (2004) Thermal-activated protein mobility and its correlation with catalysis in thermophilic alcohol dehydrogenase, *Proc. Natl. Acad. Sci. U S A 101*, 9556-9561.

190. Melander, L., and Saunders, W. H. (1987) *Reaction Rates of Isotopic Molecules*, Fourth ed., Krieger, Malabar, FL.

191. Rucker, J., Cha, Y., Jonsson, T., Grant, K. L., and Klinman, J. P. (1992) Role of internal thermodynamics in determining hydrogen tunneling in enzyme-catalyzed hydrogen transfer reactions, *Biochemistry 31*, 11489-11499.

192. Shibata, D., Steczko, J., Dixon, J. E., Hermodson, M., Yazdanparast, R., and Axelrod, B. (1987) Primary structure of soybean lipoxygenase-1, *J. Biol. Chem. 262*, 10080-10085.

193. Stallings, W. C., Kroa, B. A., Carroll, R. T., Metzger, A. L., and Funk, M. O. (1990) Crystallization and preliminary X-ray characterization of a soybean seed lipoxygenase, *J. Mol. Biol. 211*, 685-687.

194. Minor, W., Steczko, J., Stec, B., Otwinowski, Z., Bolin, J. T., Walter, R., and Axelrod, B. (1996) Crystal structure of soybean lipoxygenase L-1 at 1.4 Å resolution, *Biochemistry 35*, 10687-10701.

195. Boyington, J. C., Gaffney, B. J., and Amzel, L. M. (1993) Structure of soybean lipoxygenase-I, *Biochem. Soc. Trans. 21 (Pt 3)*, 744-748.

196. Dunham, W. R., Carroll, R. T., Thompson, J. F., Sands, R. H., and Funk, M. O., Jr. (1990) The initial characterization of the iron environment in lipoxygenase by Mossbauer spectroscopy, *Eur. J. Biochem. 190*, 611-617.

197. Glickman, M. H., and Klinman, J. P. (1996) Lipoxygenase reaction mechanism: demonstration that hydrogen abstraction from substrate precedes dioxygen binding during catalytic turnover, *Biochemistry 35*, 12882-12892.

198. Rickert, K. W., and Klinman, J. P. (1999) Nature of hydrogen transfer in soybean lipoxygenase 1: separation of primary and secondary isotope effects, *Biochemistry 38*, 12218-12228.

199. Knapp, M. J., Seebeck, F. P., and Klinman, J. P. (2001) Steric control of oxygenation regiochemistry in soybean lipoxygenase-1, *J. Am. Chem. Soc. 123*, 2931-2932.

200. Meyer, M. P., Tomchick, D. R., and Klinman, J. P. (2008) Enzyme structure and dynamics affect hydrogen tunneling: the impact of a remote side chain (I553) in soybean lipoxygenase-1, *Proc. Natl. Acad. Sci. U S A 105*, 1146-1151.

201. Sharma, S. C., and Klinman, J. P. (2008) Experimental evidence for hydrogen tunneling when the isotopic arrhenius prefactor ($A_{(H)}/A_{(D)}$) is unity, *J. Am. Chem. Soc. 130*, 17632-17633.

202. Hatcher, E., Soudackov, A. V., and Hammes-Schiffer, S. (2004) Proton-coupled electron transfer in soybean lipoxygenase, *J. Am. Chem. Soc. 126*, 5763-5775.

203. Hammes-Schiffer, S. (2006) Hydrogen tunneling and protein motion in enzyme reactions, *Acc. Chem. Res. 39*, 93-100.

204. Pazur, J. H., and Kleppe, K. (1964) The oxidation of glucose and related compounds by glucose oxidase from *Aspergillus Niger*, *Biochemistry 3*, 578-583.

205. Crueger, A., and Crueger, W. (1990) *Microbioal enzymes and biotechnology*, Elsevier Applied Science, London, UK.

206. Gibson, Q. H., Swoboda, B. E., and Massey, V. (1964) Kinetics and mechanism of action of glucose oxidase, *J. Biol. Chem. 239*, 3927-3934.

207. Hecht, H. J., Kalisz, H. M., Hendle, J., Schmid, R. D., and Schomburg, D. (1993) Crystal structure of glucose oxidase from *Aspergillus niger* refined at 2.3 A resolution, *J. Mol. Biol. 229*, 153-172.

208. Swoboda, B. E., and Massey, V. (1965) Purification and Properties of the Glucose Oxidase from *Aspergillus Niger*, *J. Biol. Chem. 240*, 2209-2215.

209. Kalisz, H. M., Hecht, H. J., Schomburg, D., and Schmid, R. D. (1991) Effects of carbohydrate depletion on the structure, stability and activity of glucose oxidase from *Aspergillus niger*, *Biochim. Biophys. Acta 1080*, 138-142.

210. Wohlfahrt, G., Trivic, S., Zeremski, J., Pericin, D., and Leskovac, V. (2004) The chemical mechanism of action of glucose oxidase from *Aspergillus niger*, *Mol. Cell. Biochem. 260*, 69-83.

211. Kiess, M., Hecht, H. J., and Kalisz, H. M. (1998) Glucose oxidase from *Penicillium amagasakiense*. Primary structure and comparison with other glucose-methanol-choline (GMC) oxidoreductases, *Eur. J. Biochem. 252*, 90-99.

212. Seymour, S. L., and Klinman, J. P. (2002) Comparison of rates and kinetic isotope effects using PEG-modified variants and glycoforms of glucose oxidase: the relationship of modification of the protein envelope to C-H activation and tunneling, *Biochemistry 41*, 8747-8758.

213. Brinkley, D. W., and Roth, J. P. (2005) Determination of a large reorganization energy barrier for hydride abstraction by glucose oxidase, *J. Am. Chem. Soc. 127*, 15720-15721.

214. Charlton, P. A., Young, D. W., Birdsall, B., Feeney, J., and Roberts, G. C. K. (1979) *J. Chem. Soc., Chem. Commun.*, 922-924.

215. Osborne, M. J., Schnell, J., Benkovic, S. J., Dyson, H. J., and Wright, P. E. (2001) Backbone dynamics in dihydrofolate reductase complexes: role of loop flexibility in the catalytic mechanism, *Biochemistry 40*, 9846-9859.

216. Epstein, D. M., Benkovic, S. J., and Wright, P. E. (1995) Dynamics of the dihydrofolate reductase-folate complex: catalytic sites and regions known to undergo conformational change exhibit diverse dynamical features, *Biochemistry 34*, 11037-11048.

217. Cameron, C. E., and Benkovic, S. J. (1997) Evidence for a functional role of the dynamics of glycine-121 of *Escherichia coli* dihydrofolate reductase obtained from kinetic analysis of a site-directed mutant, *Biochemistry 36*, 15792-15800.

218. Rajagopalan, P. T., Lutz, S., and Benkovic, S. J. (2002) Coupling interactions of distal residues enhance dihydrofolate reductase catalysis: mutational effects on hydride transfer rates, *Biochemistry 41*, 12618-12628.

219. Benkovic, S. J., and Hammes-Schiffer, S. (2003) A perspective on enzyme catalysis, *Science 301*, 1196-1202.

220. Fierke, C. A., Johnson, K. A., and Benkovic, S. J. (1987) Construction and evaluation of the kinetic scheme associated with dihydrofolate reductase from *Escherichia coli*, *Biochemistry 26*, 4085-4092.

221. Appleman, J. R., Beard, W. A., Delcamp, T. J., Prendergast, N. J., Freisheim, J. H., and Blakley, R. L. (1990) Unusual transient- and steady-state kinetic behavior is predicted by the kinetic scheme operational for recombinant human dihydrofolate reductase, *J. Biol. Chem. 265*, 2740-2748.

222. Sikorski, R. S., Wang, L., Markham, K. A., Rajagopalan, P. T., Benkovic, S. J., and Kohen, A. (2004) Tunneling and coupled motion in the *Escherichia coli* dihydrofolate reductase catalysis, *J. Am. Chem. Soc. 126*, 4778-4779.

223. Maglia, G., and Allemann, R. K. (2003) Evidence for environmentally coupled hydrogen tunneling during dihydrofolate reductase catalysis, *J. Am. Chem. Soc. 125*, 13372-13373.

224. Francisco, W. A., Knapp, M. J., Blackburn, N. J., and Klinman, J. P. (2002) Hydrogen tunneling in peptidylglycine alpha-hydroxylating monooxygenase, *J. Am. Chem. Soc. 124*, 8194-8195.

225. Wong, K. F., Selzer, T., Benkovic, S. J., and Hammes-Schiffer, S. (2005) Impact of distal mutations on the network of coupled motions correlated to hydride transfer in dihydrofolate reductase, *Proc. Natl. Acad. Sci. U S A 102*, 6807-6812.

226. Agarwal, P. K., Billeter, S. R., Rajagopalan, P. T., Benkovic, S. J., and Hammes-Schiffer, S. (2002) Network of coupled promoting motions in enzyme catalysis, *Proc. Natl. Acad. Sci. U S A 99*, 2794-2799.

227. Wang, L., Goodey, N. M., Benkovic, S. J., and Kohen, A. (2006) Coordinated effects of distal mutations on environmentally coupled tunneling in dihydrofolate reductase, *Proc. Natl. Acad. Sci. U S A 103*, 15753-15758.

228. Wang, L., Goodey, N. M., Benkovic, S. J., and Kohen, A. (2006) The role of enzyme dynamics and tunnelling in catalysing hydride transfer: studies of distal mutants of dihydrofolate reductase, *Philos. Trans. R. Soc. Lond. B Biol. Sci. 361*, 1307-1315.

229. Craig, D. H., Moody, P. C., Bruce, N. C., and Scrutton, N. S. (1998) Reductive and oxidative half-reactions of morphinone reductase from *Pseudomonas putida M10*: a kinetic and thermodynamic analysis, *Biochemistry 37*, 7598-7607.

230. Barna, T., Messiha, H. L., Petosa, C., Bruce, N. C., Scrutton, N. S., and Moody, P. C. (2002) Crystal structure of bacterial morphinone reductase and properties of the C191A mutant enzyme, *J. Biol. Chem. 277*, 30976-30983.

231. French, C. E., and Bruce, N. C. (1994) Purification and characterization of morphinone reductase from *Pseudomonas putida M10*, *Biochem. J. 301 (Pt 1)*, 97-103.

232. Basran, J., Harris, R. J., Sutcliffe, M. J., and Scrutton, N. S. (2003) H-tunneling in the multiple H-transfers of the catalytic cycle of morphinone reductase and in the reductive half-reaction of the homologous pentaerythritol tetranitrate reductase, *J. Biol. Chem. 278*, 43973-43982.

233. Hay, S., Sutcliffe, M. J., and Scrutton, N. S. (2007) Promoting motions in enzyme catalysis probed by pressure studies of kinetic isotope effects, *Proc. Natl. Acad. Sci. U S A 104*, 507-512.

234. Hay, S., Pudney, C. R., Sutcliffe, M. J., and Scrutton, N. S. (2008) Are environmentally coupled enzymatic hydrogen tunneling reactions influenced by changes in solution viscosity?, *Angew. Chem. Int. Ed. Engl. 47*, 537-540.

235. Basran, J., Sutcliffe, M. J., and Scrutton, N. S. (2001) Deuterium isotope effects during carbon-hydrogen bond cleavage by trimethylamine dehydrogenase. Implications for mechanism and vibrationally assisted hydrogen tunneling in wild-type and mutant enzymes, *J. Biol. Chem. 276*, 24581-24587.

236. Basran, J., Sutcliffe, M. J., and Scrutton, N. S. (1999) Enzymatic H-transfer requires vibration-driven extreme tunneling, *Biochemistry 38*, 3218-3222.

237. Agrawal, N., Hong, B., Mihai, C., and Kohen, A. (2004) Vibrationally enhanced hydrogen tunneling in the *Escherichia coli* thymidylate synthase catalyzed reaction, *Biochemistry 43*, 1998-2006.

238. Harris, R. J., Meskys, R., Sutcliffe, M. J., and Scrutton, N. S. (2000) Kinetic studies of the mechanism of carbon-hydrogen bond breakage by the heterotetrameric sarcosine oxidase of *Arthrobacter sp. 1-IN*, *Biochemistry 39*, 1189-1198.

239. Basran, J., Patel, S., Sutcliffe, M. J., and Scrutton, N. S. (2001) Importance of barrier shape in enzyme-catalyzed reactions. Vibrationally assisted hydrogen tunneling in tryptophan tryptophylquinone-dependent amine dehydrogenases, *J. Biol. Chem. 276*, 6234-6242.

240. Murakawa, T., Okajima, T., Kuroda, S., Nakamoto, T., Taki, M., Yamamoto, Y., Hayashi, H., and Tanizawa, K. (2006) Quantum mechanical hydrogen tunneling in bacterial copper amine oxidase reaction, *Biochem. Biophys. Res. Commun. 342*, 414-423.

241. Ikuta, S., Imamura, S., Misaki, H., and Horiuti, Y. (1977) Purification and characterization of choline oxidase from *Arthrobacter globiformis*, *J. Biochem. 82*, 1741-1749.

242. Ohishi, N., and Yagi, K. (1979) Covalently bound flavin as prosthetic group of choline oxidase, *Biochem. Biophys. Res. Commun. 86*, 1084-1088.

243. Rand, T., Halkier, T., and Hansen, O. C. (2003) Structural characterization and mapping of the covalently linked FAD cofactor in choline oxidase from *Arthrobacter globiformis*, *Biochemistry 42*, 7188-7194.

244. Deshnium, P., Los, D. A., Hayashi, H., Mustardy, L., and Murata, N. (1995) Transformation of *Synechococcus* with a gene for choline oxidase enhances tolerance to salt stress, *Plant Mol. Biol. 29*, 897-907.

245. Fan, F., Ghanem, M., and Gadda, G. (2004) Cloning, sequence analysis, and purification of choline oxidase from *Arthrobacter globiformis*: a bacterial enzyme involved in osmotic stress tolerance, *Arch. Biochem. Biophys. 421*, 149-158.

246. Gadda, G. (2003) Kinetic mechanism of choline oxidase from *Arthrobacter globiformis*, *Biochim. Biophys. Acta. 1646*, 112-118.

247. Fan, F., and Gadda, G. (2005) On the catalytic mechanism of choline oxidase, *J. Am. Chem. Soc. 127*, 2067-2074.

248. Gadda, G., Powell, N. L., and Menon, P. (2004) The trimethylammonium headgroup of choline is a major determinant for substrate binding and specificity in choline oxidase, *Arch. Biochem. Biophys. 430*, 264-273.

249. Gadda, G., Fan, F., and Hoang, J. V. (2006) On the contribution of the positively charged headgroup of choline to substrate binding and catalysis in the reaction catalyzed by choline oxidase, *Arch. Biochem. Biophys. 451*, 182-187.

250. Hoang, J. V., and Gadda, G. (2007) Trapping choline oxidase in a nonfunctional conformation by freezing at low pH, *Proteins 66*, 611-620.

251. Fan, F., and Gadda, G. (2005) Oxygen- and temperature-dependent kinetic isotope effects in choline oxidase: correlating reversible hydride transfer with environmentally enhanced tunneling, *J. Am. Chem. Soc. 127*, 17954-17961.

252. Wohlfahrt, G., Witt, S., Hendle, J., Schomburg, D., Kalisz, H. M., and Hecht, H. J. (1999) 1.8 and 1.9 A resolution structures of the *Penicillium amagasakiense* and

Aspergillus niger glucose oxidases as a basis for modelling substrate complexes, *Acta Crystallogr. D. Biol. Crystallogr. 55*, 969-977.

253. Albrecht, M., and Lengauer, T. (2003) Pyranose oxidase identified as a member of the GMC oxidoreductase family, *Bioinformatics 19*, 1216-1220.

254. Bannwarth, M., Bastian, S., Heckmann-Pohl, D., Giffhorn, F., and Schulz, G. E. (2004) Crystal structure of pyranose 2-oxidase from the white-rot fungus *Peniophora sp*, *Biochemistry 43*, 11683-11690.

255. Cavener, D. R. (1992) GMC oxidoreductases. A newly defined family of homologous proteins with diverse catalytic activities, *J. Mol. Biol. 223*, 811-814.

256. Hallberg, B. M., Henriksson, G., Pettersson, G., and Divne, C. (2002) Crystal structure of the flavoprotein domain of the extracellular flavocytochrome cellobiose dehydrogenase, *J. Mol. Biol. 315*, 421-434.

257. Henriksson, G., Johansson, G., and Pettersson, G. (2000) A critical review of cellobiose dehydrogenases, *J. Biotechnol. 78*, 93-113.

258. Hallberg, B. M., Leitner, C., Haltrich, D., and Divne, C. (2004) Crystal structure of the 270 kDa homotetrameric lignin-degrading enzyme pyranose 2-oxidase, *J. Mol. Biol. 341*, 781-796.

259. Kujawa, M., Ebner, H., Leitner, C., Hallberg, B. M., Prongjit, M., Sucharitakul, J., Ludwig, R., Rudsander, U., Peterbauer, C., Chaiyen, P., Haltrich, D., and Divne, C. (2006) Structural basis for substrate binding and regioselective oxidation of monosaccharides at C3 by pyranose 2-oxidase, *J. Biol. Chem. 281*, 35104-35115.

260. Ghanem, M., and Gadda, G. (2005) On the catalytic role of the conserved active site residue His466 of choline oxidase, *Biochemistry 44*, 893-904.

261.   Ghanem, M., and Gadda, G. (2006) Effects of reversing the protein positive charge in the proximity of the flavin N(1) locus of choline oxidase, *Biochemistry 45*, 3437-3447.

262.   Rungsrisuriyachai, K., and Gadda, G. (2008) On the role of histidine 351 in the reaction of alcohol oxidation catalyzed by choline oxidase, *Biochemistry 47*, 6762-6769.

263.   Fan, F., Germann, M. W., and Gadda, G. (2006) Mechanistic studies of choline oxidase with betaine aldehyde and its isosteric analogue 3,3-dimethylbutyraldehyde, *Biochemistry 45*, 1979-1986.

264.   Finnegan, S., and Gadda, G. (2008) Substitution of an active site valine uncovers a kinetically slow equilibrium between competent and incompetent forms of choline oxidase, *Biochemistry 47*, 13850-13861.

265.   Deshnium, P., Gombos, Z., Nishiyama, Y., and Murata, N. (1997) The action in vivo of glycine betaine in enhancement of tolerance of *Synechococcus sp.* strain PCC 7942 to low temperature, *J. Bacteriol. 179*, 339-344.

266.   Hayashi, H., Alia, Mustardy, L., Deshnium, P., Ida, M., and Murata, N. (1997) Transformation of *Arabidopsis thaliana* with the codA gene for choline oxidase; accumulation of glycinebetaine and enhanced tolerance to salt and cold stress, *Plant J. 12*, 133-142.

267.   Alia, Hayashi, H., Sakamoto, A., and Murata, N. (1998) Enhancement of the tolerance of *Arabidopsis* to high temperatures by genetic engineering of the synthesis of glycinebetaine, *Plant J. 16*, 155-161.

268.   Alia, Kondo, Y., Sakamoto, A., Nonaka, H., Hayashi, H., Saradhi, P. P., Chen, T. H., and Murata, N. (1999) Enhanced tolerance to light stress of transgenic *Arabidopsis* plants that express the codA gene for a bacterial choline oxidase, *Plant Mol. Biol. 40*, 279-288.

269.   Sakamoto, A., Valverde, R., Alia, Chen, T. H., and Murata, N. (2000) Transformation of *Arabidopsis* with the codA gene for choline oxidase enhances freezing tolerance of plants, *Plant J. 22*, 449-453.

270.   Sakamoto, A., Alia, and Murata, N. (1998) Metabolic engineering of rice leading to biosynthesis of glycinebetaine and tolerance to salt and cold, *Plant Mol. Biol. 38*, 1011-1019.

271.   Mohanty, A., Kathuria, H., Ferjani, A., Sakamoto, A., Mohanty, P., Murata, N., and Tyagi, A. K. (2002) Transgenics of an elite indica rice variety *Pusa Basmati 1* harbouring the codA gene are highly tolerant to salt stress, *Theor. Appl. Genet. 106*, 51-57.

272.   Park, E. J., Jeknic, Z., Sakamoto, A., DeNoma, J., Yuwansiri, R., Murata, N., and Chen, T. H. (2004) Genetic engineering of glycinebetaine synthesis in tomato protects seeds, plants, and flowers from chilling damage, *Plant J. 40*, 474-487.

273.   Park, E. J., Jeknic, Z., Chen, T. H., and Murata, N. (2007) The codA transgene for glycinebetaine synthesis increases the size of flowers and fruits in tomato, *Plant Biotechnol. J. 5*, 422-430.

274.   Hema, R., Senthil-Kumar, M., Shivakumar, S., Chandrasekhara Reddy, P., and Udayakumar, M. (2007) *Chlamydomonas reinhardtii*, a model system for functional validation of abiotic stress responsive genes, *Planta 226*, 655-670.

275.   Singh, A. K., Mehta, A. K., Sridhara, S., Gaur, S. N., Singh, B. P., Sarma, P. U., and Arora, N. (2006) Allergenicity assessment of transgenic mustard (*Brassica juncea*) expressing bacterial codA gene, *Allergy 61*, 491-497.

276. Rozwadowski, K. L., Khachatourians, G. G., and Selvaraj, G. (1991) Choline oxidase, a catabolic enzyme in *Arthrobacter pascens*, facilitates adaptation to osmotic stress in Escherichia coli, *J. Bacteriol. 173*, 472-478.

277. Su, J., Hirji, R., Zhang, L., He, C., Selvaraj, G., and Wu, R. (2006) Evaluation of the stress-inducible production of choline oxidase in transgenic rice as a strategy for producing the stress-protectant glycine betaine, *J. Exp. Bot. 57*, 1129-1135.

278. Keller, W. A., Datla, R. S. S., Dong, J. Z., Georges, F., Hussain, A. A. K., and Selvaraj, G. (2004) Method and compositions for modifying levels of secondary metabolic compounds in plant, *United States Patent 7279619*.

279. Michel, B., Baharoglu, Z., and Lestini, R., (Eds.) (2007) *Genetics of recombination in the model bacterium Escherichia coli* Vol. 17, Springer, Berlin.

280. Heinze, B., Hoven, N., O'Connell, T., Maurer, K. H., Bartsch, S., and Bornscheuer, U. T. (2008) Recovery of choline oxidase activity by in vitro recombination of individual segments, *Appl. Microbiol. Biotechnol. 81*, 275-282.

281. Ribitsch, D., Karl, W., Wehrschutz-Sigl, E., Tutz, S., Remler, P., Weber, H. J., Gruber, K., Stehr, R., Bessler, C., Hoven, N., Sauter, K., Maurer, K. H., and Schwab, H. (2009) Heterologous expression and characterization of choline oxidase from the soil bacterium *Arthrobacter nicotianae*, *Appl. Microbiol. Biotechnol. 81*, 875-886.

282. Quan, R., Shang, M., Zhang, H., Zhao, Y., and Zhang, J. (2004) Engineering of enhanced glycine betaine synthesis improves drought tolerance in maize, *Plant Biotechnol. J. 2*, 477-486.

283. Waditee, R., Bhuiyan, N. H., Hirata, E., Hibino, T., Tanaka, Y., Shikata, M., and Takabe, T. (2007) Metabolic engineering for betaine accumulation in microbes and plants, *J. Biol. Chem. 282*, 34185-34193.

284. Chen, T. H., and Murata, N. (2002) Enhancement of tolerance of abiotic stress by metabolic engineering of betaines and other compatible solutes, *Curr. Opin. Plant Biol. 5*, 250-257.

285. Rontein, D., Basset, G., and Hanson, A. D. (2002) Metabolic engineering of osmoprotectant accumulation in plants, *Metab. Eng. 4*, 49-56.

286. Sanchez-Aguayo, I., Rodriguez-Galan, J. M., Garcia, R., Torreblanca, J., and Pardo, J. M. (2004) Salt stress enhances xylem development and expression of S-adenosyl-L-methionine synthase in lignifying tissues of tomato plants, *Planta 220*, 278-285.

287. Shirasawa, K., Takabe, T., and Kishitani, S. (2006) Accumulation of glycinebetaine in rice plants that overexpress choline monooxygenase from spinach and evaluation of their tolerance to abiotic stress, *Ann. Bot. (Lond) 98*, 565-571.

288. Waditee, R., Bhuiyan, M. N., Rai, V., Aoki, K., Tanaka, Y., Hibino, T., Suzuki, S., Takano, J., Jagendorf, A. T., and Takabe, T. (2005) Genes for direct methylation of glycine provide high levels of glycinebetaine and abiotic-stress tolerance in *Synechococcus* and *Arabidopsis*, *Proc. Natl. Acad. Sci. U S A 102*, 1318-1323.

289. O'Callaghan, J., and Condon, S. (2000) Growth of *Lactococcus lactis* strains at low water activity: correlation with the ability to accumulate glycine betaine, *Int. J. Food Microbiol. 55*, 127-131.

290. Peddie, B. A., Chambers, S. T., and Lever, M. (1996) Is the ability of urinary tract pathogens to accumulate glycine betaine a factor in the virulence of pathogenic strains?, *J. Lab. Clin. Med. 128*, 417-422.

291. Velasco-Garcia, R., Chacon-Aguilar, V. M., Hervert-Hernandez, D., and Munoz-Clares, R. A. (2003) Inactivation of betaine aldehyde dehydrogenase from *Pseudomonas aeruginosa* and *Amaranthus hypochondriacus L.* leaves by disulfiram, *Chem. Biol. Interact. 143-144*, 149-158.

292. Ohta, M., Miura, R., Yamano, T., and Miyake, Y. (1983) Spectroscopic studies on the photoreaction of choline oxidase, a flavoprotein, with covalently bound flavin, *J. Biochem. 94*, 879-892.

293. Gadda, G. (2003) pH and deuterium kinetic isotope effects studies on the oxidation of choline to betaine-aldehyde catalyzed by choline oxidase, *Biochim. Biophys. Acta 1650*, 4-9.

294. Fan, F., and Gadda, G. (2007) An internal equilibrium preorganizes the enzyme-substrate complex for hydride tunneling in choline oxidase, *Biochemistry 46*, 6402-6408.

295. Krissinel, E., and Henrick, K. (2004) Secondary-structure matching (SSM), a new tool for fast protein structure alignment in three dimensions, *Acta Crystallogr. D60*, 2256-2268.

CHAPTER 2

Contribution of Flavin Covalent Linkage with Histidine 99 to the Reaction Catalyzed by

Choline Oxidase

(This chapter was published verbatim in Quaye, O., Cowins, S., and Gadda, G. (2009) *J. Biol. Chem.*)

2.1. Abstract

The FAD-dependent choline oxidase has a flavin cofactor covalently attached to the protein via histidine 99 through an 8α-N(3)-histidyl linkage. The enzyme catalyzes the four-electron oxidation of choline to glycine betaine, forming betaine aldehyde as an enzyme-bound intermediate. The variant form of choline oxidase in which the histidine residue has been replaced with asparagine was used to investigate the contribution of the 8α-N(3)-histidyl linkage of FAD to the protein towards the reaction catalyzed by the enzyme. Decreases of 10-fold and 30-fold in the k_{cat}/K_m and k_{cat} values were observed as compared to wild-type choline oxidase at pH 10 and 25 ^oC, with no significant effect on k_{cat}/K_{O2} using choline as substrate. Both the k_{cat}/K_m and k_{cat} values increased with increasing pH to limiting values at high pH consistent with the participation of an unprotonated group in the reductive half-reaction and the overall turnover of the enzyme. The pH independence of both $^D(k_{cat}/K_m)$ and $^Dk_{cat}$, with average values of 9.2 ± 3.3 and 7.4 ± 0.5, respectively, is consistent with absence of external forward and reverse commitments to catalysis, and the chemical step of CH bond cleavage being rate-limiting for both the reductive half-reaction and the overall enzyme turnover. Temperature dependence of the

$^{\text{D}}k_{\text{red}}$ values suggests disruption of the preorganization in the asparagine variant enzyme. Altogether, the data presented in this study are consistent with the FAD-histidyl covalent linkage being important for the optimal positioning of the hydride ion donor and acceptor in the tunneling reaction catalyzed by choline oxidase.

2.2. Introduction

A number of enzymes including dehydrogenases (*1-3*), monooxygenases (*4-7*), halogenases (*8-11*) and oxidases (*7,12,13*) employ flavin cofactors (FAD or FMN) for their catalytic processes. About a tenth of all flavoproteins have been shown to contain covalently attached cofactor which may be linked at the C8M position via histidyl, tyrosyl or cysteinyl side chains, or at the C6M position via a cysteinyl side chain (*14*). Glucooligosaccharide oxidase (*15,16*), hexose oxidase (*17*) and berberine bridge enzyme (*18,19*) are examples of flavoproteins (FAD as cofactor) with both linkages present in one flavin molecule. The covalent linkages in flavin-dependent enzymes have been shown to stabilize protein structure (*20-22*), prevent loss of loosely bound flavin cofactors (*23*), modulate the redox potential of the flavin microenvironment (*20,23-27*), facilitate electron transfer reactions (*28*), and contribute to substrate binding as in the case of the cysteinyl linkage (*20*). However, no study has implicated a mechanistic role of the flavin covalent linkages in enzymatic reactions in which a hydride ion is transferred by quantum mechanical tunneling.

The discovery of quantum mechanical tunneling in enzymatic reactions in which hydrogen atoms, protons, and hydride ions are transferred has attracted considerable interest in

enzyme studies geared towards understanding the mechanisms underlying the several orders of magnitudes in the rate enhancements of protein catalyzed reactions compared to non-enzymatic ones. Tunneling mechanisms have been shown in a wide array of cofactor-dependent enzymes including flavoenzymes. Examples of flavoenzymes in which the tunneling mechanism have been demonstrated include morphinone reductase (*29,30*), pentaerythritol tetranitrate (PETN) reductase (*29*), glucose oxidase (*31-33*) and choline oxidase (*34*). Mechanistic data on Class 2 dihydroorotate dehydrogenases, also with a flavin cofactor (FMN) covalently linked to the protein moiety (*35,36*), could only propose a mechanism that is either stepwise or concerted with significant quantum mechanical tunneling for the hydride transfer from C6 and the deprotonation at C5 in the oxidation of dihydroorotate to orotate (*37*). This leaves choline oxidase as the only characterized enzyme with a covalently attached flavin cofactor (*12,38*) where the oxidation of its substrate occurs unequivocally by quantum mechanical tunneling.

Choline oxidase from *Arthrobacter globiformis* catalyzes the two-step FAD-dependent oxidation of the primary alcohol substrate choline to glycine betaine with betaine aldehyde, which is predominantly bound to the enzyme and forms a gem-diol species, as intermediate (Scheme 2.1).
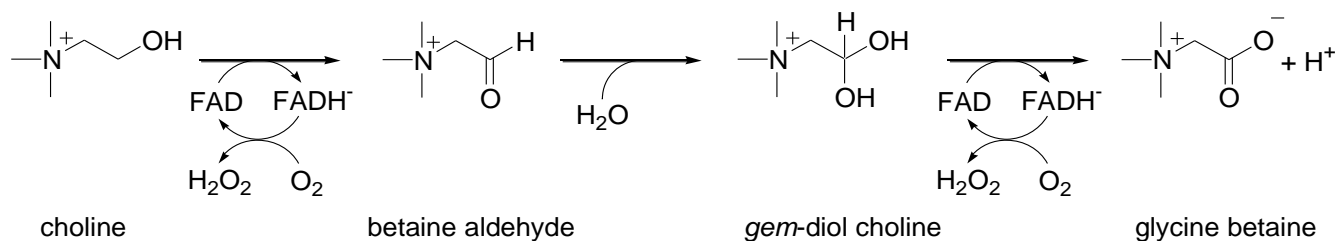
Scheme 2.1. Two-step, four-electron oxidation of choline catalyzed by choline oxidase.

Glycine betaine accumulates in the cytoplasm of plants and bacteria as a defensive mechanism against stress conditions, thus making genetic engineering of relevant plants of economic interest (*39-45*), and the biosynthetic pathway for the osmolyte being a potential drug target in human microbial infections of clinical interest (*46-48*). The first oxidation step catalyzed by choline oxidase involves the transfer of a hydride ion from a deprotonated choline to the protein bound flavin followed by reaction of the anionic flavin hydroquinone with molecular oxygen to regenerate the oxidized FAD (*for a recent review see 50*). The gem-diol choline, i.e. hydrated betaine aldehyde, is the substrate for the second oxidation step (*49*), suggesting that the reaction may follow a similar mechanism. The isoalloxazine ring of the flavin cofactor, which is buried within the protein, is physically constrained through a covalent linkage via the C(8) methyl of the flavin and the N(3) atom of the histidine side chain at position 99 (Figure 2.1) (*12*).
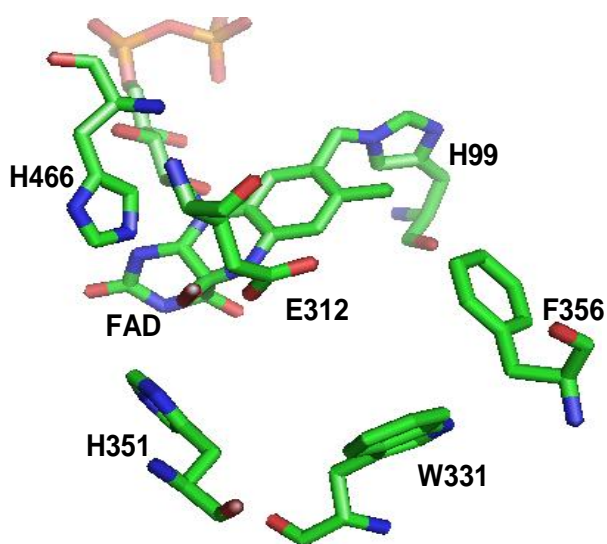
Figure 2.1. X-ray crystal structure of the active site of wild-type choline oxidase resolved to 1.86 Å (PDB 2jbv).
Note the significant distortion of the flavin ring at the C(4a) atom, which is due to the presence of a C(4a) adduct (*71*).

Also contributing to the physical constrain are the proximity of Ile103 to the pyrimidine ring and the interactions of the backbone atoms of residues H99 through Ile103 with the isoalloxazine ring. The rigid positioning of the isoalloxazine ring could only permit a solvent-excluded cavity of ~125 $Å^3$ adjacent to the re face of the FAD to accommodate a 93 $Å^3$ choline molecule in the substrate binding domain (*12*). Mechanistic data thus far obtained on choline oxidase, coupled with the crystal structure of the wild-type enzyme resolved to 1.86 Å, are consistent with a quantum tunneling mechanism for the hydride ion transfer occurring within a highly preorganized enzyme-substrate complex (Scheme 2.2) (*12,34,50*). Exploitation of the tunneling mechanism requires minimal independent movement of the hydride ion donor and acceptor, with the only dynamic motions permitted being the ones that promote the hydride transfer reaction.

In the present study, the contribution of the physically constrained flavin isoalloxazine ring to the reaction catalyzed by choline oxidase has been investigated in a variant enzyme in which the histidine residue at position 99 was replaced with an asparagine. The results suggest that although not being required per se the covalent linkage in choline oxidase contributes to the hydride tunneling reaction by either preventing independent movement or contributing to the optimal positioning of the flavin acting as hydride ion acceptor with respect to the alkoxide species acting as a donor, but however is not required for the reaction of the reduced flavin species with oxygen.
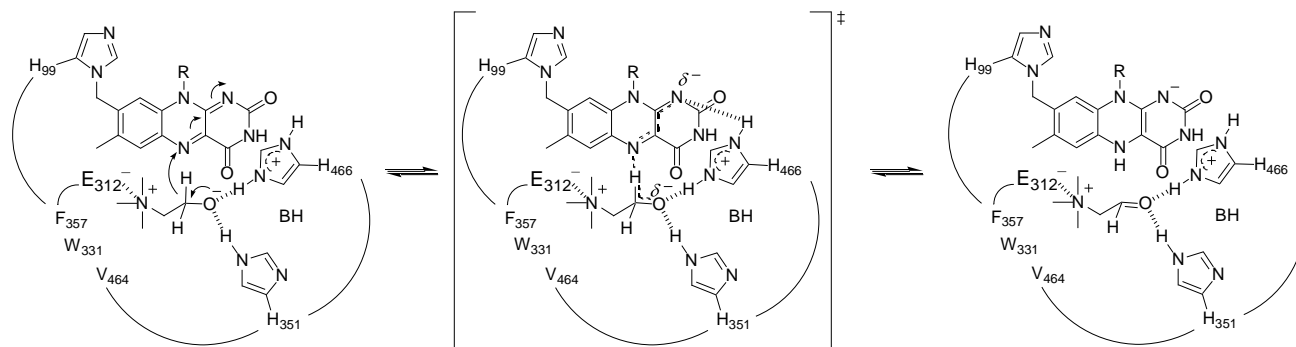
Scheme 2.2. The hydride ion transfer reaction from the α-carbon of the activated choline alkoxide species to the N(5) atom of the isoalloxazine ring of the enzyme-bound flavin in choline oxidase.

2.3. Experimental Procedures

Materials. Recombinant wild-type choline oxidase gene (pET/*codA*mg) in a permanent stock *Escherichia coli* strain XLI Blue was used as template for site-ditected mutagenesis. *E. coli* strain Rosetta (DE3)pLysS was from Novagen (Madison, WI). QIA prep Spin Miniprep kit was from Qiagen (Valencia, CA). QuickChange Site-directed mutagenesis kit was from Strategene (La Jolla, CA). Oligonucleotides for site-directed mutagenesis and sequencing of the mutant gene were from Sigma Genosys (The Woodlands, TX). Choline chloride was from ICN (Aurora, OH). 1,2-[^{2}H$_4$]-choline bromide was from Isotech Inc. (Miamisburg, OH). Glucose and glucose oxidase were from Sigma-Aldrich (St. Louis, MO). All other reagents used were of the highest purity commercially available.

Site-directed Mutagenesis, Expression and Purification of CHO-H99N. The mutant gene for the choline oxidase variant containing asparagine at position 99, CHO-H99N[1], was prepared using the pET/*codA*mg gene for the wild-type enzyme as template (*38*) with forward and reverse oligonucleotides as primers in site-directed mutagenesis. The site-directed mutagenesis was performed using the QuickChange kit, following the manufacturer's manual. Dimethylsulfoxide (2% final) was added to enhance separation of the template DNA upon denaturation. The mutation was confirmed by sequencing the resultant gene at the DNA Core Facility at Georgia State University using an Applied Biosystems Big Dye Kit on an Applied Biosystems model ABI377 DNA sequencer. The plasmid with the mutant gene (pET/*codA*mg H99N) was used to transform *E. coli* strain Rosetta(DE3)pLysS by electroporation and permanent stocks of the transformed cells prepared and stored at -80 $^{\circ}$C. The His99Asn variant of choline oxidase was expressed and purified to homogeneity with the incorporation of 10% glycerol throughout the purification procedures following the previously described purification protocol (*12,38,51*).

Biochemical Characterization of CHO-H99N. To determine whether the flavin cofactor in CHO-H99N was covalently attached to the protein, the variant enzyme was treated with 10% trichloroacetic acid (TCA) as previously described for CHO-E312D (*12*) with modifications. The extinction coefficient of the bound flavin in CHO-H99N was determined by concurrently treating free FAD with 10% TCA and subjecting the acidified free FAD to the same

---

[1]The abbreviation used is: CHO-H99N, choline oxidase variant enzyme in which histidine 99 was replaced with asparagine.

experimental conditions as the mutant enzyme. The extinction coefficient of the acidified free FAD was used as reference to determine the extinction coefficient of the CHO-H99N bound FAD.

Enzyme Assays. Enzyme activities of CHO-H99N were measured by the method of initial rates in 50 mM sodium phosphate or 50 mM sodium pyrophosphate as described previously for the wild type enzyme (*52*) by monitoring the rate of oxygen consumption with a computer-interfaced Oxy-32 oxygen monitoring system (Hansatech Instrument Inc.) at 25 $^{\circ}$C with choline or 1,2-[^{2}H$_4$]-choline as substrate.

Steady state kinetic parameters for CHO-H99N were determined at varying concentrations of choline (0.01 to 20 mM) and oxygen (0.2 to 1 mM) at pH 10. The desired oxygen concentration for each assay was obtained by bubbling the appropriate O_2/N_2 gas mixture for a minimum of 10 min to equilibrate the reaction mixture. pH profiles of the steady state kinetic parameters were obtained in the pH range from 6 to 11. All the enzyme assays for the pH profiles were conducted in 50 mM sodium pyrophosphate. Substrate kinetic isotope effect on the steady state kinetic parameters were determined by alternating varying concentrations of choline and 1,2-[^{2}H$_4$]-choline at atmospheric concentration of oxygen in the pH range of 6.5 and 10.5 at 0.5 pH unit intervals.

Rapid kinetics at varying concentrations of choline or 1,2-[^{2}H$_4$]-choline was carried out with a Hi-Tech SF-61 stopped-flow spectrophotometer thermostated from 10 to 28 $^{\circ}$C at approximately 2 $^{\circ}$C intervals. The rates of flavin reduction were monitored by measuring the decrease in absorbance at 450 nm upon mixing the oxidized enzyme with the organic substrate, both prepared in 50 mM sodium pyrophosphate, pH 9. The stopped-flow apparatus was

previously made anaerobic by treating with a mixture of glucose (5 mM) and glucose oxidase (~30 units/mL) in 100 mM sodium pyrophosphate, pH 6 overnight to scrub oxygen and rinsed with oxygen-free 50 mM sodium pyrophosphate, pH 9. The enzyme and substrate were made anaerobic as previously described (*53,54*). Equal volumes of CHO-H99N and choline (or 1,2-[^{2}H$_4$]-choline) were mixed anaerobically in the stopped-flow spectrophotometer resulting in a reaction mixture with a final enzyme concentration of ~10 µM and substrate concentrations of 0.05 to 10 mM, with each substrate concentration assayed in triplicate (differences in each set of three observed rates were less than 5%). The substrate isotopomers were alternated to determine the isotopic effect on the rate constant for flavin reduction at different temperatures.

Data Analysis. Data were fit with KaleidaGraph (Synergy Software, Reading, PA) and EnzFitter softwares (Biosoft, Cambridge, UK). Steady state kinetic parameters were determined by fitting the initial rates data to eq 1 which describes a sequential steady state kinetic mechanism where e represents the concentration of enzyme, k_{cat} is the turnover number of the enzyme at saturating substrates concentrations, and K_a and K_b represent the Michaelis constants for the organic substrate (A) and oxygen (B), respectively. The pH dependences of the steady state kinetic parameters were determined by fitting the initial rates data to eq 2, which describes a curve with a slope of + 1 and a plateau region at high pH, where C is the pH-independent value of the kinetic parameter. Stopped-flow traces were fit to eq 3, which describes a single exponential process, where k_{obs} represents the observed rate of flavin reduction, t is time, A_t is the value of absorbance at 450 nm at any given time, A is the amplitude for the total change in absorbance, and A_∞ is the absorbance at infinite time. Pre-steady state kinetic parameters were determined by fitting the observed rates data to eq 4, where k_{obs} is the observed rate for the

reduction of the enzyme bound flavin, k_{red} is the limiting rate of flavin reduction at saturating substrate concentrations and K_d is the dissociation constant for binding of the substrate to the enzyme. The temperature dependence of the rate of flavin reduction was determined by fitting the stopped-flow data with Eyring's equation (eq 5), where k_B is Boltzmann constant, h is Plank's constant, k_{red} is the limiting rate of flavin reduction at saturating substrate concentrations, R is gas constant, T is temperature, and $\Delta S^{\ddagger}$ and $\Delta H^{\ddagger}$ are the entropy and enthalpy of activations, respectively. The entropy of activation is calculated from the y-intercept and the enthalpy of activation is calculated from the slope of the Eyring plot. The temperature dependence of the kinetic isotope effect on the rate of flavin reduction was determined by fitting the data with Arrhenius equation (eq. 6), where KIE is the deuterium kinetic isotope effect on the rate of flavin reduction, A_H/A_D is the isotope effect on the preexponential factors and $[E_a(D)-E_a(H)]$ is the isotope effect on the energy of activation.

$$\frac{v}{e} = \frac{k_{cat}AB}{K_aB + K_bA + AB + K_{ia}K_b} \tag{1}$$

$$\log Y = \log \left[\frac{C}{1 + \dfrac{10^{-pH}}{10^{-pK_a}}} \right] \tag{2}$$

$$A_t = A_1 e^{-k_{obs1}t} + A_{\infty} \tag{3}$$

$$k_{obs} = \frac{k_{red}A}{K_d + A} \tag{4}$$

$$\ln(k_{red}/T) = \ln(k_B/h) + \Delta S^{\ddagger}/R - \Delta H^{\ddagger}/RT \tag{5}$$

$$\ln(KIE) = \ln[A_H/A_D] - [E_a(D) - E_a(H)/RT] \tag{6}$$

2.4. Results

Purification and Biochemical Characterization of CHO-H99N. The choline oxidase variant in which histidine 99, which participates in a covalent linkage with the C8M atom of FAD, was replaced with asparagine was expressed and purified following the same protocol previously described for wild-type choline oxidase (*38*) with the addition of 10% glycerol to all the purification solutions. Unlike the wild-type (*38,51,55*) and other choline oxidase variant enzymes (*12,56,57*) which contain a mixture of oxidized flavin and air-stable, anionic flavosemiquinone upon purification, the His99Asn mutant enzyme was purified with the bound flavin cofactor in the fully oxidized state, as indicated by the UV-visible absorbance spectrum showing absorbance maxima at 390 and 450 nm (Figure A2.1). The UV-visible absorbance spectrum of the supernatant after treatment of the variant enzyme with 10% TCA and centrifugation to remove partially denatured protein showed the presence of FAD, consistent with the flavin cofactor not being covalently bound to the protein upon substituting histidine 99 with asparagine. An extinction coefficient of 13.9 mM^{-1}cm^{-1} was determined at 450 nm for CHO-H99N, as compared to 11.4 mM^{-1}cm^{-1} for the wild-type choline oxidase (*55*). The steady state kinetic parameters with choline as substrate for CHO-H99N under atmospheric oxygen conditions are shown in Table 2.1, along with the parameters previously determined for the wild-type enzyme. Both the $^{app}k_{cat}$ and $^{app}(k_{cat}/K_m)$ values, as well as the specific activity of the mutant enzyme were significantly lower than in the wild-type enzyme, suggesting that protein flavinylation is important for the alcohol oxidation reaction catalyzed by choline oxidase.

Table 2.1. Comparison of specific activities and apparent steady state kinetic parameters of CHO-H99N with wild-type choline oxidase[a]

Enzyme	Specific Activity (U/mg)	$^{app}(k_{cat}/K_m)$ ($M^{-1}s^{-1}$)	$^{app}k_{cat}$ (s^{-1})	$^{app}K_m$ (mM)
CHO-H99N	0.28	790	1.03	1.30
CHO-WT[b]	8.0	25,000	15.0	0.60

[a]Total protein amounts were determined by the Bradford method (*70*). Specific activity was measured in atmospheric oxygen with 10 mM choline as substrate in 50 mM potassium phosphate, pH 7 and 25 °C. For the kinetic parameters, the enzymatic activities were measured at varying concentrations of choline in the range from 0.005 to 10 mM, in 50 mM potassium phosphate, pH 7 and 25 °C, using fully oxidized enzymes. [b]Data are from (*12*).

Steady State Kinetic Mechanism. The steady state kinetic parameters for the asparagine 99 mutant enzyme were determined at pH 10 and 25 °C by measuring the initial rate of oxygen consumption at varying concentrations of choline and oxygen. The data were best fit with the sequential steady state kinetic equation (eq 1), suggesting that replacement of histidine 99 with asparagine does not alter the order of substrate binding and product release with respect to the wild-type enzyme. CHO-H99N catalyzes the oxidation of choline to glycine betaine with a 10-fold decrease in the k_{cat}/K_m value, a 30-fold decrease in the k_{cat} value, but with no significant difference in the k_{cat}/K_{O2} value (Table 2.2).

Table 2.2. Comparison of steady-state kinetic parameters for CHO-H99N and wild-type choline oxidase with choline as substrate

kinetic parameters	CHO-H99N	CHO-WT[a]
k_{cat}, s^{-1}	1.86 ± 0.01	60 ± 1
k_{cat}/K_m, $M^{-1}s^{-1}$	$22,360 \pm 780$	$237,000 \pm 9000$
K_m, mM	0.08 ± 0.01	0.25 ± 0.01
K_{O2}, mM	0.015 ± 0.001	0.69 ± 0.03
k_{cat}/K_{O2}, $M^{-1}s^{-1}$	$123,730 \pm 4,400$	$86,400 \pm 3600$
$^D(k_{cat}/K_m)$[b]	9.2 ± 3.3	10.7 ± 2.6
$^Dk_{cat}$[b]	7.4 ± 0.5	7.3 ± 1.0

Steady-state kinetic parameters were determined at varying concentrations of choline and oxygen in 50 mM sodium pyrophosphate, pH 10 and 25 °C. [a]Data are from (*52*). [b]The pH-independent values are reported here.

These kinetic data suggest that the covalent linkage between His99 N(3) and the FAD C8M atom is important for the reductive half-reaction and the overall turnover of the enzyme, but it is not involved in the reaction of the reduced flavin with oxygen.

Effect of pH on the Reductive and Oxidative Half-Reactions. The pH profiles of the steady state kinetic parameters for CHO-H99N were carried out in the pH range from 6 to 11 at 25 $^{\circ}$C at varying concentrations of both choline and oxygen. The k_{cat}/K_m and k_{cat} values increased with increasing pH to limiting values at high pH (Figure 2.2), consistent with the requirement of an unprotonated group for catalysis in both the reductive half-reaction and the overall turnover of the variant enzyme. Apparent pK_a values of 8.2 ± 0.1 and 7.1 ± 0.1 were determined from the k_{cat}/K_m and k_{cat} pH profiles, respectively (Figure 2.2 and Table A2.1). There was no pH effect on the k_{cat}/K_{O2} values with an average pH-independent limiting value of 82,500 ± 32,000 M^{-1}s^{-1} in the pH range from 7 to 11 (Figure 2.2 and Table A2.1). This value is not significantly different from the pH-independent value of 86,400 M^{-1}s^{-1} that was previously reported for the wild-type enzyme (*34*), consistent with the oxidative half-reaction not being affected in the CHO-H99N variant enzyme. An average K_{O2} value of 24 μM was estimated in the pH range experimented (Table A2.1), indicating that the His99Asn enzyme is at least 90% saturated with oxygen when the initial rates of reaction are measured at atmospheric oxygen concentrations, i.e., 250 μM.
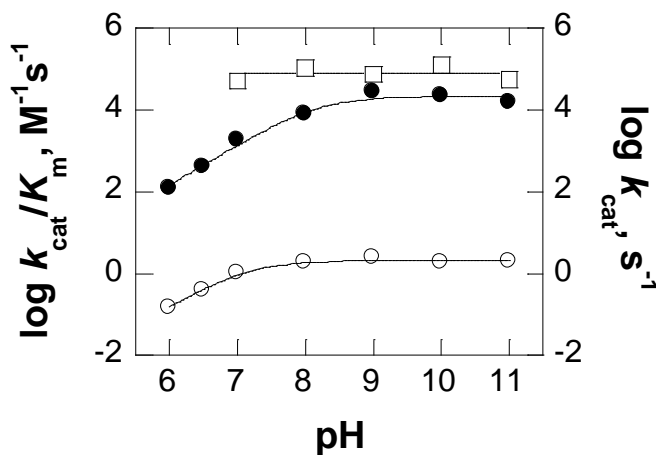
Figure 2.2. pH dependence of the k_{cat}/K_m (●), k_{cat}/K_{oxygen} (□), and k_{cat} (○) values for CHO-H99N with choline as substrates at 25 °C.
Enzymatic activities were measured at varying concentrations of choline (0.01 to 20 mM) and oxygen (0.2 to 1 mM). Data for k_{cat}/K_m and k_{cat} were fit to eqn. 2, and data for k_{cat}/K_{oxygen} were fit to y = 4.9.

Substrate Kinetic Isotope Effects. The substrate kinetic isotope effects on the k_{cat}/K_m and k_{cat} values were determined with 1,2-[^{2}H$_4$]-choline at 25 °C under air-saturated buffer conditions, ensuring at least 90 % saturation of the enzyme with oxygen due to the low K_{O2} values (*vide supra*). The k_{cat}/K_m values for both choline and 1,2-[^{2}H$_4$]-choline yielded similar pK_a values of 8.4 ± 0.1 (Figure A2.2) and resulted in a pH-independent $^D(k_{cat}/K_m)$ value of 9.2 ± 3.3 (Figure 2.3) in the pH range of 6.5 and 10.5. These results are consistent with the pK_a value of ~8.4 being the thermodynamic pK_a for the unprotonated group that participates in the reductive half-reaction catalyzed by the enzyme, and with lack of external forward and reverse commitments to catalysis (*58-60*). The pH-dependence of the k_{cat} values for both choline and 1,2-[^{2}H$_4$]-choline also yielded similar pK_a values of ≤7.0 (Figure A2.2), resulting in a pH-independent $^Dk_{cat}$ value of 7.4 ± 0.5 (Figure 2.3). The kinetic data for the pH dependence of the kinetic isotope effects of CHO-H99N are summarized in Table A2.2.
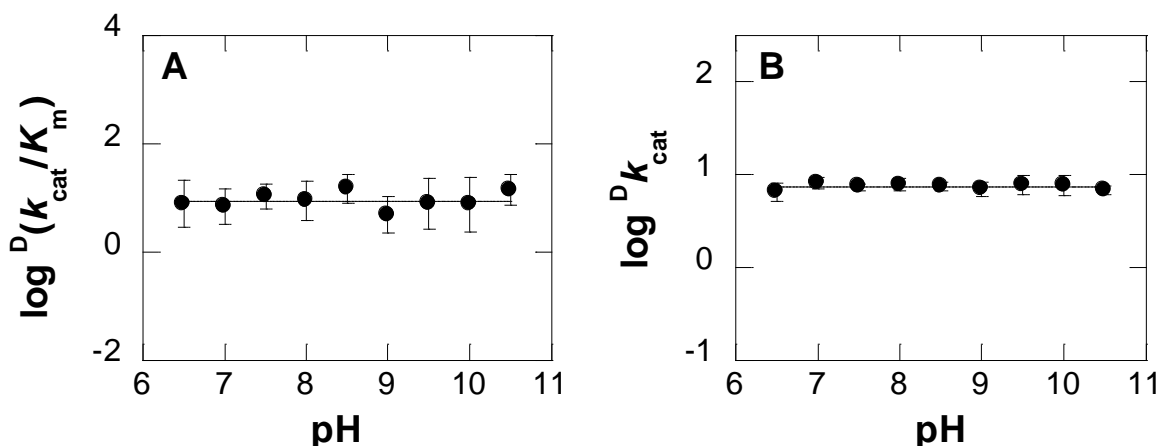
Figure 2.3. pH dependence of the $^D(k_{cat}/K_m)$ and $^Dk_{cat}$ values for CHO-H99N.
Data were fit to y = 0.94 in panel A and to y = 0.87 in panel B. Enzymatic activities were measured at varying concentrations of choline and 1,2-[^{2}H$_4$]-choline at saturating oxygen concentration under atmospheric conditions.

Effect of Temperature on the Rate Constant for Flavin Reduction. The effect of temperature on the rate constant for flavin reduction (k_{red}) and the associate kinetic isotope effects ($^Dk_{red}$) were investigated to probe the hydride transfer reaction catalyzed by CHO-H99N. The rates of flavin reduction were determined under anaerobic conditions at varying concentrations of choline or 1,2-[^{2}H$_4$]-choline from 10 to 28 ^{o}C in 50 mM sodium pyrophosphate, pH 9, using a stopped-flow spectrophotometer. The limited range of temperatures stems from the instability of the CHO-H99N enzyme at temperatures $\geq$ 30 ^{o}C over the prolonged times required for data acquisition. All the stopped-flow traces showed single exponential processes of flavin reduction with both choline and 1,2-[^{2}H$_4$]-choline, as illustrated in Figure 2.4 for the traces at 16 ^{o}C with 10 mM choline (a) and 1,2-[^{2}H$_4$]-choline (b). In all cases, the UV-visible absorbance spectrum of the reduced flavin showed a well-defined maximum at 365 nm, consistent with the presence of the anionic hydroquinone species at the end of the reduction reaction (Figure 2.4 illustrates the data at 16 ^{o}C). The observed rates of flavin reduction were fit to eq 4 to obtain the k_{red} values for choline and 1,2-[^{2}H$_4$]-choline, and the

associated kinetic isotope effects (Figure 2.4 for the data at 16 $^{\circ}$C, and Figure A2.3 for all other temperatures). The k_{red} and $^Dk_{red}$ values obtained in the temperature range from 10 to 28 $^{\circ}$C are summarized in Table A2.3.
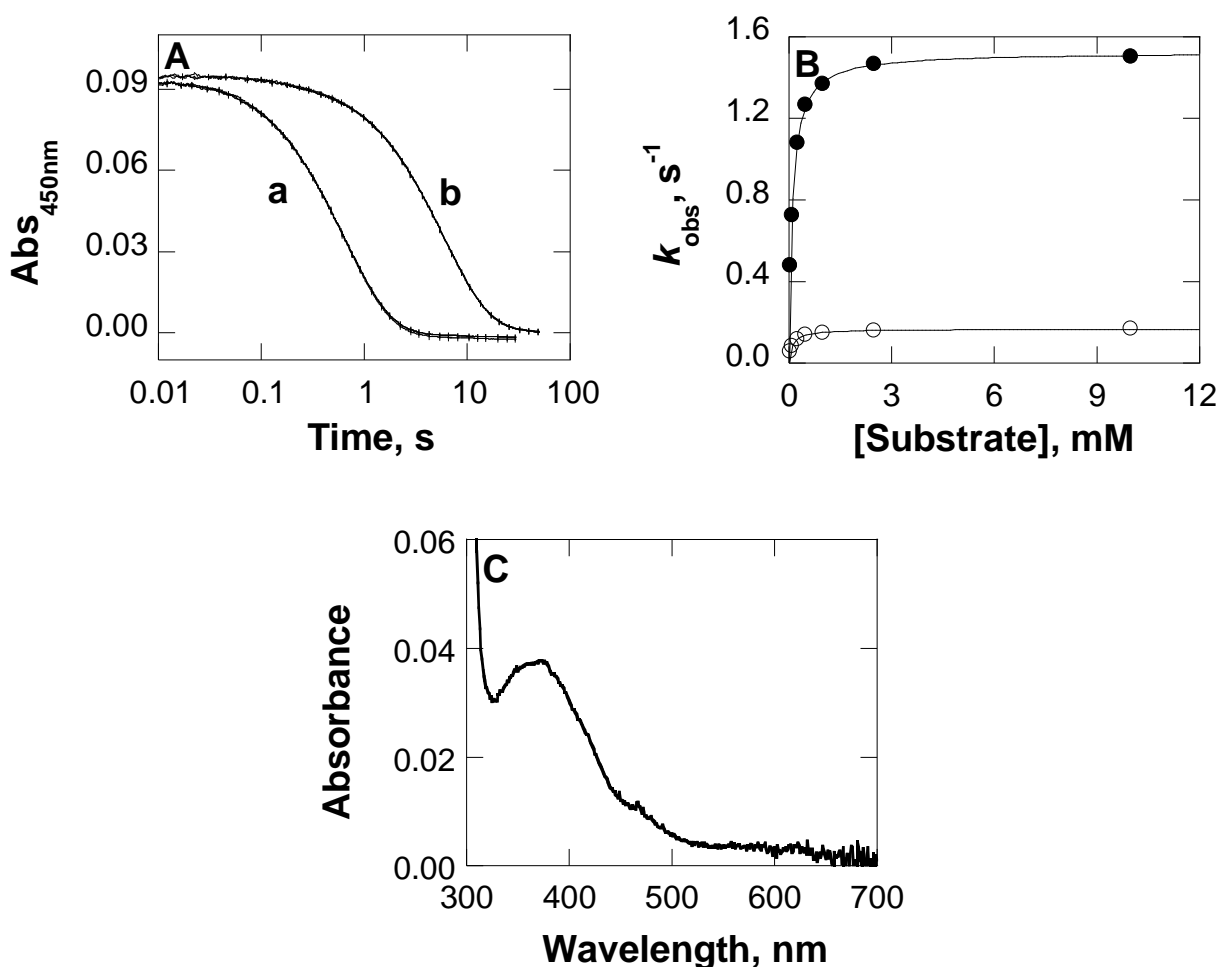
Figure 2.4. Anaerobic reductions of CHO-H99N with choline and 1,2-[^{2}H$_4$]-choline at 16.1 $^{\circ}$C and pH 9.0.
(**A**) Stopped-flow traces for choline (a) and 1,2-[^{2}H$_4$]-choline (b) at 10 mM substrate concentration. Data were fit to eq 5. Time indicated is after the end of flow, i.e., 2.2 ms. (**B**) Rates of flavin reduction as a function of substrate concentration with choline (●) and 1,2-[^{2}H$_4$]-choline (○). Data were fit to equation 6. (**C**) UV-visible absorbance spectrum of reduced flavin bound to CHO-H99N after mixing with 10 mM choline.

The k_{red} values for choline and 1,2-[^{2}H$_4$]-choline increased monotonically with increasing temperature yielding different slopes (Figure 2.5), as analyzed according to Eyring's theory. This resulted in a temperature-dependence of the $^D k_{red}$ values (Figure 2.5), with values ranging from 8.05 ± 0.13 at 28 ^{o}C to 9.17 ± 0.12 at 10 ^{o}C. Different enthalpies of activation ($\Delta H^{\ddagger}$) were determined for the cleavages of the CH and CD bonds (Table 2.3). A large isotope effect with a finite value was determined for the energy of activation for the reaction ($\Delta E_a = (E_a)_H - (E_a)_D$) (Table 2.3). Finally, a value that was close to unity was estimated for the isotope effect on the preexponential factors (A$_H$'/A$_D$') calculated from the ratio of the y-intercepts of the temperature-dependent Eyring's plots for choline and 1,2-[^{2}H$_4$]-choline (Table 2.3). All taken together, these thermodynamic data indicate that the hydride transfer reaction in the His99Asn enzyme is significantly different from that of the wild-type enzyme for which previous results showed a large and temperature-independent kinetic isotope effect on the reductive half-reaction, similar $\Delta H^{\ddagger}$ values for the cleavage of the CH and CD bonds of choline, a negligible ΔE_a value, and a large A$_H$'/A$_D$' ratio (Table 2.3).

2.5. Discussion

Previous studies established that the reaction of alcohol oxidation in choline oxidase occurs through the transfer of a hydride ion from the α-carbon of choline alkoxide to the N(5) atom of the FAD cofactor within a highly preorganized enzyme-substrate complex (*for a recent review see 50*). In such a preorganized complex, the activated alcohol substrate and the isoalloxazine of the flavin are allowed minimal independent movement because the former establishes electrostatic interactions at its opposite ends with the charged residues Glu312 and

His466 and the latter is rigidly positioned by way of a covalent linkage (Figure 2.1) to the protein moiety and several interactions with backbone atoms of amino acid residues at positions 100 to 103. In this study, the contribution of the covalent linkage between the C8M of the flavin and the N(3) atom of the histidine side chain at position 99 to the alcohol oxidation reaction in choline oxidase have been investigated using a variant form of the enzyme in which the histidine residue was replaced with an asparagine. In common with the wild-type enzyme, the histidine to asparagine variant form of choline oxidase displayed a steady state kinetic mechanism with oxygen reacting with the reduced flavin before release of the organic product of the reaction, the requirement of an unprotonated group acting as a base in the reductive half-reaction of choline oxidation, the chemical step of CH bond cleavage being rate-limiting in both the reductive half-reaction and the overall enzyme turnover, and the lack of observable ionizable groups that participate in the oxidative half-reaction in which the reduced flavin reacts with oxygen. These data collectively suggest that the enzyme containing asparagine at position 99 maintains an overall integrity that is similar to that of the wild-type enzyme, and thereby mechanistic differences between the two enzymes can be attributed to the presence or absence of the covalent flavin attachment to the protein. This conclusion is strongly reinforced by the observation that the second-order rate constant for reaction of the reduced flavin with oxygen (k_{cat}/K_{oxygen}) is essentially the same with values of ~85,000 $M^{-1}s^{-1}$ in the mutant and wild-type enzymes, since one would expect such a critical reaction of flavin oxidation to occur at significantly different rates had the protein integrity of the mutant enzyme been different from that of the wild-type enzyme.
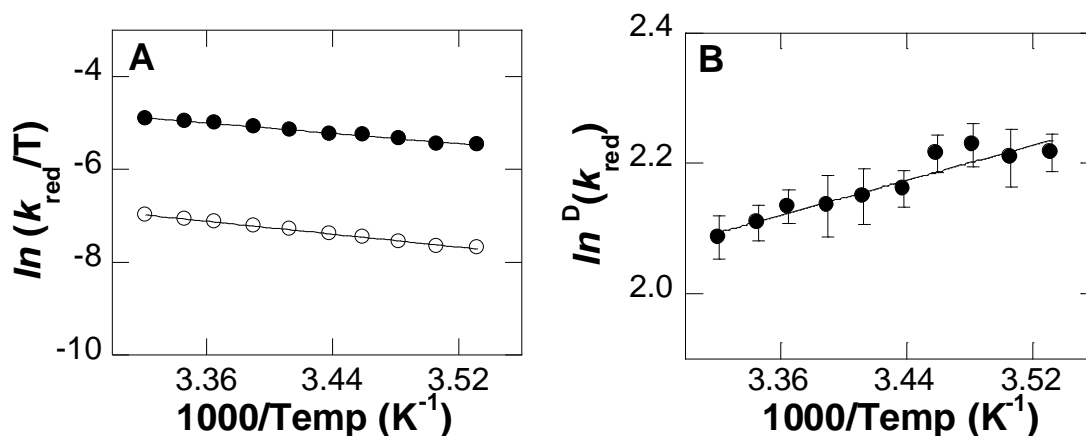
Figure 2.5. Temperature dependence of the k_{red} and $^D(k_{red})$ values for CHO-H99N with choline or 1,2-[^{2}H$_4$]-choline from 10 to 28 °C.
(A) Eyring plot of the k_{red} values versus temperature with choline (●) and 1,2-[^{2}H$_4$]-choline (○) as substrate. Data were fit to equation 7. Standard deviations associated with the measurements are ≤5% of the measured value. **(B)** Arrhenius plot of the $^D(k_{red})$ values versus temperature. Data were fit to equation 8.

Table 2.3. Comparison of the thermodynamic parameters for the reductive half-reactions catalyzed by the His99Asn and wild-type choline oxidase.

parameter	CHO-H99N[a] (k_{red})	CHO-WT[b] (k_{cat}/K_m)
$\Delta H^{\ddagger}_H$[c], kJ mol^{-1}	23 ± 1	18 ± 2
$\Delta H^{\ddagger}_D$[c], kJ mol^{-1}	29 ± 1	18 ± 5
$-T\Delta S^{\ddagger}_H$, kJ mol^{-1}	44 ± 4	24 ± 2
$-T\Delta S^{\ddagger}_D$, kJ mol^{-1}	44 ± 3	30 ± 5
$\Delta S^{\ddagger}_H$[d], kJ K^{-1}mol^{-1}	0.15 ± 0.01	0.08 ± 0.01
$\Delta S^{\ddagger}_D$[d], kJ K^{-1}mol^{-1}	0.15 ± 0.01	0.10 ± 0.02
$\Delta G^{\ddagger}_H$[d], kJ mol^{-1}	67 ± 4	42 ± 3
$\Delta G^{\ddagger}_D$[d], kJ mol^{-1}	73 ± 3	48 ± 7
ΔE_a, kJ mol^{-1}	6 ± 1	0.4 ± 4.2
A_H'/A_D'[e]	0.9 ± 0.1	14 ± 3
KIE[f]	T-dependent	T-independent

[a]Conditions: Rates of flavin reduction were measured in 50 mM sodium pyrophosphate, pH 9.0, at different temperatures under anaerobic conditions. [b]Data are from (*34*). [c]Data were calculated by using the Eyring equation (eq 7). [d]Data for 25 °C. [e]A_H'/A_D' is the ratio of the y-intercepts obtained by fitting the kinetic data with choline and 1,2-[^{2}H$_4$]-choline to the Eyring equation (eq 7). [f]KIE is the substrate kinetic isotope effect associated with the cleavage of the CH and CD bonds of choline in the reaction catalyzed y choline oxidase.

The FAD C8M covalent linkage with histidine 99 in choline oxidase is important for the reductive half-reaction in which choline is oxidized to betaine aldehyde with concomitant hydride ion transfer to the flavin, but is not involved in the oxidative half-reaction in which the flavin is oxidized with concomitant formation of hydrogen peroxide. Evidence supporting the importance of the covalent linkage to the hydride transfer reaction is the ~45-fold decrease in the rate constant for anaerobic flavin reduction (k_{red}) with choline as substrate at 25 °C with respect to the wild-type enzyme, along with the 10-fold and 30-fold decreases in the k_{cat}/K_m and k_{cat} values with choline as substrate, and the lack of significant changes in the k_{cat}/K_{oxygen} value for the His99Asn enzyme as compared to the wild-type form of choline oxidase at pH 10 and 25 °C. Similar results were observed upon replacing either one of the other two histidine residues that are located in the active site of choline oxidase, namely His351 (*54*) and His466 (*53*). Thus, while His99 (*vide infra*), His351, and His466 participate with different roles in the oxidation of choline to yield betaine aldehyde, none of them provide the electrostatic stabilization that has been shown in glucose oxidase (*61,62*) to be required for the reaction of flavin oxidation. In this regard, previous results with a substrate analog devoid of positive charge demonstrated that it is the positive charge harbored on the trimethylamine group of the enzyme-bound betaine aldehyde that plays an important role for oxygen reactivity in choline oxidase (*49,51*). In agreement with the lack of involvement of ionizable groups in the oxidative half-reaction is the observation that no pK_a values in the range between 7.0 and 11.0 were detected in the pH profile of the k_{cat}/K_{oxygen} value with the His99Asn enzyme, as also was previously reported for the His351Ala and His466Ala forms of choline oxidase (*56,57*).

The FAD-histidyl covalent linkage is important for the optimal positioning of the flavin in the enzyme-alkoxide complex that is required for the environmentally assisted tunneling of the

hydride ion in the reaction catalyzed by choline oxidase. Evidence for this conclusion comes from the comparison of the effects of temperature on the rates of anaerobic flavin reduction (k_{red}) and the related kinetic isotope effects ($^D k_{red}$) determined with a stopped-flow spectrophotometer for the His99Asn enzyme (*this study*) and the wild-type form of choline oxidase (*34*). Indeed, the reaction of hydride ion transfer in the wild-type enzyme with the flavin covalently attached to the protein has been previously shown to occur via quantum mechanical tunneling within a highly preorganized active site environment (*34,63*). Such a mechanism of hydride ion transfer is manifested mechanistically in the large kinetic isotope effects on the Eyring preexponential factors (A_H'/A_D'), temperature-independent substrate kinetic isotope effects, negligible isotope effects on the energies of activation ($\Delta E_a = (E_a)_H-(E_a)_D$), and finite and indistinguishable enthalpies of activation ($\Delta H^{\ddagger}$) for protium and deuterium transfers (*34,63*). In contrast, the reaction of hydride ion transfer in the His99Asn enzyme with the flavin non-covalently attached to the protein requires significant sampling of the reactive configuration that is conducive to the tunneling reaction, as shown by the A_H'/A_D' ratio not being significantly different from unity, the large value for the ΔE_a with protium and deuterium, the effect of temperature on the $^D k_{red}$ values with 1,2-[^{2}H$_4$]-choline, and the different $\Delta H^{\ddagger}$ values for the cleavage of the CH and CD bonds of the substrate (*64*) (Table 2.3). Such a drastic change in the mechanism of hydride transfer most likely arises from either an increased conformational freedom or a rearrangement of the position of the flavin isoalloxazine ring acting as the hydride ion acceptor with respect to the choline alkoxide acting as the hydride donor, which necessarily results from the lack of the flavin covalent attachment to the protein moiety[2]. This, in turn, establishes that the covalent linkage in

---

[2]In principle, the thermodynamic parameters of Table 3 that are associated with the hydride

flavin-dependent enzymes, besides stabilizing protein structure (*20-22*), preventing the loss of loosely bound flavin cofactors (*23*), modulating the redox potential of the flavin (*20,23-27*), and facilitating electron transfer reactions (*28*) as amply demonstrated from studies of enzymes other than choline oxidase, may also be important for the optimal positioning of the flavin in those enzymes where hydride ions are transferred through tunneling mechanisms.

The chemical step of hydride ion transfer is rate limiting in the reaction of alcohol oxidation catalyzed by the choline oxidase form with the non-covalently attached flavin. This conclusion stems from the large and pH-independent substrate kinetic isotope effects on the reductive half-reaction (k_{cat}/K_m) and the overall turnover (k_{cat}) of the His99Asn variant enzyme with 1,2-[^{2}H$_4$]-choline as substrate under steady state conditions. The enzyme with the non-covalent flavin is similar to the wild-type enzyme containing covalent flavin, in that the wild-type enzyme was also previously shown to lack external forward and reverse commitments to catalysis (52,65). Independent evidence supporting the lack of commitments to catalysis in the Asn99 variant enzyme is the lack of perturbation in the kinetic pK_a value of 8.4 ± 0.1 determined

transfer reaction catalyzed by the His99Asn enzyme do not rule out *per se* the alternate possibility that the reaction occurs with a classical over-the-barrier transition state without the involvement of tunneling (*67,68*). While the distinction between these alternate mechanisms is currently under investigation using pressure effects, the conclusion that the removal of the covalent attachment of the flavin to the protein promotes the disruption of the enzyme-substrate preorganization is valid irrespective of mechanism of reaction in the enzyme containing non-covalent flavin.

in the pH-profile for the k_{cat}/K_m value when choline is substituted with 1,2-[^{2}H$_4$]-choline as substrate. Indeed, for a substrate such as   1,2-[^{2}H$_4$]-choline that is about 9-fold slower than choline, a ΔpK_a of up to one would be expected if the CH bond cleavage were not fully rate-limiting in the reductive half-reaction where choline is oxidized to betaine aldehyde (*66*).

Although His99 is not the active site base that participates in catalysis by abstracting the hydroxyl proton of choline to activate the substrate for the hydride transfer to the flavin, it is important for the overall polarity of the active site. Evidence for these conclusions comes from the pH-profiles of the steady state kinetic parameters k_{cat}/K_m and k_{cat} showing that an unprotonated group with thermodynamic pK_a value of 8.2 to 8.4 is required for catalysis in the His99Asn enzyme, as was previously established for the wild-type enzyme where the thermodynamic pK_a value was ~7.5 (*52,65*). In this respect, the His99Asn enzyme behaves in a fashion similar to that displayed in choline oxidase variants where the other two active site histidine residues were each replaced with alanine. In those cases, a catalytic base was shown to be required for the reductive half-reaction with thermodynamic pK_a values of ~8.0 for the His351Ala enzyme (*57*) and 9.0 for the His466Ala enzyme (*56*). Consequently, it appears that all of the histidine residues located in the active site of choline oxidase modulate to different extents the polarity of the active site, which is essential for the efficient transfer of the hydroxyl proton of the alcohol substrate to an as yet unidentified base in the active site of the enzyme that triggers the subsequent hydride transfer reaction in which choline is oxidized.

The histidyl covalent attachment of the flavin to the protein moiety is required for the unusual stabilization of the anionic flavosemiquinone of choline oxidase towards molecular oxygen. Indeed, the wild-type form of choline oxidase is purified with the enzyme-bound flavin as a mixture of oxidized and anionic flavosemiquinone (*38,51,55*) and extensive incubation at

pH 6.0 is necessary to fully oxidize the flavin (*55*). In contrast, throughout the purification process of the His99Asn enzyme the enzyme-bound flavin is fully oxidized. Thus far this is the first instance among several enzymatically active variants of choline oxidase where active site residues were selectively replaced with other amino acids, such as Glu312Ala, Glu312Asp, Glu312Gln (*12*), His351Ala (*57*), Val464Thr, Val464Ala (*53*), and His466Ala[3] (*56*), in which lack of air-stabilization of the flavosemiquinone has been observed. While this results suggest an important role for protein flavinylation in the lack of reactivity of the semiquinone with oxygen, more studies will have to be carried out in order to elucidate the mechanism at a molecular level.

In conclusion, the results of the mechanistic study on the variant form of choline oxidase in which the covalent linkage between the isoalloxazine ring of the FAD and the histidine residue at position 99 is removed show the importance of the flavin C8M to N(3) histidyl linkage for the optimal positioning of the flavin in the reaction of alcohol oxidation catalyzed by the enzyme. While the enzyme with non-covalent flavin maintains mechanistic properties that are similar to those of the wild-type enzyme with covalently attached flavin, the highly preorganized active site configuration that is required for the tunneling of the hydride ion is disrupted through the lack of a covalent linkage of the flavin to the protein. This study thereby shows that protein

---

[3]The enzyme variant where the protonated histidine 466 that is located in proximity of the N(1)-C(2) locus of the enzyme-bound flavin of choline oxidase is replaced with aspartate is the only reported case thus far where the flavosemiquinone is not stabilized (*69*). However, this is due to the positioning of a negatively charged residue such as aspartate close to the N(1)-C(2) atoms of FAD, which prevents the stabilization of the negative charge that should localize in this region of the flavin upon single electron reduction from the oxidized state.

flavinylation, besides stabilizing protein structure, preventing the loss of loosely bound flavin cofactors, modulating the redox properties of the flavin, may also be important for the optimal positioning of the flavin for those hydride transfer reactions that utilize tunneling.

Supplemental Information Available. Figure A2.1 shows the UV visible absorbance spectrum of fully oxidized FAD for CHO-H99N. Figure A2.2 shows the pH dependence of the k_{cat}/K_m and k_{cat} values for CHO-H99N with choline and $1,2\text{-}[^2H_4]$-choline as substrates at 25 ^{o}C. Figure A2.3 shows the rate of flavin reduction for CHO-H99N as a function of choline or $1,2\text{-}[^2H_4]$-choline concentrations from 10 to 14 ^{o}C and from 18 to 28 ^{o}C. Table A2.1 shows the kinetic parameters for CHO-H99N from pH 6 to 11 with choline as substrate. Table A2.2 shows the kinetic parameters and kinetic isotope effect for CHO-H99N from pH 6.5 to 10.5. Table A2.3 shows temperature dependence of the pre-steady state kinetic parameters with choline and $1,2\text{-}[^2H_4]$-choline as substrates.

2.6. References

1.   Malmquist, N. A., Gujjar, R., Rathod, P. K., and Phillips, M. A. (2008) Analysis of flavin oxidation and electron-transfer inhibition in *Plasmodium falciparum* dihydroorotate dehydrogenase, *Biochemistry 47*, 2466-2475.

2.   Sygmund, C., Kittl, R., Volc, J., Halada, P., Kubatova, E., Haltrich, D., and Peterbauer, C. K. (2008) Characterization of pyranose dehydrogenase from *Agaricus meleagris* and its application in the C-2 specific conversion of D-galactose, *J. Biotechnol. 133*, 334-342.

3.   Zamocky, M., Ludwig, R., Peterbauer, C., Hallberg, B. M., Divne, C., Nicholls, P., and Haltrich, D. (2006) Cellobiose dehydrogenase--a flavocytochrome from wood-degrading, phytopathogenic and saprotropic fungi, *Curr. Protein Pept. Sci. 7*, 255-280.

4.   van Berkel, W. J., Kamerbeek, N. M., and Fraaije, M. W. (2006) Flavoprotein monooxygenases, a diverse class of oxidative biocatalysts, *J. Biotechnol. 124*, 670-689.

5.   Ballou, D. P., Entsch, B., and Cole, L. J. (2005) Dynamics involved in catalysis by single-component and two-component flavin-dependent aromatic hydroxylases, *Biochem. Biophys. Res. Commun. 338*, 590-598.

6.   Ziegler, D. M. (2002) An overview of the mechanism, substrate specificities, and structure of FMOs, *Drug Metab. Rev. 34*, 503-511.

7.   Joosten, V., and van Berkel, W. J. (2007) Flavoenzymes, *Curr. Opin. Chem. Biol. 11*, 195-202.

8.   Keller, S., Wage, T., Hohaus, K., Holzer, M., Eichhorn, E., and van Pee, K. H. (2000) Purification and Partial Characterization of Tryptophan 7-Halogenase (PrnA) from *Pseudomonas fluorescens*, *Angew. Chem. Int. Ed. Engl. 39*, 2300-2302.

9.   Dong, C., Flecks, S., Unversucht, S., Haupt, C., van Pee, K. H., and Naismith, J. H. (2005) Tryptophan 7-halogenase (PrnA) structure suggests a mechanism for regioselective chlorination, *Science 309*, 2216-2219.

10. Chen, X., and van Pee, K. H. (2008) Catalytic mechanisms, basic roles, and biotechnological and environmental significance of halogenating enzymes, *Acta Biochim. Biophys. Sin. (Shanghai) 40*, 183-193.

11. van Pee, K. H., and Patallo, E. P. (2006) Flavin-dependent halogenases involved in secondary metabolism in bacteria, *Appl. Microbiol. Biotechnol. 70*, 631-641.

12. Quaye, O., Lountos, G. T., Fan, F., Orville, A. M., and Gadda, G. (2008) Role of Glu312 in binding and positioning of the substrate for the hydride transfer reaction in choline oxidase, *Biochemistry 47*, 243-256.

13. Wong, C. M., Wong, K. H., and Chen, X. D. (2008) Glucose oxidase: natural occurrence, function, properties and industrial applications, *Appl. Microbiol. Biotechnol. 78*, 927-938.

14. Mewies, M., McIntire, W. S., and Scrutton, N. S. (1998) Covalent attachment of flavin adenine dinucleotide (FAD) and flavin mononucleotide (FMN) to enzymes: the current state of affairs, *Protein Sci. 7*, 7-20.

15. Huang, C. H., Lai, W. L., Lee, M. H., Chen, C. J., Vasella, A., Tsai, Y. C., and Liaw, S. H. (2005) Crystal structure of glucooligosaccharide oxidase from *Acremonium strictum*: a novel flavinylation of 6-S-cysteinyl, 8alpha-N1-histidyl FAD, *J. Biol. Chem. 280*, 38831-38838.

16. Lee, M. H., Lai, W. L., Lin, S. F., Hsu, C. S., Liaw, S. H., and Tsai, Y. C. (2005) Structural characterization of glucooligosaccharide oxidase from *Acremonium strictum*, *Appl. Environ. Microbiol. 71*, 8881-8887.

17. Rand, T., Qvist, K. B., Walter, C. P., and Poulsen, C. H. (2006) Characterization of the flavin association in hexose oxidase from *Chondrus crispus*, *F.E.B.S. J. 273*, 2693-2703.

18. Winkler, A., Hartner, F., Kutchan, T. M., Glieder, A., and Macheroux, P. (2006) Biochemical evidence that berberine bridge enzyme belongs to a novel family of flavoproteins containing a bi-covalently attached FAD cofactor, *J. Biol. Chem. 281*, 21276-21285.

19. Winkler, A., Lyskowski, A., Riedl, S., Puhl, M., Kutchan, T. M., Macheroux, P., and Gruber, K. (2008) A concerted mechanism for berberine bridge enzyme, *Nat. Chem. Biol.*

20. Huang, C. H., Winkler, A., Chen, C. L., Lai, W. L., Tsai, Y. C., Macheroux, P., and Liaw, S. H. (2008) Functional Roles of the 6-S-Cysteinyl, 8{alpha}-N1-Histidyl FAD in Glucooligosaccharide Oxidase from *Acremonium strictum*, *J. Biol. Chem. 283*, 30990-30996.

21. Caldinelli, L., Iametti, S., Barbiroli, A., Fessas, D., Bonomi, F., Piubelli, L., Molla, G., and Pollegioni, L. (2008) Relevance of the flavin binding to the stability and folding of engineered cholesterol oxidase containing noncovalently bound FAD, *Protein Sci. 17*, 409-419.

22. Caldinelli, L., Iametti, S., Barbiroli, A., Bonomi, F., Fessas, D., Molla, G., Pilone, M. S., and Pollegioni, L. (2005) Dissecting the structural determinants of the stability of cholesterol oxidase containing covalently bound flavin, *J. Biol. Chem. 280*, 22572-22581.

23. Hassan-Abdallah, A., Zhao, G., and Jorns, M. S. (2006) Role of the covalent flavin linkage in monomeric sarcosine oxidase, *Biochemistry 45*, 9454-9462.

24. Heuts, D. P., Winter, R. T., Damsma, G. E., Janssen, D. B., and Fraaije, M. W. (2008) The role of double covalent flavin binding in chito-oligosaccharide oxidase from *Fusarium graminearum*, *Biochem. J. 413*, 175-183.

25. Winkler, A., Kutchan, T. M., and Macheroux, P. (2007) 6-S-cysteinylation of bi-covalently attached FAD in berberine bridge enzyme tunes the redox potential for optimal activity, *J. Biol. Chem. 282*, 24437-24443.

26. Motteran, L., Pilone, M. S., Molla, G., Ghisla, S., and Pollegioni, L. (2001) Cholesterol oxidase from *Brevibacterium sterolicum*. The relationship between covalent flavinylation and redox properties, *J. Biol. Chem. 276*, 18024-18030.

27. Fraaije, M. W., van den Heuvel, R. H., van Berkel, W. J., and Mattevi, A. (1999) Covalent flavinylation is essential for efficient redox catalysis in vanillyl-alcohol oxidase, *J. Biol. Chem. 274*, 35514-35520.

28. Kim, J., Fuller, J. H., Kuusk, V., Cunane, L., Chen, Z. W., Mathews, F. S., and McIntire, W. S. (1995) The cytochrome subunit is necessary for covalent FAD attachment to the flavoprotein subunit of *p*-cresol methylhydroxylase, *J. Biol. Chem. 270*, 31202-31209.

29. Basran, J., Harris, R. J., Sutcliffe, M. J., and Scrutton, N. S. (2003) H-tunneling in the multiple H-transfers of the catalytic cycle of morphinone reductase and in the reductive half-reaction of the homologous pentaerythritol tetranitrate reductase, *J. Biol. Chem. 278*, 43973-43982.

30. Pang, J., Hay, S., Scrutton, N. S., and Sutcliffe, M. J. (2008) Deep tunneling dominates the biologically important hydride transfer reaction from NADH to FMN in morphinone reductase, *J. Am. Chem. Soc. 130*, 7092-7097.

31. Kohen, A., Jonsson, T., and Klinman, J. P. (1997) Effects of protein glycosylation on catalysis: changes in hydrogen tunneling and enthalpy of activation in the glucose oxidase reaction, *Biochemistry 36*, 2603-2611.

32. Seymour, S. L., and Klinman, J. P. (2002) Comparison of rates and kinetic isotope effects using PEG-modified variants and glycoforms of glucose oxidase: the relationship of modification of the protein envelope to C-H activation and tunneling, *Biochemistry 41*, 8747-8758.

33. Nagel, Z. D., and Klinman, J. P. (2006) Tunneling and dynamics in enzymatic hydride transfer, *Chem. Rev. 106*, 3095-3118.

34. Fan, F., and Gadda, G. (2005) Oxygen- and temperature-dependent kinetic isotope effects in choline oxidase: correlating reversible hydride transfer with environmentally enhanced tunneling, *J. Am. Chem. Soc. 127*, 17954-17961.

35. Rowland, P., Nielsen, F. S., Jensen, K. F., and Larsen, S. (1997) The crystal structure of the flavin containing enzyme dihydroorotate dehydrogenase A from *Lactococcus lactis*, *Structure 5*, 239-252.

36. Rowland, P., Bjornberg, O., Nielsen, F. S., Jensen, K. F., and Larsen, S. (1998) The crystal structure of *Lactococcus lactis* dihydroorotate dehydrogenase A complexed with the enzyme reaction product throws light on its enzymatic function, *Protein Sci. 7*, 1269-1279.

37. Fagan, R. L., Nelson, M. N., Pagano, P. M., and Palfey, B. A. (2006) Mechanism of flavin reduction in class 2 dihydroorotate dehydrogenases, *Biochemistry 45*, 14926-14932.

38. Fan, F., Ghanem, M., and Gadda, G. (2004) Cloning, sequence analysis, and purification of choline oxidase from *Arthrobacter globiformis*: a bacterial enzyme involved in osmotic stress tolerance, *Arch. Biochem. Biophys. 421*, 149-158.

39. Quan, R., Shang, M., Zhang, H., Zhao, Y., and Zhang, J. (2004) Engineering of enhanced glycine betaine synthesis improves drought tolerance in maize, *Plant Biotechnol. J. 2*, 477-486.

40. Waditee, R., Bhuiyan, N. H., Hirata, E., Hibino, T., Tanaka, Y., Shikata, M., and Takabe, T. (2007) Metabolic engineering for betaine accumulation in microbes and plants, *J. Biol. Chem. 282*, 34185-34193.

41. Chen, T. H., and Murata, N. (2002) Enhancement of tolerance of abiotic stress by metabolic engineering of betaines and other compatible solutes, *Current opinion in plant biology 5*, 250-257.

42. Rontein, D., Basset, G., and Hanson, A. D. (2002) Metabolic engineering of osmoprotectant accumulation in plants, *Metabol. Eng. 4*, 49-56.

43. Sanchez-Aguayo, I., Rodriguez-Galan, J. M., Garcia, R., Torreblanca, J., and Pardo, J. M. (2004) Salt stress enhances xylem development and expression of S-adenosyl-L-methionine synthase in lignifying tissues of tomato plants, *Planta 220*, 278-285.

44. Shirasawa, K., Takabe, T., Takabe, T., and Kishitani, S. (2006) Accumulation of glycinebetaine in rice plants that overexpress choline monooxygenase from spinach and evaluation of their tolerance to abiotic stress, *Ann. Bot. 98*, 565-571.

45. Waditee, R., Bhuiyan, M. N., Rai, V., Aoki, K., Tanaka, Y., Hibino, T., Suzuki, S., Takano, J., Jagendorf, A. T., Takabe, T., and Takabe, T. (2005) Genes for direct methylation of glycine provide high levels of glycinebetaine and abiotic-stress tolerance in *Synechococcus* and *Arabidopsis*, *Proc. Natl. Acad. Sci. U S A 102*, 1318-1323.

46. O'Callaghan, J., and Condon, S. (2000) Growth of *Lactococcus lactis* strains at low water activity: correlation with the ability to accumulate glycine betaine, *Internat. J. Food Microbiol. 55*, 127-131.

47. Peddie, B. A., Chambers, S. T., and Lever, M. (1996) Is the ability of urinary tract pathogens to accumulate glycine betaine a factor in the virulence of pathogenic strains?, *J. Lab. Clin. Med. 128*, 417-422.

48. Velasco-Garcia, R., Chacon-Aguilar, V. M., Hervert-Hernandez, D., and Munoz-Clares, R. A. (2003) Inactivation of betaine aldehyde dehydrogenase from *Pseudomonas aeruginosa* and *Amaranthus hypochondriacus L.* leaves by disulfiram, *Chemico-Biological Interactions 143-144*, 149-158.

49. Fan, F., Germann, M. W., and Gadda, G. (2006) Mechanistic studies of choline oxidase with betaine aldehyde and its isosteric analogue 3,3-dimethylbutyraldehyde, *Biochemistry 45*, 1979-1986.

50. Gadda, G. (2008) Hydride transfer made easy in the reaction of alcohol oxidation catalyzed by flavin-dependent oxidases, *Biochemistry 47*, 13745-13753.

51. Gadda, G., Powell, N. L., and Menon, P. (2004) The trimethylammonium headgroup of choline is a major determinant for substrate binding and specificity in choline oxidase, *Arch. Biochem. Biophys.430*, 264-273.

52. Fan, F., and Gadda, G. (2005) On the catalytic mechanism of choline oxidase, *J. Am. Chem. Soc. 127*, 2067-2074.

53. Finnegan, S., and Gadda, G. (2008) Substitution of an active site valine uncovers a kinetically slow equilibrium between competent and incompetent forms of choline oxidase, *Biochemistry 47*, 13850-13861.

54.   Quaye, O., and Gadda, G. (Unpublished data) Effect of conservative mutation of an active site residue involved in substrate binding on the hydride tunneling reaction catalyzed by choline oxidase; *Chapter 4 of this dissertation*.

55.   Ghanem, M., Fan, F., Francis, K., and Gadda, G. (2003) Spectroscopic and kinetic properties of recombinant choline oxidase from *Arthrobacter globiformis*, *Biochemistry 42*, 15179-15188.

56.   Ghanem, M., and Gadda, G. (2005) On the catalytic role of the conserved active site residue His466 of choline oxidase, *Biochemistry 44*, 893-904.

57.   Rungsrisuriyachai, K., and Gadda, G. (2008) On the role of histidine 351 in the reaction of alcohol oxidation catalyzed by choline oxidase, *Biochemistry 47*, 6762-6769.

58.   Cook, P. F., Blanchard, J. S., and Cleland, W. W. (1980) Primary and secondary deuterium isotope effects on equilibrium constants for enzyme-catalyzed reactions, *Biochemistry 19*, 4853-4858.

59.   Emanuele, J. J., and Fitzpatrick, P. F. (1995) Mechanistic studies of the flavoprotein tryptophan 2-monooxygenase. 1. Kinetic mechanism, *Biochemistry 34*, 3710-3715.

60.   Grissom, C. B., and Cleland, W. W. (1988) Isotope effect studies of the chemical mechanism of pig heart NADP isocitrate dehydrogenase, *Biochemistry 27*, 2934-2943.

61.   Roth, J. P., and Klinman, J. P. (2003) Catalysis of electron transfer during activation of O_2 by the flavoprotein glucose oxidase, *Proc. Natl. Acad. Sci. U S A 100*, 62-67.

62.   Su, Q., and Klinman, J. P. (1999) Nature of oxygen activation in glucose oxidase from *Aspergillus niger*: the importance of electrostatic stabilization in superoxide formation, *Biochemistry 38*, 8572-8581.

63. Fan, F., and Gadda, G. (2007) An internal equilibrium preorganizes the enzyme-substrate complex for hydride tunneling in choline oxidase, *Biochemistry 46*, 6402-6408.

64. Sharma, S. C., and Klinman, J. P. (2008) Experimental evidence for hydrogen tunneling when the isotopic arrhenius prefactor ($A_{(H)}/A_{(D)}$) is unity, *J. Am. Chem. Soc. 130*, 17632-17633.

65. Gadda, G. (2003) pH and deuterium kinetic isotope effects studies on the oxidation of choline to betaine-aldehyde catalyzed by choline oxidase, *Biochim. Biophys. Acta 1650*, 4-9.

66. Cleland, W. W. (1982) The use of pH studies to determine chemical mechanisms of enzyme-catalyzed reactions, *Methods Enzymol. 87*, 390-405.

67. Cui, Q., and Karplus, M. (2002) Quantum mechanics/molecular mechanics studies of triosephosphate isomerase-catalyzed reactions: effect of geometry and tunneling on proton-transfer rate constants, *J. Am. Chem. Soc. 124*, 3093-3124.

68. Marcus, R. A. (2006) Summarizing lecture: factors influencing enzymatic H-transfers, analysis of nuclear tunnelling isotope effects and thermodynamic versus specific effects, *Philos. Trans. R. Soc. Lond. B. Biol. Sci. 361*, 1445-1455.

69. Ghanem, M., and Gadda, G. (2006) Effects of reversing the protein positive charge in the proximity of the flavin N(1) locus of choline oxidase, *Biochemistry 45*, 3437-3447.

70. Bradford, M. M. (1976) A rapid and sensitive method for the quantitation of microgram quantities of protein utilizing the principle of protein-dye binding, *Anal. Biochem. 72*, 248-254.

2.7. Appendix
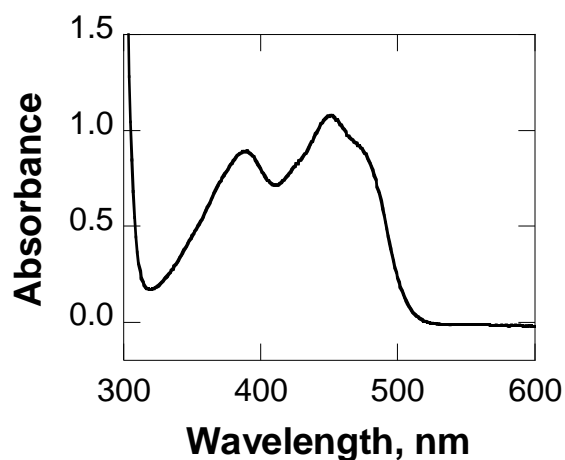
Figure A2.1. UV-visible absorbance spectrum of CHO-H99N.
Figure shows fully oxidized FAD after dialysis in 20 mM Tris-Cl, pH 8.
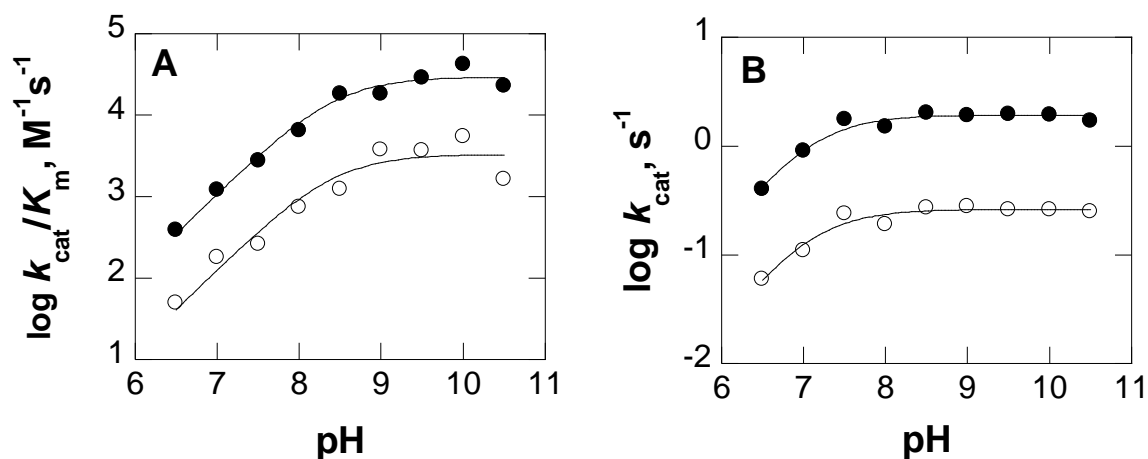
Figure A2.2. pH dependence of the k_{cat}/K_m and k_{cat} values for CHO-H99N with choline and 1,2-[^{2}H$_4$]-choline as substrates at 25 ^{o}C.
(**A**) pH-profiles for k_{cat}/K_m with choline (●) and 1,2-[^{2}H$_4$]-choline (○). (**B**) pH-profiles for k_{cat} with choline (●) and 1,2-[^{2}H$_4$]-choline (○). Enzymatic activities were measured at varying concentrations of choline and 1,2-[^{2}H$_4$]-choline at saturating oxygen concentration under atmospheric conditions. Data were fit to eq. 4.

The figure consists of six panels plotting k_{obs}, s^{-1} versus [Substrate], mM at the following temperatures: 10.1 °C, 12.2 °C, 14.2 °C, 17.9 °C, 20.0 °C, and 22.0 °C.
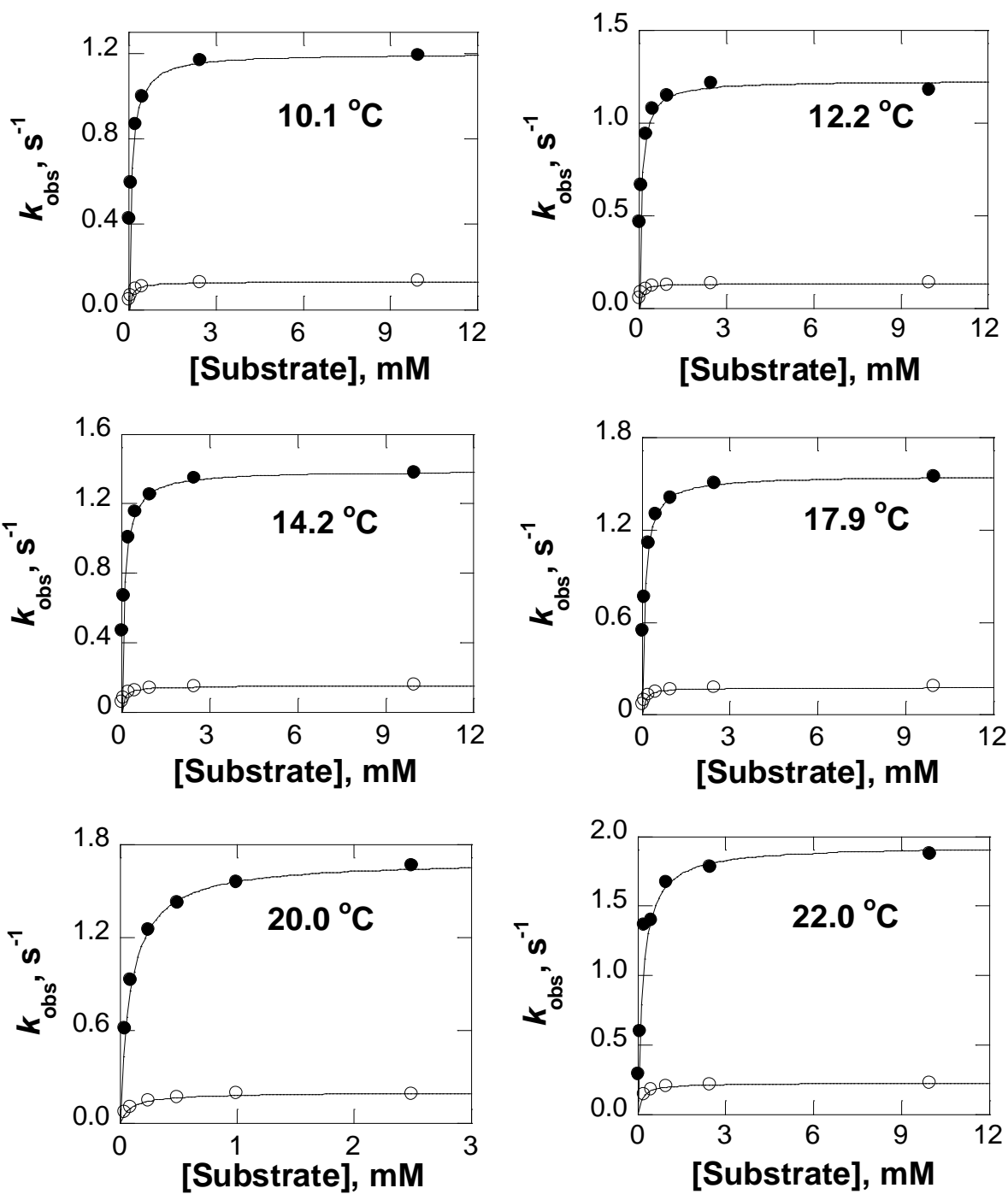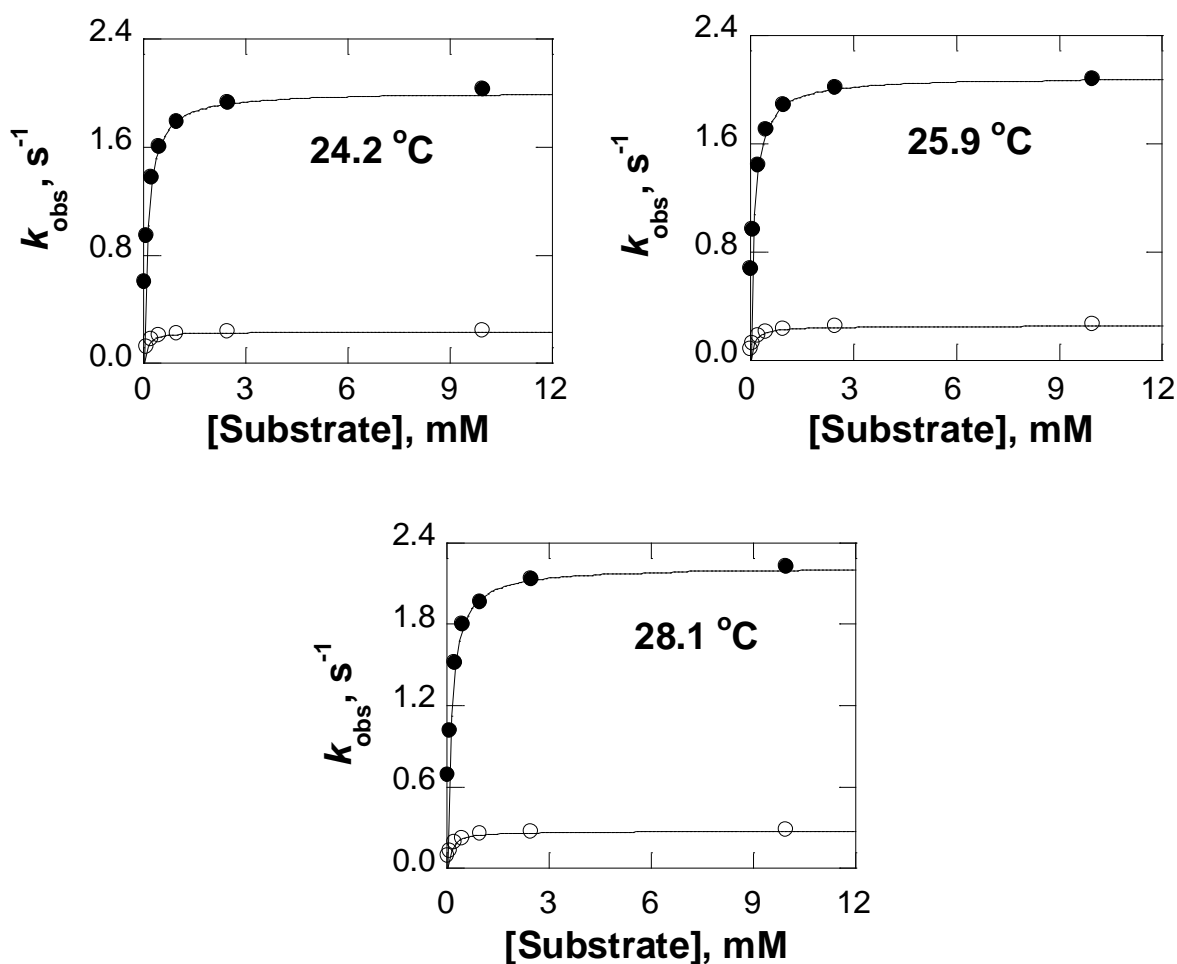
Figure A2.3. Rate of flavin reduction as a function of choline or 1,2-[^{2}H$_4$]-choline concentrations from 10 to 14 ^{o}C and from 18 to 28 ^{o}C.
($\bullet$) represents choline and ($\circ$) represents 1,2-[^{2}H$_4$]-choline. Enzymatic assays were carried out in 50 mM sodium pyrophosphate, pH 9 at varying concentration of substrate in a stopped-flow spectrophotometer under anaerobic conditions. Data were fit to equation 6.

Table A2.1. pH Dependence of Steady State Kinetic Parameters at Varying Concentrations of Oxygen with Choline as Substrate for CHO-H99N Determined at pH 10.

pH	k_{cat} (s^{-1})	k_{cat}/K_{ch} (M^{-1}s^{-1})	k_{cat}/K_{oxygen} (M^{-1}s^{-1})	K_{ch} (mM)	K_{oxygen} (μM)
6.0	0.15 ± 0.01	120 ± 10	nd	1.19 ± 0.01	nd
6.5	0.39 ± 0.01	400 ± 20	nd	0.97 ± 0.04	nd
7.0	1.07 ± 0.03	1,870 ± 230	51,880 ± 6,230	0.58 ± 0.07	21 ± 2
8.0	1.86 ± 0.01	7,720 ± 270	107,570 ± 3,920	0.24 ± 0.01	17 ± 1
9.0	2.38 ± 0.04	28,290 ± 2,970	74,250 ± 5,730	0.08 ± 0.01	32 ± 2
10.0	1.86 ± 0.01	22,360 ± 780	123,730 ± 4,400	0.08 ± 0.01	15 ± 1
11.0	1.92 ± 0.01	14,980 ± 170	54,800 ± 480	0.13 ± 0.01	35 ± 1

The k_{cat} and K_m parameters were obtained by fitting the initial rate data to $v_o/e = k_{cat}S/(K_m+S)$; the k_{cat}/K_m parameters were obtained by fitting the initial rate data to $v_o/e = k_{cat}S/[k_{cat}/[1/(k_{cat}/K_m)]+S]$.

Table A.2.2. pH Dependence of Steady State Kinetic Parameters at Atmospheric Oxygen Concentration with Choline or 1,2-[^{2}H$_4$]-Choline as Substrate for CHO-H99N Determined at pH 10.

pH	k_{cat}/K_m (H) (M^{-1}s^{-1})	k_{cat}/K_m (D) (M^{-1}s^{-1})	k_{cat} (H) (s^{-1})	k_{cat} (D) (M^{-1}s^{-1})	$^D(k_{cat}/K_m)$	$^Dk_{cat}$
6.5	390 ± 40	50 ± 20	0.41 ± 0.01	0.06 ± 0.01	7.7 ± 3.8	6.5 ± 0.8
7.0	1220 ± 160	180 ± 60	0.90 ± 0.03	0.11 ± 0.01	6.9 ± 2.7	8.1 ± 0.6
7.5	$2{,}770 \pm 220$	260 ± 50	1.75 ± 0.04	0.24 ± 0.01	10.7 ± 2.5	7.4 ± 0.3
8.0	$6{,}480 \pm 1{,}220$	740 ± 240	1.50 ± 0.06	0.19 ± 0.01	8.8 ± 3.3	7.8 ± 0.6
8.5	$18{,}220 \pm 3{,}490$	$1{,}230 \pm 150$	2.02 ± 0.08	0.27 ± 0.01	14.8 ± 3.4	7.5 ± 0.4
9.0	$18{,}320 \pm 1{,}470$	$3{,}780 \pm 1{,}820$	1.93 ± 0.03	0.28 ± 0.02	4.9 ± 2.4	7.0 ± 0.6
9.5	$28{,}740 \pm 4{,}060$	$3{,}700 \pm 1{,}890$	1.96 ± 0.06	0.26 ± 0.03	7.8 ± 4.1	7.7 ± 0.9
10.0	$41{,}920 \pm 9{,}380$	$5{,}510 \pm 2850$	1.94 ± 0.09	0.26 ± 0.03	7.6 ± 4.3	7.6 ± 0.9
10.5	$22{,}890 \pm 3{,}720$	$1{,}640 \pm 310$	1.72 ± 0.05	0.25 ± 0.01	14.0 ± 3.5	6.8 ± 0.4

The k_{cat} and K_m parameters were obtained by fitting the initial rate data to $v_o/e = k_{cat}S/(K_m+S)$; the k_{cat}/K_m parameters were obtained by fitting the initial rate data to $v_o/e = k_{cat}S/(k_{cat}/[1/(k_{cat}/K_m)]+S)$.

Table A2.3. Temperature Dependence of the k_{red} with Choline or 1,2-[^{2}H$_4$]-Choline as Substrate for CHO-H99N Determined at pH 9.

Temp (^{o}C)	Temp (K)	1000/T (K^{-1})	$(k_{red})_H$ (s^{-1})	$(k_{red})_D$ (s^{-1})	$^D(k_{red})$	$(K_d)_H$ (mM)	$(K_d)_D$ (mM)
10.1	283.1	3.532	1.20 ± 0.01	0.13 ± 0.01	9.17 ± 0.12	≤ 0.10	≤ 0.10
12.2	285.2	3.506	1.23 ± 0.02	0.14 ± 0.01	9.10 ± 0.18	≤ 0.08	≤ 0.07
14.2	287.2	3.482	1.39 ± 0.01	0.15 ± 0.01	9.28 ± 0.14	≤ 0.10	≤ 0.10
16.1	289.1	3.459	1.53 ± 0.01	0.17 ± 0.01	9.16 ± 0.12	≤ 0.11	≤ 0.10
17.9	290.9	3.438	1.55 ± 0.01	0.18 ± 0.01	8.68 ± 0.11	≤ 0.10	≤ 0.10
20.0	293.0	3.413	1.70 ± 0.02	0.20 ± 0.01	8.58 ± 0.17	≤ 0.09	≤ 0.10
22.0	295.0	3.390	1.85 ± 0.02	0.22 ± 0.01	8.46 ± 0.19	≤ 0.11	≤ 0.12
24.2	297.2	3.365	2.01 ± 0.02	0.24 ± 0.01	8.44 ± 0.10	≤ 0.12	≤ 0.10
25.9	298.9	3.346	2.09 ± 0.01	0.25 ± 0.01	8.24 ± 0.11	≤ 0.11	≤ 0.12
28.1	301.1	3.321	2.22 ± 0.02	0.28 ± 0.01	8.05 ± 0.13	≤ 0.12	≤ 0.12

The kinetic parameters were obtained by fitting the initial rate data to $k_{obs} = k_{red}S/(K_d+S)$.

CHAPTER 3

Role of Glu312 in Binding and Positioning of the Substrate for Hydride Transfer Reaction

in Choline Oxidase

(This chapter was published verbatim in Quaye, O., Lountos, G. T., Fan, F., Orville, A. M., and

Gadda, G. (2008), *Biochemistry 47*, 243-256.)

Abbreviations. CHO-E312A, choline oxidase variant with Glu312 replaced with Ala; CHO-E312Q, choline oxidase variant with Glu312 replaced with Gln; CHO-E312D, choline oxidase variant with Glu312 replaced with Asp; CHO-WT, wild-type choline oxidase; GMC oxidoreductases, Glucose-Methanol-Choline oxidoreductases. SI, Supporting Information

3.1. Abstract

Choline oxidase catalyzes the oxidation of choline to glycine betaine, a compatible solute that accumulates in pathogenic bacteria and plants to withstand osmotic and temperature stresses. The crystal structure of choline oxidase was solved to a resolution of 1.86 Å with data collected at 100 K from synchrotron x-ray radiation. The structure revealed a covalent linkage between His99Nε2 and FAD C8α atoms, and a 123 Å^3 solvent excluded cavity adjacent to the *re*-face of the flavin. A hypothetical model for choline docked into the cavity suggested that several aromatic residues and Glu312 may orient the cationic substrate for efficient catalysis.

The role of the negative charge on Glu312 was investigated by engineering variant enzymes in which Glu312 was replaced with alanine, glutamine, or aspartate. The Glu312Ala enzyme was inactive. The Glu312Gln enzyme showed a K_d value for choline at least 500-times larger than the wild-type enzyme. The Glu312Asp enzyme had a k_{cat}/K_{O2} value similar to the wild-type enzyme, but k_{cat} and k_{cat}/K_m values that were 230- and 35-times lower than in the wild-type enzyme. These data are consistent with the spatial location of the negative charge on residue 312 being important for the oxidation of the alcohol substrate. Solvent viscosity and substrate kinetic isotope effects suggested the presence of an internal equilibrium in the Glu312Asp enzyme prior to the hydride transfer reaction. All taken together the crystallographic and mechanistic data suggest that Glu312 is important for binding and positioning of the substrate in the active site of choline oxidase.

3.2. Introduction

Choline oxidase (E.C. 1.1.3.17) catalyzes the two-step oxidative conversion of choline to glycine betaine with betaine aldehyde as intermediate and molecular oxygen as final electron acceptor (Scheme 3.1). This reaction is of considerable interest for biotechnological and medical reasons, due to glycine betaine accumulating to high levels in the cytoplasm of many plants and pathogenic bacteria in response to hyperosmotic and temperature stresses ultimately resulting in the prevention of dehydration and cell death (*7, 8*). Thus, the study of choline oxidase has potential for engineering drought resistance in economically relevant plants (*9-13*) and for developing therapeutic agents targeted at the inhibition of glycine betaine biosynthesis (*14, 15*).

From a fundamental standpoint, choline oxidase serves well as a model system to investigate the mechanism of alcohol oxidation catalyzed by flavin-dependent enzymes, primarily because the chemical step in which the substrate CH bond is cleaved is not masked by other kinetic steps occurring in catalysis (*16*).
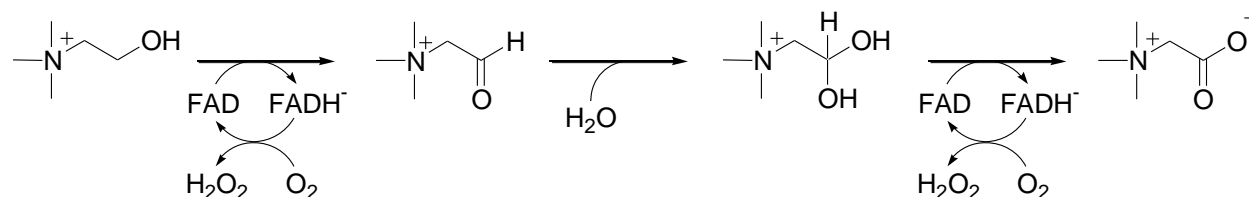
Scheme 3.1. The two-step, four-electron oxidation reaction of choline catalyzed by choline oxidase.

The elucidation at a molecular level of the catalytic mechanism of choline oxidase has been obtained from biochemical (*17-19*), mechanistic (*6, 17, 20-22*), and mutagenesis (*23, 24*) studies. As schematically illustrated in Figure 2, after the initial formation of an enzyme-choline complex, catalysis is initiated by the abstraction of the hydroxyl proton of the alcohol substrate by an as yet unidentified active site group with pK_a of ~7.5. The resulting choline-alkoxide species is transiently stabilized in the active site of the enzyme through electrostatic interaction with the positively charged side chain of His466 (*23, 24*). This interaction likely contributes to the preorganization of the enzyme-substrate complex that is required for the subsequent hydride transfer reaction from the α-carbon of the activated substrate to the N(5) atom of the flavin cofactor. The hydride transfer reaction then occurs from the activated alkoxide species quantum mechanically by exploiting the environmental vibrations of the reaction coordinate that permit a tunneling distance between the hydride donor and acceptor in the preorganized Michaelis complex (*25*),(*21, 26*). Preorganization of the substrate-enzyme complex likely requires also the

electrostatic interaction of the trimethylammonium moiety of the alcohol substrate with at least one residue in the active site of the enzyme, as suggested by mechanistic studies using an isosteric analog of choline devoid of positive charge (*19, 22*). However, in the absence of structural information, the identity of the amino acid residue that interacts with the positive charge of choline remains elusive.

In the present study, we have initially used x-ray crystallography to gain information about the active site and the residues that form the substrate binding cavity in choline oxidase. The structural information is complemented with mechanistic studies on enzyme variants in which the negative charge at position 312 in the active site of the enzyme was either removed by engineering mutant enzymes containing alanine or glutamine, or moved away from the flavin cofactor by replacing Glu312 with aspartate. The results of these studies demonstrate an important role of Glu312 for binding and positioning of the alcohol substrate for catalysis.

3.3. Experimental Procedures

Materials. *Escherichia coli* strain Rosetta(DE3)pLysS was obtained from Novagen (Madison, WI); QIAprep Spin Miniprep kit was from Qiagen (Valencia, CA); sparse-matrix screening kits were from Hampton Research (Aliso Viejo, CA) and Nextal Biotechnologies (Montreal, Quebec); QuickChange site-directed mutagenesis kit was from Stratagene (La Jolla, CA); oligonucleotides for site-directed mutagenesis and sequencing of the mutant genes were from Sigma Genosys (The Woodlands, TX); choline chloride was from ICN. All other reagents used were of the highest purity commercially available.

Crystallization and X-ray Data Collection. Recombinant wild-type choline oxidase from *Arthrobacter globiformis* was purified in high purity and yield, and converted to the oxidized form, as previously described (*19, 27*). Crystals of choline oxidase were grown by the hanging drop vapor diffusion method and initial crystallization conditions were obtained using the commercially available sparse-matrix screening kits. Diffraction-quality crystals were obtained from 2 µL of choline oxidase (4.9 mg/mL) mixed with 2 µL of reservoir solution containing 0.1 M Bis-Tris propane, pH 8.5, 1.2 M ammonium sulfate, and 10% v/v dimethylsulfoxide (DMSO), on a silanized cover slip sealed over the reservoir solution. The enzyme drops were equilibrated over 1 mL of the reservoir solution at 23 °C, from which yellow rod-like crystals of oxidized enzyme grew to maximal dimensions of 0.2 x 0.05 x 0.05 mm within two weeks. Prior to flash-freezing by quick submersion into liquid nitrogen, single crystals were transferred into 2 µL of 3.4 M sodium malonate, pH 7 (*28*), and allowed to incubate for two minutes at 23 °C. Two independent data sets were collected from two crystals held at approximately 100 K at the SER-CAT facilities at the Advanced Photon Source, Argonne National Laboratory. A 1.86 Å resolution data set was collected at beamline 22-ID using a 1 Å x-ray beam, a 0.2° oscillation angle, and a 2 s exposure time per frame. The data set at 2.69 Å resolution was collected at beamline 22-BM with a 1 Å x-ray beam, an oscillation angle of 0.5°, and a 60 s exposure time. The diffraction images were processed with HKL2000 and scaled with SCALEPACK (*29*).

Crystal Structure Determination. The diffraction data from the two data sets were consistent with either space group $P4_32_12$ or $P4_12_12$, with unit cell dimensions of $a = b = 84.4$, c

= 343.5 Å. Matthew's coefficient (*30, 31*) and solvent-content calculations suggested two protein subunits per asymmetric unit (V_M = 2.5 $Å^3$ Da^{-1}, 50% solvent content). Molecular replacement was performed using the MOLREP (*32*) from the CCP4 suite of programs (*33*) to obtain the initial phases. The search model was derived from glucose oxidase (PDB code 1CF3 (*34*)), which has 26% sequence identity with choline oxidase with *B*-factors set at 20 $Å^2$. Solvent, FAD, and divergent portions of the amino acid sequence were deleted from the search model, and conserved but non-identical residues were converted to alanine residues. Cross rotation and translation searches for two molecules in the asymmetric unit were performed with data between 15 and 3.5 Å resolution in both $P4_32_12$ and $P4_12_12$, space groups. The best solution in each space group was then subjected to rigid body refinement with data from 50 to 1.86 Å resolution using CNS (*35*). Space group $P4_32_12$ gave interpretable electron density maps that were determined to be correct. The starting model had an R-factor of 0.48 and R-free of 0.54. Phases calculated from the initial model were extracted with SIGMAA in CCP4 and were used as the starting phases in PRIME & SWITCH (*36*) as implemented in RESOLVE (*37*), which significantly improved the electron density maps. Multiple rounds of manual model rebuilding, and positional and isotropic *B*-factor refinement were carried out with O (*38*) and REFMAC5 (*39*), respectively. Progress of the refinement was monitored by R-free, which was calculated using 5% of the reflections, and cross-validated (σ_A weighted $2mF_o$-DF_c and mF_o-DF_c maps) to evaluate the model and correct errors (*40*).

After several rounds of refinement and model building, the FAD was built into the electron density. Library files containing the topology and parameter files for the FAD were prepared using the Dundee PRODRG server (*41*). Planar restraints were enforced on the oxidized isoalloxazine ring of FAD for several rounds of refinement. When the overall R-factor decreased

below 0.3, water molecules were placed with ARP/Waters (*42*), refined with REFMAC5, and manually inspected. Within each active site a single DMSO molecule, an additive used in the crystallization solution, was fit into electron density near the N5 position of the isoalloxazine ring of the flavin and refined. For comparison, a sulfate molecule was also fit in this position and refined, but inspection showed that DMSO fit the electron density better. Computational studies using density functional theory calculations (B3LYP/6-31G(d,p)) in collaboration with Drs. Keiji Morokuma and Rajeev Prabhakar are currently underway to further analyze the electronic structure of the FAD adduct and will be reported elsewhere.

Structure validation of model geometry was carried out with PROCHECK (*43, 44*). Solvent exposed surface areas were calculated with a 1.4 Å probe radius with Swiss-PDB viewer (v3.7b2) or VEGA (http://www.ddl.unimi.it). Secondary structure assignments were made using KSDSSP (*45*). Structural homologs in the Protein Data Bank were found using MSDfold. The rms differences between models were calculated with SSM (http://www.ebi.ac.uk/msd-serv/ssm), or Swiss-PDB viewer (v3.7b2). Figures showing structures were prepared using Swiss-PDBViewer (v3.7b2) and PovRay (v.3.5) or Pymol (DeLano Scientific LLC, Castro City, CA).

Site-Directed Mutagenesis. Mutant genes for choline oxidase variants CHO-E312A, CHO-E312Q and CHO-E312D, were prepared using the pET/*codA*mg plasmid for the wild-type enzyme as template (*27*), and forward and reverse oligonucleotides as primers for site-directed mutagenesis. Site-directed mutagenesis was carried out using the QuikChange[TM] Site-Directed Mutagenesis kit, following the manufacturer's instruction manual in the presence of 2% DMSO. The resulting mutant genes (pET/*codA*mg-E312A, -E312Q and -E312D) were sequenced at the

DNA Core Facility at Georgia State University using an Applied Biosystems Big Dye Kit on an Applied Biosystems model ABI 377 DNA Sequenser to confirm the presence of the mutant genes in their correct orientations. As an expression host, competent cells of *E. coli* strain Rosetta(DE3)pLysS were transformed with the mutant plasmids by electroporation, and permanent stocks of the transformed cells were prepared and stored at -80 ^{o}C.

Expression and Purification of Choline Oxidase Variants. The variant enzymes were expressed and purified to homogeneity as previously described for wild-type choline oxidase (*19, 27*). To increase the stability of the variant enzymes during purification, 10% glycerol was incorporated in the buffers throughout the purification steps with the exception of the dialysis step at pH 6 in which the anionic semiquinone form of the enzyme was converted to the oxidized form (*19*). Enzymes stored at − 20 ^{o}C in 20 mM Tris-Cl, pH 8, were found to be stable for at least six months.

Biochemical Studies. In order to ascertain that FAD was covalently bound to the proteins, the purified enzymes were treated with 10% trichloroacetic acid (TCA) after recording the spectra for the bound flavin. The enzyme-TCA mixtures were incubated for 30 min on ice and centrifuged at 20,000 g for 10 min. The flavin spectra of the supernatants were recorded again to check the presence of unbound FAD. All UV-visible absorbance spectra were recorded using an Agilent Technologies diode-array spectrophotometer Model HP 8453.

Kinetic Assays. Enzyme activities of CHO-E312Q and CHO-E312D were measured by the method of initial rates in 50 mM potassium phosphate or 50 mM sodium pyrophosphate as

described for wild-type choline oxidase (*16*). The enzymatic activities were measured by monitoring the rate of oxygen consumption with a computer-interfaced Oxy-32 oxygen-monitoring system (Hansatech Instrument) at 25 $^{\circ}$C.

Steady-state kinetic parameters for CHO-E312D were determined at varying concentrations of choline between 0.01 and 20 mM, and oxygen between 0.03 and 1.1 mM, after equilibrating the reaction mixture at the desired concentration of oxygen by bubbling the appropriate O_2/N_2 gas mixture for a minimum of 10 min. The pH profiles of the kinetic parameters with choline as substrate for CHO-E312D were carried out at atmospheric oxygen concentration due to the low K_m values for oxygen determined at pH 5 and 10. All enzyme assays were conducted in 50 mM sodium pyrophosphate, with the exception of pH 7 where 50 mM potassium phosphate was used. Substrate kinetic isotope effects on the steady-state kinetic parameters were determined by alternating varying concentrations of the substrate isoptomers, choline and 1,2-[^{2}H$_4$]-choline, at atmospheric concentration of oxygen. Solvent viscosity effects on steady-state kinetic parameters were measured in 50 mM sodium pyrophosphate, pH 10 at 25 $^{\circ}$C, using glucose and sucrose as viscosigens; the relative viscosity values at 25 $^{\circ}$C were calculated according to the reference values at 20 $^{\circ}$C from Lide (*46*).

Rates of flavin reduction with varying concentrations of substrate (choline or 1,2-[^{2}H$_4$]-choline), measured in rapid kinetics, were carried out on a Hi-Tech SF-61 stopped-flow spectrophotometer thermostated at 25 $^{\circ}$C in 50 mM sodium pyrophosphate, pH 10. Reduction of the oxidized enzyme-bound flavin upon mixing with substrate was monitored as a decrease in absorbance at 450 nm. The enzyme was previously made anaerobic by alternately applying vacuum and flushing with oxygen-free argon for 25-cycles and mounted onto the stopped-flow also previously treated with 0.26 mM degassed dithionite or a mixture of glucose (5 mM)-

glucose oxidase (3600 units) to scrub oxygen. The substrate was flushed with oxygen-free argon for at least 15 min prior to mounting onto the stopped-flow. Equal volumes of CHO-E312Q or CHO-E312D and substrate were mixed anaerobically in the stopped-flow yielding a final enzyme concentration of ~20 µM.

Data Analysis. Data were fit with KaleidaGraph software (Synergy Software, Reading, PA) and EnzFitter software (Biosoft, Cambridge, UK). Stopped-flow traces were fit to equations 1 and 2, which describe single- and double-exponential processes, respectively. Here, k_{obs}, k_{obs1}, and k_{obs2}, represent first-order rate constants, t is time, A_t is the value of absorbance at 450 nm at any given time, A, A_1 and A_2 are the amplitudes of the absorbance changes, and A_∞ is the absorbance at infinite time. Pre-steady state kinetic parameters were determined by using equation 3, where k_{obs} is the observed first-order rate for the reduction of the enzyme bound flavin at any given concentration of substrate, k_{red} is the limiting first-order rate constant for flavin reduction at saturated substrate concentration, and K_d is the dissociation constant for binding of the substrate to the enzyme. Steady-state kinetic parameters in atmospheric oxygen were determined by fitting the initial rates at different concentrations of substrate to the Michaelis-Menten equation for one substrate. Steady-state kinetic parameters at varying concentrations of choline and oxygen were determined by fitting the initial rates data to equation 4, which describes a steady-state kinetic mechanism with intersecting lines in double reciprocal plots. Here, e represents the concentration of enzyme, k_{cat} is the turnover number of the enzyme at infinite substrates concentrations, and K_a and K_b represent the Michaelis constants for the organic substrate (A) and oxygen (B). The pH dependences of the steady-state kinetic parameters with choline were determined by fitting the initial rates data to equation 5, which describes a

curve with a slope of +1 and a plateau region at high pH. Here, C is the pH-independent value of the kinetic parameter of interest. Solvent viscosity effects on the k_{cat}/K_m and k_{cat} values for choline were fit to equation 6, where $(k)_o$ and $(k)_\eta$ are the kinetic parameters of interest in the absence and presence of viscosigen, respectively, S is the degree of viscosity dependence and η_{rel} is the relative viscosity.

$$A_t = Ae^{-k_{obs}t} + A_\infty \tag{1}$$

$$A_t = A_1 e^{-k_{obs1}t} + A_2 e^{-k_{obs2}t} + A_\infty \tag{2}$$

$$k_{obs} = \frac{k_{red}A}{K_d + A} \tag{3}$$

$$\frac{v}{e} = \frac{k_{cat}AB}{K_aB + K_bA + AB + K_{ia}K_b} \tag{4}$$

$$\log Y = \log\left[\frac{C}{1 + \dfrac{10^{-pH}}{10^{-pK_a}}}\right] \tag{5}$$

$$\frac{(k)_o}{(k)_\eta} = S(\eta_{rel} - 1) + 1 \tag{6}$$

3.4. Results

Crystal Structure Determination. The x-ray data collection and atomic model refinement statistics are listed in Table 3.1. X-ray diffraction data were obtained with synchrotron radiation from two independent crystals of choline oxidase; although nearly identical structures were obtained from both data sets, one crystal diffracted to higher resolution (1.86 Å compared to 2.69 Å). That data set consists of 381317 observations of 97546 unique reflections in the resolution range 50 to 1.86 Å. The overall completeness of 92.3% (63.2% in the highest resolution shell) and overall R_{sym} of 7.2% (31.5% in the highest resolution shell) indicated the data are of good quality. The structure was solved by molecular replacement with a search model based upon glucose oxidase from *Aspergillus niger* (PDB code: 1CF3) (*34*). The atomic model was refined against the 1.86 Å resolution dataset to a final R-factor of 0.161 and R-free of 0.202. An overall coordinate error of the model based on R-factor of 0.13 Å was determined. The final model had a correlation coefficient of 0.967. Ramachandran analysis of the crystal structures showed that 89.4% of the residues are in the most favored region, 10% in the additionally allowed regions, 0.6% in the generously allowed regions, and 0.1% in the disallowed regions. Ala230 in the A chain was flagged as being in the disallowed region but the electron density maps indicate this residue fits well in the observed density.

Table 3.1. X-ray diffraction data collection and model refinement statistics

Crystal ID	Crystal 1	Crystal 2
X-ray Wavelength (Å)	1.0	1.0
Resolution Range (Å)[a]	50-1.86 (1.91-1.86)	50-2.69 (2.76-2.69)
Space group	$P4_32_12$	$P4_32_12$
Unit Cell Dimensions (Å)		
$a = b =$	84.4	84.4
$c =$	343.5	343.7
Total Reflections	381317	196964

Unique Reflections	97546	33722
Multiplicity	3.9 (2.8)	5.8 (2.4)
Completeness (%)	92.3 (63.2)	94.2 (69.7)
R_{sym} (%)[b]	7.2 (31.5)	10.8 (27.1)
$I/(\sigma)I$[c]	17.7 (2.3)	15.6 (2.8)
Model Refinement Statistics		
Resolution Range (Å)	50-1.86	50-2.69
No. of Reflections	92403	31943
No. of protein atoms	8171	8168
No. of water molecules	960	152
R-factor	0.161	0.157
R-free[d]	0.202	0.219
Average B-factors (Å^2)		
Protein	22.5	25.5
Water	32.6	17.5
FAD (2)	17.4	20.4
O_2^- (2)	24.8	37.2
DMSO (2)	40.0	44.1
Rms deviations for ideal		
Bond length (Å)	0.014	0.018
Bond angles (°)	1.5	1.7
Correlation coefficient	0.967	0.954
Estimated coordinate error (Å)	0.128	0.219

[a] Values for the highest resolution shell of data are given in parentheses. [b] R_{sym} (I) gives the average agreement between the independently measured intensities such as $\Sigma_h \Sigma_i |I_i - I| / \Sigma_h \Sigma_i I$, where I is the mean intensity of the i observations of reflection h. [c] I/σ(I) is the root-mean-square value of the intensity measurements divided by their estimated standard deviation. [d] Calculated with 5% of the data.

Overall Structure Description. The x-ray structure revealed that choline oxidase crystallized as a homodimer with approximate dimensions of 88 Å x 70 Å x 46 Å (Figure 3.1), in agreement with solution measurements showing a dimeric structure under native conditions (*27*). Each monomer contains 546 residues; however, the last 19 residues in the C-terminal portion of each monomer were not visible in the electron density maps and were not included in the final model. Non-crystallographic symmetry restraints were not applied during refinement. The two monomers in the asymmetric unit of the holoenzyme overlaid with an r.m.s. deviation of 0.23 Å over 527 common C_α atoms. The buried surface area at the subunit interface was approximately 2430 Å^2, which corresponds to approximately 13% of the total surface area for each monomer.

The dimer interface included two sets of six identical intersubunit contacts between charge-complementary residues clustered on the outer edges of the interface. These are: Asp72-Lys398 (4.1 Å), Asp250-Glu53 (4.3 Å), Arg255-Glu370 (3.2 Å), Asp358-Arg396 (2.4 Å), Arg363-Asp394 (4.2 Å), and Arg363-Asp397 (2.9 Å). In contrast, the central portion of the dimer interface contained very few close contacts between subunits, which include Asp72-Lys398 (4.1 Å).
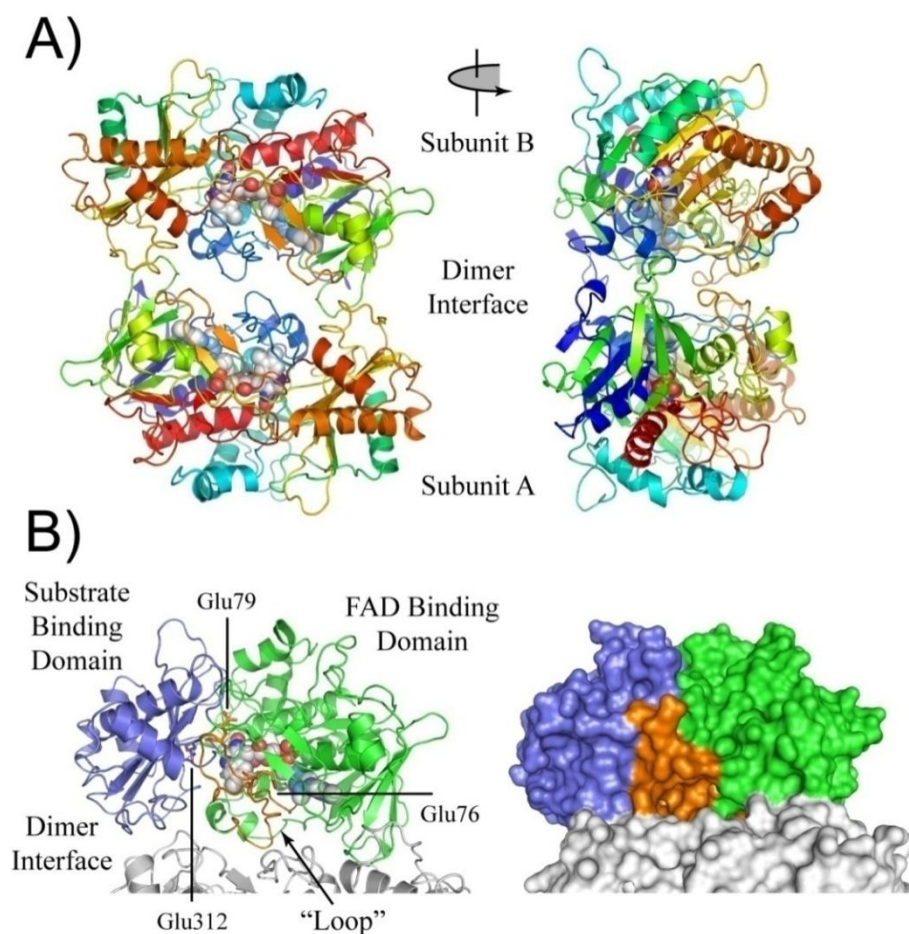
Figure 3.1. The three-dimensional structure of choline oxidase refined to 1.86 Å resolution.
A) Two orthogonal views of the choline oxidase homodimer illustrated with a cartoon ribbon trace of the protein backbone. Each subunit is colored from blue to red starting at the N-terminal. The FAD is shown as CPK atoms with the C, N, and O atoms colored in gray, blue, and red, respectively. **B)** A single subunit of choline oxidase illustrating the domain architecture (see the text for a discussion). The view is similar to that of part A (left) above. The space-filled view is shown on the right with the surfaces colored according to the FAD binding (blue), substrate binding (green) and "loop" (orange) regions, respectively.

The protein fold of each choline oxidase subunit resembles that of other members of the Glucose-Methanol-Choline (GMC) oxidoreductase enzyme superfamily (*5, 34, 47-55*). The structure-based sequence alignment is quantified in Table A3.1 and shown in Figure A3.1 in the Supporting Information. The two-domain topology is similar to that of glucose oxidase and the bacterial flavoenzyme *p*-hydroxybenzoate hydroxylase, with a typical PHBH-fold (*56*). The FAD-binding domain is formed primarily by residues 1-159, 201-311, and 464-527 (Figure 3.1). This domain consists of a six-stranded parallel β-sheet that is flanked on one side by a three-stranded anti-parallel β-sheet and further surrounded by eight α-helices. The substrate binding domain is formed primarily by residues 160-200 and 312-463. The topology of the substrate binding domain consists of a distorted six-stranded anti-parallel β-sheet, which forms the bottom of the choline oxidase active site and is flanked on the other side by three α-helices that protrude into the bulk solvent.

A common feature of other members of the GMC family is a loop that forms a lid over the putative substrate binding site (*48, 50, 51, 55*). In choline oxidase, this loop region is composed of residues 64-95 (Figure 3.1, Figure A3.1). The average *B*-factors of these residues is 20 $Å^2$, indicating that the loop is well defined in the crystal structure. A portion of the loop is shielded from bulk solvent by the second monomer of the dimer; however, residues 74-85 extend into the bulk solvent. The loop is amphiphatic, with hydrophobic residues directed toward the interior and hydrophilic residues directed toward the external surface.

FAD Binding Site. The FAD isoalloxazine ring is buried within the protein such that no parts are visible from the molecular surface of the protein[4]. Solvent-accessible surface

---

[4]An outstanding feature of the electron density for the FAD is that the isoalloxazine ring is not planar, as anticipated for oxidized flavin. However, the observed distortions also differ significantly from the structures of reduced flavins, which typically exhibit an approximately 150° angle along the N5-N10 axis defined by the dimethylbenzene and pyrimidine rings (*1, 2*). In contrast, the dimethylbenzene and piperazine rings in choline oxidase are essentially flat and coplanar, but the plane of the pyrimidine ring is at an approximately 120° angle to the former plane. The pyrimidine ring is also significantly distorted from planarity and adopts a "half-boat" configuration. In this orientation, all atoms in the pyrimidine are in the same plane with the exception of C4a, which lies approximately 0.5 Å above the plane defined by the pyrimidine ring. In this context, a greater than +4σ positive difference peak extending from the C4a atom was still present upon convergence of the refinement. These features all suggest that the C4a atom of FAD is sp^3 hybridized, consistent with a covalent adduct involving this position of the flavin being present in the crystals. It is noteworthy to note that the crystallization materials and conditions did not include any reagent known to form a C4a adduct with FAD. Moreover, the crystallographic data indicate that the C4a adduct contains either one or two C, N, or O atoms. The aerobic crystals do contain O_2, which is known to react with reduced flavins at the C4a position of the isoalloxazine ring in flavin-dependent monooxygenases and possibly in flavoprotein oxidases (*3*). Therefore, at this stage of the investigation we have modeled an O_2 molecule bound to the C4a atom. This unusual covalent adduct with the FAD C4a atom is

calculations indicate that only 21.5 Å^2 (2.1%) of the entire FAD surface area is exposed to the

solvent. The electron density maps clearly indicate that the FAD is covalently linked to the His99

Nε2 atom via the FAD C8M atom of the isoalloxazine ring (Figure 3.2). This contrasts to

previous mass spectrometric studies by other authors that proposed His87 as the residue

covalently attached to the FAD^{C8M} (57). Indeed, His87 is part of the loop that covers the active

site cavity (*see above*) and is located approximately 7.7 Å away from the FAD C8M atom.
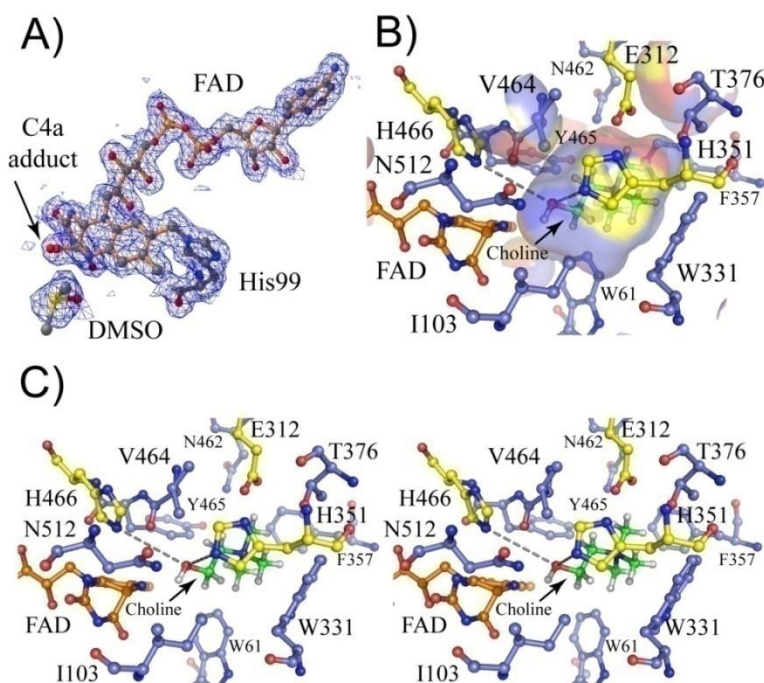
Figure 3.2. The active site of choline oxidase.
A) An example of the typical $2mF_o\text{-}DF_c$ electron density at 1.86 Å resolution (1 ⬚ contour) associated with an active site DMSO molecule, the FAD, a C4a adduct (see footnote[1]) and the His99 residue. The DMSO molecule binds at the bottom of the solvent excluded cavity and comes within 2.7 Å of the FAD N5 atom. **B)** The solvent excluded cavity illustrated with semi-transparent surfaces calculated after removal of the C4a adduct and the DMSO molecule. The

---

currently under investigation using structural and computational approaches, and the results of

these studies will be reported elsewhere.

surfaces are colored according to the atom forming its border with generally hydrophobic and hydrophilic residues shown with their carbon atoms colored in either blue or yellow, respectively. The cavity volume of greater than 120 Å^3 is of sufficient size to accommodate a choline molecule (shown with green carbon atoms). The choline molecule was manually docked into the cavity to maximize the potential interactions between the substrate and catalytically important residues such as His351, His466, FAD^{N5} and Glu312 (see text). **C)** A divergent stereo view of the hypothetical docked choline molecule into the active site of choline oxidase. The view and coloring scheme are identical to that of part B above.

Substrate Binding Site. Upon completion of the refinement, electron density with greater than $+4.5\sigma$ positive difference features was still present approximately 4 Å from the N5 atom of the isoalloxazine ring. The shape and size of the electron density clearly indicated that this species was not a water molecule. The crystallization solution used contained DMSO and ammonium sulfate. Refinement of either DMSO or sulfate ion indicated that the former ligand fits well into the electron density, but the latter does not. As illustrated in Figure 3.2, the methyl groups of DMSO project toward Val464 (3.7 Å) and His351 (3.5 Å), whereas the oxygen atom of DMSO is within hydrogen bonding distance with Ser101 Oγ (2.7 Å) and the FAD N5 atom (2.7 Å). The average refined *B*-factor for the DMSO atoms was 40.0 Å^2, which is roughly double that of the protein or the FAD (Table 3.1). Our steady-state kinetic analyses indicated that DMSO is a weak competitive inhibitor with respect to choline, with a K_I value of 460 ± 4 mM (Fan and Gadda; unpublished observations).

Analysis of the molecular surfaces of the protein reveals a solvent excluded cavity, with a volume of approximately 125 Å^3, located within the substrate binding domain. The cavity is adjacent to the *re*-face of the FAD and is of sufficient size to accommodate a choline molecule (93 Å^3), provided that the DMSO ligand in the current structure is displaced. The cavity is partially surrounded by the hydrophobic residues Trp61, Trp331, Phe357, and Val464 (Figure 3.2), which form an aromatic cage. The polar residues bordering the cavity include Glu312,

His351, and His466, of which the latter two are near the FAD isoalloxazine ring. Of particular importance is the side chain of Glu312, which forms the "top" of the aromatic cage and is the only negatively charged residue lining the active site cavity.

Docking of Choline into the Substrate Binding Cavity. Earlier mechanistic studies with substrate and product analogs established that the positive charge on the trimethylammonium moiety of choline plays an important role in substrate binding and specificity in the reaction catalyzed by choline oxidase (*19, 22*). In order to gain insights into the enzyme and substrate interactions, we manually docked choline into the cavity (Figure 3.2). The side chain of Glu312 is approximately 3 Å from the positively charged trimethylammonium moiety of choline, which suggests an ionic pair. Although other orientations are possible, in the illustrated configuration choline appears to be poised to initiate the reductive half-reaction (i.e., oxidation of choline). For example, the choline hydroxyl O atom is approximately 4 Å from the side chains of His351, His466 and Asn512, of which the former two are good candidates to serve as an active site base. Moreover, the C1 atom of choline is less than 4 Å from the side chain of Ser101 and the flavin N5 atom, which is the locus to accept the hydride transfer reaction.

Expression and Purification of CHO-E312A, CHO-E312Q and CHO-E312D. Choline oxidase variants in which glutamate at position 312 was replaced with alanine, glutamine or aspartate were expressed and purified at pH 8 in the presence of 10% glycerol, following the same protocol used for the wild-type enzyme (*27*). The addition of glycerol throughout the purification steps resulted in increased stability of the mutant enzyme. A mixture of anionic semiquinone and oxidized flavin species were present upon isolation of the mutant

enzymes (Figure A3.2), which was also observed for purification of the wild-type enzyme (*19, 27*). The fully oxidized and active enzymes, which were used in this study, were obtained by treatment at pH 6, as previously reported for the wild-type enzyme (*58*). UV-visible absorbance spectra of the supernatants after treatment of the three variant enzymes with 10% TCA and centrifugation, showed no peaks around 370 and 450 nm, consistent with the flavin cofactor being covalently bound to the proteins. Thus, substitution of Glu312 with alanine, glutamine, or aspartate, did not affect the covalent linkage of the flavin to the protein. There was no detectable activity for the alanine variant with up to 100 mM choline as substrate. In contrast, the glutamine and aspartate variants were able to oxidize choline. Table 3.2 reports the specific activities and apparent steady state kinetic parameters determined at atmospheric oxygen at pH 7 for the mutant enzymes.

Table 3.2. Comparison of specific activities and apparent steady-state kinetic parameters of CHO-E312D, CHO-E312Q, CHO-E312A with wild.type choline oxidase[a]

Enzyme	Total Protein, mg	Specific Activity, U/mg	$^{App}k_{cat}/K_m$, $M^{-1}s^{-1}$	$^{App}k_{cat}$, s^{-1}	$^{App}K_m$, mM
CHO-E312D	190	0.17	1500	0.26	0.17
CHO-E312Q	104	0.013	1.8	0.21	116
CHO-E312A	120	-[b]	-	-	-
CHO-WT	220	8	25,000	15	0.6

[a]Total protein amounts were determined by the Bradford method (*78*). Enzymatic activities were measured at varying concentrations of choline in the range from 0.005 to 250 mM, in 50 mM potassium phosphate, pH 7 and 25 °C, using fully oxidized enzymes. [b]No oxygen consumption was determined when 11 μM enzyme was assayed with 100 mM choline; for comparison, with the wild-type enzyme at a concentration of 0.1 μM and 10 mM choline the rate of oxygen consumption is ~15 s^{-1}.

Reductive Half-reaction of CHO-E312Q with Choline. The involvement of the negative charge of Glu312 in binding choline was determined by directly measuring and comparing the thermodynamic equilibrium constants (K_d) with choline as substrate for CHO-E312Q and the wild-type enzyme. Thus, the Glu312 enzyme variant was mixed anaerobically

with different concentrations of choline up to 250 mM in a stopped-flow spectrophotometer at pH 10 and 25 $^{\circ}$C, and the resulting rates of flavin reduction were measured. The high pH was chosen to avoid artifactual contributions originating from pH effects, since previous results with the wild-type enzyme (*17, 58*), as well as CHO-E312D (*this study*), showed that the kinetic parameters become pH-independent at high pH. With CHO-E312Q, the observed rates of flavin reduction were hyperbolically dependent on the concentration of choline, yielding a K_d value ≥150 mM[5] (Figure A3.3). This value was at least 500-times larger than the K_d value of ~0.3 mM previously reported for the wild-type enzyme under the same conditions (*16*), suggesting that the negative charge at position 312 is important for binding of the alcohol substrate in choline oxidase. Flavin reduction was followed by a slow kinetic step with a rate of ~0.01 s^{-1}, which was independent of the concentration of choline. This was tentatively assigned to the release of the product of the reaction from the reduced enzyme.

Kinetic and Mechanistic Studies with CHO-E312D. The Glu312Asp enzyme variant was investigated in its mechanistic properties in order to establish how the spatial location of the

---

[5]At concentrations of choline >250 mM inflated rates of flavin reduction in the stopped-flow spectrophotometer were observed. While such a kinetic behavior was not investigated further, an accurate determination of the K_d value for binding of choline to CHO-E312Q could not be carried out because the enzyme could not be saturated with the substrate. For this reason, only a limiting lower value of 150 mM is reported for K_d.

negative charge on residue 312 in the active site of the enzyme may affect catalysis in the enzyme.

The steady-state kinetic mechanism was determined at pH 10, by measuring initial rates of oxygen consumption at varying concentrations of both choline and oxygen. As for the case of the wild-type enzyme (*16, 58*), the best fit of the data was obtained to an equation describing a sequential steady-state kinetic mechanism. As illustrated in Table 3.3, substitution of Glu312 with aspartate resulted in a 230-fold decrease in the k_{cat} value and a 30-fold decrease in the k_{cat}/K_m value with choline, indicating that Glu312 participates in the reductive half-reaction in which the alcohol substrate is oxidized. An upper limiting value of 2 μM could be estimated for the K_m value for oxygen from the fit of the steady-state kinetic data. Consistent with a K_m value for oxygen in the low micromolar range, the apparent rates of reaction determined as a function of [oxygen] with 10 mM choline showed that the enzyme was at least 75-80% saturated at a concentration of oxygen of 10 μM (Figure A3.4). From the k_{cat} and K_{O2} values, a limiting lower k_{cat}/K_{O2} value of 76,000 could be estimated. As shown in Table 3.3, such a value is not significantly different from that previously determined with the wild-type enzyme, consistent with substitution of Glu312 with aspartate having a negligible effect on the oxidative half-reaction in which the enzyme-bound reduced flavin is reoxidized with formation of hydrogen peroxide.

Table 3.3. Comparison of the kinetic parameters with choline as substrate for CHO-E312D and wild-type choline oxidase at pH 10

kinetic parameters	CHO-E312D[a]	CHO-WT[b]
k_{cat}, s^{-1}	0.26 ± 0.004	60 ± 1
k_{cat}/K_m, M^{-1}s^{-1}	7100 ± 400	237,000 ± 9000
K_m, mM	0.04 ± 0.002	0.25 ± 0.01
K_{O2}, mM	≤ 0.002[c]	0.69 ± 0.03
k_{cat}/K_{O2}, M^{-1}s^{-1}	≥ 76,000[d]	86,400 ± 3600
k_{red}, s^{-1}	0.36 ± 0.01	93 ± 1

K_d, mM	~0.1	0.29 ± 0.01
$^D k_{red}$	9.3 ± 0.2	8.9 ± 0.2
$^D(k_{cat}/K_m)^e$	4.4 ± 1.2	10.7 ± 2.6
$^D k_{cat}{}^e$	7.1 ± 1.3	7.5 ± 0.3

[a]Steady-state kinetic parameters were determined at varying concentrations of choline and oxygen in 50 mM sodium pyrophosphate, pH 10 and 25 °C. [b]Data are from (16). [c]Estimated upper limiting value. [d]Estimated lower limiting value calculated from the k_{cat} value experimentally determined and the estimated upper limiting K_{O2} value. [e]The pH-independent values are reported here.

The reductive-half reaction of CHO-E312D was investigated using a stopped-flow spectrophotometer to determine the rate of flavin reduction (k_{red}) and the K_d value for binding of choline. As for the case of the wild-type enzyme (16), no intermediates were observed with the enzyme undergoing a two-electron reduction to the hydroquinone state. The rate of flavin reduction was the same between 1 and 10 mM choline (Figure A3.5), yielding a well-defined k_{red} value that was 260-fold lower than in the wild-type enzyme (Table 3.3). A K_d value of ~0.1 mM could only be estimated from the kinetic data, due to the impossibility of maintaining pseudo-first order conditions in the stopped-flow at concentrations of choline lower than 50 μM. However, such a K_d value was not significantly different from that of ~0.3 mM determined previously for the wild-type enzyme, suggesting similar chemical binding affinities in choline oxidase containing glutamate and aspartate at position 312.

Substitution of choline with 1,2-[^{2}H$_4$]-choline resulted in a slower rate of flavin reduction at pH 10, yielding a $^D k_{red}$ value of 9.3 ± 0.2. This value was not significantly different from the $^D k_{red}$ value of ~9 recently reported for the wild-type enzyme (16), consistent with cleavage of the CH bond of choline being rate-limiting in the reductive half-reaction.

The pH profiles of the steady-state kinetic parameters with choline as substrate for CHO-E312D were determined in the pH range from 5 to 10 in air-saturated buffer at 25 °C, corresponding to an [oxygen] of 250 μM. At pH 5 and 10 the K_{O2} values were ≤2 μM (Figure A3.4), thereby ensuring that the enzyme was saturated with oxygen throughout the pH range

tested. As shown in Figure 3.3, the k_{cat}/K_m and k_{cat} values were pH independent at high pH and decreased with decreasing pH, consistent with the requirement of an unprotonated group in the reaction catalyzed by the Glu312Asp variant enzyme. An apparent pK_a value of 7.6 ± 0.04 was determined from the k_{cat}/K_m pH-profile. Substitution of choline with 1,2-[^{2}H$_4$]-choline did not results in changes in the apparent pK_a (7.6 ± 0.1) (Figure 3.3), suggesting that the value of 7.6 is likely a true thermodynamic pK_a value (*59*) that is not perturbed by kinetic commitments (*60*). In agreement with these conclusions, the resulting $^D(k_{cat}/K_m)$ value was pH-independent between pH 6 and 10 (Figure 3.4). The $^Dk_{cat}$ value was also pH-independent and, interestingly, significantly larger than the $^D(k_{cat}/K_m)$ value, with an average value of 7.1 ± 1.3 compared to 4.4 ± 1.2, respectively. These data suggest the presence of a pH-independent, internal equilibrium in the enzyme-substrate complex occurring prior to the cleavage of the substrate CH bond (*60*).
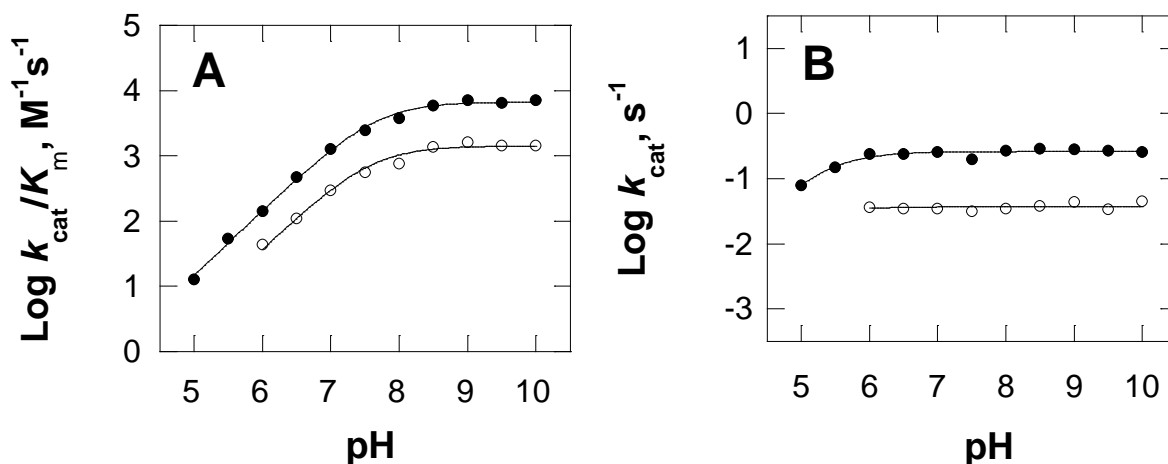
Figure 3.3. pH dependence of the k_{cat}/K_m and k_{cat} values for CHO-E312D with choline and 1,2-[^{2}H$_4$]-choline as substrates at 25 °C.
A) pH-profiles for k_{cat}/K_m with choline (●) and 1,2-[^{2}H$_4$]-choline (○). Data were fit to eqn. 2. **B)** pH-profiles for k_{cat} with choline (●) and 1,2-[^{2}H$_4$]-choline (○). Data were fit to eqn. 2.
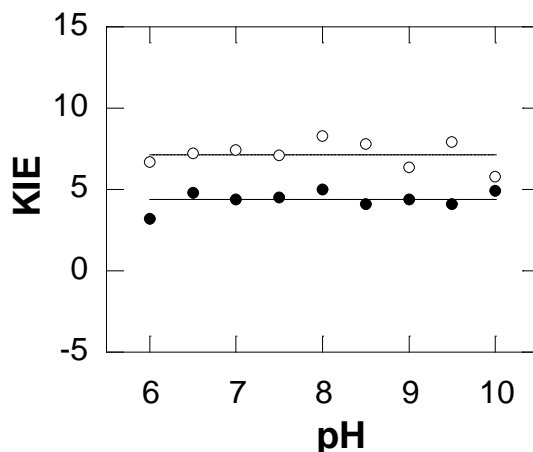
Figure 3.4. pH dependence of $^D(k_{cat}/K_m)$ (●) and $^Dk_{cat}$ (○) values. CHO-E312D activity was measured at varying concentrations of choline or 1,2-[^{2}H$_4$]-choline under atmospheric oxygen conditions. The data for $^Dk_{cat}$ and $^Dk_{cat}/K_m$ were fit to y = 7.1 and y = 4.4, respectively.

The effects of solvent viscosity on the k_{cat}/K_m and k_{cat} values with choline as substrate for CHO-E312D were determined at pH 10 to further probe for the presence of internal equilibria in the reductive half-reaction and the overall turnover of the enzyme, as previously reported for flavocytochrome b$_2$ (*61*). Initial rates of reaction were measured at varying concentrations of choline in air-saturated, 50 mM sodium pyrophosphate, pH 10, at 25 ^{o}C, in the presence of increasing amounts of glucose or sucrose as viscosigens. As shown in Figure 3.5, both the k_{cat}/K_m and k_{cat} values increased monotonically with increasing viscosity of the solvent, consistent with the presence of internal equilibria in both the reductive half-reaction and the overall turnover of the enzyme. Table 3.4 summarizes the effect of solvent viscosity on the k_{cat}/K_m and k_{cat} values for the Glu312Asp enzyme variant.
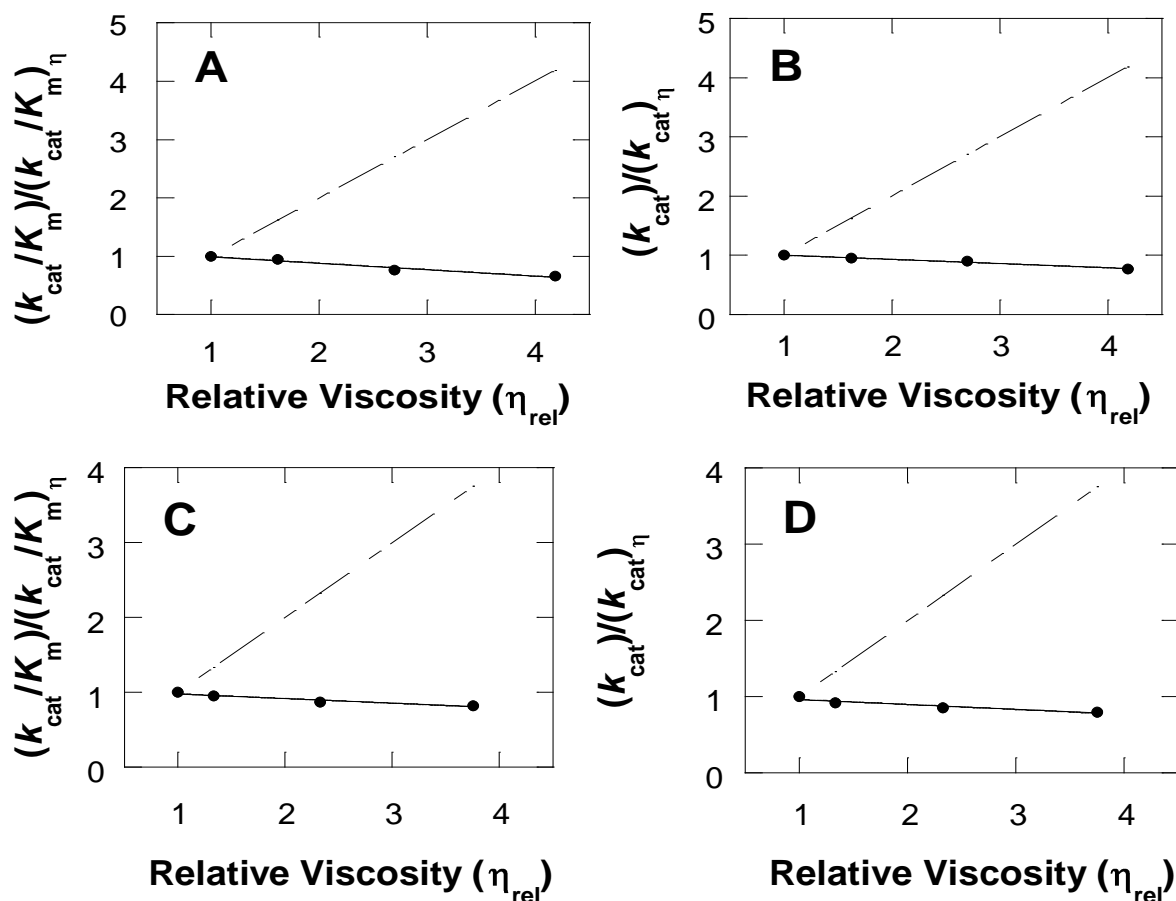
Figure 3.5. Effects of solvent viscosity on the k_{cat}/K_m (●) and k_{cat} (○) values with choline as substrate for CHO-E312D with glucose or sucrose as viscosigen at pH 10.

A) Normalized k_{cat}/K_m values as a function of relative solvent viscosity with glucose as viscosigen. **B)** Normalized k_{cat} values as a function of relative solvent viscosity with glucose as viscosigen. **C)** Normalized k_{cat}/K_m values as a function of relative solvent viscosity with sucrose as viscosigen. **D)** Normalized k_{cat} values as a function of relative solvent viscosity with sucrose as viscosigen. Solid lines represent fits of the experimental data using eq. 6. Dashed lines with a slope of one describe the case hypothetical cases for fully diffusion-controlled reactions. The values of the relative viscosities of the reaction mixture at 25 °C were calculated according to the values at 20 °C from Lide (*46*). CHO-E312D activity was measured at varying concentrations of choline under atmospheric oxygen conditions.

Table 3.4. Effect of solvent viscosity on the steady-state kinetic paramaters for CHO-E312D at pH 10

kinetic parameters	viscosigen	viscosity effect
k_{cat}/K_m, $M^{-1}s^{-1}$	glucose	-0.11 ± 0.02
k_{cat}/K_m, $M^{-1}s^{-1}$	sucrose	-0.06 ± 0.01
k_{cat}, s^{-1}	glucose	-0.07 ± 0.01
k_{cat}, s^{-1}	sucrose	-0.07 ± 0.02

Viscosity effect values are relative to the values in the absence of viscosigen.

3.5. Discussion

A detailed picture of the reaction mechanism of choline oxidase has emerged from previous pH and kinetic isotope effect studies (*16, 17, 58*), as well as mechanistic studies with substrate and product analogues (*6, 19, 22*), and site-directed mutants (*23, 24*). The high resolution structure of the wild-type enzyme reported in this study provides a structural framework within which previous mechanistic results can be further interpreted, as well as important information about residues that form the active site of choline oxidase. Furthermore, the mechanistic data presented on Glu312 enzyme variants shed light on the roles this residue play in binding and correct positioning of the alcohol substrate for the hydride transfer reaction of choline oxidation catalyzed by choline oxidase.

Mechanistic Insights from the Crystal Structure of Wild-type Choline Oxidase. The active site of choline oxidase is formed by a cavity of approximately 125 $\mathring{A}^3$ facing the *re*-face of FAD, which is completely secluded from the exterior of the protein by a long loop region composed of residues 64 to 95. Whereas about 60% of this loop is shielded from bulk solvent by the presence of the other subunit in the dimeric enzyme, residues 74 to 85 extend into the bulk solvent, suggesting that this portion of the loop may form a lid that allows entry of the substrate and exit of the reaction product to and from the active site. Similar loop regions that cover the active site have been previously observed in other members of the Glucose-Methanol-Choline (GMC) oxidoreductase enzyme superfamily, such as glucose oxidase (*52, 62*), pyranose 2-oxidase (*48, 51*), cholesterol oxidase (*5, 55*), and the flavin domain of cellobiose dehydrogenase (*50*). During catalysis in choline oxidase, opening and closing of the lid must necessarily follow

the association of choline to form the catalytically relevant enzyme-substrate complex and precede the dissociation of glycine betaine from the enzyme-product complex[6]. The molecular mechanism underlying the entry and exit of organic ligands to and from the active site of choline oxidase, as well as in other members of the GMC superfamily, has not been investigated to date, and represents an important question that has now the potential to be addressed.

As illustrated in Figure 3.2, the active site of choline oxidase is lined by both hydrophobic and hydrophilic residues playing important roles in both substrate binding and catalysis. The side chains of Trp61, Trp331, and Phe357, form a hydrophobic cage on the active site surface that is adjacent to the isoalloxazine ring of the flavin and, along with the negatively charged side chain of Glu312, constitute the site of interaction for binding the trimethylammoniun moiety of the choline substrate via cation-π and electrostatic interactions. The importance of the negative charge at position 312 for binding of the substrate is demonstrated by the ~500-fold increase in the K_d value for choline binding observed upon

---

[6]It is assumed here that the lid topping the active site cavity is closed not only in the enzyme devoid of ligands, as observed in this study, but also when the enzyme is in complex with the substrate, as reported previously for another member of the GMC oxidoreductase superfamily, cholesterol oxidase (*4, 5*). This assumption is based on the observation that, upon docking of choline in the active site of the enzyme, all the residues proposed to participate in substrate binding and catalysis appear to be spatially positioned in a fashion that is consistent with all the available mechanistic and biochemical data. A closed-lid configuration during enzymatic turnover is also consistent with earlier kinetic data showing that the betaine aldehyde intermediate predominantly remains bound at the active site during turnover with choline (*6*).

substitution of Glu312 with glutamine that was determined in this study by anaerobic stopped-flow spectrophotometry. Since glutamine is isosteric with glutamate, one can assume similar binding modes of choline in the Glu312Gln and wild-type enzymes, allowing for an energetic contribution of ~15 kJ mol^{-1} to be estimated for the ionic interaction of the negative charge at position 312 and the positive charge of choline. This value agrees well with the value of ~13 kJ mol^{-1} that was recently estimated from mechanistic studies on choline oxidase with the choline analog devoid of positive charge, 3,3-dimethyl-butan-1-ol (*22*). An aromatic cage structurally surrounding a negatively charged amino acid residue appears to be a common feature in enzymes and proteins that bind ligands containing trimethylammoniun groups, as it has been previously observed in phospholipase C (*63*), acetylcholinesterase (*64-66*), CTP:phosphocholine cytidylyltransferase (*67*), and the periplasmic ligand-binding proteins pro-X and Opu-C (*68-70*).

Previous mechanistic studies have established that the oxidation of choline catalyzed by choline oxidase occurs through a highly asynchronous chemical mechanism, in which formation of a choline alkoxide species is followed by a hydride transfer reaction from this activated species of the substrate to the enzyme-bound flavin (Scheme 3.2) (*16*). A group with a thermodynamic pK_a of 7.5 has been proposed to be responsible for the abstraction of the hydroxyl H$^+$ from the alcohol substrate (*16, 17, 58*). The structure of choline oxidase indicates that Glu312, His351, and His466, are the only residues lining the active site cavity of the enzyme with the ability to act as general base. The side chain of Glu312 can be immediately ruled out as being responsible for choline activation because it is ~8 Å from the N5 atom of FAD, a distance that is too long for such a catalytic role. In agreement with this conclusion, site-directed mutagenesis data on enzyme variants containing glutamine or aspartate at position 312 are consistent with Glu312 participating in substrate binding (*vide infra*). Recent mechanistic data on

mutant forms of choline oxidase in which His466 is replaced by other amino acids strongly suggest that this residue is likely not the group responsible for the removal of the hydroxyl H^+ of choline, but rather point out that His466 is protonated during the reductive half-reaction in which choline is oxidized by choline oxidase (Scheme 3.2.) (*23, 24*). Indeed, with the His466Ala mutant enzyme the enzymatic activity could be partially rescued with imidazolium, but not imidazole (*23*), and both the k_{cat} and k_{cat}/K_m pH profiles still showed the requirement for a catalytic base (*23*). Furthermore, the His466Asp enzyme was completely devoid of enzymatic activity with choline, both under catalytic turnover or anaerobic conditions (*24*). Thus, based on the structural information now available it appears that His351 may serve as general base in the oxidation reaction catalyzed by choline oxidase. This hypothesis is currently under study with the characterization of mutant variants of choline oxidase in which His351 has been replaced with amino acids carrying other functional groups.
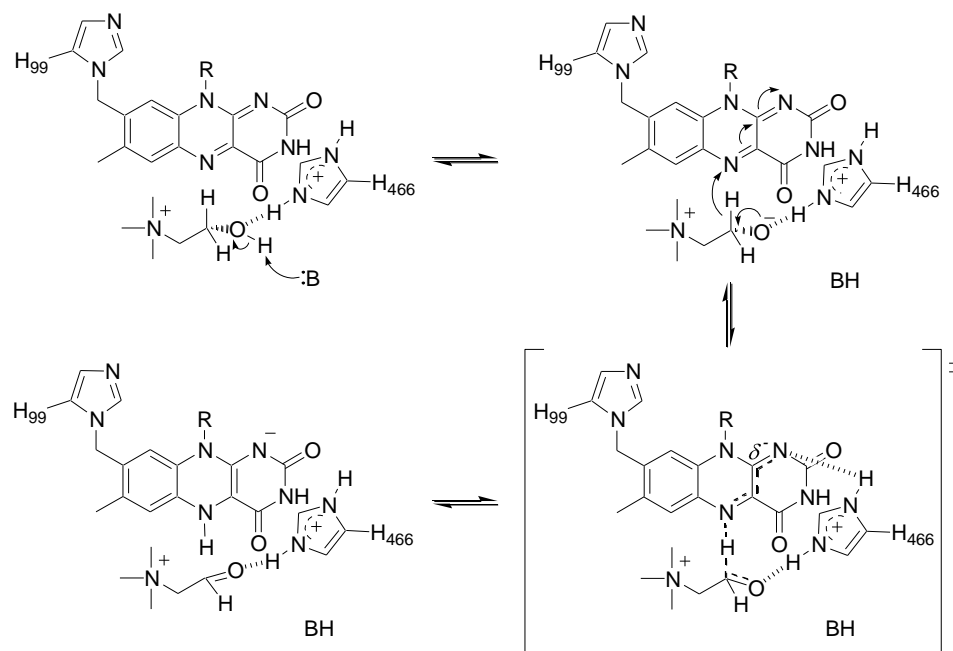
Scheme 3.2. Chemical mechanism for the oxidation of choline to betaine aldehyde catalyzed by choline oxidase.

Recent mechanistic data have established that in choline oxidase the hydride transfer reaction occur within a highly preorganized enzyme-substrate complex (*21*), by exploiting the mechanical effects that result in the tunneling of the hydride ion from the α-carbon of the choline alkoxide to the flavin N(5) atom (*20*) (Scheme 3.2). This, in turn, requires minimal independent movement of the activated choline alkoxide relative to the isoalloxazine ring of the flavin, so that the only dynamical motions that are permitted in the activated enzyme-substrate complex are those resulting in the hydride transfer reaction. The active site cavity of choline oxidase, which has a volume slightly larger than that of choline, as well as the location of the groups involved in substrate binding and catalysis are fully consistent with this mechanistic hypothesis (Figure 3.2). Indeed, the isoalloxazine ring of the cofactor, which acts as hydride acceptor in the oxidation reaction, is physically constrained by the covalent linkage of the FAD C8M atom with His99, the proximity of Ile103 to the pyrimidine ring, and several contacts with the backbone atoms between His99 and Ile103. To a similar extent, the choline alkoxide species that donates the hydride in the oxidation reaction is physically constrained by electrostatic interactions of its positively charged trimethylammonium group with Glu312 at one extremity, and its negatively charged alkoxide O atom with the positively charged side chain of His466 at the opposite end (*23, 24*).

Mechanistic Insights on the Role of Glu312 in Choline Oxidase. The mutant form of choline oxidase in which Glu312 is replaced with aspartate is properly folded and functional, as suggested by the steady-state and rapid kinetic data presented in this study. The Glu312Asp enzyme variant showed the same sequential steady-state kinetic mechanism of reaction of the wild-type enzyme. Moreover, pH profiles of the k_{cat}/K_m values for choline and 1,2-[^{2}H$_4$]-choline

as substrate for the Glu312Asp enzyme variant identified a pK_a value of ~7.5 for the general base that activates choline in catalysis, which is similar to the value previously reported for the wild-type enzyme (*17, 58*). Finally, both the $^Dk_{red}$ and K_d values with choline as substrate for CHO-E312D were not significantly different from those of the wild-type enzyme. Consequently, the comparison of the mechanistic properties of the Glu312Asp and the wild-type enzymes could provide direct evidence on the importance of spatial location of the negative charge on residue 312 in the reaction catalyzed by choline oxidase.

The spatial location of the negative charge on residue 312 is important for the oxidation of the alcohol substrate, but not for the following oxidation of the enzyme-bound reduced flavin. This conclusion is supported by the 30-fold decrease in the k_{cat}/K_m value for choline and the lack of significant changes in the k_{cat}/K_m value for oxygen observed with the Glu312Asp enzyme variant as compared to the wild-type enzyme determined at pH 10. The lack of involvement of Glu312 in the oxidative half-reaction is in agreement with previous pH profile data on the wild-type enzyme (*17, 58*), showing that no ionizable groups with pK_a values between 6 and 10 participate in the oxidation of the reduced flavin.

Substitution of Glu312 with an aspartate residue significantly affects the hydride transfer reaction that results in the reduction of the flavin cofactor, but has little if any effect on the binding of the substrate in the active site of the enzyme. Evidence supporting this conclusion comes from anaerobic substrate reduction experiments using a stopped-flow spectrophotometer, showing that in the Glu312Asp enzyme the k_{red} value at pH 10 is 260-times lower than in the wild-type enzyme, whereas the K_d value is not significantly changed. In the wild-type form of choline oxidase (*20*), the hydride ion tunnels from the α-carbon of the activated substrate to the enzyme-bound flavin N(5) atom, with little independent movements of the hydride donor and

acceptor other than those conducive to tunneling of the hydride ion. Due to the larger distance between the donor and acceptor of the hydride ion that necessarily arises from moving the negative charge on residue 312 away from the flavin cofactor, one can speculate that the mode of hydride ion transfer in the Glu312Asp mutant enzyme may be significantly altered with respect to the wild-type enzyme. In this respect, the large deuterium kinetic isotope effect determined here for the Glu312Asp mutant enzyme, with a $^D k_{red}$ value of ~9, bodes well as an essential prerequisite for future mechanistic studies aimed at investigating the mode of hydride ion transfer in the Glu312Asp enzyme.

The thermodynamic pK_a of ~7.5 for the group that act as a general base in the oxidation of choline is not affected by the substitution of Glu312 with an aspartate residue, as suggested by the comparison of the mechanistic data presented here for CHO-E312D and previous data for the wild-type enzyme (*17, 58*). Evidence for the value of ~7.5 determined in the k_{cat}/K_m pH profile with CHO-E312D being a thermodynamic pK_a value comes from kinetic isotope effects data, showing that the $^D(k_{cat}/K_m)$ value is pH-independent between pH 6 and 10. This is consistent with lack of external commitments to catalysis in the mutant enzyme, which would perturb the observed kinetic pK_a value away from its thermodynamic value (*59*). The observation that the same pK_a value is seen in the k_{cat}/K_m pH profiles with choline and 1,2-$[^2H_4]$-choline provides independent support for the observed pK_a being a thermodynamic value. Indeed, a value significantly lower than 7.5 would be expected with a slower substrate such as 1,2-$[^2H_4]$-choline, for which CD bond cleavage is at least 4-times slower than CH bond cleavage in the reductive half-reaction (*71*).

Upon substitution of Glu312 with aspartate, the enzyme-substrate Michaelis complex undergoes a kinetically relevant, pH-independent, isomerization prior to the hydride ion transfer

reaction. Evidence supporting this conclusion comes from the effects of solvent viscosity on the k_{cat}/K_m value with choline as substrate for CHO-E312D. Indeed, the normalized k_{cat}/K_m values decreased monotonically with increasing relative viscosity of the solvent, irrespective of the use of glucose or sucrose as solvent viscosigen. These data cannot be explained with solvent viscosity reporting on the contribution of substrate binding steps on the overall rate for the reductive half-reaction in which choline is oxidized to betaine aldehyde, for which normalized k_{cat}/K_m values are expected not to change or to increase to various extent with increasing relative viscosity (*72-75*). In contrast, the effects of solvent viscosity observed with CHO-E312D can be readily explained with the presence of a conformational change in the enzyme-substrate complex that is sensitive to the viscosity of the solvent. Independent evidence for the presence of a kinetically relevant conformational change in the enzyme-substrate complex comes from kinetic isotope effects on the k_{cat}/K_m value with choline as substrate for CHO-E312D, showing pH-independent $^D(k_{cat}/K_m)$ values significantly lower than the $^Dk_{cat}$ values. It is well established that kinetic isotope effects determined using the steady-state kinetic approach may be significantly lower than their intrinsic values in the presence of commitments to catalysis (*60*). In choline oxidase, both the external forward commitment to catalysis and the reverse commitment to catalysis are pH-dependent, since they both include the chemical step in which the hydroxyl proton is abstracted from the alcohol substrate. However, these commitments to catalysis can be immediately ruled out as being responsible for lowering the observed $^D(k_{cat}/K_m)$ value because both the pH-independence of the $^D(k_{cat}/K_m)$ values and the similarity in the pK_a values of ~7.5 determined from the pH profiles of the k_{cat}/K_m values with choline and 1,2-[^{2}H$_4$]-choline argue against the presence of pH-dependent commitments to catalysis (*60, 76, 77*). Consequently, any decrease in the observed $^D(k_{cat}/K_m)$ values seen with CHO-E312D must necessarily arise from a

pH-independent, internal equilibrium, involving the enzyme-substrate complex. In this regard, an internal equilibrium of the type described here has been recently proposed for the wild-type form of choline oxidase from the comparison of the effects of pH and temperature on the kinetic isotope effects in reversible and irreversible catalytic regimes (*21*).

Conclusions. The results of the crystallographic and mechanistic investigations presented in this study demonstrate the important role of Glu312 for binding and positioning of the alcohol substrate for catalysis in choline oxidase. The negative charge on residue 312 is involved in an electrostatic interaction with the positive charge of the alcohol substrate that anchors the non-reactive end of the substrate in the active site of the enzyme. The spatial location of the negative charge in the active site is important for correct positioning of the substrate for the hydride transfer reaction from the activated choline alkoxide to the flavin N(5) atom. Moreover, the crystal structure of choline oxidase provides detailed structural information that correlates well with the mechanistic information that is available on the enzyme. It shows that the active site of choline oxidase is well-suited to maximize productive binding of the alcohol substrate, so that the catalytic base that activates the substrate, the positive charge that stabilizes the activated alkoxide species, and the isoalloxazine ring of the flavin, are efficiently positioned for a hydride transfer reaction occurring within a highly preorganized enzyme-substrate complex. Finally, the availability of the three-dimensional structure of the enzyme represents an essential prerequisite for future mechanistic studies aimed at establishing the contribution of selected active site residues that do not participate directly in catalysis, e.g., Glu312, toward hydride transfer and tunneling in the oxidation of alcohol substrate catalyzed by flavin-dependent enzymes.

Supporting Information Available. Figure A3.1 shows a structure based sequence alignment with homologs of choline oxidase with known x-ray structures. Figure A3.2 shows the UV visible absorbance spectra of a mixture of flavin semiquinone and oxidized and fully oxidized FAD for CHO-E312A. Figure A3.3 shows the rate of flavin reduction Rate of flavin reduction in CHO-E312Q as a function of choline or $1,2-[^2H_4]$-choline concentrations. Figure A3.4 shows the estimation of K_m for oxygen in CHO-E312D at pH 5 and 10. Figure A3.5 shows the rate of flavin reduction in CHO-E312D as a function of choline or $1,2-[^2H_4]$-choline concentrations. Table A3.1 presents the quantitative structural similarity between choline oxidase and selected homologues. Table A3.2 shows the kinetic parameters and kinetic isotope effect for CHO-E312D between pH 5 and 10. Table A3.3 shows the solvent viscosity effects on steady state kinetic parameters for CHO-E312D with choline as substrate, and glucose and sucrose as viscosigens.

3.6. References

1. Dixon, D. A., Lindner, D. L., Branchaud, B., and Lipscomb, W. N. (1979) Conformations and electronic structures of oxidized and reduced isoalloxazine, *Biochemistry 18*, 5770-5775.

2. Lennon, B. W., Williams, C. H., Jr., and Ludwig, M. L. (1999) Crystal structure of reduced thioredoxin reductase from Escherichia coli: structural flexibility in the isoalloxazine ring of the flavin adenine dinucleotide cofactor, *Protein Sci. 8*, 2366-2379.

3. Sheng, D., Ballou, D. P., and Massey, V. (2001) Mechanistic studies of cyclohexanone monooxygenase: chemical properties of intermediates involved in catalysis, *Biochemistry 40*, 11156-11167.

4. Lario, P. I., Sampson, N., and Vrielink, A. (2003) Sub-atomic resolution crystal structure of cholesterol oxidase: what atomic resolution crystallography reveals about enzyme mechanism and the role of the FAD cofactor in redox activity, *J. Mol. Biol. 326*, 1635-1650.

5. Li, J., Vrielink, A., Brick, P., and Blow, D. M. (1993) Crystal structure of cholesterol oxidase complexed with a steroid substrate: implications for flavin adenine dinucleotide dependent alcohol oxidases, *Biochemistry 32*, 11507-11515.

6. Fan, F., Germann, M. W., and Gadda, G. (2006) Mechanistic studies of choline oxidase with betaine aldehyde and its isosteric analogue 3,3-dimethylbutyraldehyde, *Biochemistry 45*, 1979-1986.

7.	Bae, J. H., Anderson, S. H., and Miller, K. J. (1993) Identification of a high-affinity glycine betaine transport system in *Staphylococcus aureus*, *Appl. Environ. Microbiol. 59*, 2734-2736.

8.	Pichereau, V., Bourot, S., Flahaut, S., Blanco, C., Auffray, Y., and Bernard, T. (1999) The osmoprotectant glycine betaine inhibits salt-induced cross-tolerance towards lethal treatment in *Enterococcus faecalis*, *Microbiol. 145 (Pt 2)*, 427-435.

9.	Chen, T. H., and Murata, N. (2002) Enhancement of tolerance of abiotic stress by metabolic engineering of betaines and other compatible solutes, *Curr. Opin. Plant Biol. 5*, 250-257.

10.	Rontein, D., Basset, G., and Hanson, A. D. (2002) Metabolic engineering of osmoprotectant accumulation in plants, *Metabol. Eng. 4*, 49-56.

11.	Sanchez-Aguayo, I., Rodriguez-Galan, J. M., Garcia, R., Torreblanca, J., and Pardo, J. M. (2004) Salt stress enhances xylem development and expression of S-adenosyl-L-methionine synthase in lignifying tissues of tomato plants, *Planta 220*, 278-285.

12.	Shirasawa, K., Takabe, T., Takabe, T., and Kishitani, S. (2006) Accumulation of glycinebetaine in rice plants that overexpress choline monooxygenase from spinach and evaluation of their tolerance to abiotic stress, *Ann. Bot. (Lond) 98*, 565-571.

13.	Waditee, R., Bhuiyan, M. N., Rai, V., Aoki, K., Tanaka, Y., Hibino, T., Suzuki, S., Takano, J., Jagendorf, A. T., Takabe, T., and Takabe, T. (2005) Genes for direct methylation of glycine provide high levels of glycinebetaine and abiotic-stress tolerance in *Synechococcus* and *Arabidopsis*, *Proc. Natl. Acad. Sci. U.S.A. 102*, 1318-1323.

14.   O'Callaghan, J., and Condon, S. (2000) Growth of *Lactococcus lactis* strains at low water activity: correlation with the ability to accumulate glycine betaine, *Int. J. Food Microbiol. 55*, 127-131.

15.   Velasco-Garcia, R., Chacon-Aguilar, V. M., Hervert-Hernandez, D., and Munoz-Clares, R. A. (2003) Inactivation of betaine aldehyde dehydrogenase from *Pseudomonas aeruginosa* and *Amaranthus hypochondriacus L.* leaves by disulfiram, *Chem. Biol. Interact. 143-144*, 149-158.

16.   Fan, F., and Gadda, G. (2005) On the catalytic mechanism of choline oxidase, *J. Am. Chem. Soc. 127*, 2067-2074.

17.   Gadda, G. (2003) pH and deuterium kinetic isotope effects studies on the oxidation of choline to betaine-aldehyde catalyzed by choline oxidase, *Biochim. Biophys. Acta 1650*, 4-9.

18.   Gadda, G., and McAllister-Wilkins, E. E. (2003) Cloning, expression, and purification of choline dehydrogenase from the moderate halophile *Halomonas elongata*, *Appl. Environ. Microbiol. 69*, 2126-2132.

19.   Gadda, G., Powell, N. L., and Menon, P. (2004) The trimethylammonium headgroup of choline is a major determinant for substrate binding and specificity in choline oxidase, *Arch. Biochem. Biophys. 430*, 264-273.

20.   Fan, F., and Gadda, G. (2005) Oxygen- and temperature-dependent kinetic isotope effects in choline oxidase: correlating reversible hydride transfer with environmentally enhanced tunneling, *J. Am. Chem. Soc. 127*, 17954-17961.

21.   Fan, F., and Gadda, G. (2007) An internal equilibrium preorganizes the enzyme-substrate complex for hydride tunneling in choline oxidase, *Biochemistry 46*, 6402-6408.

22. Gadda, G., Fan, F., and Hoang, J. V. (2006) On the contribution of the positively charged headgroup of choline to substrate binding and catalysis in the reaction catalyzed by choline oxidase, *Arch. Biochem. Biophys. 451*, 182-187.

23. Ghanem, M., and Gadda, G. (2005) On the catalytic role of the conserved active site residue His466 of choline oxidase, *Biochemistry 44*, 893-904.

24. Ghanem, M., and Gadda, G. (2006) Effects of reversing the protein positive charge in the proximity of the flavin N(1) locus of choline oxidase, *Biochemistry 45*, 3437-3447.

25. Pudney, C. R., Hay, S., Sutcliffe, M. J., and Scrutton, N. S. (2006) Alpha-secondary isotope effects as probes of "tunneling-ready" configurations in enzymatic H-tunneling: insight from environmentally coupled tunneling models, *J. Am. Chem. Soc. 128*, 14053-14058.

26. Rajagopalan, P. T., and Benkovic, S. J. (2002) Preorganization and protein dynamics in enzyme catalysis, *Chem. Rec. 2*, 24-36.

27. Fan, F., Ghanem, M., and Gadda, G. (2004) Cloning, sequence analysis, and purification of choline oxidase from *Arthrobacter globiformis*: a bacterial enzyme involved in osmotic stress tolerance, *Arch. Biochem. Biophys. 421*, 149-158.

28. Holyoak, T., Fenn, T. D., Wilson, M. A., Moulin, A. G., Ringe, D., and Petsko, G. A. (2003) Malonate: a versatile cryoprotectant and stabilizing solution for salt-grown macromolecular crystals, *Acta. Crystallogr. 59*, 2356-2358.

29. Otwinowski, Z., and Minor, W. (1997) Processing the x-ray diffraction data collected in oscillation mode, *Methods Enzymol. 276*, 20.

30. Kantardjieff, K. A., and Rupp, B. (2003) Matthews coefficient probabilities: Improved estimates for unit cell contents of proteins, DNA, and protein-nucleic acid complex crystals, *Protein Sci. 12*, 1865-1871.

31. Matthews, B. W. (1968) Solvent content of protein crystals, *J. Mol. Biol 33*, 491-497.

32. Vagin, A. A. a. T., A (1997) *J. Appl. Crystallogr. 30.*

33. Collaborative Computational Project, N. (1994) The CCP4 Suite.

34. Wohlfahrt, G., Witt, S., Hendle, J., Schomburg, D., Kalisz, H. M., and Hecht, H. J. (1999) 1.8 and 1.9 A resolution structures of the *Penicillium amagasakiense* and *Aspergillus niger* glucose oxidases as a basis for modelling substrate complexes, *Acta Crystallogr. 55*, 969-977.

35. Brunger, A. T., Adams, P. D., Clore, G. M., DeLano, W. L., Gros, P., Grosse-Kunstleve, R. W., Jiang, J. S, Kuszewski, J., Nilges, M., Pannu N. S., Read, R. J., Rice, L. M., Simonson, T. and Warren, G. L. (1998) Crystallography & NMR system: A new software suite for macromolecular structure determination, *Acta. Crystallogr. D54*, 16.

36. Terwilliger, T. C. (2004) Using prime-and-switch phasing to reduce model bias in molecular replacement, *Acta Crystallogr. D60*, 6.

37. Terwilliger, T. C. (2003) SOLVE and RESOLVE: automated structure solution and density modification, *Methods Enzymol. 374*, 16.

38. Kleywegt, G. J. a. J., T. A. (1997) Model building and refinement practice, *Methods Enzymol. 277*, 23.

39. Pannu, N. S., Murshudov, G. N., Dodson, E. J. and Read, R. J. (1998) Incorporation of prior phase information strengthens maximum-likelihood structure refinement, *Acta Crystallogr. D54*, 10.

40. Read, R. J. (1997) Model phases: Probabilities and bias, *Methods Enzymol. 277*, 19.

41. van Aalten, D. M., Bywater, R., Findlay, J. B., Hendlich, M., Hooft, R. W., and Vriend, G. (1996) PRODRG, a program for generating molecular topologies and unique molecular descriptors from coordinates of small molecules, *J. Comput. Aided Mol. Des. 10*, 255-262.

42. Lamzin, V. S. a. W., K. S. (1993) Automated refinement of protein models, *Acta Crystallogr. D49*, 19.

43. Laskowski, R. A., Moss, D. S., and Thornton, J. M. (1993) Main-chain bond lengths and bond angles in protein structures, *J. Mol. Biol. 231*, 1049-1067.

44. Morris, A. L., MacArthur, M. W., Hutchinson, E. G., and Thornton, J. M. (1992) Stereochemical quality of protein structure coordinates, *Proteins 12*, 345-364.

45. Kabsch, W., and Sander, C. (1983) Dictionary of protein secondary structure: pattern recognition of hydrogen-bonded and geometrical features, *Biopolymers 22*, 2577-2637.

46. Lide, D. R. (2000) Handbook of Chemistry and Physics, (Ed, -. Ed.), pp pp8-57, CRC Press, Boca Raton, Fl.

47. Albrecht, M., and Lengauer, T. (2003) Pyranose oxidase identified as a member of the GMC oxidoreductase family, *Bioinformatics (Oxford, England) 19*, 1216-1220.

48. Bannwarth, M., Bastian, S., Heckmann-Pohl, D., Giffhorn, F., and Schulz, G. E. (2004) Crystal structure of pyranose 2-oxidase from the white-rot fungus *Peniophora sp*, *Biochemistry 43*, 11683-11690.

49. Cavener, D. R. (1992) GMC oxidoreductases. A newly defined family of homologous proteins with diverse catalytic activities, *J. Molecul. Biol. 223*, 811-814.

50. Hallberg, B. M., Henriksson, G., Pettersson, G., and Divne, C. (2002) Crystal structure of the flavoprotein domain of the extracellular flavocytochrome cellobiose dehydrogenase, *J. Mol. Biol. 315*, 421-434.

51. Hallberg, B. M., Leitner, C., Haltrich, D., and Divne, C. (2004) Crystal structure of the 270 kDa homotetrameric lignin-degrading enzyme pyranose 2-oxidase, *J. Mol. Biol. 341*, 781-796.

52. Hecht, H. J., Kalisz, H. M., Hendle, J., Schmid, R. D., and Schomburg, D. (1993) Crystal structure of glucose oxidase from *Aspergillus niger* refined at 2.3 Å resolution, *J. Mol. Biol. 229*, 153-172.

53. Henriksson, G., Johansson, G., and Pettersson, G. (2000) A critical review of cellobiose dehydrogenases, *J. Biotechnol. 78*, 93-113.

54. Kiess, M., Hecht, H. J., and Kalisz, H. M. (1998) Glucose oxidase from *Penicillium amagasakiense*. Primary structure and comparison with other glucose-methanol-choline (GMC) oxidoreductases, *Eur. J. Biochem. 252*, 90-99.

55. Yue, Q. K., Kass, I. J., Sampson, N. S., and Vrielink, A. (1999) Crystal structure determination of cholesterol oxidase from Streptomyces and structural characterization of key active site mutants, *Biochemistry 38*, 4277-4286.

56. Fraaije, M. W., and Mattevi, A. (2000) Flavoenzymes: diverse catalysts with recurrent features, *Trends Biochem. Sci. 25*, 126-132.

57. Rand, T., Halkier, T., and Hansen, O. C. (2003) Structural characterization and mapping of the covalently linked FAD cofactor in choline oxidase from *Arthrobacter globiformis*, *Biochemistry 42*, 7188-7194.

58. Ghanem, M., Fan, F., Francis, K., and Gadda, G. (2003) Spectroscopic and kinetic properties of recombinant choline oxidase from *Arthrobacter globiformis*, *Biochemistry 42*, 15179-15188.

59. Cook, P. F., Blanchard, J. S., and Cleland, W. W. (1980) Primary and secondary deuterium isotope effects on equilibrium constants for enzyme-catalyzed reactions, *Biochemistry 19*, 4853-4858.

60. Cleland, W. W. (1982) The use of isotope effects to determine transition-state structure for enzymic reactions, *Methods Enzymol. 87*, 625-641.

61. Sobrado, P., and Fitzpatrick, P. F. (2003) Solvent and primary deuterium isotope effects show that lactate CH and OH bond cleavages are concerted in Y254F flavocytochrome b2, consistent with a hydride transfer mechanism, *Biochemistry 42*, 15208-15214.

62. Hecht, H. J., Schomburg, D., Kalisz, H., and Schmid, R. D. (1993) The 3D structure of glucose oxidase from *Aspergillus niger*. Implications for the use of GOD as a biosensor enzyme, *Biosens. Bioelectron 8*, 197-203.

63. Martin, S. F., Follows, B. C., Hergenrother, P. J., and Trotter, B. K. (2000) The choline binding site of phospholipase C (*Bacillus cereus*): insights into substrate specificity, *Biochemistry 39*, 3410-3415.

64. Pomponi, M., Sacchi, S., Colella, A., Patamia, M., and Marta, M. (1998) The role of TRP84 in catalytic power and the specificity of AChE, *Biophys. Chem. 72*, 239-246.

65. Gasch, A. P., Spellman, P. T., Kao, C. M., Carmel-Harel, O., Eisen, M. B., Storz, G., Botstein, D., and Brown, P. O. (2000) Genomic expression programs in the response of yeast cells to environmental changes, *Mol. Biol. Cell 11*, 4241-4257.

66. Harel, M., Kryger, G., Rosenberry, T. L., Mallender, W. D., Lewis, T., Fletcher, R. J., Guss, J. M., Silman, I., and Sussman, J. L. (2000) Three-dimensional structures of *Drosophila melanogaster* acetylcholinesterase and of its complexes with two potent inhibitors, *Protein Sci. 9*, 1063-1072.

67. Kwak, B. Y., Zhang, Y. M., Yun, M., Heath, R. J., Rock, C. O., Jackowski, S., and Park, H. W. (2002) Structure and mechanism of CTP:phosphocholine cytidylyltransferase (LicC) from *Streptococcus pneumoniae*, *J. Biol. Chem. 277*, 4343-4350.

68. Horn, C., Sohn-Bosser, L., Breed, J., Welte, W., Schmitt, L., and Bremer, E. (2006) Molecular determinants for substrate specificity of the ligand-binding protein OpuAC from *Bacillus subtilis* for the compatible solutes glycine betaine and proline betaine, *J. Mol. Biol. 357*, 592-606.

69. Schiefner, A., Breed, J., Bosser, L., Kneip, S., Gade, J., Holtmann, G., Diederichs, K., Welte, W., and Bremer, E. (2004) Cation-pi interactions as determinants for binding of the compatible solutes glycine betaine and proline betaine by the periplasmic ligand-binding protein ProX from *Escherichia coli*, *J. Biol. Chem. 279*, 5588-5596.

70. Schiefner, A., Holtmann, G., Diederichs, K., Welte, W., and Bremer, E. (2004) Structural basis for the binding of compatible solutes by ProX from the hyperthermophilic archaeon *Archaeoglobus fulgidus*, *J. Biol. Chem. 279*, 48270-48281.

71. Cleland, W. W. (1982) The use of pH studies to determine chemical mechanisms of enzyme-catalyzed reactions, *Methods Enzymol. 87*, 390-405.

72. Agmon, N. (1985) A diffusion Michaelis-Menten mechanism: continuous conformational change in enzymatic kinetics, *J. Theoret. Biol. 113*, 711-717.

73.   Sobrado, P., Daubner, S. C., and Fitzpatrick, P. F. (2001) Probing the relative timing of hydrogen abstraction steps in the flavocytochrome b2 reaction with primary and solvent deuterium isotope effects and mutant enzymes, *Biochemistry 40*, 994-1001.

74.   Somogyi, B., Norman, J. A., Zempel, L., and Rosenberg, A. (1988) Viscosity and transient solvent accessibility of Trp-63 in the native conformation of lysozyme, *Biophys. Chem. 32*, 1-13.

75.   Su, Q., and Klinman, J. P. (1999) Nature of oxygen activation in glucose oxidase from Aspergillus niger: the importance of electrostatic stabilization in superoxide formation, *Biochemistry 38*, 8572-8581.

76.   Emanuele, J. J., and Fitzpatrick, P. F. (1995) Mechanistic studies of the flavoprotein tryptophan 2-monooxygenase. 1. Kinetic mechanism, *Biochemistry 34*, 3710-3715.

77.   Grissom, C. B., and Cleland, W. W. (1988) Isotope effect studies of the chemical mechanism of pig heart NADP isocitrate dehydrogenase, *Biochemistry 27*, 2934-2943.

78.   Bradford, M. M. (1976) A rapid and sensitive method for the quantitation of microgram quantities of protein utilizing the principle of protein-dye binding, *Anal. Biochem. 72*, 248-254.

3.7. Appendix

```
CHO                     ~~a~~  ---1-->  ~~~~~b~~~~~~    -2->        ~~~c~~
CHO       -------------mhidnienlsdREFDYIVVGGGSAGAAVAARLSEDpaVSVALVEAGPddrgvpevlq   57
GOX 1cf3  ---------gieaslltdpkdvsgRTVDYIIAGGGLTGLTTAARLTENpnISVLVIESGSyesdrgpiie   63
HNL 1ju2  lattsdhdfsylsfaydatdleleGSYDYVIVGGGTSGCPLAATLSEK--YKVLVLERGS----------   58
CDH 1naa  ----------------------TPYDYIIVGAGPGGIIAADRLSEAg-KKVLLLERGGpstkqtggty  259
COX 1n4w  ----------------------GYVPAVVIGTGYGAAVSALRLGEAg-VQTLMLEMGQlwnqpgpdgn   53
P2Ox 2f5v ---------------------mdIKYDVVIVGSGPIGCTYARELVGAg-YKVAMFDIGEidsglkigah   89


CHO       ~~~c~~~~
CHO       ldrwme llesgydw--------------------------------dypiepqengnsfmrharak   92
GOX 1cf3  dlnaygdifgssvdh--------------------------------ayetvelatnnqtalirsgn   98
HNL 1ju2  ----------------------------------------------------------------   58
CDH 1naa  vapwatssgltkfdipgl---------------------------feslftdsnpfwwckditvfagc  300
COX 1n4w  ifcgmlnpdkrsswfknrteaplgsf-------------lwldvvnrnidpyagvldrvnydqmsvyvgr  110
P2Ox 2f5v kkntveyqknidkfvnviqgqlmsvsvpvntlvvdtlsptswqastffvrngsnpeqdplrnlsgqavtr  159


CHO       ~~d~~~                              ~~~e~~
CHO       vmg gCSSH-------------------------------------NSCIAFWAPRE-DL-  112
GOX 1cf3  glggSTLV-------------------------------------NGGTWTRPHKA-QV-  119
HNL 1ju2  ----LPTAypnvltadgfvynlqqeddgktpverfvsedgidnvrgrvlggtsiiNAGVYARANTS-IY-  122
CDH 1naa  lvggGTSV-------------------------------------NGALYWYPNDG-DF-  321
COX 1n4w  gvggGSLV-------------------------------------NGGMAVEPKRSyFEe  133
P2Ox 2f5v vvggMSTH-------------------------------------WTCATPRFDREqRPl  182


CHO       ~~~~~~      ~~~~~~f~~~~~~ -3>              ~~g~~
CHO       --------DeweakygatgWnaeaAWPLYKRL-Etnedagpd---------aphhgdsGPvHLMN-V---  160
```

```
GOX 1cf3    --------DswetvfgnegWnwdnVAAYSLQA-ErarapnakqiaaghyfnaschgvnGTvHAGP-R---  176
HNL 1ju2    --------Sasg-----vdWdmdlVNQTYEWV-E-----------------------DT-IVYK-P---  149
CDH 1naa    --------Sssvg--wpssWt--nHAPYTSKL-S----------------------SRlPSTD-Hpst  353
COX 1n4w    ilp--rvdSs--------eM----YDRYFPRAnS----------------------ML-RVNH-Idt-  162
P2Ox 2f5v   lvkddadaDd--------aE----WDRLYTKA-E----------------------SYfQTGTdQ---  212
```

```
CHO                      ~~~~~~~h~~ ~ ~~~          -4->
CHO         ---P----Pk---DPTGVALLDA-C--EQagiprakf-ntgttvvnGANFFQINRR--Ad----------  204
GOX 1cf3    ---DtgddY----SPIVKALMSA-V--EDrgvptkkd--fgcgdphGVSMFPNTLH--Ed----------  222
HNL 1ju2    ---N----S----QSWQSVTKTA-F--LEagvhpnhg--fsldheeGTRITGSTFD--Nk----------  191
CDH 1naa    dgqR----Yl---EQSFNVVSQL-L--KGqgynqatindnpnykdhVFGYSAFDFL--N-----------  400
COX 1n4w    -kwF----EdtewYKFARVSREQaGkaGL-----------------GTVFVPNVYDfgYmqreaagevpk  210
P2Ox 2f5v   ---F----Ke---SIRHNLVLNK-La-EEykg------------qrDFQQIPLAATr-Rspt--------  249
```

```
CHO                      ~~~i~~~        ~j~~  ~~~k~~~    ~~~l~~~
CHO         ------------GtRSsSSVSyIH-P--Ive----qANFTLLTGLRARQLVFdAd---rRCTGVDIV-Ds  251
GOX 1cf3    ------------QvRSdAAREwLL-P--Nyq----rPNLQVLTGQYVGKVLLsQngttpRAVGVEFG-Th  272
HNL 1ju2    -----------gTrHA-ADEL-LN-KgnS-------NNLRVGVHASVEKIIFsNap-glTATGVIYR-Ds  238
CDH 1naa    ------------GkRAgPVATyLQ-Ta-La-----rPNFTFKTNVMVSNVVR-Ng---sQILGVQTN-D-  445
COX 1n4w    salateviygnnHgKQsLDKTyLA-AalGt------GKVTIQTLHQVKTIRQtKd----GGYALTVE-Qk  268
P2Ox 2f5v   ----------fvE-WS-SANTvFDlQn-Rpntdape ERFNLFPAVACERVVRnAln--sEIESLHIHdLi  304
```

```
CHO         -   ---5-- - --->   ~~~~~~m~~~~~~    ~~~~n~~       ~
CHO         a----fgHt----HRLTAR--N-EvVL--STGAIDTPKLLMLSG----IGpaahlae-----------hg  293
GOX 1cf3    k-----gNt----HNVYAK--H-EvLL--AAGSAVSPTILEYSG----IGmksilep-----------lg  313
HNL 1ju2    n-----gTp----HQAFVR--SkG-EVivSAGTIGTPQLLLSG----VGpesylss-----------ln  281
CDH 1naa    -------PtlgpnGFIPVTpkG-RvIL--SAGAFGTSRILFQSG----IGptdmiqtvqsnptaaaalpp  501
COX 1n4w    dtdgkllA-----TKEISC--R-YlFL--GAGSLGSTELLVRARdtgtLP------------------  308
P2Ox 2f5v   s-----gD-----RFEIKA--D-VyVL--TAGAVHNTQLLVNSG----FGqlgrpn------------p  342
```

```
CHO                           --6-  >
CHO        ievlVDSpGVGEHLQD-HPEGVVQFE----AK-------------------------------------  320
GOX 1cf3   idtvVDL-PVGLNLQD-QTTATVRSR----IT-------------------------------------  339
HNL 1ju2   ipvvLSHpYVGQFLHD-NPRNFINIL----PP-------------------------------------  308
CDH 1naa   qnqwINL-PVGMNAQD-NPSINLVFT----HP-------------------------------------  527
COX 1n4w   ----NLNsEVGAGWGPnGNIMTARANhmwnPT-------------------------------------  336
P2Ox 2f5v  tnppELLpSLGSYITE-QSLVFCQTV----MStelidsvksdmtirgtpgeltysvtytpgastnkhpdw 407


CHO                                          --7->
CHO        ----------------Qp-----mVa-----------------------eSvq--wwE-IGIFT--Pta  340
GOX 1cf3   ----------------Sag----aG------------------------Qg-----Q-AAWFA--Tfn  355
HNL 1ju2   ----------------Np-----iEp-----------------------Ti-----VtVLGIS--N--  323
CDH 1naa   ----------------Si------DayenwadvwsnprpadaaqylanqsgVfagaspK-LNFWR--Ays  572
COX 1n4w   ----------------Ga------Hq-----------------------Ss----iPaLGIDAw-Dns  354
P2Ox 2f5v  wnekvknhmmqhqedpLpipfedpE-------------------------P------Q-VTTLFqpSh-  443


CHO                                         --8-->
CHO        dg-----------------------------------------------ldrpDLMMHYGS----Vpfd  358
GOX 1cf3   etfgdysekahellntkleqwaeeavarggfhnttalliqyenyrdwivnhnvaYSELFLDTa---G---  419
HNL 1ju2   ------------------------------------------------------DFYQCSFS----Slpf  335
CDH 1naa   gsd---------------------------------------------gftrYAQGTVRP----Gaas  591
COX 1n4w   ------------------------------------------------dsSVFAEIAP----Mpag  368
P2Ox 2f5v  ------------------------------------------------PWHTQIHRdafsYgav  459


CHO                ~~~o   ~~   ----9-->        ~p~            ~q~
CHO        mntlr------hgypttenGFSLTPNVt--HaRSR--G-TVRLRS--------Rdfr-dkPMVD--PrYf  406
GOX 1cf3   -------------------VASFDVWDl--LpFTR--G-YVHILD--------KdpylhhFAYD--PqYf  455
HNL 1ju2   ttppfgffpsssyplpnstFAHFASKVa--GpLSY--G-SLTLKS--------SsnvrvsPNVK--FnYy  390
CDH 1naa   vnss--------lpynasqIFTITVYLstgI-QSR--G-RIGIDAa-------Lr-----GTVLtpP-Wl  636
COX 1n4w   l--------------etwVSLYLAIT---KnPQR--GtFVYDAAt-------D------RAKL--NwTr  403
P2Ox 2f5v  qqs-----------idsrlIVDWRFFG---RtEPKeeN-KLWFSDkitdaynmPq-----PTFD--FrF-  506
```

```
CHO       ~~~~~~~~~~~r~~~ ~~ ~~~~~~     ~    ---10- >          ~~~   s
CHO       tDpeGHDmRVMVAGIRKAR-EI-Aaqpam--------aewtgRE-L--S--------Pgveaqtde---e  452
GOX 1cf3  lN--ELDlLGQAAATQLAR-NI-Snsgam--------qtyfaGE-T--I--------Pgdnlaydadlsa  502
HNL 1ju2  sN--LTDlSHCVSGMKKIG-EL-LstdalkpykvedlpgvegFN-Il-G--------Iplpkdqtdd-aa  445
CDH 1naa  vN--PVDkTVLLQALHDVV-SN-Igsi------------pglTM-I--T--------Pdvtqtl------  673
COX 1n4w  dQnaPAV-NAAKALFDRINkANgT------------------IY-R--Ydlfgtqlkaf-----------  440
P2Ox 2f5v -Pa-GRTsKEAEDMMTDMC-VMsAki---------------gGFlPgsL--------P-----------  538


CHO       ~~~s~~~~~  ~                   11> ~~t~~        ~
CHO       lqdyirkT---HN----TvYHPVGTVRMGave-demSPLDPELRVKGvT-GLRVADASVMpE-Hv-TVNP  511
GOX 1cf3  wteyipyH---FRp---N-YHGVGTCSMMpke--mgGVVDNAARVYGvQ-GLRVIDGSIPpT-Qm-SSHV  560
HNL 1ju2  fetfcreS---VA----SyWHYHGGCLVG-------KVLDGDFRVTGiN-ALRVVDGSTF-P-YtpASHP  498
CDH 1naa  -eeyvdaYdpaTMn---S-NHWVSSTTIGssp--qsAVVDSNVKVFGtN-NLFIVDAGIIpH-Lp-TGNP  733
COX 1n4w  ------aD---DF----C-YHPLGGCVLG-------KATDDYGRVAGyK-NLYVTDGSLIpG-Sv-GVNP  486
P2Ox 2f5v -------Q---FMepglV-LHLGGTHRMGfdekednCCVNTDSRVFG-FkNLFLGGCGNIpTaY--GANP  594


CHO       ~~~~~~u~~~~~~~~~
CHO       NITVMMIGERCADLIR---------  527
GOX 1cf3  MTVFYAMALKISDAILedyasmq--  583
HNL 1ju2  QGFYLMLGRYVGIKILqersasd--  521
CDH 1naa  QGTLMSAAEQAAAKILalaggp---  755
COX 1n4w  FVTITALAERNVERIIkqdv-----  506
P2Ox 2f5v TLTAMSLAIKSCEYIKqnftpspft  619
```

Figure A5.1. Structurally based amino acid sequence alignment and secondary structure assignment for choline oxidase and selected homologs with the Secondary Structure Matching server *(1)*.

CHO, choline oxidase from *Arthrobacter globiformis*, GI:31979241 and the structure reported here; GOX, glucose oxidase from *Aspergillus niger*, PDB code 1cf3; HNL, hydroxynitrile lyase from *Prunus dulcis* (almond), PDB code 1ju2, gi|23200196; CDH, cellobiose dehydrogenase from *Phanerochaete chrysosporium*, PDB code 1naa; COX, cholesterol oxidase from *Brevibacterium*

sterolicum, PDB code 1n4w; P2Ox, pyranose 2-oxidase from *Peniophora* sp. SG, PDB code 2f5v. Residues that are 100% conserved are highlighted in green, those that form the putative choline binding site in CHO are in yellow, those that form the loop are boxed in red, and those that comprise the substrate binding domain are boxed in black. The secondary structure for choline oxidase is indicated by dashed arrows under magenta and tildes' under cyan for β-strands and α-helixes, respectively.

1.   Krissinel, E., and Henrick, K. (2004) Secondary-structure matching (SSM), a new tool for fast protein structure alignment in three dimensions, *Acta Crystallogr. D60*, 2256-2268.
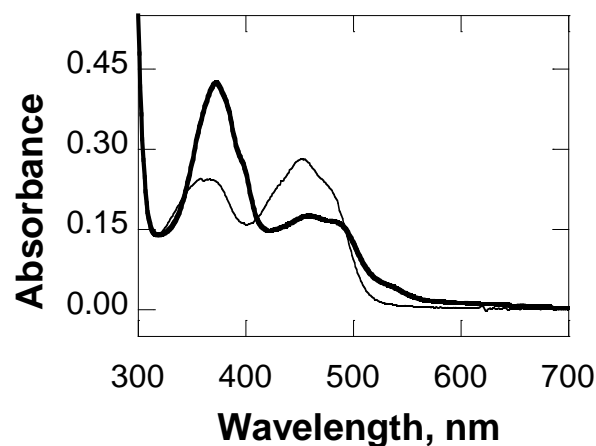
Figure A3.2. UV-visible absorbance spectra for CHO-E312A.
Thick line represents a mixture of anionic semiquinone and oxidized flavin as purified in 200 mM Tris-Cl, pH 8. Thin line represents fully oxidized flavin after dialysis in 20 mM sodium phosphate and 20 mM sodium pyrophosphate, pH 6, and 20 mM Tris-Cl, pH 8.
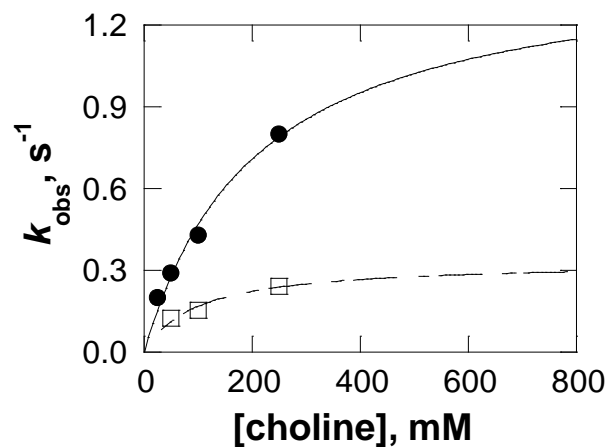
Figure A3.3. Rate of flavin reduction in CHO-E312Q as a function of choline or 1,2-[^{2}H$_4$]-choline concentrations. (●) represents choline and (○) represents 1,2-[^{2}H$_4$]-choline. Experiments were carried out in 50 mM sodium pyrophosphate, pH 10 and 25 ^{o}C at varying concentrations of choline. Data were fit to equation 5.

Figure A3.4. Estimation of K_m for oxygen in CHO-E312D at pH 5 and 10.

Panel A represents the plot of v_o, s^{-1} versus $[O_2]$, μM at pH 5. Panel B represents the plot of v_o, s^{-1} versus $[O_2]$, μM at pH 10. Apparent steady state kinetics to determine the K_m for oxygen was carried out at varying concentrations of oxygen between 4.3 and 247 μM, and at fixed choline concentration of 400 mM. The reaction was started in 50 mM sodium pyrophosphate, pH 5 or 10, by the addition of CHO-E312D to a final concentration of ~3 μM in a total reaction volume of 1 ml at 25 $^{\circ}C$. In both plots, the rate of the reaction v_o, s^{-1} on the ordinate axis was plotted against the log of the concentration of oxygen on the abscissa axis.
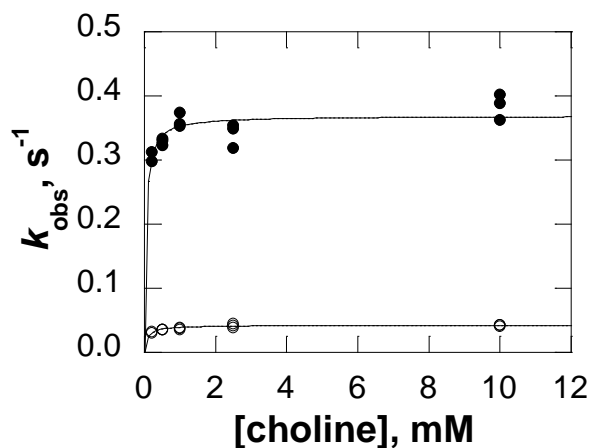
Figure A3.5. Rate of flavin reduction in CHO-E312D as a function of choline or 1,2-[$^2H_4$]-choline concentrations. (●) represents choline and (○) represents 1,2-[$^2H_4$]-choline. Experiments were carried out in 50 mM sodium pyrophosphate, pH 10 and 25 $^{\circ}C$ at varying concentrations of choline. Data were fit to equation 5.

Table A3.1. Structural Similarity between Choline Oxidase and Selected Homologues[a]

|	GOX, 1cf3[b]	HNL, 1ju2[c]	CDH, 1naa[d]	COX, 1n4w[e]	P2Ox, 2f5v[f]
r.m.s. Δ (Å)[g]					
CHO	1.6	2.1	1.7	2.6	2.5
GOX, 1cf3		2.6	2.2	2.9	2. 6
HNL, 1ju2			2.5	3.2	2.9
CDH, 1naa				2.8	2.8
COX, 1n4w					3.2
Q-Score[h]					
CHO	0.241	0.231	0.254	0.204	0.187
GOX, 1cf3		0.177	0.193	0.168	0.164
HNL, 1ju2			0.197	0.17	0.161
CDH, 1naa				0.186	0.164
COX, 1n4w					0.156
Sequence Identity					
CHO	0.299	0.253	0.244	0.172	0.192
GOX, 1cf3		0.237	0.24	0.188	0.162
HNL, 1ju2			0.24	0.169	0.159
CDH, 1naa				0.182	0.198
COX, 1n4w					0.153

[a] Structures were superimposed using the multiple alignment function in the Secondary Structure Matching server (*295*). [b]glucose oxidase; [c]hydroxynitrile lyase; [d]cellobiose dehydrogenase; [e]cholesterol oxidase; [f]pyranose-2-oxidase; [g]Root mean squared difference. [h]The Q score is defined as $N_{align} * N_{align}/ (1+(RMSD/R_o)^2) * N_{res1} * N_{res2}$, where N_{align} is the length of alignment and N_{res1} and N_{res2} are the number of total residues in the choline oxidase and target structure.

Table A3.2. pH-Dependence of the Steady State Kinetic Parameters with Choline or 1,2-[^{2}H$_4$]-Choline as Substrate for CHO-E312D Determined at 0.25 mM Oxygen and 25 ^{o}C.

These data were used for Figures 3,4 and 5.

pH	$(k_{cat}/K_m)_H$ M^{-1}s^{-1}	$(k_{cat})_H$ s^{-1}	$(K_m)_H$ mM^{-1}	$(k_{cat}/K_m)_D$ M^{-1}s^{-1}	$(k_{cat})_D$ s^{-1}	$(K_m)_D$ mM^{-1}	$^D(k_{cat}/K_m)$	$^D(k_{cat})_H$
5.0	16 ± 1	0.07 ± 0.01	4.63 ± 0.40	nd	nd	nd	nd	nd
5.5	54 ± 7	0.18 ± 0.01	3.29 ± 0.70	nd	nd	nd	nd	nd
6.0	140 ± 6	0.24 ± 0.01	1.68 ± 0.09	44 ± 4	0.036 ± 0.001	0.81 ± 0.08	3.2 ± 0.7	6.7 ± 0.3
6.5	476 ± 33	0.26 ± 0.01	0.55 ± 0.05	108 ± 9	0.035 ± 0.001	0.32 ± 0.03	4.8 ± 0.9	7.2 ± 0.4
7.0	1303 ± 297	0.26 ± 0.01	0.20 ± 0.02	297 ± 20	0.035 ± 0.001	0.12 ± 0.01	4.4 ± 0.8	7.4 ± 0.4
7.5	2460 ± 154	0.21 ± 0.01	0.09 ± 0.01	585 ± 60	0.030 ± 0.001	0.05 ± 0.01	4.5 ± 0.7	7.1 ± 0.2
8.0	3790 ± 157	0.27 ± 0.01	0.04 ± 0.01	756 ± 110	0.033 ± 0.001	0.04 ± 0.01	5.0 ± 0.2	7.9 ± 0.1
8.5	5837 ± 349	0.29 ± 0.01	0.05 ± 0.01	1385 ± 60	0.038 ± 0.001	0.03 ± 0.01	4.1 ± 0.3	7.8 ± 0.1
9.0	7239 ± 577	0.28 ± 0.01	0.04 ± 0.01	1629 ± 120	0.044 ± 0.001	0.03 ± 0.01	4.4 ± 0.2	6.4 ± 0.1
9.5	6390 ± 583	0.27 ± 0.01	0.04 ± 0.01	1434 ± 120	0.034 ± 0.001	0.02 ± 0.01	4.1 ± 0.7	7.9 ± 0.3
10.0	7097 ± 394	0.26 ± 0.01	0.04 ± 0.01	1449 ± 260	0.045 ± 0.002	0.03 ± 0.01	4.9 ± 0.9	5.8 ± 0.2

The k_{cat} and K_m parameters were obtained by fitting the initial rate data to v$_o$/e = k_{cat}S/(K_m+S); the k_{cat}/K_m parameters were obtained by fitting the initial rate data to v$_o$/e = k_{cat}S/{k_{cat}/[1/(k_{cat}/K_m)]+S}. nd : not determined ; due to data inconsistency with 1,2-[^{2}H$_4$]-choline at pH 5 and 5.5.

Table A3.3. Solvent viscosity effects on steady state kinetic parameters for CHO-E312D with choline as substrate and glucose and sucrose as viscosigens at 0.25 mM Oxygen and 25 $^{\circ}$C.

kinetic parameters				
glucose				
Relative viscosity	1.00	1.62	2.70	4.19
k_{cat}/K_m, M^{-1}s^{-1}	5050 ± 260	5380 ± 170	6670 ± 480	7620 ± 410
Viscosity effect on k_{cat}/K_m	1.00	0.94	0.76	0.66
k_{cat}, s^{-1}	0.19 ± 0.01	0.20 ± 0.01	0.22 ± 0.01	0.25 ± 0.01
Viscosity effect on k_{cat}	1.00	0.95	0.90	0.77
sucrose				
Relative viscosity	1.00	1.33	2.33	3.75
k_{cat}/K_m, M^{-1}s^{-1}	4400 ± 240	4610 ± 290	5030 ± 280	5340 ± 380
Viscosity effect on k_{cat}/K_m	1.00	0.95	0.87	0.82
k_{cat}, s^{-1}	0.21 ± 0.01	0.23 ± 0.01	0.25 ± 0.01	0.26 ± 0.01
Viscosity effect on k_{cat}	1.00	0.92	0.85	0.80

The kinetic parameters were obtained by fitting the initial rates to the Michaelis-Menten equation and the viscosity effects on the parameters obtained from $(k)_o/(k)_\eta = S(\eta_{rel}-1)+1$.

CHAPTER 4

Effect of a Conservative Mutation of an Active Site Residue Involved in Substrate Binding on the Hydride Tunneling Reaction Catalyzed by Choline Oxidase

4.1. Abstract

Quantum mechanical tunneling has been extensively demonstrated to date in enzymatic reactions where hydride ions, protons, or hydrogen atoms are transferred. These transfer reactions have been shown to occur either with or without distance and geometry sampling of the reactive configurations conducive to the transfer reactions. The reaction of alcohol oxidation catalyzed by choline oxidase is a documented example of an enzymatic reaction in which a hydride ion tunnels without appreciable sampling, and occurring within a highly preorganized enzyme-substrate complex [Gadda, G. (2008) Biochemistry 47, 13745-13753]. In the present study, a glutamate residue (312) that participates in substrate binding has been replaced with aspartate by site-directed mutagenesis, in order to alter the relative positioning of the hydride donor and acceptor in the active site of the enzyme. The effect of temperature on the rate constants for anaerobic hydride transfer reaction (k_{red}) with choline and 1,2-[^{2}H$_4$]-choline as substrate for the enzyme containing aspartate at position 312 were determined at pH 8.0 using a stopped-flow spectrophotometer. The thermodynamic parameters associated with the enzymatic reaction and the temperature effects on the kinetic isotope effects are consistent with significant distance and geometry sampling of the reactive configuration that is required for the tunneling of the hydride ion in the aspartate-containing enzyme. This allowed us to estimate the effect of

disrupting the relative positioning of the hydride donor and acceptor to the rate constant for the tunneling of the hydride ion within the active site of wild-type choline oxidase, and how a conservative substitution of an active site residue involved in substrate binding but not directly in catalysis can affect the catalytic mechanism of an enzymatic reaction.

4.2. Introduction

Quantum mechanical tunneling has been implicated in enzymatic reactions where hydrogen atoms, protons or hydride ions are transferred (*1-15*). Well characterized examples include, but are not limited to, choline oxidase,(*9, 16, 17*) alcohol dehydrogenase (*2, 18-22*), dihydrofolate reductase (*13, 23-25*), lipoxygenase-1 (*26-28*), morphinone reductase (*4, 29, 30*), pentaerythritol tetranitrate (PETN) reductase (*4*), and glucose oxidase (*31-33*). The charged or neutral hydrogen transfers catalyzed by these enzymes have been shown to occur either with or without appreciable distance and geometric sampling of the reactive configurations conducing to the reactions. Transfer reactions without sampling occur in a relatively rigid or preorganized active site environment with minimal reorientations of the active site geometry, whereas sampling is associated with conformational motions that reorganize the active site environment to achieve the overall geometry required for the reaction (*34, 35*). Preorganization of the reactive configurations coupled with the minimized reorganization of the active site has been accepted as an important factor to the enhancement of catalytic reactions (*36-38*). Different effects of temperature on the rate constants for the transfer reactions using protiated and deuterated (or in limited cases tritiated) substrates, along with their associated primary kinetic isotope effects,

have been mainly used to decipher between the two cases of tunneling (for recent reviews see *14, 32, 39*). Pressure effects have also emerged more recently as probes to investigate mechanisms of transfer reactions (*39, 40*).

The reaction of alcohol oxidation catalyzed by choline oxidase (E.C. 1.1.3.17; choline-oxygen 1-oxidoreductase) is a documented example of an enzymatic oxidation involving the transfer of a hydride ion within a highly preorganized enzyme-substrate complex where tunneling occurs without appreciable distance and geometric sampling (for a recent review on the topic see *9*). Preorganization is attained through a conformational change of the enzyme-substrate complex that is associated with the deprotonation of the alcohol substrate to yield the corresponding activated alkoxide species and is kinetically independent from the subsequent reaction of hydride ion transfer (Scheme 4.1), as indicated by kinetic isotope effects studies on the wild-type and some active site variants of the enzyme (Figure 4.1) (*9, 41-43*). Electrostatic interactions of the trimethylammonium headgroup and the alkoxide oxygen atom of the activated alcohol substrate with the side chains of Glu312 and His466, respectively, contribute to assemble the hydride donor and acceptor in a configuration that is required for the subsequent tunneling of the hydride ion (*43-45*). Limited independent movement between the alkoxide C-H bond at the α-carbon which acts as the hydride donor and the N(5) atom of the flavin isoalloxazine ring acting as the hydride acceptor has been proposed to be a major contributor to the full tunneling transfer of the hydride ion, as suggested by temperature effects studies on the reaction catalyzed by choline oxidase (*16, 41*). A recent study on choline oxidase showed that upon shortening the negatively charged side chain at position 312 with the conservative replacement of glutamate to aspartate, the limiting rate constant for flavin reduction (k_{red}) decreases from 93 s^{-1} to 0.4 s^{-1} (*43*). This suggests that besides participating in substrate binding, as demonstrated by at least a 500-

fold increase in the K_d value for choline when glutamate 312 is substituted with glutamine (*43*), Glu312 also plays a major role in positioning the substrate for efficient hydride transfer (*43*). However, how the hydride ion transfer reaction is affected by the conservative replacement of glutamate with aspartate has yet to be addressed at a mechanistic level.
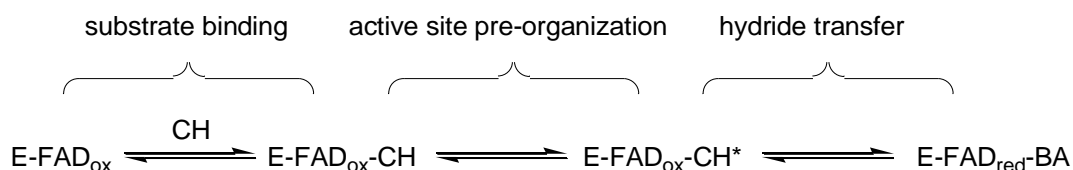
Scheme 4.1. Preorganization of the activated enzyme-substrate complex in the reaction of alcohol oxidation catalyzed by choline oxidase.
E, enzyme; FAD_{ox}, oxidized flavin; FAD_{red}, reduced flavin; CH, choline; BA, betaine aldehyde.

In this study, we have investigated the effect of temperature on the k_{red} values with choline or 1,2-[$^2H_4$]-choline as substrate for the choline oxidase variant containing aspartate at position 312 using anaerobic stopped-flow spectrophotometry. The thermodynamic parameters associated with the enzymatic reaction and the temperature effects on the substrate kinetic isotope are consistent with a tunneling reaction in the aspartate-containing enzyme occurring with significant distance and geometry sampling of the reactive configuration that conduce to the transfer reaction. The mechanistic data presented herein, when compared to a previously reported analysis on the mechanism of hydride transfer in the wild-type enzyme, provided a quantitative analysis of the effect of altering the relative positioning of the hydride donor and acceptor to the hydride tunneling reaction in choline oxidase. The study also serves as an example of how a conservative substitution of a residue involved in substrate binding can have an effect on catalytic events without affecting the kinetic parameters that report on substrate binding.
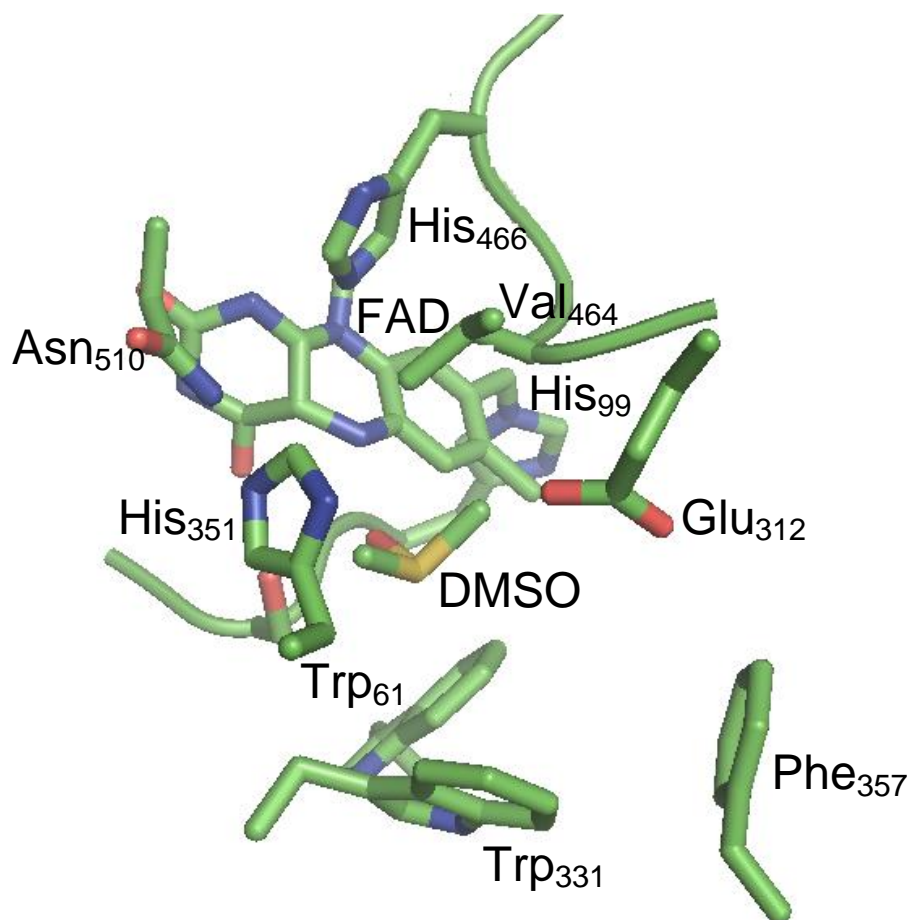
Figure 4.1. X-ray crystal structure of the active site of wild-type choline oxidase resolved to 1.86 Å (PDB 2jbv).
DMSO was used as an additive during the crystallization process. Note the significant distortion of the flavin ring at the C(4a) atom, which originates from the presence of a C(4a)-flavin adduct (not shown here) (51).

4.3. Experimental Procedures

Materials. Plasmid pET/*codA* E312D harboring the gene for recombinant choline oxidase was used to express the enzyme variant with aspartate instead of glutamate at position 312 in *Escherichia coli* strain Rosetta (DE3)pLysS (*43*). Choline chloride was from ICN (Aurora, OH). 1,2-[^{2}H$_4$]-Choline bromide was from Isotech Inc. (Miamisburg, OH). Glucose and glucose

oxidase were from Sigma-Aldrich (St. Louis, MO). All other reagents used were of the highest purity commercially available.

Kinetic Assays. The variant of choline oxidase with aspartate instead of glutamate at position 312 was expressed and purified to homogeneity as previously described (*43, 46, 47*). Pre-steady state measurements were carried out anaerobically on a Hi-Tech SF-61 stopped-flow spectrophotometer thermostated from 7 to 37 $^{\circ}$C in the presence of a mixture of glucose (5 mM) and glucose oxidase (0.5 μM) as previously described (*42*). The addition of glucose and glucose oxidase to the enzyme and substrate was required to scavenge trace amounts of oxygen due to the low K_{m} values for oxygen of ≤2 μM previously determined for the Glu312Asp enzyme (*43*). Equal volumes of enzyme and choline (or 1,2-[^{2}H$_4$]-choline) were anaerobically mixed in the stopped-flow spectrophotometer resulting in a reaction mixture with a final enzyme concentration of ~0.01 mM and substrate concentrations of 0.05 to 10 mM. The substrate isotopomers were alternated to determine the isotopic effect on the reaction of flavin reduction at the different temperatures, with each substrate concentration assayed in triplicate.

Data Analysis. Stopped-flow traces were fit to eq. 1, which describes a single exponential process where k_{obs} is the observed rate for the reduction of the enzyme-bound flavin at any given concentration of substrate, t is time, A is the value of absorbance at 450 nm at any given time, B is the amplitude for the total change in absorbance, and C is the absorbance at 450 nm at infinite time. Pre-steady state kinetic parameters were determined by using eq. 2, where A is the concentration of substrate, k_{red} is the limiting first-order rate constant for flavin reduction at saturating substrate concentrations and K_{d} is the dissociation constant for binding of the substrate

to the enzyme. The temperature dependences of the rate of flavin reduction at saturating concentration of the substrate were determined by fitting the stopped-flow data with the Eyring equation (eq 3), where k_B is Boltzmann constant, h is Plank's constant, k_{red} is the limiting first-order rate constant for flavin reduction at saturating substrate concentrations, R is gas constant, T is temperature, and $\Delta S^{\ddagger}$ and $\Delta H^{\ddagger}$ are the entropy and enthalpy of activations, respectively. The temperature dependence of the kinetic isotope effect was determined by fitting the data with the Arrhenius equation (eq. 4), where $^D(k_{red})$ is the substrate kinetic isotope effect on the limiting rate constants for flavin reduction when the enzyme is saturated with the substrate, A_H/A_D is the isotope effect on the preexponential factors and $[E_a(D)-E_a(H)]$ is the isotope effect on the energy of activation. Data were fit with KaleidaGraph software (Synergy Software, Reading, PA).

$$A = Be^{-k_{obs}t} + C \tag{1}$$

$$k_{obs} = \frac{k_{red}A}{K_d + A} \tag{2}$$

$$\ln\left(k_{red}/T\right) = \ln\left(k_B/h\right) + \Delta S^{\ddagger}/R - \Delta H^{\ddagger}/RT \tag{3}$$

$$\ln{}^D\left(k_{red}\right) = \ln\left[A_H/A_D\right] + \left[E_a(D) - E_a(H)\right]/RT \tag{4}$$

4.4. Results

The effect of temperature on the rate constants for flavin reduction (k_{red}) with choline or 1,2-[$^2H_4$]-choline as substrate for the choline oxidase variant with aspartate instead of glutamate at position 312 was investigated between 7 and 37 $^{\circ}$C. The enzyme (0.01 mM final) was mixed anaerobically with varying concentrations of organic substrate (between 0.05 and 10 mM final)

in a stopped-flow spectrophotometer in 50 mM sodium pyrophosphate, pH 8.0, to determine the k_{red} and K_d values. As illustrated in the example (Figure 4.2) for the data at 37 ^{o}C, at all concentrations of substrates the stopped-flow traces at 450 nm showed single exponential decays from the oxidized to the anionic hydroquinone enzyme-bound flavin species, in keeping with previous observations reported for the wild-type form of the enzyme (*16*).
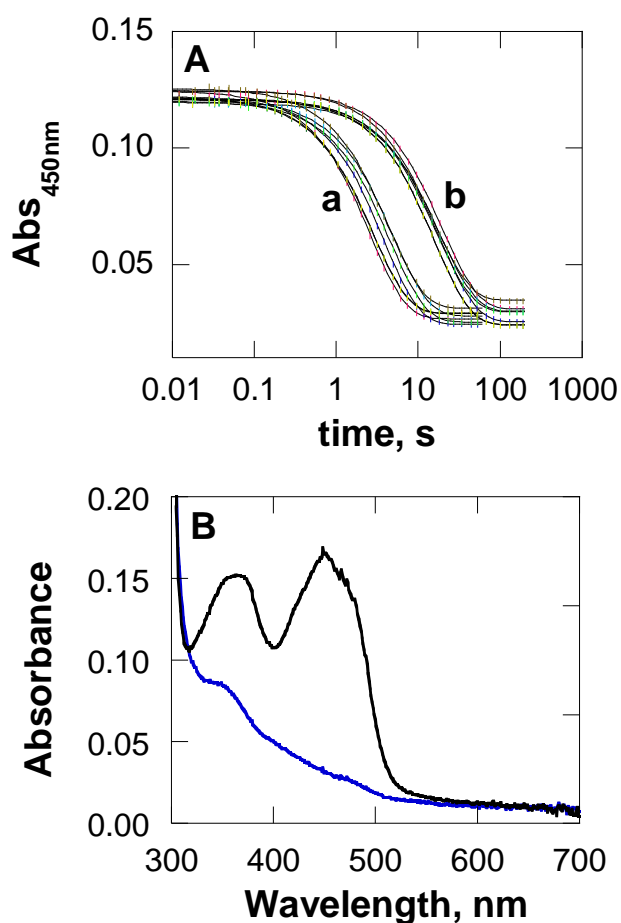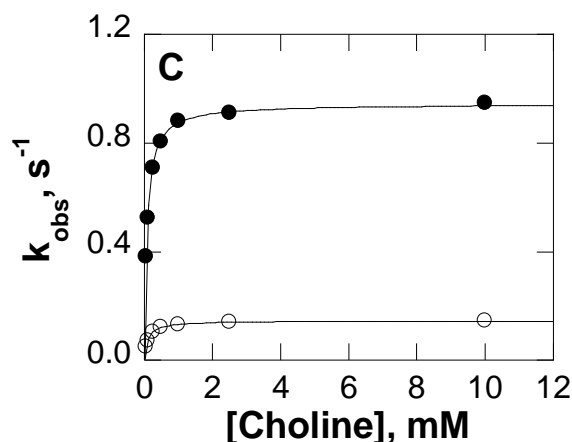
Figure 4.2. Anaerobic reductions of the Glu312Asp variant of choline oxidase with choline and 1,2-[^{2}H$_4$]-choline at 37 ^{o}C.
(A) Stopped-flow traces for choline (a) and 1,2-[^{2}H$_4$]-choline (b) at 0.05, 0.1, 0.25, 0.5, 1.0, 2.5 and 10.0 mM substrate concentrations in 50 mM sodium pyrophosphate, pH 8.0. Data were fit to eq 1. Time indicated is after the end of flow, i.e., 2.2 ms. (B) UV-visible absorbance spectra for the oxidized (black line) and two-electron reduced (blue thick line) enzyme-bound flavin. (C) Rates of flavin reduction in the Glu312Asp enzyme as a function of substrate concentration with choline ($\bullet$) and 1,2-[^{2}H$_4$]-choline ($\circ$). Data were fit to eq 2.

At each substrate concentration the observed rates of flavin reduction determined in triplicate differed from one another by $\leq$ 3%, as exemplified in Table A4.1 for the data at 37 ^{o}C. The averaged observed rates of flavin reduction (k_{obs}) were hyperbolically dependent on the concentration of the substrate (Figure 4.2), allowing for the determination of the limiting rate constants for flavin reduction (k_{red}) and the macroscopic equilibrium constants for substrate binding to the enzyme (K_d) by using eq. 2. The kinetic data for all of the temperatures in the range from 7 to 34 ^{o}C are summarized in Figure A4.1 and Tables A4.2 to A4.4. Over the range of temperatures considered, the k_{red} values ranged from 0.209 $\pm$ 0.002 to 0.943 $\pm$ 0.007 s^{-1} with choline and from 0.025 $\pm$ 0.001 to 0.146 $\pm$ 0.001 s^{-1} with 1,2-[^{2}H$_4$]-choline, yielding large isotope effects on the limiting rates for flavin reduction ($^D k_{red}$) from 6.4 to 8.4 (Table A4.4). In all cases, the K_d values could only be estimated as being $\leq$ 0.1 mM since the requirement for

pseudo-first order conditions in the anaerobic reduction of the enzyme with substrate prevented

the use of concentrations of choline or 1,2-[^{2}H$_4$]-choline lower than 0.05 mM (Table A4.4).

The analysis of the temperature dependence of the k_{red} values determined with choline and

1,2-[^{2}H$_4$]-choline as substrate for the Glu312Asp enzyme according to Eyring formalism (eq. 3)

is shown in Figure 4.3.
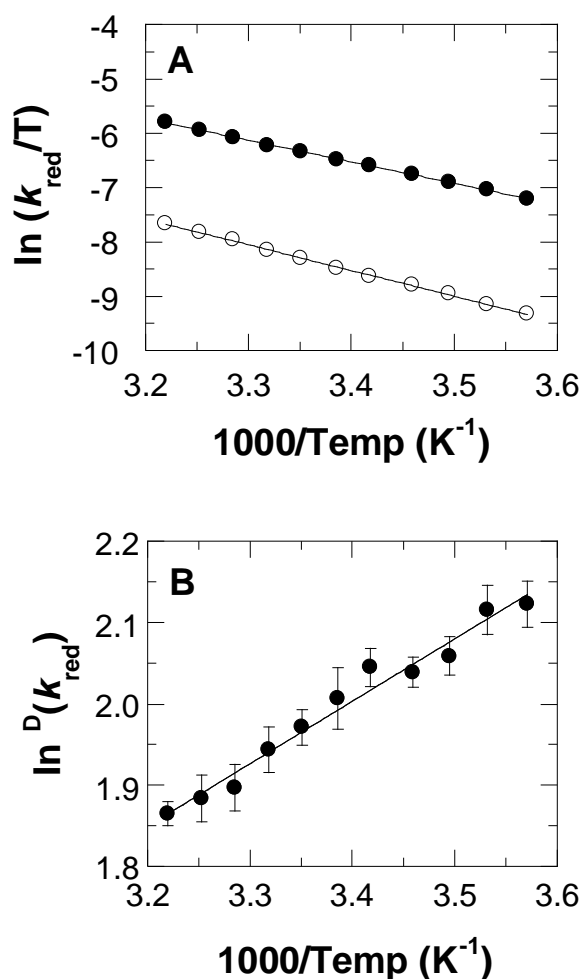
Figure 4.3. Temperature dependence of the rate k_{red} and $^D(k_{red})$ values for the Glu312Asp variant of choline oxidase with choline and 1,2-[^{2}H$_4$]-choline.
(A) Eyring plot of the k_{red} values versus temperature with choline (●) and 1,2-[^{2}H$_4$]-choline (○) as substrate; data were fit to eq 3. Standard deviations associated with the measurements are ≤4% of the measured value. (B) Arrhenius plot of the $^D(k_{red})$ values versus temperature; data were fit to eq 4.

The k_{red} values increased monotonically with increasing temperature, with 1,2-[^{2}H$_4$]-choline showing a steeper slope than choline (-4.73 $\pm$ 0.05 versus -3.95 $\pm$ 0.03). Thus, the enthalpies of activation ($\Delta H^{\ddagger}$) for the hydride ion transfer reaction were ~39 kJ mol^{-1} for 1,2-[^{2}H$_4$]-choline and ~33 kJ mol^{-1} for choline. For comparison, a previous investigation of the temperature dependence of the reductive half-reaction with the wild-type enzyme using a steady state approach yielded slopes that were similar to one another with choline and 1,2-[^{2}H$_4$]-choline, corresponding to $\Delta H^{\ddagger}$ values of ~18 kJ mol^{-1} (*16*). Similar entropies of activation ($-T\Delta S^{\ddagger}$) of ~40 kJ mol^{-1} were observed with choline and 1,2-[^{2}H$_4$]-choline as substrate for the Glu312Asp enzyme, yielding an isotope effect on the Eyring preexponential factor of ~0.9. This value contrasts with the value of ~14 previously reported for the wild-type form of choline oxidase, where the $-T\Delta S^{\ddagger}$ values were 24 and 30 kJ mol^{-1} with choline and 1,2-[^{2}H$_4$]-choline (*16*).

As shown in Figure 4.3, the analysis of the $^D(k_{red})$ values according to the Arrhenius formalism demonstrated that the kinetic isotope effects decreased monotonically with increasing temperature. The corresponding difference in the activation energy for the reaction of hydride ion transfer catalyzed by the Glu312Asp enzyme for the cleavage of the CH and CD bonds (ΔE_a), which could be estimated from the slope of the line in the Arrhenius plot of the $^D(k_{red})$ values, had a finite value of ~6.5 kJ mol^{-1}. In comparison, previous studies on the wild-type enzyme showed a ΔE_a value that was not significantly different from zero (*16*). Table 4.1 summarizes the thermodynamic parameters determined from the temperature dependence of the reductive half-reaction catalyzed by the Glu312Asp variant enzyme and the parameters for wild-type choline oxidase determined from a previous study.

Table 4.1. Comparison of the thermodynamic parameters for the reductive half-reactions catalyzed by the Glu312Asp and wild-type choline oxidase.

parameter	CHO-E312D[a] (k_{red})	CHO-WT[b] (k_{cat}/K_m)
$\Delta H^{\ddagger}_{H}{}^{c}$, kJ mol^{-1}	32.9 ± 0.2	18 ± 2
$\Delta H^{\ddagger}_{D}{}^{c}$, kJ mol^{-1}	39.3 ± 0.4	18 ± 5
$-T\Delta S^{\ddagger}_{H}$, kJ mol^{-1}	41.7 ± 0.6	24 ± 2
$-T\Delta S^{\ddagger}_{D}$, kJ mol^{-1}	40.1 ± 0.9	30 ± 5
$\Delta S^{\ddagger}_{H}{}^{d}$, kJ K^{-1}mol^{-1}	0.14 ± 0.01	0.08 ± 0.01
$\Delta S^{\ddagger}_{D}{}^{d}$, kJ K^{-1}mol^{-1}	0.13 ± 0.01	0.10 ± 0.02
$\Delta G^{\ddagger}_{H}{}^{d}$, kJ mol^{-1}	75 ± 1	42 ± 3
$\Delta G^{\ddagger}_{D}{}^{d}$, kJ mol^{-1}	79 ± 1	48 ± 7
ΔE_a, kJ mol^{-1}	6.50 ± 0.5	0.4 ± 4.2
$A_H{}'/A_D{}'{}^{e}$	0.91 ± 0.02	14 ± 3
KIE^{f}	T-dependent	T-independent

[a]Conditions: Rates of flavin reduction were measured in 50 mM sodium pyrophosphate, pH 8.0, at different temperatures under anaerobic conditions. [b]Data are from (16). [c]Data were calculated by using the Eyring equation (eq 3). [d]Data for 25 °C. [e]A_H'/A_D' is the ratio of the y-intercepts obtained by fitting the kinetic data with choline and 1,2-[^{2}H$_4$]-choline to the Eyring equation (eq 3). [f]KIE is the substrate kinetic isotope effect associated with the cleavage of the CH and CD bonds of choline in the reaction catalyzed y choline oxidase.

4.5. Discussion

The mechanism of hydride ion transfer in a choline oxidase variant with a conservative mutation of an active site residue involved in substrate binding (i.e., Glu312 to Asp) has been investigated in the present study. The mechanistic data on the enzyme containing aspartate at

position 312 have been compared to the mechanistic data that were previously reported for the wild-type enzyme in order to estimate the effect of disrupting the relative positioning of the hydride donor and acceptor to the rate of hydride tunneling in wild-type choline oxidase.

The transfer of the hydride ion in the reaction catalyzed by the choline oxidase variant containing aspartate at position 312 occurs through environmentally coupled tunneling with significant distance and geometric sampling of the reactive configurations that conduce to the transfer reaction. Evidence supporting this conclusion comes from the thermodynamic parameters that are associated with the temperature effects on the k_{red} and $^Dk_{red}$ values with choline and 1,2-[^{2}H$_4$]-choline as substrates determined by following the anaerobic reduction of the enzyme-bound flavin using a stopped-flow spectrophotometer. The temperature dependence of the kinetic isotope effects and the finite enthalpies of activation ($\Delta H^{\ddagger}$) that differ from one another for protium and deuterium transfers immediately rule out a tunneling reaction from a highly preorganized enzyme-substrate complex with no appreciable sampling of distance and geometry as previously reported for the wild-type enzyme (*16*). Indeed, a mode of tunneling reaction of the type reported for the wild-type enzyme is expected to yield kinetic isotope effects that are independent of temperature, and $\Delta H^{\ddagger}$ values for the transfer of protium and deuterium with finite values not different from one another (*4, 5, 11, 16*). Further evidence that is consistent with distance and geometry sampling of the reactive configurations that conduce to tunneling comes from the isotope effect on the Eyring preexponential factors (A_H'/A_D'), with a value that is not significantly larger than unity. In this regard, while transfer reactions where sampling is present are commonly associated with A_H'/A_D' values that are smaller than unity (i.e., <0.7) (*32, 35, 49, 50*), a report on lipoxygenase-1 by Klinman's group recently showed that in some instances tunneling of hydrogen atoms in enzyme catalyzed reactions where distance and

geometry sampling is prominent can also be associated with A_H'/A_D' values close to unity (*51*). In contrast, transfer reactions where tunneling occurs without sampling of the reactive configurations, i.e., within a highly preorganized enzyme-substrate complex, commonly display A_H'/A_D' values that are significantly larger than unity (i.e., >1.7) (*1, 5, 16, 27, 52-56*). Evidence in support of distance and geometry sampling also comes from the finite value for the difference in the energies of activation ($\Delta E_a = (E_a)_H-(E_a)_D$) for protium and deuterium transfers (*14, 16, 27*). Contrastingly, a ΔE_a value not significantly different from zero would be expected for a tunneling reaction within a highly preorganized active site as previously reported for the wild-type form of choline oxidase (*1, 16, 35*).

In principle, an alternate mechanism where the hydride ion is transferred through a transition state occurring over the energetic barrier that separates the alkoxide-oxidized flavin and the aldehyde-reduced flavin complexes, i.e., in the absence of tunneling, could also be considered. Indeed, all of the earmarks for such a mechanism are observed experimentally in the reaction catalyzed by the Glu312Asp enzyme, i.e., A_H'/A_D' values that are close to unity, temperature dependent kinetic isotope effects where $\Delta H^{\ddagger}$ values for protium and deuterium transfers are different from one another, and large ΔE_a value in the order of ~5 kJ mol^{-1} (*57*). If this were the case, it could be reasonably envisaged that the substitution of glutamate with aspartate at position 312 might have altered the relative positioning of the α-carbon of the choline alkoxide acting as the donor of the hydride ion and the N(5) atom of the flavin acting as the hydride ion acceptor to an extent that is not compatible any more with a tunneling reaction. While such an alternative mechanism cannot out rightly be rule out *a priori* with the data at hand, the similar magnitudes of the kinetic isotope effects determined with the Glu312 and Asp312 enzymes argue in favor of environmentally coupled tunneling being involved in the reaction catalyzed by the mutant

enzyme. Indeed, one would expect kinetic isotope effects with similar magnitudes once the correct geometry and distance of the configuration that is required for the tunneling of the hydride ion from the donor to the acceptor is achieved irrespective of whether the transfer reaction displays sampling. A hydride transfer mechanism similar to that of the aspartate-containing enzyme shown in this study has recently been reported for a variant form of choline oxidase in which the histidine residue involved in covalent linkage with FAD was replaced with asparagine (CHO-H99N) (*58*). Thus, suggesting similar modes of active site reorganization in the two variant enzymes of choline oxidase upon disrupting the relative positioning of the hydride donor and acceptor in the wild-type enzyme.

Reorientation of the relative positioning of the hydride ion donor and acceptor that is required to achieve the correct geometry and distance for the tunneling of the hydride ion in the reaction catalyzed by the aspartate-containing variant of choline oxidase accounts for a two-order of magnitude decrease in the rate of hydride ion transfer. Evidence supporting this conclusion comes from the comparison of the mechanism and the rates of hydride ion transfer determined in this study with the choline oxidase variant containing aspartate at position 312 and previous studies on the wild-type enzyme containing glutamate (*16, 17*). Indeed, while in the wild-type enzyme the transfer of a hydride ion occurs at a rate of 93 s^{-1} within a highly preorganized enzyme-substrate complex without appreciable distance sampling (*16*), the hydride ion transfer reaction occurs at a rate of 0.4 s^{-1} (at 25 $^{\circ}$C) with significant distance and geometric sampling of the reactive configurations in the Glu312Asp enzyme. These results are also in agreement with coupled catalytic motions being important for reorientation of the donor and acceptor in the active site of the aspartate-containing enzyme, since these motions would be minimal in the hydride ion transfer reaction catalyzed by the wild-type enzyme (*34, 59*). Furthermore, these data

agree well with recent observations suggesting that enzymes appear to reduce reorganizational motions to a minimum in favor of a relatively rigid active site configuration to be efficient catalysts (*36, 37*). Even though not directly involved in catalysis, the active site glutamate residue at position 312 in choline oxidase that is primarily involved in substrate binding has been demonstrated to contribute to the overall preorganization of the enzyme-substrate complex in choline oxidase, with no significant effect on substrate binding upon conservatively replacing the residue with aspartate.

Conclusion. The conservative replacement of the negatively charged residue at position 312 from glutamate to aspartate has a significant effect on both the rate constant for the hydride ion transfer and the mechanism of the reaction catalyzed by choline oxidase. The transfer of the hydride ion in the reaction catalyzed by the variant form of choline oxidase containing aspartate occurs through environmentally coupled tunneling with significant distance and geometric sampling of the reactive configurations. A ~200-fold decrease in the rate constant for the reaction in the Glu312Asp enzyme is associated with reorientation of the relative positioning of the hydride donor and acceptor due to loss of the high level of preorganization of the enzyme-substrate complex that is observed in the wild-type enzyme. While this study provides a quantitative analysis of the effect of altering the relative positioning of the hydride donor and acceptor to the hydride ion tunneling reaction catalyzed by choline oxidase, it also represents an example of how the selected, conservative substitution of an active site residue that is involved in substrate binding, but not directly in catalysis, can have an exclusive effect on the kinetic parameters related to catalytic events, without affecting those reporting on substrate binding.

Supporting Information Available. Figure A4.1 shows the rate of flavin reduction as a function of substrate concentrations from 7.0 to 34 $^{\circ}$C. Table A4.1 shows the average observed rates of flavin reduction for CHO-E312D at different choline concentrations from 7 to 34 $^{\circ}$C. Table A4.2 shows the average observed rates of flavin reduction for CHO-E312D at different 1,2-[^{2}H$_4$]-choline concentrations from 7 to 34 $^{\circ}$C. Table A4.3 shows temperature dependence of the pre-steady state kinetic parameters with choline and 1,2-[^{2}H$_4$]-choline as substrates.

4.6. References

1.   Agrawal, N., Hong, B., Mihai, C., and Kohen, A. (2004) Vibrationally enhanced hydrogen tunneling in the *Escherichia coli* thymidylate synthase catalyzed reaction, *Biochemistry 43*, 1998-2006.

2.   Bahnson, B. J., Park, D. H., Kim, K., Plapp, B. V., and Klinman, J. P. (1993) Unmasking of hydrogen tunneling in the horse liver alcohol dehydrogenase reaction by site-directed mutagenesis, *Biochemistry 32*, 5503-5507.

3.   Banacky, P. (1981) Dynamics of proton transfer and enzymatic activity, *Biophys. Chem. 13*, 39-47.

4.   Basran, J., Harris, R. J., Sutcliffe, M. J., and Scrutton, N. S. (2003) H-tunneling in the multiple H-transfers of the catalytic cycle of morphinone reductase and in the reductive

half-reaction of the homologous pentaerythritol tetranitrate reductase, *J. Biol. Chem. 278*, 43973-43982.

5.   Basran, J., Sutcliffe, M. J., and Scrutton, N. S. (1999) Enzymatic H-transfer requires vibration-driven extreme tunneling, *Biochemistry 38*, 3218-3222.

6.   Bruno, W. J., and Bialek, W. (1992) Vibrationally enhanced tunneling as a mechanism for enzymatic hydrogen transfer, *Biophys. J. 63*, 689-699.

7.   Cha, Y., Murray, C. J., and Klinman, J. P. (1989) Hydrogen tunneling in enzyme reactions, *Science 243*, 1325-1330.

8.   Fagan, R. L., Nelson, M. N., Pagano, P. M., and Palfey, B. A. (2006) Mechanism of flavin reduction in class 2 dihydroorotate dehydrogenases, *Biochemistry 45*, 14926-14932.

9.   Gadda, G. (2008) Hydride transfer made easy in the reaction of alcohol oxidation catalyzed by flavin-dependent oxidases, *Biochemistry 47*, 13745-13753.

10.   Garcia-Viloca, M., Alhambra, C., Truhlar, D. G., and Gao, J. (2003) Hydride transfer catalyzed by xylose isomerase: mechanism and quantum effects, *J. Comput. Chem. 24*, 177-190.

11.   Jonsson, T., Edmondson, D. E., and Klinman, J. P. (1994) Hydrogen tunneling in the flavoenzyme monoamine oxidase B, *Biochemistry 33*, 14871-14878.

12.   Karsten, W. E., Hwang, C. C., and Cook, P. F. (1999) Alpha-secondary tritium kinetic isotope effects indicate hydrogen tunneling and coupled motion occur in the oxidation of L-malate by NAD-malic enzyme, *Biochemistry 38*, 4398-4402.

13.   Maglia, G., and Allemann, R. K. (2003) Evidence for environmentally coupled hydrogen tunneling during dihydrofolate reductase catalysis, *J. Am. Chem. Soc. 125*, 13372-13373.

14. Sutcliffe, M. J., Masgrau, L., Roujeinikova, A., Johannissen, L. O., Hothi, P., Basran, J., Ranaghan, K. E., Mulholland, A. J., Leys, D., and Scrutton, N. S. (2006) Hydrogen tunnelling in enzyme-catalysed H-transfer reactions: flavoprotein and quinoprotein systems, *Philos. Trans. R. Soc. Lond. B. Biol. Sci. 361*, 1375-1386.

15. Valley, M. P., and Fitzpatrick, P. F. (2004) Comparison of enzymatic and non-enzymatic nitroethane anion formation: thermodynamics and contribution of tunneling, *J. Am. Chem. Soc. 126*, 6244-6245.

16. Fan, F., and Gadda, G. (2005) Oxygen- and temperature-dependent kinetic isotope effects in choline oxidase: correlating reversible hydride transfer with environmentally enhanced tunneling, *J. Am. Chem. Soc. 127*, 17954-17961.

17. Fan, F., and Gadda, G. (2005) On the catalytic mechanism of choline oxidase, *J. Am. Chem. Soc. 127*, 2067-2074.

18. Billeter, S. R., Webb, S. P., Agarwal, P. K., Iordanov, T., and Hammes-Schiffer, S. (2001) Hydride transfer in liver alcohol dehydrogenase: quantum dynamics, kinetic isotope effects, and role of enzyme motion, *J. Am. Chem. Soc. 123*, 11262-11272.

19. Chin, J. K., and Klinman, J. P. (2000) Probes of a role for remote binding interactions on hydrogen tunneling in the horse liver alcohol dehydrogenase reaction, *Biochemistry 39*, 1278-1284.

20. Liang, Z. X., Lee, T., Resing, K. A., Ahn, N. G., and Klinman, J. P. (2004) Thermal-activated protein mobility and its correlation with catalysis in thermophilic alcohol dehydrogenase, *Proc. Natl. Acad. Sci. U S A 101*, 9556-9561.

21.   Rubach, J. K., and Plapp, B. V. (2003) Amino acid residues in the nicotinamide binding site contribute to catalysis by horse liver alcohol dehydrogenase, *Biochemistry 42*, 2907-2915.

22.   Rubach, J. K., Ramaswamy, S., and Plapp, B. V. (2001) Contributions of valine-292 in the nicotinamide binding site of liver alcohol dehydrogenase and dynamics to catalysis, *Biochemistry 40*, 12686-12694.

23.   Garcia-Viloca, M., Truhlar, D. G., and Gao, J. (2003) Reaction-path energetics and kinetics of the hydride transfer reaction catalyzed by dihydrofolate reductase, *Biochemistry 42*, 13558-13575.

24.   Pang, J., Pu, J., Gao, J., Truhlar, D. G., and Allemann, R. K. (2006) Hydride transfer reaction catalyzed by hyperthermophilic dihydrofolate reductase is dominated by quantum mechanical tunneling and is promoted by both inter- and intramonomeric correlated motions, *J. Am. Chem. Soc. 128*, 8015-8023.

25.   Wang, L., Goodey, N. M., Benkovic, S. J., and Kohen, A. (2006) Coordinated effects of distal mutations on environmentally coupled tunneling in dihydrofolate reductase, *Proc. Natl. Acad. Sci. U S A 103*, 15753-15758.

26.   Knapp, M. J., and Klinman, J. P. (2002) Environmentally coupled hydrogen tunneling. Linking catalysis to dynamics, *Eur. J. Biochem. 269*, 3113-3121.

27.   Knapp, M. J., Rickert, K., and Klinman, J. P. (2002) Temperature-dependent isotope effects in soybean lipoxygenase-1: correlating hydrogen tunneling with protein dynamics, *J. Am. Chem. Soc. 124*, 3865-3874.

28. Tejero, I., Garcia-Viloca, M., Gonzalez-Lafont, A., Lluch, J. M., and York, D. M. (2006) Enzyme dynamics and tunneling enhanced by compression in the hydrogen abstraction catalyzed by soybean lipoxygenase-1, *J. Phys. Chem. B 110*, 24708-24719.

29. Pang, J., Hay, S., Scrutton, N. S., and Sutcliffe, M. J. (2008) Deep tunneling dominates the biologically important hydride transfer reaction from NADH to FMN in morphinone reductase, *J. Am. Chem. Soc. 130*, 7092-7097.

30. Pudney, C. R., Hay, S., Sutcliffe, M. J., and Scrutton, N. S. (2006) Alpha-secondary isotope effects as probes of "tunneling-ready" configurations in enzymatic H-tunneling: insight from environmentally coupled tunneling models, *J. Am. Chem. Soc. 128*, 14053-14058.

31. Kohen, A., Jonsson, T., and Klinman, J. P. (1997) Effects of protein glycosylation on catalysis: changes in hydrogen tunneling and enthalpy of activation in the glucose oxidase reaction, *Biochemistry 36*, 2603-2611.

32. Nagel, Z. D., and Klinman, J. P. (2006) Tunneling and dynamics in enzymatic hydride transfer, *Chem. Rev. 106*, 3095-3118.

33. Seymour, S. L., and Klinman, J. P. (2002) Comparison of rates and kinetic isotope effects using PEG-modified variants and glycoforms of glucose oxidase: the relationship of modification of the protein envelope to C-H activation and tunneling, *Biochemistry 41*, 8747-8758.

34. Liu, H., and Warshel, A. (2007) The catalytic effect of dihydrofolate reductase and its mutants is determined by reorganization energies, *Biochemistry 46*, 6011-6025.

35.   Meyer, M. P., Tomchick, D. R., and Klinman, J. P. (2008) Enzyme structure and dynamics affect hydrogen tunneling: the impact of a remote side chain (I553) in soybean lipoxygenase-1, *Proc. Natl. Acad. Sci. U S A 105*, 1146-1151.

36.   Roca, M., Liu, H., Messer, B., and Warshel, A. (2007) On the relationship between thermal stability and catalytic power of enzymes, *Biochemistry 46*, 15076-15088.

37.   Smith, A. J., Muller, R., Toscano, M. D., Kast, P., Hellinga, H. W., Hilvert, D., and Houk, K. N. (2008) Structural reorganization and preorganization in enzyme active sites: comparisons of experimental and theoretically ideal active site geometries in the multistep serine esterase reaction cycle, *J. Am. Chem. Soc. 130*, 15361-15373.

38.   Warshel, A., Sharma, P. K., Kato, M., Xiang, Y., Liu, H., and Olsson, M. H. (2006) Electrostatic basis for enzyme catalysis, *Chem. Rev. 106*, 3210-3235.

39.   Hay, S., and Scrutton, N. S. (2008) Incorporation of hydrostatic pressure into models of hydrogen tunneling highlights a role for pressure-modulated promoting vibrations, *Biochemistry 47*, 9880-9887.

40.   Hay, S., Sutcliffe, M. J., and Scrutton, N. S. (2007) Promoting motions in enzyme catalysis probed by pressure studies of kinetic isotope effects, *Proc. Natl. Acad. Sci. U S A 104*, 507-512.

41.   Fan, F., and Gadda, G. (2007) An internal equilibrium preorganizes the enzyme-substrate complex for hydride tunneling in choline oxidase, *Biochemistry 46*, 6402-6408.

42.   Finnegan, S., and Gadda, G. (2008) Substitution of an active site valine uncovers a kinetically slow equilibrium between competent and incompetent forms of choline oxidase, *Biochemistry 47*, 13850-13861.

43. Quaye, O., Lountos, G. T., Fan, F., Orville, A. M., and Gadda, G. (2008) Role of Glu312 in binding and positioning of the substrate for the hydride transfer reaction in choline oxidase, *Biochemistry 47*, 243-256.

44. Ghanem, M., and Gadda, G. (2005) On the catalytic role of the conserved active site residue His466 of choline oxidase, *Biochemistry 44*, 893-904.

45. Ghanem, M., and Gadda, G. (2006) Effects of reversing the protein positive charge in the proximity of the flavin N(1) locus of choline oxidase, *Biochemistry 45*, 3437-3447.

46. Cleland, W. W. (1980) Measurement of isotope effect by the equilibrium perturbation technique, in *Methods Enzymol.* (Purich, D. L., Ed.), pp 104-125, New York.

47. Lewis, C. A., Jr., and Wolfenden, R. (1977) Antiproteolytic aldehydes and ketones: substituent and secondary deuterium isotope effects on equilibrium addition of water and other nucleophiles, *Biochemistry 16*, 4886-4890.

48. (Previous studies established that in the Glu312Asp enzyme the k_{cat}/K_m for choline between pH 8.0 and 10.0 and the substrate kinetic isotope effects from pH 6.0 to 10.0 that are associated with the reductive half-reaction in which a hydride ion is transferred from the substrate to the enzyme-bound isoalloxazine ring of the flavin are pH-independent. The lack of pH effects allowed the choice of a pH value at which the mutant enzyme was stable in the anaerobic tonometer for the prolonged times required to perform the stopped-flow experiment, i.e., pH 8.0.).

49. Chowdhury, S., and Banerjee, R. (2000) Evidence for quatum mechanical tunneling in the coupled cobalt-carbon bond homolysis substrate radical generation reaction catalyzed by methylmalonyl-CoA mutase, *J. Am. Chem. Soc. 122*, 5417-5418.

50.   Whittaker, M. M., Ballou, D. P., and Whittaker, J. W. (1998) Kinetic isotope effects as probes of the mechanism of galactose oxidase, *Biochemistry 37*, 8426-8436.

51.   Sharma, S. C., and Klinman, J. P. (2008) Experimental Evidence for Hydrogen Tunneling when the Isotopic Arrhenius Prefactor ($A_{(H)}/A_{(D)}$) is Unity, *J. Am. Chem. Soc. 130*, 17632-17633.

52.   Basran, J., Patel, S., Sutcliffe, M. J., and Scrutton, N. S. (2001) Importance of barrier shape in enzyme-catalyzed reactions. Vibrationally assisted hydrogen tunneling in tryptophan tryptophylquinone-dependent amine dehydrogenases, *J. Biol. Chem. 276*, 6234-6242.

53.   Francisco, W. A., Knapp, M. J., Blackburn, N. J., and Klinman, J. P. (2002) Hydrogen tunneling in peptidylglycine alpha-hydroxylating monooxygenase, *J. Am. Chem. Soc. 124*, 8194-8195.

54.   Kohen, A., Cannio, R., Bartolucci, S., and Klinman, J. P. (1999) Enzyme dynamics and hydrogen tunnelling in a thermophilic alcohol dehydrogenase, *Nature 399*, 496-499.

55.   Sikorski, R. S., Wang, L., Markham, K. A., Rajagopalan, P. T., Benkovic, S. J., and Kohen, A. (2004) Tunneling and coupled motion in the *Escherichia coli* dihydrofolate reductase catalysis, *J. Am. Chem. Soc. 126*, 4778-4779.

56.   Wang, L., Tharp, S., Selzer, T., Benkovic, S. J., and Kohen, A. (2006) Effects of a distal mutation on active site chemistry, *Biochemistry 45*, 1383-1392.

57.   Melander, L., and Saunders, W. H. (1987) *Reaction Rates of Isotopic Molecules*, Fourth ed., Krieger, Malabar, FL.

58.   Quaye, O., Gadda, G., and Cowins, S. (2009) Contribution of flavin covalent linkage with histidine 99 to the reaction catalyzed by choline oxidase, *J. Biol. Chem. 284(25)*, 16990-16997.

59.   Marti, S., Andres, J., Moliner, V., Silla, E., Tunon, I., and Bertran, J. (2003) Preorganization and reorganization as related factors in enzyme catalysis: the chorismate mutase case, *Chemistry 9*, 984-991.

4.7. Appendix

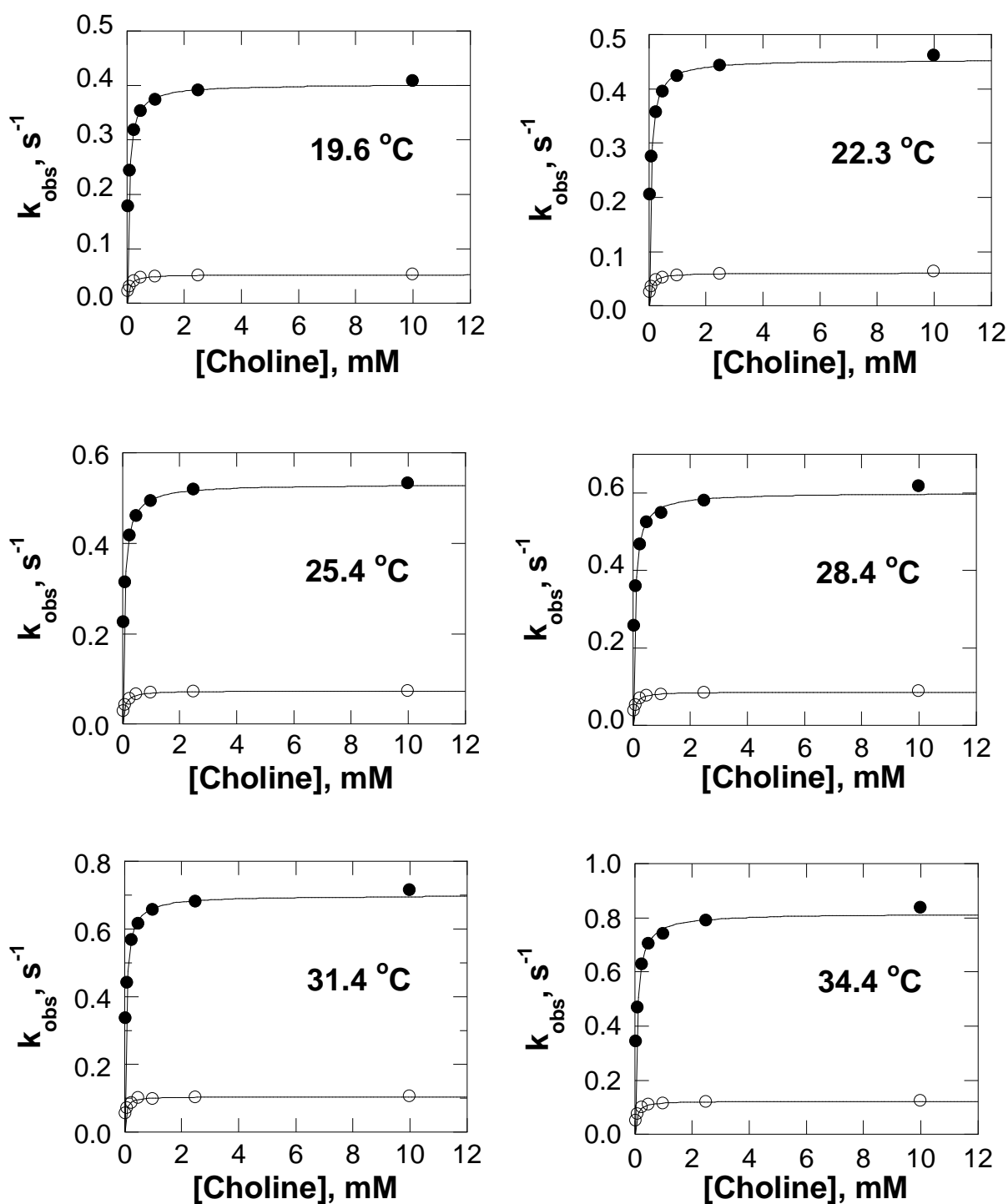<p align="center"><u>**SUPPORTING INFORMATION**</u></p>
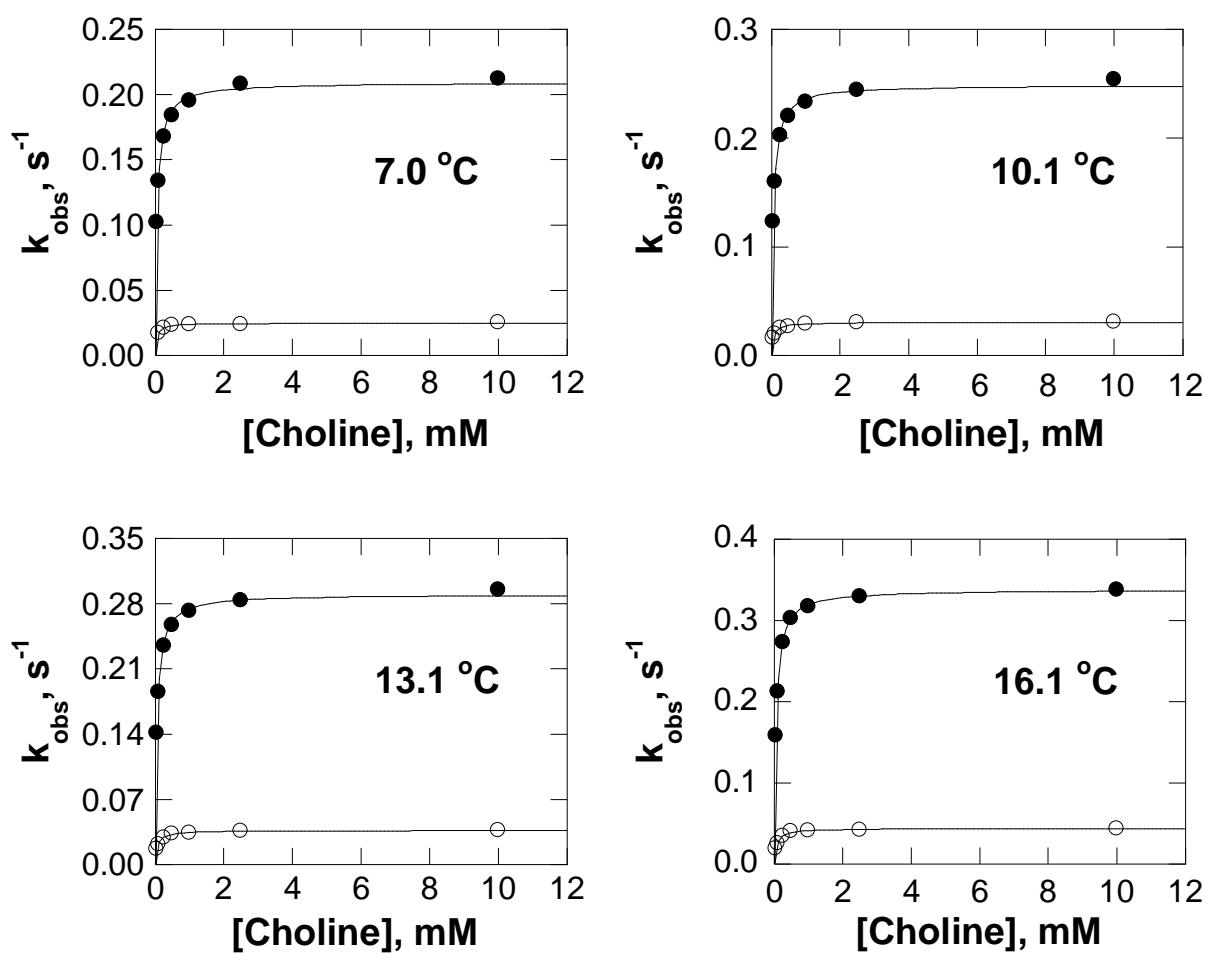
Figure A4.1. Rate of flavin reduction as a function of substrate concentrations from 7.0 to 34 °C.

(●) represents choline and (○) represents 1,2-[²H₄]-choline. Enzymatic assays were carried out in 50 mM sodium pyrophosphate, pH 8 at varying concentration of substrate in a stopped-flow spectrophotometer under anaerobic conditions. Data were fit to equation 2.

Table A4.1. Average observed rates of flavin reduction (k_{obs}) for CHO-E312D at different concentrations of choline determined at pH 8 in the temperature range from 7 to 34 °C.

Temperature (°C)	Average k_{obs}, at different choline concentrations (s⁻¹) [a]						
	0.05 (mM)	0.1 (mM)	0.25 (mM)	0.5 (mM)	1.0 (mM)	2.5 (mM)	10.0 (mM)
7.0	0.102 ± 0.001	0.134 ± 0.001	0.168 ± 0.001	0.184 ± 0.001	0.195 ± 0.001	0.208 ± 0.001	0.212 ± 0.001
10.1	0.123 ± 0.001	0.160 ± 0.001	0.202 ± 0.001	0.220 ± 0.001	0.233 ± 0.001	0.244 ± 0.001	0.254 ± 0.001
13.1	0.141 ± 0.001	0.185 ± 0.001	0.235 ± 0.003	0.257 ± 0.001	0.272 ± 0.001	0.284 ± 0.001	0.295 ± 0.001
16.1	0.158 ± 0.001	0.213 ± 0.001	0.273 ± 0.001	0.303 ± 0.001	0.318 ± 0.001	0.330 ± 0.001	0.338 ± 0.001
19.6	0.117 ± 0.001	0.243 ± 0.001	0.318 ± 0.001	0.353 ± 0.001	0.373 ± 0.001	0.390 ± 0.001	0.408 ± 0.001
22.3	0.205 ± 0.001	0.275 ± 0.001	0.357 ± 0.002	0.395 ± 0.005	0.423 ± 0.002	0.443 ± 0.001	0.461 ± 0.001
25.4	0.226 ± 0.001	0.314 ± 0.001	0.418 ± 0.001	0.460 ± 0.001	0.493 ± 0.002	0.519 ± 0.001	0.532 ± 0.001
28.4	0.257 ± 0.001	0.359 ± 0.001	0.467 ± 0.003	0.524 ± 0.002	0.548 ± 0.002	0.580 ± 0.001	0.617 ± 0.001
31.4	0.336 ± 0.002	0.442 ± 0.001	0.568 ± 0.005	0.615 ± 0.001	0.656 ± 0.003	0.681 ± 0.001	0.715 ± 0.001
34.4	0.343 ± 0.007	0.468 ± 0.002	0.628 ± 0.009	0.704 ± 0.003	0.740 ± 0.008	0.789 ± 0.004	0.837 ± 0.001

[a]Ave k_{obs} is the mean average of triplicate observed rates of flavin reduction at each concentration of choline . The observed rates were measured anaerobically with the stopped-flow spectrophotometer by monitoring absorbance at 450 nm and the traces fit to equation 1.

Table A4.2. Average observed rates of flavin reduction (k_{obs}) for CHO-E312D at different concentrations of 1,2-[^{2}H$_4$]-choline determined at pH 8 in the temperature range from 7 to 34 ^{o}C.

Temperature (^{o}C)	Average k_{obs}, at different 1,2-[^{2}H$_4$]-choline concentrations (s^{-1})						
	0.05 (mM)	0.1 (mM)	0.25 (mM)	0.5 (mM)	1.0 (mM)	2.5 (mM)	10.0 (mM)
7.0	0.014 ± 0.001	0.017 ± 0.001	0.021 ± 0.001	0.023 ± 0.001	0.024 ± 0.001	0.024 ± 0.001	0.025 ± 0.001
10.1	0.016 ± 0.001	0.020 ± 0.001	0.025 ± 0.001	0.027 ± 0.001	0.029 ± 0.001	0.030 ± 0.001	0.031 ± 0.001
13.1	0.017 ± 0.001	0.022 ± 0.001	0.029 ± 0.001	0.033 ± 0.001	0.034 ± 0.001	0.036 ± 0.001	0.037 ± 0.001
16.1	0.019 ± 0.001	0.026 ± 0.001	0.035 ± 0.001	0.040 ± 0.001	0.041 ± 0.001	0.042 ± 0.001	0.044 ± 0.001
19.6	0.022 ± 0.001	0.030 ± 0.001	0.040 ± 0.001	0.046 ± 0.001	0.049 ± 0.001	0.050 ± 0.001	0.053 ± 0.001
22.3	0.025 ± 0.001	0.035 ± 0.001	0.047 ± 0.001	0.051 ± 0.001	0.056 ± 0.001	0.058 ± 0.001	0.063 ± 0.001
25.4	0.029 ± 0.001	0.042 ± 0.001	0.055 ± 0.001	0.066 ± 0.001	0.069 ± 0.001	0.071 ± 0.001	0.073 ± 0.001
28.4	0.038 ± 0.001	0.052 ± 0.001	0.069 ± 0.001	0.077 ± 0.001	0.080 ± 0.002	0.083 ± 0.001	0.087 ± 0.002
31.4	0.055 ± 0.001	0.072 ± 0.009	0.086 ± 0.004	0.100 ± 0.002	0.098 ± 0.001	0.103 ± 0.001	0.105 ± 0.001
34.4	0.050 ± 0.001	0.074 ± 0.003	0.099 ± 0.008	0.110± 0.003	0.113 ± 0.003	0.120 ± 0.001	0.123 ± 0.001

[a]Ave k_{obs} is the mean average of triplicate observed rates of flavin reduction at each concentration of 1,2-[^{2}H$_4$]-choline . The observed rates were measured anaerobically with the stopped-flow spectrophotometer by monitoring absorbance at 450 nm and the traces fit to equation 1.

Table A4.3. Temperature dependence of the pre-steady state kinetic parameters with choline or 1,2-[^{2}H$_4$]-choline as substrate for CHO-E312D determined at pH 8 .

Temperature (°C)	Temperature (K)	(1000/T) (K^{-1})	$(k_{red})_H$ (s^{-1})	$(k_{red})_D$ (s^{-1})	$^D(k_{red})$	$(K_d)_H$ (mM)	$(K_d)_D$ (mM)
7.0	280.0	3.571	0.209 ± 0.002	0.025 ± 0.001	8.36 ± 0.11	≤0.06	≤0.05
10.1	283.1	3.532	0.249 ± 0.002	0.030 ± 0.001	8.30 ± 0.12	≤0.06	≤0.05
13.1	286.1	3.495	0.290 ± 0.002	0.037 ± 0.001	7.84 ± 0.09	≤0.06	≤0.06
16.1	289.1	3.459	0.338 ± 0.001	0.044 ± 0.001	7.68 ± 0.07	≤0.06	≤0.07
19.6	292.6	3.418	0.402 ± 0.003	0.052 ± 0.001	7.73 ± 0.09	≤0.07	≤0.07
22.3	295.3	3.386	0.454 ± 0.004	0.061 ± 0.001	7.44 ± 0.14	≤0.07	≤0.08
25.4	298.4	3.351	0.531 ± 0.003	0.074 ± 0.001	7.18 ± 0.08	≤0.07	≤0.08
28.4	301.4	3.318	0.601 ± 0.007	0.086 ± 0.001	6.99 ± 0.10	≤0.07	≤0.06
31.4	304.4	3.285	0.700 ± 0.007	0.105 ± 0.001	6.67 ± 0.10	≤0.06	≤0.05
34.4	307.4	3.253	0.816 ± 0.010	0.124 ± 0.001	6.58 ± 0.10	≤0.07	≤0.07
37.6	310.6	3.220	0.943 ± 0.007	0.146 ± 0.001	6.46 ± 0.05	≤0.08	≤0.10

The kinetic parameters were obtained by fitting the initial rate data to $k_{obs} = k_{red}S/(K_d+S)$.

CHAPTER 5

Alcohol Oxidation in Choline Oxidase: Perspectives of Charge and Distance in the Substrate for Rescuing the Activity of the Glu312Asp Mutant Enzyme Using the Substrate Analogue (3-hydroxypropyl)trimethylammonium

(The author's contribution to this project involved pre-steady state experiments and the analysis of all the data. Tran-Bao Nguyen performed all of the steady state kinetics)

5.1. Abstract

In a recent combined crystallographic and mechanistic study, the oxidative conversion of choline to glycine betaine was shown to decrease 230-fold upon replacing an active site glutamate residue at position 312, which is involved in substrate binding, with an aspartate suggesting that the spatial location of the negative charge is important for correct positioning of the substrate for the hydride tunneling reaction in choline oxidase. pH and solvent viscosity effects on steady state kinetic parameters, and the rate of flavin reduction for CHO-E312D with 3-HPTA as substrate were used as mechanistic tools to further probe the role of Glu312. The steady state kinetic data at low pH were best fit to a sequential mechanism, whereas the data at high pH fit best to a rapid equilibrium sequential mechanism with $K_a \ll K_{ia}$. An increase in the k_{cat} and k_{red} values of ~20-fold upon replacing choline with 3-HPTA suggests a partial rescue of CHO-E312D activity with the substrate analogue. All the kinetic parameters increased with increasing pH to limiting values at high pH consistent with the requirement for unprotonated species in the reductive and oxidative half-reactions, and the overall turnover of the reaction

catalyzed by CHO-E312D with 3-HPTA as substrate. The effects of solvent viscosity on k_{cat}/K_{O2} and k_{cat} suggest a change in conformation of the enzyme-betaine aldehyde complex upon interacting with oxygen, and the presence of an internal equilibrium in the overall enzyme turnover, respectively. The data presented in this study substantiate the importance of the side chain at position 312 for the relative positioning of the hydride donor and acceptor for the hydride transfer reaction catalyzed by choline oxidase.

5.2. Introduction

Choline oxidase catalyzes the four-electron oxidative conversion of choline to glycine betaine with the formation of betaine aldehyde as an enzyme-bound intermediate using molecular oxygen as the final electron acceptor (Scheme 5.1). Glycine betaine accumulation is triggered in the cytoplasm of a number of plants and pathogenic bacteria in response to hyperosmotic and adverse temperature conditions to prevent dehydration and eventual cell death (*1, 2*). A better understanding of the reaction catalyzed by choline oxidase might consequently result in the development of therapeutic agents with the glycine betaine biosynthetic pathway as target for the management of microbial infections (*3-5*), thus making the enzyme a subject of medical interest. Biotechnologically, beneficial plants such as crops which lack the property of salt accumulation can be genetically engineered with choline oxidase to withstand adverse environmental conditions (*6-12*). Choline oxidase provides the basis for deciphering the mechanism of alcohol oxidation for which flavin-dependent enzymes achieve the oxidation of alcohols to carboxylic acids with the formation of aldehyde intermediates.
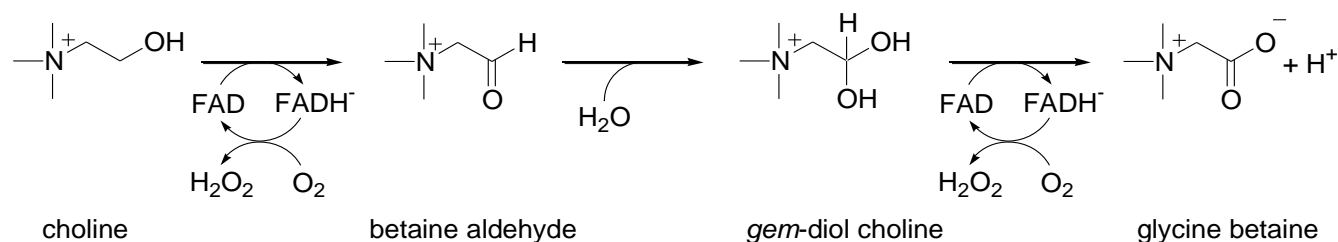
Scheme 5.1. Two-step, four-electron oxidation of choline catalyzed by choline oxidase.

Biochemical (*13, 14*), mechanistic (*15-20*), mutagenesis (*20-23*) and crystallographic (*20*) studies have been used to elucidate the catalytic mechanism by which choline is oxidized by choline oxidase. The oxidation of choline by choline oxidase is shown to occur by quantum mechanical hydride tunneling in a highly preorganized active site environment which is achieved via an enthalpically unfavorable internal equilibrium [see (*24*) for a recent review]. The organic substrate binds to the enzyme, containing oxidized FAD, in a solvent excluded cavity partially surrounded by hydrophobic residues to form an enzyme-choline complex. The hydroxyl proton is abstracted by a yet to be identified active site base from the alcohol substrate after substrate binding to form a transiently stabilized enzyme-alkoxide species followed by a hydride transfer from the substrate α-carbon to the N5 position of the flavin cofactor. The hydride transfer reaction results in the oxidation of choline to betaine aldehyde with concomitant reduction of the oxidized flavin bound to choline oxidase to form an anionic flavin hydroquinone-bound enzyme in complex with the reaction intermediate (*18*). The anionic flavin hydroquinone is subsequently re-oxidized by reacting with molecular oxygen to regenerate the oxidized flavin-bound enzyme.

The crystal structure of choline oxidase recently resolved to 1.86 Å revealed Glu312 as the only negatively charged residue in the active site of the enzyme, forming part of the solvent excluded cavity within the substrate binding domain (*20*) (Figure 5.1). The glutamate residue at position 312 was shown to be involved in substrate binding through an electrostatic interaction

with the positively charged trimethylammonium headgroup of choline by replacing the negatively charged residue with a glutamine in a choline oxidase mutant enzyme, CHO-E312Q. As evidence for this for this conclusion, a K_d value of at least 500-fold larger than the value previously obtained for the wild-type enzyme was determined for CHO-E312Q with choline as substrate (20). The importance of the spatial location for correct positioning of the substrate towards the hydride transfer reaction was demonstrated in another choline oxidase mutant enzyme in which the active site glutamate residue was replaced with an aspartate (CHO-E312D). A decrease of 260-fold in the rate of flavin reduction compared to wild-type choline oxidase and the presence of a kinetically relevant conformational change in the enzyme-substrate Michaelis complex were observed in the aspartae variant enzyme (20). These results coupled with the temperature dependence of the kinetic isotope effect on the rate constant for flavin reduction and the associated thermodynamic parameters in comparison with the wild-type enzyme (unpublished data) are consistent with disruption of the highly preorganized enzyme substrate complex in the Glu312Asp enzyme, which is required for the hydride tunneling reaction catalyzed by choline oxidase. The disruption is due to displacement of the substrate in the aspartate variant with choline as substrate, resulting in a larger distance between the hydride ion donor and acceptor upon replacing the glutamate residue with aspartate.

In this study, a substrate analogue which has one additional methylene group compared to choline, (3-hydroxypropyl)trimethylammonium (3-HPTA), was used as a substrate for CHO-E312D in a mechanistic study to further probe the role of the side chain at position 312 with respect to the relative positioning of the substrate hydride donor and flavin hydride acceptor. The substrate analogue was used to compensate for the resultant larger distance due to the shortening of the side chain at position 312 in CHO-E312D. The results herein demonstrate the requirement

of an unprotonated species for the reactivity of the reduced flavin species with oxygen for the aspartate variant enzyme with 3-HPTA as substrate, and substantiate the importance of the glutamate side chain in the relative positioning of the hydride donor and acceptor for the hydride ion tunneling reaction in choline oxidase.
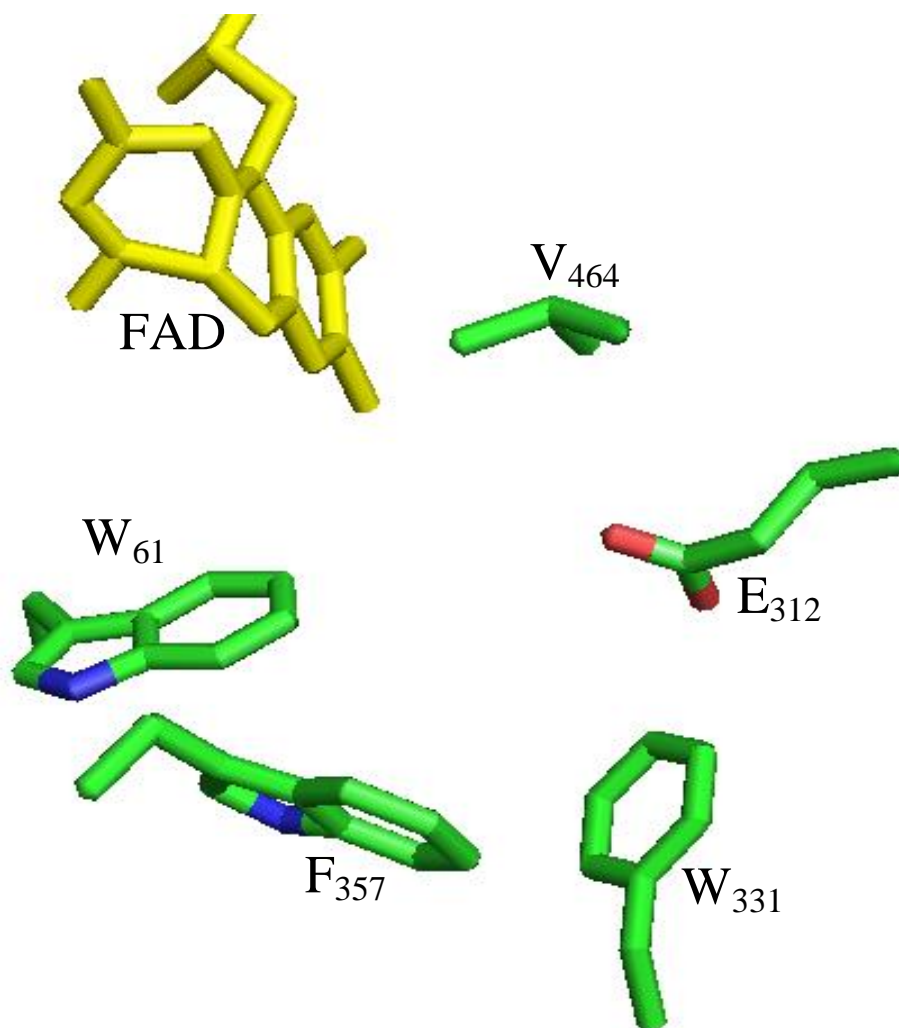

Figure 5.1. X-ray crystal structure of the active site of wild-type choline oxidase resolved to 1.86 Å (PDB 2jbv).
Picture shows the substrate binding cavity partially surrounded by hydrophobic residues to form an aromatic cage.

5.3. Experimental Procedures

Materials. Recombinant choline oxidase gene (pET/*codA* E312D) in *Escherichia coli* strain Rosetta (DE3)pLysS was used to express CHO-E312D. (3-Hydroxypropyl)-trimethylammonium (3-HPTA) iodide, sucrose, glucose and glucose oxidase were from Sigma-Aldrich (St. Louis, MO). All other reagents used were of the highest purity commercially available.

Enzyme Assays. The gene for choline oxidase variant enzyme in which the active site glutamate residue at position 312 has been replaced with an aspartate, CHO-E312D, was expressed and purified to homogeneity as previously described (*14, 20, 25*).

Rapid kinetics at varying concentrations of 3-HPTA was carried out at pH 10 and 25 °C with a Hi-Tech SF-61 stopped-flow spectrophotometer under anaerobic conditions with the addition of glucose and glucose oxidase as previously described (*26, 27*). The rates of flavin reduction were measured by monitoring the decrease in absorbance at 450 nm upon mixing the oxidized enzyme with the organic substrate. Glucose and glucose oxidase (oxygen scrubbing system) were added to the enzyme and substrate to scavenge lurking traces of oxygen that may be present before mixing. Equal volumes of CHO-E312D and 3-HPTA were anaerobically mixed in the stopped-flow spectrophotometer resulting in a reaction mixture with a final enzyme concentration of ~10 μM and substrate concentrations of 0.1 to 15 mM, with each substrate concentration assayed in triplicate.

Enzyme activities for CHO-E312D with 3-HPTA as substrate were measured by the method of initial rates in 50 mM sodium pyrophosphate by monitoring the rate of oxygen

consumption with a computer-interfaced Oxy-32 oxygen monitoring system (Hansatech Instrument Inc.) at 25 $^{\circ}$C as described previously for the wild type and CHO-E312D enzymes (*16, 20*). Steady state kinetic parameters for CHO-E312D were determined at varying concentrations of 3-HPTA (0.1 to 10 mM) and oxygen (0.2 to 1 mM) at pH 10. The desired oxygen concentration for each assay was obtained by bubbling the appropriate O_2/N_2 gas mixture for a minimum of 10 min to equilibrate the reaction mixture. pH profiles of the steady state kinetic parameters were obtained between pH 5.5 and 10. The effect of solvent viscosity on the kinetic parameters were measured at pH 10 using sucrose as viscosigen, with the relative viscosity values at 25 $^{\circ}$C calculated according to the reference values at 20 $^{\circ}$C from Lide (*28*).

Data Analysis. Data were fit with KaleidaGraph (Synergy Software, Reading, PA) and EnzFitter softwares (Biosoft, Cambridge, UK). Stopped-flow traces were fit to eq 1, which describes a double-exponential process, where k_{obs1} and k_{obs2} represent the observed rates of flavin reduction, t is time, A_t is the value of absorbance at 450 nm at any given time, A is the amplitude of the total change in absorbance, and A_∞ is the absorbance at infinite time. Pre-steady state kinetic parameters were determined by fitting the observed rates data to eq 2, where k_{obs} is the observed rate for the reduction of the enzyme bound flavin, k_{red} is the limiting rate constant of flavin reduction at saturated substrate concentration and K_d is the dissociation constant for binding of the substrate to the enzyme. Steady state kinetic parameters were determined by fitting the initial rates data for pH 9 and 10 to eq 3 which describes a sequential steady state kinetic mechanism with the organic substrate (A) (3-HPTA) in rapid equilibrium with the enzyme ($K_a << K_{ia}$). Initial rates for pH 5.5 to 8 fitted to eq 4 which describes sequential steady state kinetic mechanism, where e represents the concentration of enzyme, k_{cat} is the turnover

number of the enzyme at saturating substrates concentrations, and K_a and K_b represent the Michaelis constants for the organic substrate (A) and oxygen (B), respectively. The pH dependences of the steady state kinetic parameters were determined by fitting the initial rates data to eq 5, which describes a curve with a slope of + 1 and a plateau region at high pH, where C is the pH-independent value of the kinetic parameter. Effects of solvent viscosity on k_{cat}/K_{O2} and k_{cat} values were fit to eq 6, where $(k)_o$ and $(k)_\eta$ are the kinetic parameters of interest in the absence and presence of viscosigen, respectively, S is the degree of viscosity dependence and η_{rel} is the relative viscosity.

$$A_t = A_1 e^{-k_{obs1}t} + A_2 e^{-k_{obs2}t} + A_\infty \tag{1}$$

$$k_{obs} = \frac{k_{red}A}{K_d + A} \tag{2}$$

$$\frac{v}{e} = \frac{k_{cat}AB}{K_bA + AB + K_{ia}K_b} \tag{3}$$

$$\frac{v}{e} = \frac{k_{cat}AB}{K_aB + K_bA + AB + K_{ia}K_b} \tag{4}$$

$$\log Y = \log\left[\frac{C}{1 + \dfrac{10^{-pH}}{10^{-pK_a}}}\right] \tag{5}$$

$$\frac{(k)_o}{(k)_\eta} = S(\eta_{rel} - 1) + 1 \tag{6}$$

5.4. Results

Reductive Half-Reaction. The choline oxidase variant in which the glutamate residue at position 312 was replaced with an aspartate was expressed and purified following previously described procedures with the addition of 10% glycerol to all the purification solutions (*20, 25*). The reductive half-reaction of CHO-E312D was investigated pH 10 and 25 $^{\circ}$C to determine the limiting rate constant for flavin reduction (k_{red}) and the thermodynamic binding constant (K_d) at varying concentrations of 3-HPTA using a stopped-flow spectrophotometer. The stopped-flow traces showed double exponential processes of flavin reduction as shown in Figure 5.2 for the traces at 15 mM substrate concentration. The data for the fast observed rate of flavin reduction (k_{obs} 1) which increases with increasing concentration of 3-HPTA to a limiting value at high substrate concentration were fit to eq 2 yielding a k_{red} value that was ~20-fold higher than that for CHO-E312D with choline as substrate (*20*), with no significant difference in the estimated binding constants (K_d) for the two substrates (Figure 5.2 and Table 5.1). As shown in Figure 5.2 and Table A5.1 of the Supporting Information, the slow observed rate (k_{obs} 2) is independent of the concentration of 3-HPTA with a limiting value of ~0.1 s^{-1}. For all the concentrations of 3-HPTA used, the enzyme undergoes two-electron reduction to form a flavin hydroquinone (Figure 5.2) suggesting no observed intermediates as for the case of wild-type choline oxidase (*16*) and the aspartate mutant with choline as substrate (*20*).

Steady State Kinetic Mechanism. The steady state kinetic mechanism and parameters for CHO-E312D at pH 10 and 25 $^{\circ}$C were determined by measuring the initial rates of oxygen consumption at varying concentrations of both 3-HPTA and oxygen. The data were best fit to a

sequential steady state kinetic mechanism with $K_a \ll K_{ia}$ (eq 3) suggesting that the substrate is in rapid equilibrium with the enzyme. As shown in Table 5.1, the k_{cat} value for CHO-E312D with 3-HPTA as substrate was ~20 times larger than the value for the enzyme with choline as substrate (20) and consistent with partial rescue of activity in the aspartate variant enzyme with the substrate analogue. A decrease of at least 7-fold in the k_{cat}/K_{O_2} value resulted from substituting choline with 3-HPTA, suggesting that the oxidative half-reaction in which oxygen reacts with the reduced flavin-bound enzyme species is adversely affected by the substrate analogue.
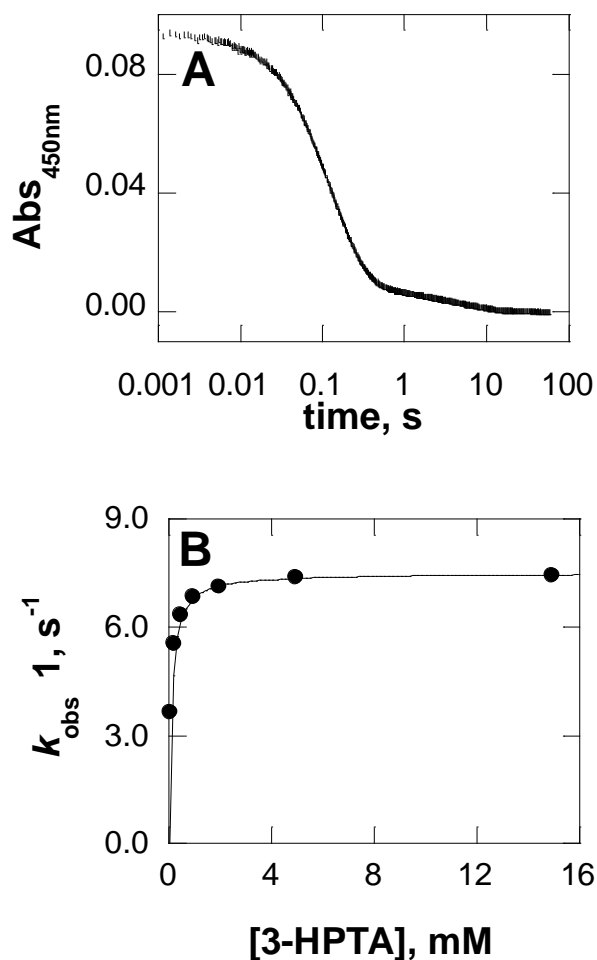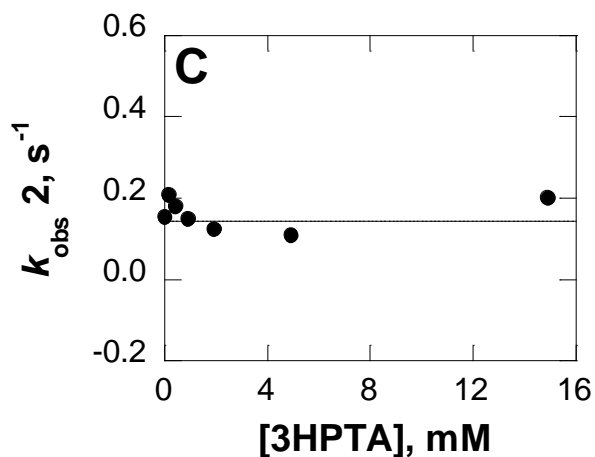
Figure 5.2. Rate of flavin reduction in CHO-E312D as a function of 3-HPTA concentration. Experiments were carried out in 50 mM sodium pyrophosphate, pH 10 and 25 °C. Data were fit to $k_{obs} = k_{red}S/(K_d+S)$.

Table 5.1. Steady state and pre-steady state kinetic parameters for CHO-E312D with 3-HPTA and choline as substrates at pH 10 and 25 °C.

Kinetic parameters	3-HPTA	choline[a]
k_{cat} (s^{-1})	5.04 ± 0.02	0.26 ± 0.01
k_{cat}/K_m (M^{-1}s^{-1})	nd	$7,100 \pm 400$
K_{cat}/K_{O2} (M^{-1}s^{-1})	$11,100 \pm 90$	$\geq 76,000$
K_m (mM)	nd	0.04 ± 0.01
K_{O2} (mM)	0.45 ± 0.01	≤ 0.002
k_{red} (s^{-1})	7.51 ± 0.06	0.36 ± 0.01
K_d (mM)	~0.1	~0.1

Experiments were carried out in 50 mM sodium pyrophosphate and the data fit to $v_o/[E] = k_{cat}S/(K_m+S)$. [a]Data with choline as substrate are from ref *(16)*.

pH Dependence of Steady State Kinetic Parameters. pH dependences of the steady state kinetic parameters for CHO-E312D were carried out in the pH range of 5.5 to 10 at varying concentrations of 3-HPTA and oxygen to determine the pK_a of functional groups that are involved in the catalytic oxidation of the organic substrate analogue. The double reciprocal plots for the oxidation of 3-HPTA showed converging lines between pH 5.5 and 10, consistent with

the kinetic mechanism being sequential steady state throughout the pH range (Figure 5.3). The lines for the plots of $[E]/v_o$ versus $1/[\text{oxygen}]$ at different fixed concentrations of 3-HPTA from pH 5.5 to 8, however, intersect on the left of the y-axis whereas the lines for the plots at pH 9 and 10 intersect on the y-axis, suggesting that the k_{cat} is not dependent on the concentration of 3-HPTA at high pH (Figure 5.3). All the kinetic parameters (k_{cat}/K_m, k_{cat}/K_{O2} and k_{cat}) increased with increasing pH to limiting values at high pH as shown in Figure 5.4, consistent with the requirement of an unprotonated species in both the reductive and oxidative half-reactions, and the overall turnover of the enzyme for catalysis. An apparent pK_a value of 6.7 was estimated from the pH dependence of the k_{cat}/K_m values (in the pH range of 5.5 and 8 due to the change in the steady-state kinetic mechanism caused by small K_m values for the organic substrate analogue at pH 9 and 10) (Figure 5.4) compared to a pK_a value of 7.6 for the same kinetic parameter but with choline as substrate for CHO-E312D (Table 5.2). The perturbed pK_a value (shift in the value with 3-HPTA as substrate) suggests the presence of a partially rate-limiting step in the reductive half-reaction of the catalytic oxidation of 3-HPTA by the aspartate choline oxidase variant. The similarities in the limiting values of the pH dependence of the k_{cat}/K_m values with 3-HPTA and choline as substrates (Table 5.2) suggest similar specificities of the native substrate and the substrate analogue to the mutant enzyme. A pK_a value of ≤ 6 was obtained from the dependence of k_{cat} values on pH compared to the pK_a value of 6.7 from the k_{cat}/K_m pH-profile suggesting that steps occurring after the chemical step are partially rate-limiting in the overall turnover of the enzyme. The limiting value of $\sim 10,700$ $M^{-1}s^{-1}$ obtained from the pH dependence of the k_{cat}/K_{O2} values with 3-HPTA as substrate (Figure 5.4) compared to the limiting value of at least 76,000 $M^{-1}s^{-1}$ for the mutant enzyme with choline as substrate is consistent with lower

reactivity of oxygen with the reduced enzyme species of CHO-E312D with the substrate analogue.

Table 5.2. Kinetic parameters and pK_a values determined from pH-profiles for CHO-E312D with choline and 3-HPTA as substrates determined at pH 10 and 25 °C.

Kinetic parameters	Substrates	Limiting Values	pK_a
k_{cat} (s^{-1})	choline[a]	0.26 ± 0.01	≤ 6
	3-HPTA	4.77 ± 0.33	≤ 6
k_{cat}/K_m (M^{-1}s^{-1})	choline[a]	$6{,}690 \pm 380$	7.6 ± 0.1
	3-HPTA	$\sim 7{,}300 \pm 1200$	$\sim 6.7 \pm 0.1$
K_{cat}/K_{O2} (M^{-1}s^{-1})	choline[a]	$\geq 76{,}000$[b]	nd[c]
	3-HPTA	$10{,}650 \pm 630$	5.9 ± 0.1

[a]Data with choline as substrate were from Quaye *et al*., 2008 (*20*). [b]Estimated lower limiting value was calculated from the k_{cat} value experimentally determined and the estimated upper limiting value for K_m. [c]not determined:
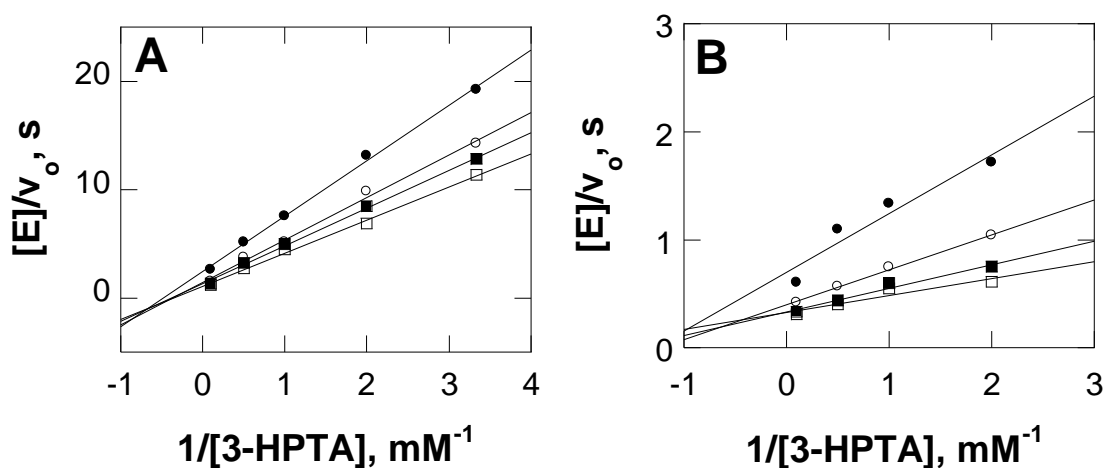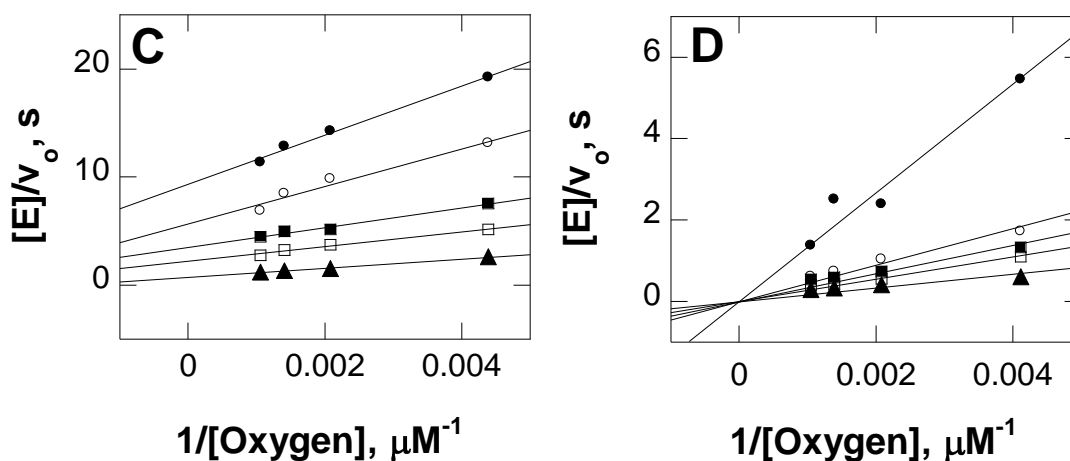
Figure 5.3. Double reciprocal plots for the rates of 3-HPTA oxidation by CHO-E312D. Panels A and B are $[E]/v_o$ versus 1/[3-HPTA] plots at pH 5.5 and 10, respectively, and different fixed concentrations of oxygen: (○) 0.24 mM; (■) 0.48 mM; (□) 0.72 mM; (●) 0.96 mM. Panels C and D are $[E]/v_o$ versus 1/[oxygen] plots at pH 5.5 and 10, respectively, and different fixed concentrations of 3-HPTA: (○) 0.1 mM; (■) 0.5 mM; (□) 1.0 mM; (●) 2.0 mM; (▲) 10.0 mM. CHO-E312D activity was measured at varying concentrations of choline and oxygen in 50 mM sodium pyrophosphate pH 10 and 25 °C. Data of Panels A and C were fit to eq 4 and data for Panels B and D were fit to eq 3.
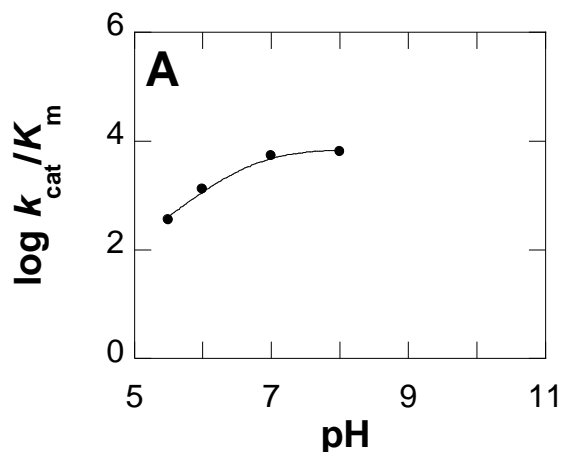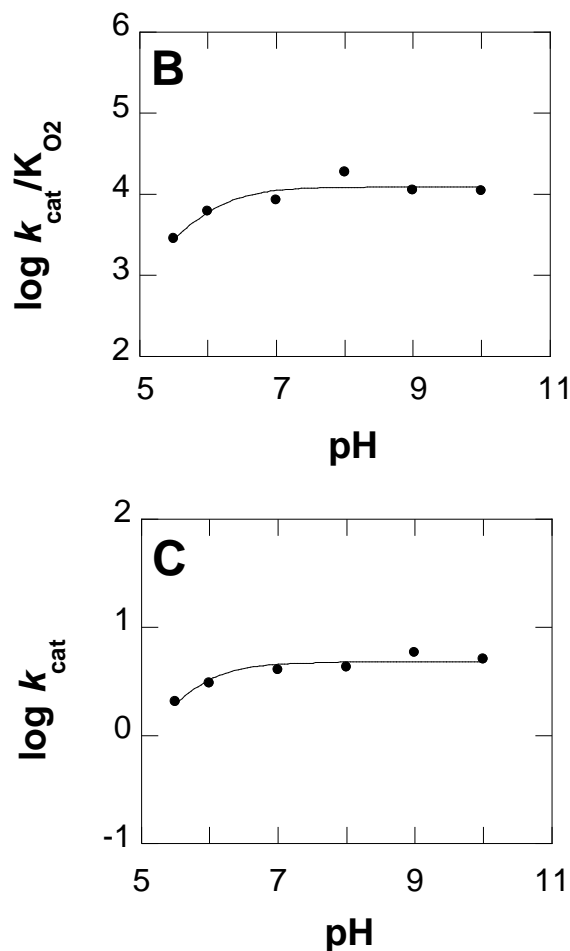
Figure 5.4. pH dependence of k_{cat}, k_{cat}/K_{mO2} and k_{cat}/K_m values for CHO-E312D with 3-HPTA as substrate.
Panels A, B and C represent the pH profiles for log k_{cat}, log k_{cat}/K_{mO2} and log k_{cat}/K_m, respectively. CHO-E312D activity was measured at varying concentrations of choline and oxygen in 50 mM sodium pyrophosphate buffer. Data were fit to equation 5.

Effect of Solvent Viscosity on Steady State Kinetic Parameters. Using sucrose as viscosigen at pH 10 and 25 °C, the effect of solvent viscosity on the k_{cat}/K_{O2} and k_{cat} values were determined to probe the presence of internal equilibria in the oxidative half-reaction and the overall turnover of the enzyme. The steady state kinetic parameters were determined by measuring the initial rates of reaction at varying concentrations of 3-HPTA and oxygen in the absence and presence of increasing amounts of sucrose, and the data fit to the rapid equilibrium

steady state kinetic mechanism equation (eq 3). There is an inverse solvent viscosity effect on k_{cat}/K_{O2} but with slight decrease in the k_{cat}/K_{O2} values with increasing relative viscosity between 1.33 and 6.06 after the introduction of the lowest amount of viscosigen (Figure 5.5). Similar observation has previously been made for the k_{cat}/K_m values of homoisocitrate dehydrogenase with magnesium isocitrate as substrate and glycerol as viscosigen (*29*). The phenomenon suggests initial stabilization of an enzyme conformation and minimal limitation of oxygen reactivity in the oxidative half-reaction due to increasing relative viscosity. As shown in Figure 5.5, the k_{cat} value increased monotonically with increasing relative viscosity resulting in an inverse viscosity effect which is consistent with the presence of an internal equilibrium in the overall turnover of the enzyme. A summary of the effect of solvent viscosity on the k_{cat}/K_{O2} and k_{cat} values for CHO-E312D is shown in Table 5.3.

Table 5.3. Solvent viscosity effect on steady state kinetic parameters for CHO-E312D with sucrose as viscosigen at pH 10 and 25 °C.

Kinetic Parameter	Viscosity Effect[a]
K_{cat}/K_{O2} (M^{-1}s^{-1})	0.15 ± 0.02
k_{cat} (s^{-1})	-0.09 ± 0.05

[a]Viscosity effect values are relative to the values in the absence of viscosigen.
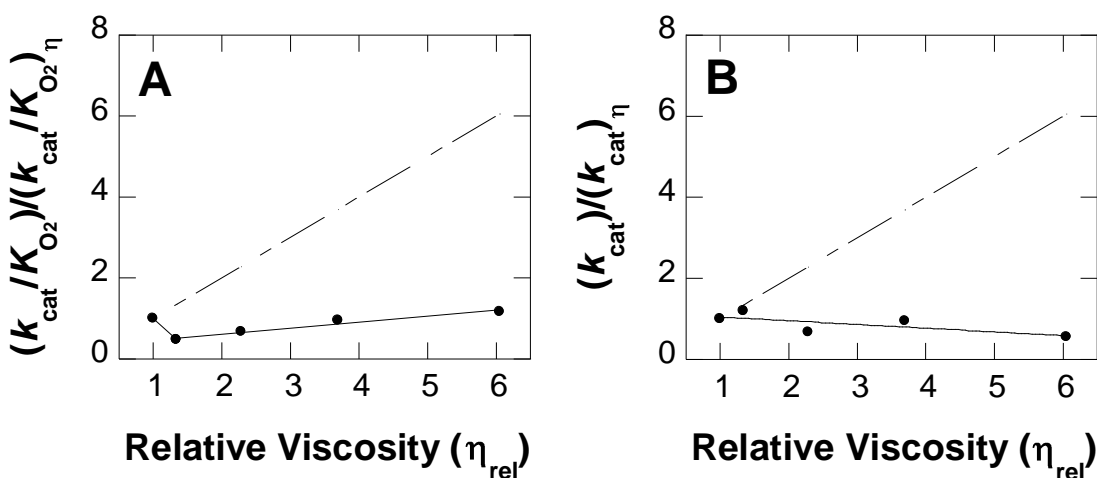
Figure 5.5. Effect of solvent viscosity on steady-state kinetic parameters for CHO-E312D with 3-HPTA as substrate and sucrose as viscosigen at pH 10.

Panels A and B show normalized k_{cat}/K_{mO2} and k_{cat} values, respectively, as a function of relative solvent viscosity. Solid lines represent fits of the experimental data using equation 6. Dashed lines with a slope of one describe a fully diffusion-controlled reaction. The values of the relative viscosities of the reaction mixture at 25 ^{o}C were calculated according to the values at 20 ^{o}C from Lide (ref.). CHO-E312D activity was measured at varying concentrations of choline and oxygen in 50 mM sodium pyrophosphate buffer in the absence and presence of increasing concentrations of sucrose as viscosigen.

5.5. Discussion

In this study, the enzymatic oxidation of (3-hydroxypropyl)trimethylammonium to an aldehyde, with the aldehyde species probably further oxidized to propiobetaine, by the variant form of choline oxidase in which the glutamate residue at position 312 was replaced with an aspartate (CHO-E312D) has been investigated. The aspartate variant was previously constructed using site-directed mutagenesis to investigate the importance of the spatial location of the only negatively charged amino acid residue in the active site of choline oxidase (*20*). The shortening of the side chain at position 312 resulted in a change in the kinetic mechanism of alcohol oxidation in the aspartate containing enzyme from a quantum mechanical hydride ion tunneling in the wild-type enzyme to either environmentally assisted tunneling or over-the-barrier transition state (*30*). The change in hydride transfer mechanism is associated with a two-order of magnitude decrease in the rate flavin reduction. The sharp contrast in the kinetic mechanism is due to disruption of the highly preorganized enzyme-substrate complex caused by a larger distance between the alkoxide hydride ion donor and the flavin hydride ion acceptor upon replacing the glutamate with an aspartate and using choline as substrate. The substrate analogue

(3-HPTA), which has one additional methylene group compared to choline, was used as substrate for CHO-E312D to compensate for the larger distance between the hydride ion donor and acceptor to further understand the importance of the side chain at position 312 for the relative positioning of the hydride donor and acceptor for the hydride transfer reaction catalyzed by choline oxidase.

The enzymatic activity of the Glu312Asp variant enzyme was partially rescued upon replacing choline with 3-HPTA as substrate. Evidence for the partial rescue of activity in CHO-E312D comes from the limiting rate constant for flavin reduction and the overall enzyme turnover for the mutant enzyme with the substrate analogue determined at pH 10 and 25 $^{\circ}$C as compared to choline as substrate under the same experimental conditions of pH and temperature. The ~20-fold increase in k_{red} and k_{cat} values with the substitution of choline with 3-HPTA as substrate for the aspartate-containing enzyme is probably due to a shorter distance between the hydride ion donor (activated 3-HPTA) and acceptor (N5 atom of the flavin). Even though CHO-E312D activity with 3-HPTA could not be totally rescued compared to the wild-type enzyme with choline as substrate, the data suggest that the spatial location of the negative charge is important for the reaction catalyzed by choline oxidase. The inability of the total activity to be rescued may partly be due to the CHO-E312D-activated 3-HPTA complex not being as highly preorganized as is the wild-type enzyme. The lack of high preorganization is probably contributed by the kinetically relevant internal equilibrium previously shown to be present in the Glu312Asp enzyme with choline as substrate (*20*). The similarity in the increase in k_{red} and k_{cat} values with the substitution of choline with 3-HPTA as substrate is an independent evidence of the hydride transfer step being fully rate-limiting in the catalytic mechanism of CHO-E312D.

The reactivity of the reduced flavin species with oxygen in the oxidative-half reaction catalyzed by CHO-E312D is adversely affected by the presence of the bulky substrate analogue. This conclusion is supported by the decrease of at least 7-fold in the k_{cat}/K_{O_2} value for the variant enzyme with 3-HPTA compared to the value for the enzyme previously determined with choline as substrate at pH 10 and 25 °C. The decrease in the rate of oxidation of the reduced flavin species is consistent with lack of easy access of oxygen to the oxidative reaction center or activation of molecular oxygen or both. The k_{cat}/K_{O_2} values for CHO-E312D with 3-HPTA increased with increasing pH to a limiting value at high pH consistent with the requirement of an unprotonated species in the oxidative half-reaction. The limiting k_{cat}/K_{O_2} value is ~8-fold lower compared to the value in wild-type choline oxidase with choline as substrate. Since similar limiting values were estimated for the CHO-E312D and wild-type choline oxidase with choline as substrate, the decrease in the limiting value for the mutant enzyme with 3-HPTA could be due to steric hindrance and the bulky nature of the substrate analogue preventing easy accessibility of molecular oxygen to the reactivity site, and not due to the spatial location of the negative charge at position 312. Independent evidence supporting the conclusion was obtained from the inverse effect of solvent viscosity on k_{cat}/K_{O_2}, which is consistent with the stabilization of an enzyme-intermediate-oxygen ternary complex conformation followed by slight decreases in the kinetic parameter with increasing amounts of the viscosigen (*29*). The slight but monotonical increase of the inverse solvent viscosity effect on k_{cat}/K_{O_2} is an indication of the presence of a diffusion-controlled step in the oxidative half-reaction after the stabilization of the ternary complex conformation. In agreement with this explanation, analysis of the molecular surfaces of the crystal structure of wild-type choline oxidase showed a solvent-excluded cavity with a volume of ~125 Å^3, just large enough to accommodate choline with a volume of 93 Å^3.

A kinetic step(s) other than the chemical step is partially rate-limiting in the reductive half-reaction. This conclusion was evident in the pK_a value obtained from the k_{cat}/K_m pH profile for the ionizable group that acts as a base in the aspartate-containing enzyme with 3-HPTA as substrate compared to the pK_a value for the wild-type enzyme and CHO-E312D both with choline as substrate. A shift in the pK_a value to 6.7 for CHO-E312D with 3-HPTA compared to the thermodynamic value of ~7.5 for wild-type choline oxidase and the Glu312Asp enzyme with choline as substrate is consistent with the presence of an external commitment to catalysis in the reductive half-reaction catalyzed by the aspartate-containing enzyme with the substrate analogue. The thermodynamic constant for binding of the substrate to the enzyme (K_d) in CHO-E312D is similar for both choline and 3-HPTA as substrates, suggesting similar binding modes for the two substrates. Even though the presence of an external commitment to catalysis will be probed further in a later study using substrate kinetic isotope effect, the partially rate-limiting step other than the chemical step is likely not due to the kinetically relevant internal equilibrium previously as shown in CHO-E312D with choline as substrate (20). Since the external forward commitment to catalysis shown in CHO-E312D is affected by pH, is probably due to deprotonation of the substrate analogue to form the activated substrate which is subsequently followed by the hydride ion transfer step.

The change in the kinetic mechanism of CHO-E312D with 3-HPTA from low to high pH is probably due to an increase in k_1 with increasing pH. Comparison of the pK_a values from the k_{cat}/K_m and k_{cat} pH-profiles suggest the presence of a partially rate-limiting step other than the chemical step in the overall turnover of the Glu312Asp enzyme. This observation is supported by a lower k_{cat} value of ~5 s^{-1} compared to the k_{red} value of 7.5 s^{-1}. The sequential mechanism of the aspartate-containing enzyme with 3-HPTA, as for the case of the wild-type enzyme with choline

as substrate, suggests that the substrate analogue is oxidized to the aldehyde intermediate upon binding CHO-E312D with subsequent interaction of the enzyme-intermediate complex with oxygen to form a ternary complex. The partially rate-limiting step other than the chemical step in the overall enzyme turnover for CHO-E312D with 3-HPTA could either be the hydride ion transfer from the aldehyde intermediate to the N5 position of the flavin cofactor or the release of the final product. The effect of solvent viscosity on k_{cat} values with sucrose as solvent viscosigen does not implicate any involvement of the product release step in the overall turnover rate of the Glu312Asp enzyme with 3-HPTA as substrate. In the event where the product released step contributes to the overall rate of enzyme turnover, the normalized k_{cat} values are expected to increase with increasing relative viscosity (*31-34*). The observed effect of solvent viscosity on k_{cat} suggests that the product released step is not partially rate-limiting in the overall turnover of CHO-E312D and consistent with the hydride ion transfer from the aldehyde intermediate being the other rate-limiting step in the overall turnover of the enzyme. With the hydride transfer steps for the oxidation of 3-HPTA and the aldehyde intermediate contributing to the overall enzyme turnover as for the case of wild-type choline oxidase, the rate of flavin reduction (k_{red}) of the betaine aldehyde analogue to propiobetaine with a value of 15 s^{-1} can be estimated from eq 7. The ratio of k_{cat} to k_{cat}/K_m in terms of kinetic rate constants gives an equation that describes K_m and is shown in eq 8. An increase in k_1 with increasing pH agrees with a resulting decrease in K_m and is consistent with the observed change in the kinetic mechanism of CHO-E312D with 3-HPTA at low and high pH.

$$k_{cat} = \frac{k_3 k_7}{k_3 + k_7} \tag{7}$$

$$K_m = \frac{k_7(k_2 + k_3)}{k_1(k_3 + k_7)} \tag{8}$$

In conclusion, the mechanistic data for the mutant enzyme of choline oxidase in which the active site residue at position 312 was replaced with an aspartate with 3-HPTA as substrate demonstrated the importance of the glutamate side chain in the relative positioning of the hydride donor and acceptor for the catalytic oxidation of choline by choline oxidase. The larger distance between the hydride donor and acceptor in CHO-E312D compared to the wild-type enzyme, created by the displacement of the negative charge and ultimately altered the positioning of choline was compensated for by the use of 3-HPTA with an additional carbon-carbon bond compared to choline. The compensation, however, did not result in total rescue of activity of CHO-E312D due to a poorly preorganized active site environment in the mutant enzyme. The poor preorganization in CHO-E312 coupled with the bulky nature of the substrate analogue might have resulted in conformational changes in the oxidative half-reaction and the overall turnover of the mutant enzyme. Altogether, the data presented suggest that the distance between the hydride donor and acceptor alone is not enough for the hydride tunneling oxidation of choline catalyzed by choline oxidase.

5.6. References

1.   Bae, J. H., Anderson, S. H., and Miller, K. J. (1993) Identification of a high-affinity glycine betaine transport system in *Staphylococcus aureus*, *Appl.Environ. Microbiol. 59*, 2734-2736.

2.   Pichereau, V., Bourot, S., Flahaut, S., Blanco, C., Auffray, Y., and Bernard, T. (1999) The osmoprotectant glycine betaine inhibits salt-induced cross-tolerance towards lethal treatment in *Enterococcus faecalis*, *Microbiology 145*, 427-435.

3.   O'Callaghan, J., and Condon, S. (2000) Growth of *Lactococcus lactis* strains at low water activity: correlation with the ability to accumulate glycine betaine, *Internat. J. Food Microbiol. 55*, 127-131.

4.   Velasco-Garcia, R., Chacon-Aguilar, V. M., Hervert-Hernandez, D., and Munoz-Clares, R. A. (2003) Inactivation of betaine aldehyde dehydrogenase from *Pseudomonas aeruginosa* and *Amaranthus hypochondriacus L.* leaves by disulfiram, *Chemico-Biol. Int. 143-144*, 149-158.

5.   Peddie, B. A., Chambers, S. T., and Lever, M. (1996) Is the ability of urinary tract pathogens to accumulate glycine betaine a factor in the virulence of pathogenic strains?, *J. Lab. Clin. Med. 128*, 417-422.

6.   Chen, T. H., and Murata, N. (2002) Enhancement of tolerance of abiotic stress by metabolic engineering of betaines and other compatible solutes, *Curr. Opin. Plant Biol. 5*, 250-257.

7.   Rontein, D., Basset, G., and Hanson, A. D. (2002) Metabolic engineering of osmoprotectant accumulation in plants, *Metabol. Eng. 4*, 49-56.

8.   Sanchez-Aguayo, I., Rodriguez-Galan, J. M., Garcia, R., Torreblanca, J., and Pardo, J. M. (2004) Salt stress enhances xylem development and expression of S-adenosyl-L-methionine synthase in lignifying tissues of tomato plants, *Planta 220*, 278-285.

9. Shirasawa, K., Takabe, T., Takabe, T., and Kishitani, S. (2006) Accumulation of glycinebetaine in rice plants that overexpress choline monooxygenase from spinach and evaluation of their tolerance to abiotic stress, *Annal. Bot. 98*, 565-571.

10. Waditee, R., Bhuiyan, M. N., Rai, V., Aoki, K., Tanaka, Y., Hibino, T., Suzuki, S., Takano, J., Jagendorf, A. T., Takabe, T., and Takabe, T. (2005) Genes for direct methylation of glycine provide high levels of glycinebetaine and abiotic-stress tolerance in *Synechococcus* and *Arabidopsis*, *Proc. Natl. Acad. Sci. U S A 102*, 1318-1323.

11. Quan, R., Shang, M., Zhang, H., Zhao, Y., and Zhang, J. (2004) Engineering of enhanced glycine betaine synthesis improves drought tolerance in maize, *Plant Biotechnol. J. 2*, 477-486.

12. Waditee, R., Bhuiyan, N. H., Hirata, E., Hibino, T., Tanaka, Y., Shikata, M., and Takabe, T. (2007) Metabolic engineering for betaine accumulation in microbes and plants, *J. Biol. Chem. 282*, 34185-34193.

13. Gadda, G. (2003) pH and deuterium kinetic isotope effects studies on the oxidation of choline to betaine-aldehyde catalyzed by choline oxidase, *Biochim. Biophys. Acta 1650*, 4-9.

14. Gadda, G., Powell, N. L., and Menon, P. (2004) The trimethylammonium headgroup of choline is a major determinant for substrate binding and specificity in choline oxidase, *Arch. Biochem. Biophys. 430*, 264-273.

15. Fan, F., and Gadda, G. (2005) Oxygen- and temperature-dependent kinetic isotope effects in choline oxidase: correlating reversible hydride transfer with environmentally enhanced tunneling, *J. Am. Chem. Soc.127*, 17954-17961.

16. Fan, F., and Gadda, G. (2005) On the catalytic mechanism of choline oxidase, *J. Am. Chem. Soc. 127*, 2067-2074.

17. Fan, F., and Gadda, G. (2007) An internal equilibrium preorganizes the enzyme-substrate complex for hydride tunneling in choline oxidase, *Biochemistry 46*, 6402-6408.

18. Gadda, G. (2003) Kinetic mechanism of choline oxidase from *Arthrobacter globiformis*, *Biochim. Biophys.Acta 1646*, 112-118.

19. Gadda, G., Fan, F., and Hoang, J. V. (2006) On the contribution of the positively charged headgroup of choline to substrate binding and catalysis in the reaction catalyzed by choline oxidase, *Arch. Biochem. Biophys. 451*, 182-187.

20. Quaye, O., Lountos, G. T., Fan, F., Orville, A. M., and Gadda, G. (2008) Role of Glu312 in binding and positioning of the substrate for the hydride transfer reaction in choline oxidase, *Biochemistry 47*, 243-256.

21. Ghanem, M., and Gadda, G. (2005) On the catalytic role of the conserved active site residue His466 of choline oxidase, *Biochemistry 44*, 893-904.

22. Ghanem, M., and Gadda, G. (2006) Effects of reversing the protein positive charge in the proximity of the flavin N(1) locus of choline oxidase, *Biochemistry 45*, 3437-3447.

23. Rungsrisuriyachai, K., and Gadda, G. (2008) On the role of histidine 351 in the reaction of alcohol oxidation catalyzed by choline oxidase, *Biochemistry 47*, 6762-6769.

24. Gadda, G. (2008) Hydride transfer made easy in the reaction of alcohol oxidation catalyzed by flavin-dependent oxidases, *Biochemistry 47*, 13745-13753.

25. Fan, F., Ghanem, M., and Gadda, G. (2004) Cloning, sequence analysis, and purification of choline oxidase from *Arthrobacter globiformis*: a bacterial enzyme involved in osmotic stress tolerance, *Arch. Biochem. Biophys. 421*, 149-158.

26. Finnegan, S., and Gadda, G. (2008) Substitution of an active site valine uncovers a kinetically slow equilibrium between competent and incompetent forms of choline oxidase, *Biochemistry 47*, 13850-13861.

27. Quaye, O., Cowins, S., and Gadda, G. (2009) Contribution of flavin covalent linkage with histidine 99 to the reaction catalyzed by choline oxidase, *J. Biol. Chem. 284*, 16990-16997.

28. Lide, D. R. (2000) Handbook of Chemistry and Physics, (Ed, -. Ed.), pp pp8-57, CRC Press, Boca Raton, Fl.

29. Lin, Y., Volkman, J., Nicholas, K. M., Yamamoto, T., Eguchi, T., Nimmo, S. L., West, A. H., and Cook, P. F. (2008) Chemical mechanism of homoisocitrate dehydrogenase from Saccharomyces cerevisiae, *Biochemistry 47*, 4169-4180.

30. Quaye, O., and Gadda, G. (2009) Effect of a conservative mutation of an active site residue involved in substrate binding on the hydride tunneling reaction catalyzed by choline oxidase, *Submitted for publication in Arch. Biochem. Biophys.*

31. Agmon, N. (1985) A diffusion Michaelis-Menten mechanism: continuous conformational change in enzymatic kinetics, *J. Theor. Biol. 113*, 711-717.

32. Sobrado, P., Daubner, S. C., and Fitzpatrick, P. F. (2001) Probing the relative timing of hydrogen abstraction steps in the flavocytochrome b2 reaction with primary and solvent deuterium isotope effects and mutant enzymes, *Biochemistry 40*, 994-1001.

33. Somogyi, B., Norman, J. A., Zempel, L., and Rosenberg, A. (1988) Viscosity and transient solvent accessibility of Trp-63 in the native conformation of lysozyme, *Biophys. Chem. 32*, 1-13.

34.   Su, Q., and Klinman, J. P. (1999) Nature of oxygen activation in glucose oxidase from

       Aspergillus niger: the importance of electrostatic stabilization in superoxide formation,

       Biochemistry 38, 8572-8581.

5.7. Appendix

Table A5.1. pH-Dependence of Steady State Kinetic Parameters for CHO-E312D Determined at Varying Concentrations of 3-HPTA and Oxygen at 25 $^{\circ}$C . These data were used for Figures 3,4 and 5.

pH	k_{cat}/K_m $(M^{-1}s^{-1})$	k_{cat}/K_{O2} $(M^{-1}s^{-1})$	k_{cat} (s^{-1})	K_m (mM)	K_{O2} (mM)
5.5	350 ± 20	2850 ± 140	2.05 ± 0.04	5.90 ± 0.31	0.72 ± 0.03
6.0	1310 ± 390	6190 ± 1550	3.04 ± 0.30	2.30 ± 0.64	0.49 ± 0.11
7.0	5400 ± 970	8500 ± 850	4.04 ± 0.16	0.75 ± 0.13	0.47 ± 0.04
8.0	6240 ± 1420	18600 ± 2970	4.24 ± 0.18	0.68 ± 0.15	0.23 ± 0.01
9.0	nd	11300 ± 80	5.82 ± 0.02	nd	0.52 ± 0.01
10.0	nd	11100 ± 90	5.04 ± 0.02	nd	0.45 ± 0.01

The k_{cat} and K_m parameters were obtained by fitting the initial rate data to $v_o/e = k_{cat}S/(K_m+S)$; the k_{cat}/K_m parameters were obtained by fitting the initial rate data to $v_o/e = k_{cat}S/\{k_{cat}/[1/(k_{cat}/K_m)]+S\}$. nd : not determined ; due to data inconsistency with 1,2-[$^2H_4$]-choline at pH 5 and 5.5.

Table A5.2. Solvent viscosity effects on steady state kinetic parameters for CHO-E312D with 3-HPTA as substrate and sucrose as viscosigen at 25 $^{\circ}$C.

A

Relative Viscosity	k_{cat} (s^{-1}) With No Viscosigen	k_{cat} (s^{-1}) With Viscosigen	Viscosity Effect
1.00	5.04 ± 0.02	NA	1.00
1.34	4.51 ± 0.02	3.77 ± 0.13	1.20
2.29	3.31 ± 0.14	3.11 ± 0.20	1.06
3.70	4.42 ± 0.17	4.60 ± 0.25	0.96
6.06	3.20 ± 0.02	5.72 ± 0.14	0.56

B

Relative Viscosity	k_{cat}/K_m (M^{-1}s^{-1}) With No Viscosigen	k_{cat}/K_m (M^{-1}s^{-1}) With Viscosigen	Viscosity Effect
1.00	11100 ± 90	NA	1.00
1.34	6300 ± 50	13500 ± 1200	0.47
2.29	7200 ± 740	10640 ± 2070	0.68
3.70	7660 ± 720	7970 ± 920	0.96
6.06	9310 ± 120	7900 ± 380	1.18

(A) Viscosity effect on kcat. (B) Viscosity effect on k_{cat}/K_m. Kinetic parameters were obtained by fitting the initial rates to the rapid equilibrium steady state kinetic mechanism equation (eq X) and the viscosity effects on the parameters obtained from $(k)_o/(k)_\eta = S(\eta_{rel}-1)+1$.

CHAPTER 6

Probing the Mechanism of Hydride Ion Transfer in Choline Oxidase Variant Enzymes

(The experiments in this chapter were carried out by the author with the help of Sam Hay and Chris Pudney, and supervised by Nigel Scrutton and Giovanni Gadda)

6.1. Abstract

The mechanisms of hydrogen atom transfer in enzymatic reactions where the transfers occur via quantum mechanical tunneling have been typically demonstrated using the temperature dependence approach. Recent studies suggest that there are instances when hydrogen atom transfer with significant distance and geometry sampling that can be associated with isotope effects on the pre-exponential factors that are close to unity, and the phenomenon not necessarily indicative of an over-the-barrier transition state mechanism. The mechanism of choline oxidation by choline oxidase is via tunneling of a hydride ion from the substrate hydride donor to the flavin hydride acceptor in a highly pre-organized active site environment. Previous data on the effect of temperature on the k_{red} and $^D k_{red}$ values of variant forms of choline oxidase in which histidine 99 and glutamate 312 were singly replaced with asparagine and aspartate, respectively, resulted in A_H/A_D values that are close to unity compared to ~14 in the wild-type enzyme and suggestive of a hydride ion transfer mechanism that is significantly different in the variant enzymes.

In this study, the true identities of the mechanism of hydride ion transfer in the His99Asn and Glu312Asp variant enzymes were investigated by probing the effect of hydrostatic pressure on the rate constant for flavin reduction using high pressure stopped-flow spectrophotometry. The rate of flavin reduction increases with increasing pressure to different slopes with choline

and 1,2-[^{2}H$_4$]-choline in CHO-H99N resulting in a pressure-dependent kinetic isotope effect and suggesting a tunneling mechanism with sampling of the reactive configurations. On the other hand, the rate of flavin reduction increases with increasing pressure to similar slopes with the isotopic substrates in CHO-E312D, thus yielding a pressure-independent kinetic isotope effect and consistent with a transition state mechanism. Redox potentials of the wild-type and two variant enzymes are consistent with the covalent linkage being important for the driving force in choline oxidase.

6.2. Introduction

The mechanism of hydrogen atom transfer in enzymatic reactions has been investigated in a number of enzyme systems including flavoproteins. Quantum mechanical tunneling has been demonstrated in a number of hydrogen transfer reactions and shown to occur either without significant sampling or with extensive distance and geometry sampling of the reactive configurations (*1-15*). Temperature dependence of the rate of flavin reduction and kinetic isotope effect have been typically used to indicate the mode of hydrogen transfer in enzymatic reactions; however, data on some enzyme systems do not conform to the tunneling models and require correction factors. Hydrogen tunneling with minimal or no sampling is associated with temperature independence of the kinetic isotope effect, isotope effects on the Eyring or Arrhenius pre-exponential factors (A_H/A_D) that are significantly larger than unity (i.e., >1.7), enthalpies of activations ($\Delta H^{\ddagger}$) for the transfer of protium and deuterium having finite values not different from one another, and negligible differences in the energies of activation ($\Delta E_a = (E_a)_H$-

$(E_a)_D$) for protium and deuterium transfers (*14, 16, 17*). On the other hand, transfer reactions where distance sampling is significant are commonly associated with, temperature dependent kinetic isotope effects with finite but different $\Delta H^{\ddagger}$ values for protium and deuterium transfers, finite ΔE_a values, and A_H/A_D values that are smaller than unity (i.e., <0.7) (*18-20*). However, a study by the group of Klinman have demonstrated that tunneling of hydrogen atom in enzyme catalyzed reactions where distance sampling is prominent can also be associated with A_H/A_D values close to unity (*21*). This suggests that the isotope effect on the preexponential factors alone without the other thermodynamic parameters associated with the hydrogen atom transfer reaction is not sufficient for correct interpretation of the data. Transfer reactions that occur via over-the-barrier transition state mechanism have also been categorized using the temperature dependence approach and also associated with temperature dependent kinetic isotope effects where $\Delta H^{\ddagger}$ values for protium and deuterium transfers are different from one another, A_H/A_D values that are close to unity (i.e., between 0.7 and 1.7), and large ΔE_a values in the order of ~5 kJ mol^{-1} (*22*).

The effect of hydrostatic pressure on the rate of hydrogen atom transfer, apart from temperature, has also been used to study tunneling reactions (*23-26*). Pressure effects are associated with differences in vibrational frequencies of isotopic and non-isotopic atoms but stretching vibrations are insensitive to pressures of a few kilobars (*27*). Inflated kinetic isotope effects that do not conform to semi-classical transition state theory have been shown to be dependent on pressure in the range from 1 to 2,000 bar and consistent with the presence of a tunneling mechanism (*25*). Since substrate kinetic isotope effects for non-tunneling reactions arise from a single transition state, these reactions are independent of pressure (*24*), thus

providing the basis for differentiating between quantum tunneling and over-the-barrier transition state mechanisms.

Choline oxidase from *Arthrobacter globiformis* catalyzes the oxidation of choline to glycine betaine in a two-step, FAD-dependent reaction with betaine aldehyde as intermediate and molecular oxygen as the primary electron acceptor. The reaction of alcohol oxidation in choline oxidase involves the transfer of a hydride ion from the α-carbon of the deprotonated substrate to the N(5) position of the flavin isoalloxazine ring. Accumulated mechanistic data for the wild-type enzyme are consistent with the hydride transfer reaction occurring via quantum mechanical tunneling in a highly preorganized active site environment (see (*9*) for recent review). A thermodynamically relevant internal equilibrium which is associated with proton abstraction from choline has been shown to be important for the enzyme-substrate pre-organization that is required for the hydride transfer reaction (*28*). For structural insights into the mechanistic properties of choline oxidase, the X-ray crystal structure of the choline oxidizing enzyme was solved to 1.86 Å (*29*). The isoalloxazine ring of the flavin cofactor is physically constrained through a covalent linkage via the C(8)M atom of the flavin and the N(3) atom of the histidine residue at position 99, and adjacent to the re face of the FAD ring is a solvent exclusion cavity of with a volume of ~125 Å^3 to accommodate a choline molecule of ~93 Å^3. Substitution of the histidine residue with asparagine resulted in a variant form of choline oxidase with a non-covalently bound flavin cofactor (*30*). Mechanistic data for the asparagine 99 enzyme are consistent with the FAD-histidyl covalent linkage being important for the optimal positioning of the hydride ion donor and acceptor in the reaction catalyzed by choline oxidase. A glutamate residue at position 312, which is the only negatively charged residue in the active site of choline oxidase and shown to be involved in substrate binding (*29*). Replacement of the negatively

charged residue with aspartate revealed a kinetically relevant internal equilibrium in the reaction catalyzed by the variant enzyme. The effect of temperature on the kinetic isotope effect of the rate of flavin reduction in the aspartate 312 variant enzyme is consistent with a hydride transfer reaction that is significantly different from that of the wild-type enzyme (see Chapter IV).

In this study, the effect of hydrostatic pressure on the rate of flavin reduction in the asparagine 99 and aspartate 312 variant enzymes has been investigated using a high pressure stopped-flow spectrophotometer to probe the mechanism of hydride ion transfer in the two enzymes. The data herein presented are consistent with a tunneling mechanism with extensive distance and geometry sampling of the reactive configurations for the hydride transfer reaction in CHO-H99N, and an over-the-barrier transition state mechanism for the hydride transfer reaction in CHO-E312D. Redox potential data suggest that even though the covalent linkage in choline oxidase is important for the driving force in the enzyme, the hydride transfer reaction is not significantly affected by a change in driving force.

6.3. Experimental Procedures

Materials. Plasmids harboring the recombinant choline oxidase genes pET/codAmg for the wild-type enzyme, pET/codA H99N for CHO-H99N, and pET/codA E312D for CHO-E312D were used to express the various enzymes in *E. coli* strain Rosetta (DE3)pLysS (*29-32*). Choline chloride was from ICN (Aurora, OH). Glycine betaine, glucose, glucose oxidase and 1,2-[^{2}H$_4$]-choline bromide, methyl viologen, benzyl viologen, hydroxyl naphthoquinone, phenazine

methyosulfate, ferrocene dicarboxylic acid and sodium dithionite were from Sigma-Aldrich (St. Louis, MO). All other reagents were of the highest purity commercially available.

Kinetic Assays. The wild-type enzyme and the variant forms of choline oxidase in which the histidine at position 99 or glutamate at position 312 were replaced with asparagines and aspartate, respectively, were expressed with 60 μM isopropylthiogalactopyranoside (IPTG) and purified to homogeneity as previously described (*29-32*). Pre-steady state kinetic measurements were performed with a Hi-Tech Scientific HPSF-56 High Pressure Stopped-flow spectrophotometer (TgK Scientific, Bradford on Avon, UK). The experiments were carried out at 25 $^{\circ}$C in 100 mM Tris-Cl, pH 8, at hydrostatic pressures in the range from 1 to 1,500 bar under anaerobic condition. The choice of Tris buffer was to minimize changes in pH due to pressure changes since Tris has a small volume of ionization (*33*). The experimental set-up was made anaerobic with the addition of ~10 units/mL glucose oxidase and 50 mM glucose to the enzyme and substrate in a final volume of 4 mL each as previously described (*34*). The samples were immediately loaded into the stopped-flow syringes and mounted into the stopped-flow spectrophotometer. The set-up was incubated for a minimum of 30 min, long enough to scrub the system of oxygen such that no re-oxidation of the enzyme was observed upon mixing the enzyme and substrate. Reduction of the flavin was monitored at 450 nm. The wild-type enzyme was used to determine the thermodynamic binding constant (K_d) for interaction of the substrate with the enzyme in Tris-Cl, pH 8. Previous mechanistic data indicate that there is no significant difference in the binding constant for the wild-type, asparagines 99 variant and aspartate 312 variant enzymes (*29, 30*). The wild-type enzyme was therefore used to determine the effect of pressure on the K_d values. Equal volumes of the enzymes and substrates (choline or 1,2-[^{2}H$_4$]-

choline) were anaerobically mixed in the high pressure stopped-flow spectrophotometer at varying hydrostatic pressure to a final enzyme concentration of ~20 µM and a final substrate concentration of ~50 mM thereby ensuring saturation of the enzyme with the substrate. The rate constants for flavin reduction for the isotopic substrates were measured to determine the effect of pressure on the kinetic isotope effect of flavin reduction. The observed rate at each substrate concentration was measured in triplicate.

Potentiometric Titrations. The reduction-oxidation titrations for the wild-type, asparagine 99 and aspartate 312 enzymes were carried out under anaerobic conditions in a glove box at 15 ^{o}C and in Tris-Cl, pH 8. The enzymes were liganded with the addition of 1.5 M glycine betaine in a final concentration of ~40 µM and a final volume of 5 mL. The enzyme solutions were prepared by gel-filteration to change the buffer to 100 mM Tris-Cl, pH 8, which was previously made anaerobic by flushing with nitrogen gas for at least 1 hr. Equilibration during the reductive titrations was ensured by adding 0.3 µM methyl viologen, 1.0 µM benzyl viologen, 7.0 µM hydroxyl naphthoquinone, 2.0 µM phenazine methosulfate, and 2.8 µM ferrocene dicarboxylic acid as redox mediators. Hydroxy naphthoquinone, phenazine methyosulfate, and ferrocene dicarboxylic acid were freshly prepared due to their relatively short life span. Sodium dithionite, also prepared fresh, was used as a reductant in the electrochemical titrations. UV-visible absorbance spectra of the enzymes were recorded with a computer interfaced spectrophotometer connected to the solutions, after equilibration of the potential upon each addition of the sodium dithionite to obtain a change in potential of about +4 to +6 mV.

Data Analysis. Data were fit with KaleidaGraph software (Synergy Software, Reading, PA). Stopped-flow traces were fit to eq 1 which describes a single exponential process where k_{obs} is the observed rate of flavin reduction at any given concentration of substrate, t is time, A_t is the absorbance at 450 nm at any given time, A is the amplitude for the total change in absorbance, and A_∞ is the absorbance at infinite time. The pre-steady state kinetic data were fit to eq 2 to determine the kinetic parameters, where S is the concentration of substrate, k_{red} is the limiting first-order rate constant for flavin reduction at saturating substrate concentrations and K_d is the dissociation constant for binding of the substrate to the enzyme. The dependence of pressure on the rate of flavin reduction at saturating substrate concentrations was determined by fitting the stopped-flow data to eq 3, where k_{red} is the rate of flavin reduction, k_o is the rate constant extrapolated to 0 bar, p is pressure $\Delta V_p^\ddagger$ is the apparent difference between the volume of the reactant state and the transition state, R_p is the gas constant when the pressure is measured in bars, and T is temperature.

The reduction potentials of the enzymes were determined by fitting the data to the Nernst equation (eq 4), where E_h is the measured electrode potential after equilibration at each point in the titration, E'_m is the mid-point redox potential, R is gas constant, T is temperature, n is the number of electron transferred, and F is Faraday's constant.

$$A_t = A e^{-k_{obs}t} + A_\infty \tag{1}$$

$$k_{obs} = \frac{k_{red}S}{K_d + S} \tag{2}$$

$$\ln k_{red} = \ln k_0 - \Delta V^\ddagger p / R_p T \tag{3}$$

$$E_h = E'_m + \frac{2.303\ RT}{nF}\ \log\ \frac{[\text{FAD}_{\text{Ox or Sq}}]}{[\text{FAD}_{\text{Sq or Red}}]} \tag{4}$$

6.4. Results

Effect of Pressure on Flavin Reduction. The effect of pressure on the rate of flavin reduction for the mutant enzymes choline oxidase in which histidine 99 and glutamate 312 have been replaced with asparagine and aspartate, respectively, were investigated to probe the mode of hydride ion transfer in the variant enzymes. The rate constants for flavin reduction (k_{red}) with choline or 1,2-[^{2}H$_4$]-choline as substrate for CHO-H99N and CHO-E312D at varying hydrostatic pressures in the range from 1 to 1500 bar were determined under anaerobic conditions at saturating substrate concentration. As illustrated as an example for the experiment with the wild-type enzyme at 50 mM choline and 1.25 kbar, the absorbance at 450 nm decreased in a single exponential fashion as the oxidized flavin species is reduced to anionic hydroquinone upon mixing the enzymes with substrate and fitting the data to eq 1 (Figure 6.1). Averaged observed rates of flavin reduction increase with increasing choline concentration to limiting values for wild-type choline oxidase and the data fit to eq 2 to determine k_{red} and K_d at the different hydrostatic pressures (Figure 6.2). The rate constant for flavin reduction for wild-type choline oxidase increases with increasing pressure whereas the binding constant is independent of pressure with a limiting value of 3.0 ± 0.2 mM. Based on the pressure independence of the K_d values for the wild-type enzyme, saturating concentration of choline or 1,2-[^{2}H$_4$]-choline was used to determine the dependence of the rate of flavin reduction in the asparagine 99 and aspartate 312 variant enzymes. The rate of flavin reduction increases monotonically with increasing pressure in CHO-H99N to different slopes with choline and 1,2-[^{2}H$_4$]-choline yielding large kinetic isotope effect that is also dependent on pressure (Figure 6.3), consistent with a tunneling mechanism for the hydride ion transfer reaction. The rate constant for flavin reduction

for CHO-E312D however increases monotonically with increasing pressure to similar slopes

with choline and 1,2-[^{2}H$_4$]-choline, resulting in pressure-independent kinetic isotope effect

(Figure 6.4). The data for the effect of pressure on the hydride ion transfer reaction in the

aspartate variant enzyme suggest lack of a tunneling mechanism and therefore consistent with an

over-the-barrier transition state mechanism. The k_{red} values ranged from 0.69 to 2.85 s^{-1} and 0.073

to 0.298 s^{-1} with choline and 1,2-[^{2}H$_4$]-choline as substrates, respectively, in CHO-H99N, and

0.108 ± to 0.297 s^{-1} and 0.0113 to 0.0316 s^{-1} with the same substrates in CHO-E312D throughout

the pressure range considered. A summary of the pre-steady state kinetic parameters for CHO-

H99N and CHO-E312D are shown in Tables A6.1 and A6.2, respectively. A change in activation

volume ($\Delta V^{\ddagger}$) of -21.6 ± 0.7 and -17.5 ± 0.9 cm^3 mol^{-1} were determined for CHO-H99N with

choline and 1,2-[^{2}H$_4$]-choline as substrates, respectively, resulting in a $\Delta\Delta V^{\ddagger}$ value of -4.1 ± 1.1,

where $\Delta\Delta V^{\ddagger} = \Delta V_H^{\ddagger} - \Delta V_D^{\ddagger}$. In CHO-E312D, similar $\Delta V^{\ddagger}$ values of ~-16 cm^3 mol^{-1} were obtained

for the isotopic substrates and yielding a $\Delta\Delta V^{\ddagger}$ value that is not significantly different from zero.
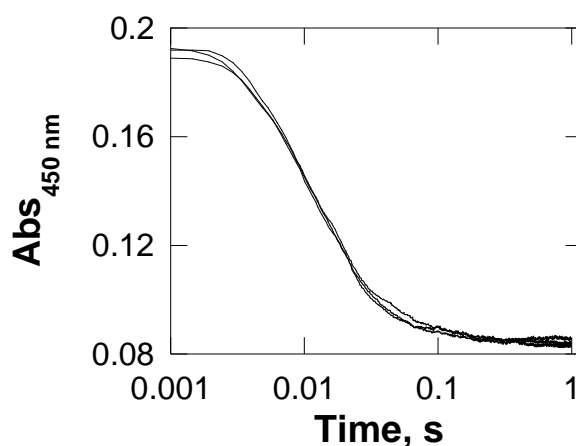

Figure 6.1. Stopped-flow traces for wild-type choline oxidase with 50 mM choline at 1.25 kbar. Flavin reduction was conducted under anaerobic condition at 4 oC in Tris-Cl, pH 8 and data fit to eq. 1.
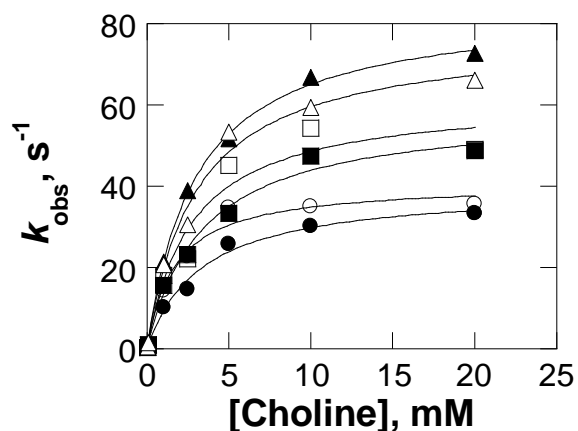
Figure 6.2. Dependence of choline concentration on rate of flavin reduction for wild-type choline oxidase at varying hydrostatic pressure.
(■) 0.01 kbar, (□) 0.25 kbar, (○) 0.50 kbar (●) 0.75 kbar (▲) 1.00 kbar (△) 1.25 kbar. Enzymatic activities were measured at 4 oC in Tris-Cl, pH 8 and data fit to eq. 2.
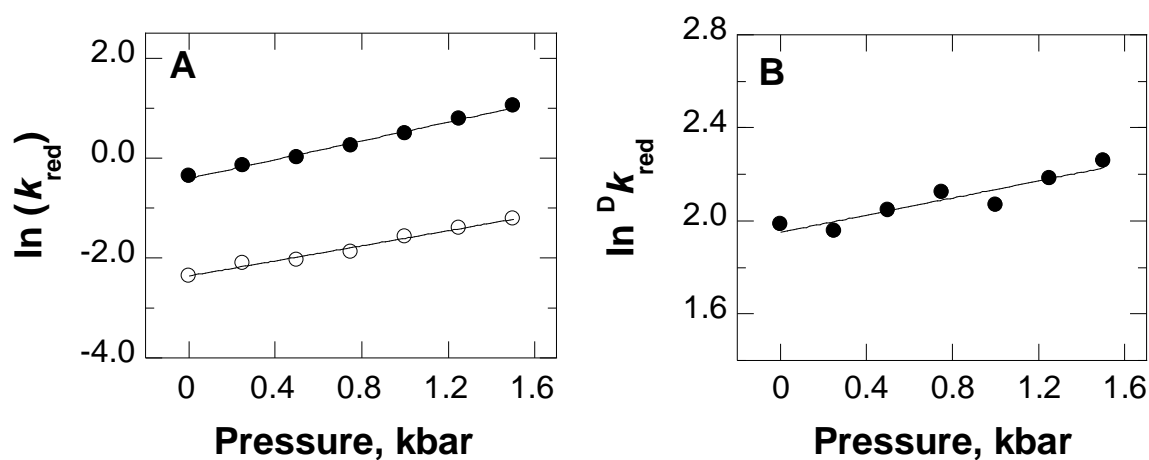
Figure 6.3. Pressure dependence of k_{red} and $^Dk_{red}$ for CHO-H99N.
(A) Plot of k_{red} values versus pressure with choline (●) and 1,2-[$^2H_4$]-choline (○) as substrates. Data were fit to eq y. (B) Plot of $^Dk_{red}$ versus pressure. Data were fit to a line.

Figure 6.4. Pressure dependence of k_{red} and $^Dk_{red}$ for CHO-E312D.
(A) Plot of k_{red} values versus pressure with choline (●) and 1,2-$[^2H_4]$-choline (○) as substrates. Data were fit to eq y. (B) Plot of $^Dk_{red}$ versus pressure. Data were fit to y = 2.23.
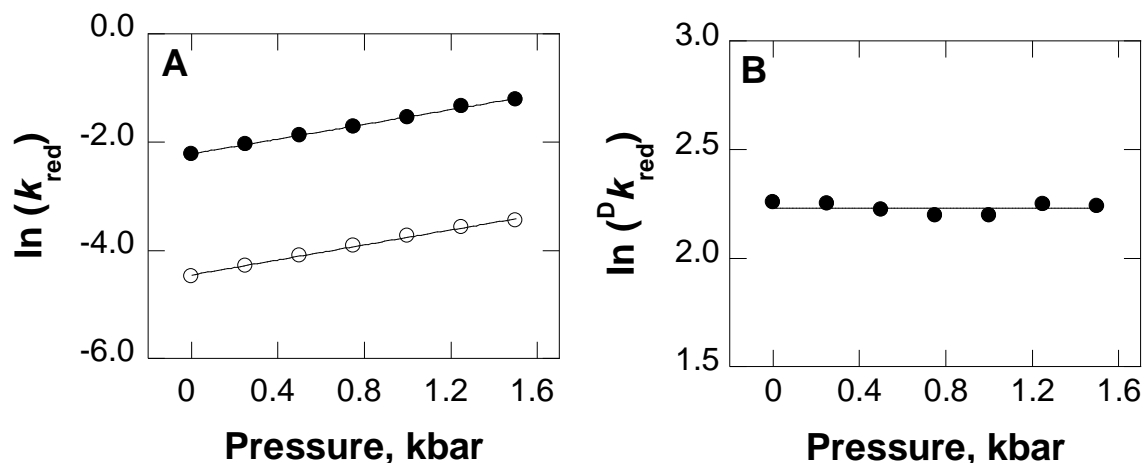
Redox Pontentiometry. The redox potentials of the wild-type and two variant enzymes in complex with glycine betaine were determined at pH 8 and 15 ^{o}C by the reductive titration of the enzymes with sodium dithionite as reductant. The oxidized flavin bound to the wild-type and aspartate 312 enzymes were reduced to anionic hydroquinone with the stabilization of the semiquinone species. However, no significant formation of the flavin semiquinone species was observed in the asparagine variant enzyme suggesting that the covalent linkage is important for the stabilization of the flavin semiquinone. A fit of the redox potentials data to the Nernst equation (eq 4) showed similar values for the wild-type and CHO-E312D variant enzymes suggesting similar driving forces in the two enzymes with lower values observed in CHO-H99N (Figure 6.5 and Table 6.1).
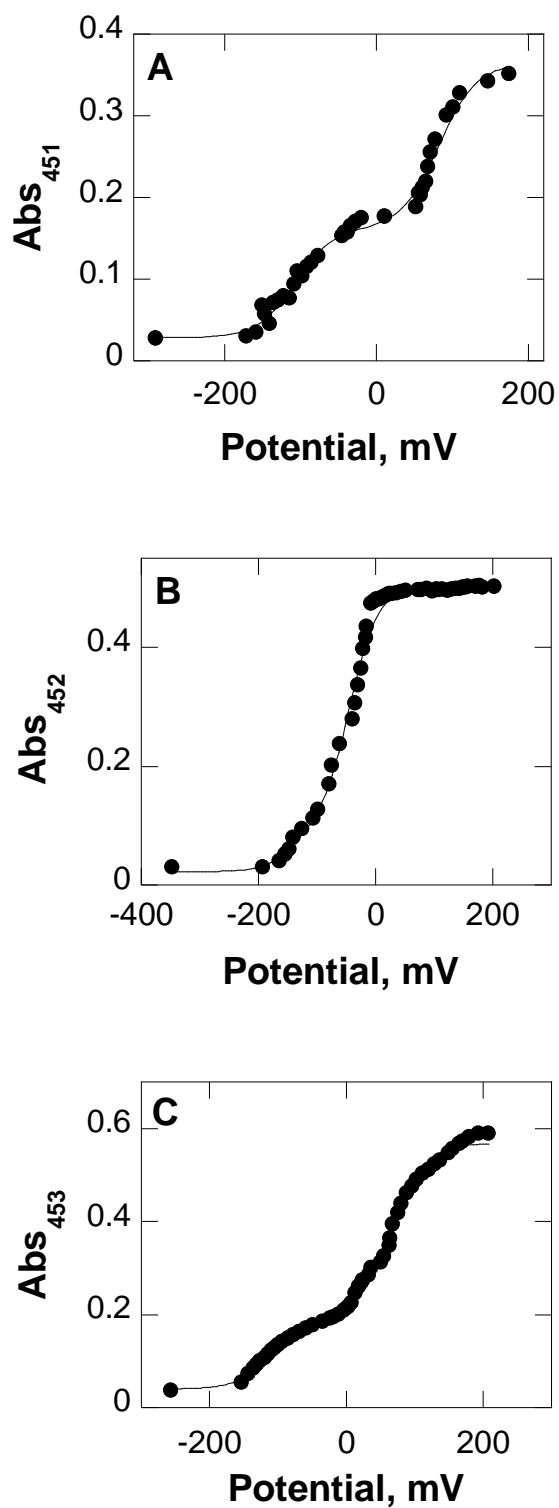
Figure 6.5. Anaerobic redox titrations of wild-type choline oxidase.

(A) CHO-H99N (B) and CHO-E312D (C). Reductive titrations of the enzymes were carried out in a glove box in Tris-Cl, pH 8 and 15 °C using sodium dithionite as reductant. Data were fit to eq 4.

Table 6.1. Anaerobic redox potential values for wild-type choline oxidase, CHO-H99N and CHO-E312D.

Enzyme	E_1 (mV)	E_2 (mV)	E_m (mV)[a]
CHO-WT	+ 82 ± 3	-107 ± 5	-13 ± 6
CHO-H99N	- 44 ± 3	- 144 ± 24	-94 ± 24
CHO-E312D	+ 68 ± 2	- 109 ± 5	-41 ± 5

Reductive titration of the enzymes were carried out in Tris-Cl, pH 8 and 15 °C. Data were fit to eq 4. [a]Data were calculated as the average of E_1 and E_2.

6.5. Discussion

The mechanism of hydride ion transfer in the oxidation of choline by choline oxidase is a documented example of a quantum mechanical tunneling reaction that occurs in highly pre-organized active site environment (*9*). Previous mechanistic data for variant forms of choline oxidase in which the active site residues His99 and Glu312 were replaced with asparagine and aspartate, respectively, are consistent with the residues being involved in the reductive half-reaction but not playing any significant roles in the oxidative half-reaction (*29, 30*). Studies on the effect of temperature on the rate of flavin reduction in the variant enzymes resulted in dependences of the kinetic isotope effects, large and finite enthalpies of activation that are significantly different from each other for C-H and C-D bond cleavages, isotope effects on the Eyring's pre-exponential factors that are close to unity, and large and finite changes in activation energies, suggesting mechanisms of hydride ion transfer that are consistent with either an environmentally assisted tunneling or over-the-barrier transition state [(*30*) and Chapter IV]. Whether environmentally assisted tunneling or over-the-barrier transition state, these

mechanisms are significantly different from that of the wild-type enzyme. In this study, the effects of hydrostatic pressure on the rate of flavin reduction have been exploited to determine the true identities of the mechanisms of hydride ion transfers in the variant enzymes.

The hydride ion transfer reaction in the His99Asn variant enzyme is via an environmentally assisted tunneling mechanism. Evidence supporting this conclusion comes from pressure dependence of the primary kinetic isotope effects on the rate of flavin reduction. The increases in the k_{red} values with increasing pressure are likely due to compression of the hydride ion transfer distance between the donor and acceptor. However, the pressure dependence of the kinetic isotope effect suggests differences in the modes of hydride and deuteride transfers other than the transfer distance (34). Substrate isotope effects, more often than not, arise from a single transition state and are usually pressure-independent (35). Since the zero point energies for the protiated and deuterated substrates cannot be changed by changes in pressure, the differences in the modes of transfer for the hydride and deuteride is likely due to dynamic motions affecting the reaction coordinates (35).

The hydride ion transfer reaction in the Glu312Asp variant enzyme is probably via over-the-barrier transition state mechanism. This conclusion is supported by the effect of pressure on the kinetic isotope effect of flavin reduction. The increases in the k_{red} values with increasing pressure to similar effects suggest similar modes of transfer for the hydride and deuteride atoms in CHO-E312D. The independence of the substrate kinetic isotope effect on pressure arise from a single transition state for non-tunneling reactions since the formation of the transition state is dependent on the energy of the reaction (24). The lack of effect of hydrostatic pressure may be due to the kinetic isotope effect arising exclusively from the zero point energies of the isotopic substrates. The change in the mechanism of hydride transfer from tunneling with minimal

sampling to over-the-barrier transition state is probably due to a larger distance between the substrate hydride donor and the flavin hydride acceptor upon replacing the glutamate residue with aspartate and therefore shortening the side chain at the 312 position.

The flavin covalent linkage is important for the driving force in choline oxidase. Evidence for this conclusion comes from the redox potential data for CHO-H99N compared to the wild-type enzyme and CHO-E312D. The similar redox potentials for wild-type choline oxidase and CHO-E312D (Table 6.1), in which the covalent linkage is present, are consistent with similar driving forces in the two enzymes. A decrease in the midpoint potential of ~120 mV in CHO-H99N for the reduction of the oxidized bound flavin to the flavin semiquinone, suggests a decrease in the driving force for the variant enzyme with the non-covalently linked flavin cofactor. Similar decreases in the midpoint potential have been shown in other enzymes with covalently bound flavins where the covalent linkages have been removed by site-directed mutagenesis (*36-40*). The decrease in midpoint potential does not, however, seem to have an effect on the rate of flavin reduction as suggested by the higher k_{red} values obtained for CHO-H99N (Table A6.1) compared to CHO-E312D (Table A6.2), and consistent with the hydride transfer reaction not significantly affected by the driving force in choline oxidase. If the hydride transfer was affected by the driving force, the k_{red} values for CHO-H99N were expected to be lower than the rate constants for flavin reduction in CHO-E312D.

In summary, the results presented in this study on the mechanistic investigation of the effect of hydrostatic pressure on the rate of flavin reduction with choline and 1,2-[^{2}H$_4$]-choline for the variant forms of choline oxidase are consistent with environmentally assisted tunneling mechanism for the hydride transfer reaction in CHO-H99N and over-the-barrier transition state mechanism for the reaction in CHO-E312D. The histidine residue at position 99 and the

glutamate resiude at position 312 are both important for the oxidation of choline by choline oxidase since replacement of the residues using site-directed mutagenesis resulted in significant changes in the mechanism for the reaction of hydride transfer. Previous mechanistic data on the effect of temperature on the rate of flavin reduction suggest that the residues are important for preorganization of the enzyme-substrate complex that preceed that hydride transfer reaction. The change in the mechanism of hydride transfer in CHO-E312D from tunneling with minimal sampling to over-the-barrier transition state is primarily due to a larger distance between the hydride donor and acceptor upon replacing glutamate with aspartate. Midpoint potential data suggest that even though the covalent linkage of the flavin cofactor to histidine 99 is important for the driving force in choline oxidase, the hydride transfer reaction is not significantly affected by a change in the driving force.

6.6. References

1. Agrawal, N., Hong, B., Mihai, C., and Kohen, A. (2004) Vibrationally enhanced hydrogen tunneling in the Escherichia coli thymidylate synthase catalyzed reaction, *Biochemistry 43*, 1998-2006.

2. Bahnson, B. J., Park, D. H., Kim, K., Plapp, B. V., and Klinman, J. P. (1993) Unmasking of hydrogen tunneling in the horse liver alcohol dehydrogenase reaction by site-directed mutagenesis, *Biochemistry 32*, 5503-5507.

3. Banacky, P. (1981) Dynamics of proton transfer and enzymatic activity, *Biophys. Chem. 13*, 39-47.

4. Basran, J., Harris, R. J., Sutcliffe, M. J., and Scrutton, N. S. (2003) H-tunneling in the multiple H-transfers of the catalytic cycle of morphinone reductase and in the reductive half-reaction of the homologous pentaerythritol tetranitrate reductase, *J. Biol. Chem. 278*, 43973-43982.

5. Basran, J., Sutcliffe, M. J., and Scrutton, N. S. (1999) Enzymatic H-transfer requires vibration-driven extreme tunneling, *Biochemistry 38*, 3218-3222.

6. Bruno, W. J., and Bialek, W. (1992) Vibrationally enhanced tunneling as a mechanism for enzymatic hydrogen transfer, *Biophys. J. 63*, 689-699.

7. Cha, Y., Murray, C. J., and Klinman, J. P. (1989) Hydrogen tunneling in enzyme reactions, *Science 243*, 1325-1330.

8. Fagan, R. L., Nelson, M. N., Pagano, P. M., and Palfey, B. A. (2006) Mechanism of flavin reduction in class 2 dihydroorotate dehydrogenases, *Biochemistry 45*, 14926-14932.

9. Gadda, G. (2008) Hydride Transfer Made Easy in the Reaction of Alcohol Oxidation Catalyzed by Flavin-dependent Oxidases, *Biochemistry 47*, 13745-13753.

10. Garcia-Viloca, M., Alhambra, C., Truhlar, D. G., and Gao, J. (2003) Hydride transfer catalyzed by xylose isomerase: mechanism and quantum effects, *J. Comput. Chem. 24*, 177-190.

11. Jonsson, T., Edmondson, D. E., and Klinman, J. P. (1994) Hydrogen tunneling in the flavoenzyme monoamine oxidase B, *Biochemistry 33*, 14871-14878.

12. Karsten, W. E., Hwang, C. C., and Cook, P. F. (1999) Alpha-secondary tritium kinetic isotope effects indicate hydrogen tunneling and coupled motion occur in the oxidation of L-malate by NAD-malic enzyme, *Biochemistry 38*, 4398-4402.

13. Maglia, G., and Allemann, R. K. (2003) Evidence for environmentally coupled hydrogen tunneling during dihydrofolate reductase catalysis, *J. Am. Chem. Soc. 125*, 13372-13373.

14. Sutcliffe, M. J., Masgrau, L., Roujeinikova, A., Johannissen, L. O., Hothi, P., Basran, J., Ranaghan, K. E., Mulholland, A. J., Leys, D., and Scrutton, N. S. (2006) Hydrogen tunnelling in enzyme-catalysed H-transfer reactions: flavoprotein and quinoprotein systems, *Philos. Trans. R. Soc. Lond. B. Biol. Sci. 361*, 1375-1386.

15. Valley, M. P., and Fitzpatrick, P. F. (2004) Comparison of enzymatic and non-enzymatic nitroethane anion formation: thermodynamics and contribution of tunneling, *J. Am. Chem. Soc. 126*, 6244-6245.

16. Hay, S., and Scrutton, N. S. (2008) Incorporation of hydrostatic pressure into models of hydrogen tunneling highlights a role for pressure-modulated promoting vibrations, *Biochemistry 47*, 9880-9887.

17. Nagel, Z. D., and Klinman, J. P. (2006) Tunneling and dynamics in enzymatic hydride transfer, *Chem. Rev. 106*, 3095-3118.

18. Meyer, M. P., Tomchick, D. R., and Klinman, J. P. (2008) Enzyme structure and dynamics affect hydrogen tunneling: the impact of a remote side chain (I553) in soybean lipoxygenase-1, *Proc. Natl. Acad. Sci. U S A 105*, 1146-1151.

19. Wang, L., Goodey, N. M., Benkovic, S. J., and Kohen, A. (2006) Coordinated effects of distal mutations on environmentally coupled tunneling in dihydrofolate reductase, *Proc. Natl. Acad. Sci. U S A 103*, 15753-15758.

20. Wang, L., Tharp, S., Selzer, T., Benkovic, S. J., and Kohen, A. (2006) Effects of a distal mutation on active site chemistry, *Biochemistry 45*, 1383-1392.

21. Sharma, S. C., and Klinman, J. P. (2008) Experimental Evidence for Hydrogen Tunneling when the Isotopic Arrhenius Prefactor (A(H)/A(D)) is Unity, *J. Am. Chem. Soc. 130*, 17632-17633.

22. Melander, L., and Saunders, W. H. (1987) *Reaction Rates of Isotopic Molecules*, Fourth ed., Krieger, Malabar, FL.

23. Northrop, D. B., and Cho, Y. K. (2000) Effect of pressure on deuterium isotope effects of yeast alcohol dehydrogenase: evidence for mechanical models of catalysis, *Biochemistry 39*, 2406-2412.

24. Northrop, D. B. (2002) Effects of high pressure on enzymatic activity, *Biochim. Biophys. Acta 1595*, 71-79.

25. Northrop, D. B. (2006) Unusual origins of isotope effects in enzyme-catalysed reactions, *Philos. Trans. R. Soc. Lond. B. Biol. Sci. 361*, 1341-1349.

26. Quirk, D. J., and Northrop, D. B. (2001) Effect of pressure on deuterium isotope effects of formate dehydrogenase, *Biochemistry 40*, 847-851.

27. Isaacs, N. S., Javaid, K., and Rannala, E. (1978) *J. Chem. Soc. Perkin. Trans. 2*, 709-711.

28. Fan, F., and Gadda, G. (2007) An internal equilibrium preorganizes the enzyme-substrate complex for hydride tunneling in choline oxidase, *Biochemistry 46*, 6402-6408.

29. Quaye, O., Lountos, G. T., Fan, F., Orville, A. M., and Gadda, G. (2008) Role of Glu312 in binding and positioning of the substrate for the hydride transfer reaction in choline oxidase, *Biochemistry 47*, 243-256.

30. Quaye, O., Cowins, S., and Gadda, G. (2009) Contribution of flavin covalent linkage with histidine 99 to the reaction catalyzed by choline oxidase, *J. Biol. Chem. 284*, 16990-16997.

31. Fan, F., Ghanem, M., and Gadda, G. (2004) Cloning, sequence analysis, and purification of choline oxidase from Arthrobacter globiformis: a bacterial enzyme involved in osmotic stress tolerance, *Arch. Biochem. Biophys. 421*, 149-158.

32. Gadda, G., Powell, N. L., and Menon, P. (2004) The trimethylammonium headgroup of choline is a major determinant for substrate binding and specificity in choline oxidase, *Arch. Biochem. Biophys. 430*, 264-273.

33. Kitamura, Y., and Itoh, T. (1987) *J. Solution Chem. 16*, 715-725.

34. Hay, S., Sutcliffe, M. J., and Scrutton, N. S. (2007) Promoting motions in enzyme catalysis probed by pressure studies of kinetic isotope effects, *Proc. Natl. Acad. Sci. U S A 104*, 507-512.

35. Isaacs, N. S. (1984) The effect of pressure on kinetic isotope effects, in *Isotope Effects in Organic Chemistry* (Buncel, E., and Lee, C. C., Eds.), pp 67-105, Elservier, Amsterdam.

36. Fraaije, M. W., van den Heuvel, R. H., van Berkel, W. J., and Mattevi, A. (1999) Covalent flavinylation is essential for efficient redox catalysis in vanillyl-alcohol oxidase, *J. Biol. Chem. 274*, 35514-35520.

37. Motteran, L., Pilone, M. S., Molla, G., Ghisla, S., and Pollegioni, L. (2001) Cholesterol oxidase from Brevibacterium sterolicum. The relationship between covalent flavinylation and redox properties, *J. Biol. Chem. 276*, 18024-18030.

38. Winkler, A., Kutchan, T. M., and Macheroux, P. (2007) 6-S-cysteinylation of bi-covalently attached FAD in berberine bridge enzyme tunes the redox potential for optimal activity, *J. Biol. Chem. 282*, 24437-24443.

39.   Winkler, A., Motz, K., Riedl, S., Puhl, M., Macheroux, P., and Gruber, K. (2009) Structural and mechanistic studies reveal the functional role of bicovalent flavinylation in berberine bridge enzyme, *J. Biol. Chem.*

40.   Efimov, I., Cronin, C. N., and McIntire, W. S. (2001) Effects of noncovalent and covalent FAD binding on the redox and catalytic properties of p-cresol methylhydroxylase, *Biochemistry 40*, 2155-2166.

6.7. Appendix

Table A6.1. Pressure Dependence of average k_{red} values for CHO-H99N with choline and 1,2-[^{2}H$_4$]-choline as Substrates at pH 8 and 4 ^{o}C

Pressure (bar)	k_{red}(H)	k_{red}(D)	$^D k_{red}$
1	0.67 ± 0.06	0.095 ± 0.004	7.1 ± 0.7
250	0.86 ± 0.01	0.122 ± 0.001	7.1 ± 0.1
500	1.02 ± 0.04	0.131 ± 0.007	7.8 ± 0.5
750	1.28 ± 0.06	0.154 ± 0.004	8.3 ± 0.5
1,000	1.64 ± 0.05	0.208 ± 0.005	7.9 ± 0.3
1,250	2.19 ± 0.07	0.247 ± 0.003	8.9 ± 0.3
1,500	2.85 ± 0.02	0.298 ± 0.005	9.6 ± 0.2

k_{red} values were determined at 50 mM substrate concentrations which is ~95% saturation of the enzyme.

Table A6.2. Pressure Dependence of average k_{red} values for CHO-E312D with choline and 1,2-[^{2}H$_4$]-choline as Substrates at pH 8 and 4 ^{o}C

Pressure (bar)	k_{red}(H)	k_{red}(D)	$^D k_{red}$
1	0.108 ± 0.001	0.0113 ± 0.0002	9.6 ± 0.2
250	0.131 ± 0.001	0.0138 ± 0.0001	9.5 ± 0.1
500	0.153 ± 0.002	0.0166 ± 0.0001	9.2 ± 0.1
750	0.179 ± 0.004	0.0200 ± 0.0001	9.0 ± 0.2
1,000	0.215 ± 0.006	0.0239 ± 0.0004	9.0 ± 0.3
1,250	0.264 ± 0.003	0.0278 ± 0.0001	9.5 ± 0.1
1,500	0.297 ± 0.004	0.0316 ± 0.0001	9.4 ± 0.1

k_{red} values were determined at 50 mM substrate concentrations which is ~95% saturation of the enzyme.

CHAPTER 7

General Discussion

Enzymes have long been known as biological catalysts that speed up the rate of reactions. However, the mechanisms by which most enzymes (usually enzymes of the same group) catalyze their reactions are yet to be fully understood. This dissertation used choline oxidase as a model enzyme to contribute to the understanding of the quantum mechanical tunneling mechanism for the transfer of hydride ions.

Choline oxidase catalyzes the two-step, four electron oxidation of choline to glycine betaine with betaine aldehyde as the intermediate with molecular oxygen as the final electron acceptor. The betaine aldehyde intermediate is predominantly bound to the enzyme during catalysis and almost entirely forms a gem-diol when in solution. The first oxidation step in the reaction catalyzed by choline oxidase involves the transfer of a hydride ion from the α-carbon of choline to the N(5) position of the enzyme-bound flavin to form betaine aldehyde and anionic flavin hydroquinone, followed by reactivity of the flavin hydroquinone with oxygen and a concomitant release of hydrogen peroxide (*1-3*). The second oxidation step involves a hydride ion transfer from the gem-diol aldehyde intermediate to form glycine betaine and the reduced flavin which is also subsequently oxidized by molecular oxygen. Previous mechanistic data have shown that the hydride ion transfer step, which is rate limiting in both the reductive half-reaction and the overall turnover of the enzyme, occurs via a quantum mechanical tunneling mechanism in a highly preorganized enzyme-substrate complex and follows a fast hydroxyl proton abstraction. This conclusion was obtained from substrate, solvent and multiple kinetic isotope effects, and the effect of temperature on the isotope effects and its associating thermodynamic parameters. In order to understand at the molecular level the mechanism of hydride ion transfer

in the reaction catalyzed by choline oxidase, this dissertation has complemented the previous data on the wild-type enzyme with structural studies and compared the wild-type enzyme with mutant forms of choline oxidase in which a glutamate residue at position 312 was replaced with alanine, glutamine or aspartate, and in which a histidine residue at position 99 was replaced with asparagine.

The crystal structure of choline oxidase resolved to 1.86 Å provided insights about the overall organization of the active site and different domains of the wild-type enzyme. The enzyme crystallized as a homodimer with approximate dimensions of 88 Å × 70 Å × 46 Å with each monomer containing 546 amino acid residues (*4*). The two monomers are in contact with each other at an interface that has two sets of six identical charge complementary residues clustered at the outer edges, where as the central portion of the dimer interface contains very few close contacts between the subunits. The protein fold of each monomer is similar to a typical PHBH (*p*-hydroxybenzoate hydroxylase) and resembles that of other members of the GMC oxidoreductase enzyme superfamily including the presence of a loop that forms a lid over the substrate binding site (*4*). Even though the loop is thought to allow access and exit of ligands (substrate and product) to and from the active site, respectively, its catalytic importance has not been investigated in any of the members of the enzyme superfamily. The isoalloxazine ring of the flavin cofactor is buried within the protein (in the solvent inaccessible region) and covalently linked to histidine 99 and not histidine 87 as previously reported (*5*). The covalent linkage suggests that the FAD is physically constrained in the active site of the enzyme and does not move freely relative to the substrate. A volume of ~125 $Å^3$ located within the substrate binding domain and adjacent the *re* face of the FAD likely to be the cavity for substrate binding. The cavity is partially surrounded by hydrophobic residues which form an aromatic cage and polar

residues including His466, His 351 and Glu312 which is the only negatively charged residue in the active site. The docking of choline to its most probable position in the active site structure of choline oxidase suggests an electrostatic interaction between the positively charged trimethylammonium headgroup of the substrate and the glutamate residue at position 312. Indeed, this is consistent with previous mechanistic data using substrate and product analogues suggesting that the positive charge on the trimethylammonium moiety of choline is important for substrate binding and specificity in the reaction catalyzed by choline oxidase (*6*). The importance of the negative charge at position 312 in substrate binding was investigated by replacing the glutamate residue with a glutamine. The value of at least ~500-fold increase in the thermodynamic equilibrium constant (K_d) determined by anaerobic stopped-flow spectrophotometry for the glutamine variant enzyme compared to the wild-type enzyme is consistent with the negative charge being involved in substrate binding since glutamine is isosteric with glutamate. An energetic contribution of ~15 kJ/mol was estimated for the electrostatic interaction at position 312 and not significantly different from the value of ~13 kJ/mol also estimated in an independent mechanistic study using 3,3-dimethylbutan-1-ol as substrate (*7*).

The quantum mechanical tunneling for the hydride ion transfer in a highly preorganized enzyme-substrate complex established for wild-type choline oxidase suggests the requirement of the hydride donor and acceptor to be in close proximity for the reaction to occur. The effect of substrate positioning relative to the FAD was investigated in a variant enzyme of choline oxidase in which the glutamate residue at position 312 was replaced with an aspartate. Since aspartate is one carbon-carbon bond length shorter than glutamate, the objective was to displace the substrate by that distance relative to the flavin and determine what effect that has on the reaction catalyzed

by choline oxidase. The substitution of Glu312 with aspartate resulted in over 200-fold decrease in the rate of flavin reduction as well as the overall turnover of the enzyme, and a 30-fold decrease in the reductive half-reaction but no significant effect on the oxidative half-reaction (*4*). This is consistent with the Glu312 participating in the reductive half-reaction but not being involved in the reactivity of the reduced flavin species with molecular oxygen. Substitution of choline with 1,2-[^{2}H$_4$]-choline in a pH dependence study with the Glu312Asp variant enzyme suggests that the replacement of glutamate with aspartate did not affect the active site base but demonstrated the presence of a kinetically relevant internal equilibrium in the reductive half-reaction which was confirmed by the effect of solvent viscosity on the steady state kinetic parameters. In agreement with this observation, a thermodynamically relevant internal equilibrium was previously shown in the wild-type enzyme under reversible catalytic regime (*8*). The internal equilibrium has been proposed to be triggered by the proton abstraction step which results in the formation of the choline alkoxide species. All together, the data on the mechanistic characterization of the Glu312Asp enzyme in comparison to wild-type choline oxidase suggest that positioning of the substrate is important for the reaction catalyzed by the wild-type enzyme, and displacement of the substrate position results in disruption of the highly preorganized active site.

The effect of temperature on the limiting rate constant for the anaerobic hydride transfer reaction for Glu312Asp mutant enzyme was investigated to determine the mode of hydride transfer and the effect of a conservative mutation of the active site residue involved in substrate binding on the hydride tunneling mechanism in choline oxidase. The k_{red} values for choline and 1,2-[^{2}H$_4$]-choline increased monotonically with increasing temperature with different slopes as analyzed according to Eyring's formalism resulting in an increasing kinetic isotope effects on the

rate constant for flavin reduction with increasing temperature, as analyzed according to Arrhenius formalism, within the range from 7 to 37 $^\circ$C. Previous mechanistic data for the temperature dependence of the reductive half-reaction with the wild-type enzyme using steady state kinetic studies approach yielded similar slopes for choline and 1,2-[^{2}H$_4$]-choline and a corresponding temperature independent kinetic isotope effect. The dependence of k_{red} on temperature and the associating thermodynamic parameters as compared to the data for the wild-type enzyme are consistent with the hydride transfer reaction in the aspartate enzyme occurring through an environmentally coupled tunneling mechanism with significant distance and geometry sampling of the reactive configurations. An alternate mechanism where the hydride ion is transferred through over-the-barrier transition state mechanism without tunneling could be considered since all the earmarks for such a mechanism are observed in the effect of temperature on the reaction catalyzed by the Glu312Asp enzyme and the associated thermodynamic parameters. In this regards, the data would suggest that substitution of the glutamate residue with aspartate at position 312 might have altered the relative positioning of the substrate hydride ion donor and the flavin hydride ion acceptor to an extent that does not favor the tunneling mechanism anymore. However, the similarity in the magnitudes of the kinetic isotope effects determined in the wild-type and aspartate enzymes does not rule out an environmentally assisted tunneling mechanism for the transfer of the hydride ion. Reorientation of the relative positioning of the hydride ion donor and hydride ion acceptor or the environmental assistance required to achieve the correct geometry and distance for the tunneling of the hydride ion in the reaction catalyzed by the Glu312Asp variant enzyme is accounted for by a two-order of magnitude decrease in the rate of hydride ion transfer. This was evidenced in the over 200-fold decrease in the rate of flavin reduction for the aspartate mutant enzyme compared to wild-type choline

oxidase with choline as substrate. The reorientation of the relative positioning of the hydride ion donor and acceptor must have been necessarily employed due to the disruption of the highly preorganized active site in the aspartate-containing enzyme. The data presented on the effect of temperature on the rate of hydride ion transfer suggest that, even though not directly involved in catalysis, the glutamate residue at position 312 in the active site of choline oxidase, which is primarily involved in substrate binding, contributes to the overall preorganization of the enzyme-choline alkoxide complex.

The structural characterization of the wild-type choline oxidase using X-ray crystallography showed that the isoalloxazine ring of the FAD cofactor is physically constrained by a covalent attachment at the C(8) methyl position with histidine 99 via an 8α-N3-hystidyl linkage (*4*). The rigid positioning of the cofactor coupled with previous mechanistic characterization of the enzyme suggest that the covalent linkage might be important for the relative positioning of the hydride ion donor and acceptor needed for the hydride ion transfer reaction to occur in a highly preorganized active site. The tunneling mechanism requires minimal independent movement of the donor and acceptor with only dynamic motions that promote the hydride transfer reaction permitted. The contribution of the physically constrained flavin cofactor to the reaction catalyzed by choline oxidase was investigated in a variant enzyme in which the histidine residue at position 312 was replaced with asparagine. The His99Asn variant enzyme was purified with fully oxidized FAD, unlike the wild-type and other mutant enzymes which were purified containing a mixture of oxidized and air-stable anionic semiquinone flavin species (*1, 6, 9-11*). The FAD cofactor was non-covalently bound to the enzyme suggesting that flavinylation is important for the stabilization of the anionic flavin semiquinone (*10*). The His99Asn variant displayed a steady state kinetic mechanism and reactivity with oxygen that are

similar to that of the wild-type, suggesting that the asparagine mutant enzyme maintains an overall integrity that is not significantly different from the wild-type enzyme. Thus, mechanistic data in the variant enzyme that are not in keeping with the wild-type enzyme can be attributed to the absence of the covalent linkage. There were 10- and 30-fold decreases in k_{cat} and k_{cat}/K_m, respectively, compared to the wild-type enzyme suggesting that the covalent linkage is important for the reductive half-reaction and the overall turnover catalyzed by choline oxidase, without a significant involvement in the oxidative half-reaction. Even though shown to modulate the polarity of the active site, the requirement of an unprotonated species in the asparagine variant is consistent with the histidine residue at position 99 not being the active site base and also not the positively charged group that is required for re-oxidation of the flavin as for the case of glucose oxidase (*12, 13*). The other histidine residues, His351 and His466, have also previously been shown in independent studies not to be the unprotonated species for catalysis and not required for flavin re-oxidation (*9, 11*). The positive charge on the trimethylammonium headgroup of choline has been shown to play a role in the reactivity of the reduced flavin with oxygen, by using a substrate analogue that is devoid of the charge (*6, 14*).

The effect of temperature on the rate of flavin reduction (k_{red}) and the associated kinetic isotope ($^D k_{red}$) were investigated under anaerobic conditions from 10 to 28 ^{o}C to probe the hydride transfer reaction catalyzed by the His99Asn variant enzyme. The k_{red} values for choline and 1,2-[$^2H_4$]-choline increased monotonically with increasing temperature with different slopes as analyzed according to Eyring's formalism (*10*). This gives rise to an isotope effect on the Eyring's preexponential factors close to unity, different enthalpies of activation for the C-H and C-D bond cleavages, and similar entropies of activation, suggesting that the hydride ion transfer reaction is enthalpically driven. The $^D k_{red}$ values increase with decreasing temperature, resulting

in a large isotope effect on the energies of activation for the protium and deuterium transfers. In the wild-type enzyme in which the flavin is covalently attached to the protein, the reaction of hydride ion transfer occurs via quantum mechanical tunneling with minimal vibrations only affecting the reaction coordinate. The mechanism is associated with temperature independence kinetic isotope effects, similar enthalpies of activation for the C-H and C-D bond cleavages, negligible isotope effect on the energies of activation and large kinetic isotope effect on the Eyring preexponential factors (*10*). The differences in the thermodynamic parameters for the asparagine variant enzyme compared to the wild-type suggest a different mechanism for the hydride transfer reaction in CHO-H99N attributable to the absence of the covalent linkage. All together, the data on the effect of temperature on the rate of flavin reduction is consistent with the hydride ion transfer reaction occurring by environmentally assisted tunneling (*10*). As previously mentioned for the Glu312Asp variant enzyme, the change in mechanism is likely due to disruption of the active site preorganization and/or geometry upon removal of the covalent linkage (*4*). The FAD-histidyl linkage is therefore important for the preorganization of the enzyme-substrate complex that is required for the quantum mechanical tunneling of the hydride ion in choline oxidase. This observation adds to the various roles that flavin covalent linkages have been shown to play which include the stabilization of protein structure (*15-17*), prevention of the loss of loosely bound cofactor (*18*), modulation of redox potential of the flavin (*17-22*), and facilitation of electron transfer reactions (*23*) among others.

In the reaction catalyzed by the mutant enzyme of choline oxidase in which the active site residue at position 312 was replaced with aspartate, it was demonstrated that the rate of hydride ion transfer was decreased by over 200-fold and the mechanism perturbed due to disruption of the highly preorganized active site (*4*). Disruption of the active site preorganization is likely due

to displacement of the substrate relative to the flavin cofactor upon replacing the glutamate with aspartate suggesting that the spatial location of the negative charge at position 312 is important for correct positioning of the substrate for the hydride tunneling reaction in choline oxidase. The substrate analogue which has one carbon-carbon chain more than choline, 3-HPTA, was used as substrate for the Glu312Asp variant enzyme in order to compensate for the shortening of the side chain at position 312 upon replacing glutamate with aspartate. The rate of flavin reduction for the mutant enzyme under anaerobic conditions using stopped-flow spectrophotometer with 3-HPTA as substrate was ~20-fold higher than the rate for the same enzyme but with choline as substrate. Since the over 200-fold decrease in activity for CHO-E312D compared to the wild-type enzyme could not be rescued, the data suggest a partial rescue of the CHO-E312D activity with the substitution of choline with 3-HPTA as substrate. The inability of total activity rescue may partly be due to the CHO-E312D-activated 3-HPTA complex not being highly preorganized as for the case of the wild-type enzyme. The lack of high preorganization is probably due to a change in the overall active site geometry that is required for the hydride ion transfer reaction and therefore results in the presence of the kinetically relevant internal equilibrium that was previously shown in the Glu312Asp enzyme with choline as substrate (*4*). The reactivity of the reduced flavin with oxygen was, however, affected by 3-HPTA. This could be due to bulkiness of the substrate analogue thus preventing easy accessibility of molecular oxygen to the site for flavin re-oxidation. The solvent viscosity effect on the oxidative half-reaction is consistent with the stabilization of an enzyme-intermediate-oxygen ternary complex conformation. This explanation agrees with the analysis of the molecular surfaces of the crystal structure of wild-type choline oxidase which showed a solvent-excluded cavity with a volume of ~125 Å^3, just large enough to accommodate choline with a volume of 93 Å^3. The similarity in the thermodynamic constant for

binding of choline and 3-HPTA in CHO-E312D suggests similar binding modes for both substrates. The mechanistic data for the Glu312Asp variant enzyme with 3-HPTA as substrate compared to the data for the same enzyme with choline as substrate suggest that replacement of glutamate with aspartate created a larger distance between the hydride donor and acceptor. However, compensation of the distance between the donor and acceptor by using 3-HPTA as substrate for CHO-E312D did not fully rescue the activity of the aspartate mutant enzyme due to altered active site geometry.

In order to confirm the mechanisms of hydride ion transfer in the aspartate 312 and asparagine 99 variant enzymes of choline oxidase, the effects of hydrostatic pressure on the rate constants for flavin reduction in the mutant enzymes were investigated using high stopped-flow spectrophotometry. The rate constants for flavin reduction with both choline and $1,2\text{-}[^{2}H_4]$-choline increased with increasing pressure to similar slopes in CHO-E312D, resulting in a pressure-independent kinetic isotope effect and suggesting a transition state mechanism for the hydride transfer in the aspartate variant enzyme. The rate constants for flavin reduction for the isotopic substrates increase with increasing pressure to different slopes in CHO-H99N, yielding a pressure-dependent kinetic isotope effect and consistent with a tunneling mechanism with sampling of the reactive configurations. For definite conclusions on the mechanisms of hydride ion transfers in the variant enzymes, pressure effect on the rate constant for flavin reduction in wild-type choline oxidase will be studied and compared to the effects in CHO-E312D and CHO-H99N. Redox potentials of the wild-type and two variant enzymes suggest that the covalent linkage is important for the driving force in choline oxidase, however, the hydride transfer reaction is not significantly modulated by the driving force.

Overall, the results presented in this dissertation have provided insight into the oxidation of choline catalyzed by choline oxidase with respect to some of the key active site residues that contribute to the enzyme-substrate preorganization required for the quantum mechanical tunneling of the hydride ion. Glutamate residue at position 312, which is the only negatively charged residue in the active site of choline oxidase is involved in substrate binding through electrostatic interaction. The residue also correctly positions the substrate relative to the flavin for the hydride transfer reaction in the choline oxidixing enzyme. Histidine at position 99 is involved in a covalent linkage with the isoalloxazine ring of the flavin between the N(3) atom of the side chain and the C(8) methyl of the cofactor. The histidine residue physically constrains the flavin, rigidly positioning the cofactor relative to the substrate for the hydride transfer reaction. With the involvement of other residues in the stabilization of the enzyme-substrate complex (not subjects in this dissertation) (*9, 11*), it is apparent that preorganization in choline oxidase is a collective responsibility of a number of active site residues.

7.1. References

1. Fan, F., Ghanem, M., and Gadda, G. (2004) Cloning, sequence analysis, and purification of choline oxidase from *Arthrobacter globiformis*: a bacterial enzyme involved in osmotic stress tolerance, *Arch. Biochem. Biophys. 421*, 149-158.

2. Gadda, G. (2003) Kinetic mechanism of choline oxidase from *Arthrobacter globiformis*, *Biochim. Biophys. Acta 1646*, 112-118.

3. Ohta, M., Miura, R., Yamano, T., and Miyake, Y. (1983) Spectroscopic studies on the photoreaction of choline oxidase, a flavoprotein, with covalently bound flavin, *J. Biochem. 94*, 879-892.

4. Quaye, O., Lountos, G. T., Fan, F., Orville, A. M., and Gadda, G. (2008) Role of Glu312 in binding and positioning of the substrate for the hydride transfer reaction in choline oxidase, *Biochemistry 47*, 243-256.

5. Rand, T., Halkier, T., and Hansen, O. C. (2003) Structural characterization and mapping of the covalently linked FAD cofactor in choline oxidase from *Arthrobacter globiformis*, *Biochemistry 42*, 7188-7194.

6. Gadda, G., Powell, N. L., and Menon, P. (2004) The trimethylammonium headgroup of choline is a major determinant for substrate binding and specificity in choline oxidase, *Arch. Biochem. Biophys. 430*, 264-273.

7. Gadda, G., Fan, F., and Hoang, J. V. (2006) On the contribution of the positively charged headgroup of choline to substrate binding and catalysis in the reaction catalyzed by choline oxidase, *Arch. Biochem. Biophys. 451*, 182-187.

8. Fan, F., and Gadda, G. (2005) Oxygen- and temperature-dependent kinetic isotope effects in choline oxidase: correlating reversible hydride transfer with environmentally enhanced tunneling, *J. Am. Chem. Soc. 127*, 17954-17961.

9. Ghanem, M., and Gadda, G. (2005) On the catalytic role of the conserved active site residue His466 of choline oxidase, *Biochemistry 44*, 893-904.

10. Quaye, O., Cowins, S., and Gadda, G. (2009) Contribution of flavin covalent linkage with histidine 99 to the reaction catalyzed by choline oxidase, *J. Biol. Chem. 284(25)*, 16990-16997.

11. Rungsrisuriyachai, K., and Gadda, G. (2008) On the role of histidine 351 in the reaction of alcohol oxidation catalyzed by choline oxidase, *Biochemistry 47*, 6762-6769.

12. Su, Q., and Klinman, J. P. (1999) Nature of oxygen activation in glucose oxidase from *Aspergillus niger*: the importance of electrostatic stabilization in superoxide formation, *Biochemistry 38*, 8572-8581.

13. Roth, J. P., and Klinman, J. P. (2003) Catalysis of electron transfer during activation of O_2 by the flavoprotein glucose oxidase, *Proc. Natl. Acad. Sci. U S A 100*, 62-67.

14. Fan, F., Germann, M. W., and Gadda, G. (2006) Mechanistic studies of choline oxidase with betaine aldehyde and its isosteric analogue 3,3-dimethylbutyraldehyde, *Biochemistry 45*, 1979-1986.

15. Caldinelli, L., Iametti, S., Barbiroli, A., Bonomi, F., Fessas, D., Molla, G., Pilone, M. S., and Pollegioni, L. (2005) Dissecting the structural determinants of the stability of cholesterol oxidase containing covalently bound flavin, *J. Biol. Chem. 280*, 22572-22581.

16. Caldinelli, L., Iametti, S., Barbiroli, A., Fessas, D., Bonomi, F., Piubelli, L., Molla, G., and Pollegioni, L. (2008) Relevance of the flavin binding to the stability and folding of engineered cholesterol oxidase containing noncovalently bound FAD, *Protein Sci. 17*, 409-419.

17. Huang, C. H., Winkler, A., Chen, C. L., Lai, W. L., Tsai, Y. C., Macheroux, P., and Liaw, S. H. (2008) Functional roles of the 6-S-cysteinyl, 8alpha-N1-histidyl FAD in glucooligosaccharide oxidase from *Acremonium strictum*, *J. Biol. Chem. 283*, 30990-30996.

18. Hassan-Abdallah, A., Zhao, G., and Jorns, M. S. (2006) Role of the covalent flavin linkage in monomeric sarcosine oxidase, *Biochemistry 45*, 9454-9462.

19.   Fraaije, M. W., van den Heuvel, R. H., van Berkel, W. J., and Mattevi, A. (1999) Covalent flavinylation is essential for efficient redox catalysis in vanillyl-alcohol oxidase, *J. Biol. Chem. 274*, 35514-35520.

20.   Heuts, D. P., Winter, R. T., Damsma, G. E., Janssen, D. B., and Fraaije, M. W. (2008) The role of double covalent flavin binding in chito-oligosaccharide oxidase from *Fusarium graminearum*, *Biochem. J. 413*, 175-183.

21.   Motteran, L., Pilone, M. S., Molla, G., Ghisla, S., and Pollegioni, L. (2001) Cholesterol oxidase from *Brevibacterium sterolicum*. The relationship between covalent flavinylation and redox properties, *J. Biol. Chem. 276*, 18024-18030.

22.   Winkler, A., Kutchan, T. M., and Macheroux, P. (2007) 6-S-cysteinylation of bi-covalently attached FAD in berberine bridge enzyme tunes the redox potential for optimal activity, *J. Biol. Chem. 282*, 24437-24443.

23.   Kim, J., Fuller, J. H., Kuusk, V., Cunane, L., Chen, Z. W., Mathews, F. S., and McIntire, W. S. (1995) The cytochrome subunit is necessary for covalent FAD attachment to the flavoprotein subunit of *p*-cresol methylhydroxylase, *J. Biol. Chem. 270*, 31202-31209.